AD NUMBER

AD472900

LIMITATION CHANGES

TO:

Approved for public release; distribution is unlimited. Document partially illegible.

FROM:

**Distribution authorized to U.S. Gov't. agencies and their contractors;
Administrative/Operational Use; JUN 1965. Other requests shall be referred to Army Electronics Command, Attn: AMSEL-KL-PB, Fort Monmouth, NJ. Document partially illegible.**

AUTHORITY

usaec ltr, 1 may 1968

SECURITY MARKING

The classified or limited status of this report applies to each page, unless otherwise marked.
Separate page printouts MUST be marked accordingly.

THIS DOCUMENT CONTAINS INFORMATION AFFECTING THE NATIONAL DEFENSE OF THE UNITED STATES WITHIN THE MEANING OF THE ESPIONAGE LAWS, TITLE 18, U.S.C., SECTIONS 793 AND 794. THE TRANSMISSION OR THE REVELATION OF ITS CONTENTS IN ANY MANNER TO AN UNAUTHORIZED PERSON IS PROHIBITED BY LAW.

NOTICE: When government or other drawings, specifications or other data are used for any purpose other than in connection with a definitely related government procurement operation, the U. S. Government thereby incurs no responsibility, nor any obligation whatsoever; and the fact that the Government may have formulated, furnished, or in any way supplied the said drawings, specifications, or other data is not to be regarded by implication or otherwise as in any manner licensing the holder or any other person or corporation, or conveying any rights or permission to manufacture, use or sell any patented invention that may in any way be related thereto.

HYDROCARBON-AIR
FUEL CELL

Report No. 7

Contract No. DA 36-039 AMC-03743(E)

ARPA Order No. 247

Task No. 7900.21.903.01.00.

Semi-Annual Report No. 3, 1 Jan. 1965 - 30 June 1965

U.S. Army Electronics Command

Fort Monmouth, New Jersey

ESSO RESEARCH AND ENGINEERING COMPANY
PROCESS RESEARCH DIVISION
LINDEN, NEW JERSEY

PcRD-4M-65

HYDROCARBON-AIR FUEL CELL

REPORT NO. 7

CONTRACT NO. DA 36-039 AMC-03743(E)
ARPA ORDER NO. 247
TASK NO. 7900.21.903.01.00.

SEMI-ANNUAL REPORT NO. 3, 1 JAN. 1965 - 30 JUNE 1965

OBJECT: CONDUCT INVESTIGATIONS LEADING TO THE DEVELOPMENT OF HYDROCARBON AND METHANOL FUEL CELLS

Authored by:

William R. Epperly
Eugene L. Holt
Hugh H. Horowitz
Duane G. Levine
Charles E. Morrell
Barry L. Tarmy
James A. Wilson
Morton Beltzer
George Ciprios
I-Ming Feng
Donald E. LeClair
Martin Lieberman
John M. Matsen
Andreas W. Moerikofer
Eugene H. Okrent
Robert K. Resnik
Joseph A. Shropshire
Charles E. Thompson
Herbert H. Vickers
Elliot A. Vogelfanger
Abraham A. Zimmerman

The work performed under this contract was made possible by the support of the Advanced Research Projects Agency under Order No. 247, through the U.S. Army Electronics Command.

Esso Research and Engineering Company
Process Research Division
Linden, New Jersey

CONTENTS

CONTENTS

ILLUSTRATIONS

TABLES

APPENDIX ILLUSTRATIONS

APPENDIX TABLES

SECTION 1

PURPOSE

The purpose of these investigations is to perform research on the basic components of fuel cells using electrolyte-soluble carbonaceous fuels and fuel cells using hydrocarbon fuels. One objective, which is a continuation of the work carried out under contracts DA 36-039 SC-89156 and DA 36-039 AMC-00134(E), is to improve the performance of methanol-air fuel cells and to incorporate improved components into multicell batteries to study the engineering problems of multicell operation. A second objective is to determine the feasibility of hydrocarbon-air fuel cells.

The major emphasis of the program is on the simultaneous research and development on all basic aspects of the cells to optimize performance of the entire cell and to take into account interactions between components.

This work is aimed toward the development of practical fuel cells using hydrocarbons or their partially oxygenated derivatives as fuels and air as oxidant. The fuels must be capable of reacting to carbon dioxide, be reasonably available, and pose no unusual corrosion, toxicity, or handling problems. Also, the cell must use a CO_2-rejecting electrolyte and operate at temperatures up to about 200°C. Other desired requirements include high electrical output per unit volume and weight, high efficiency, long life, high reliability, reasonable cost, particularly catalyst cost, and ruggedness.

The program is divided into seven parts. These are referred to as Tasks A through G in this report. Tasks A and D describe studies of catalysis and structure at the hydrocarbon and methanol electrodes, respectively. Air electrode research is discussed in Task E. Task B includes work to assess performance in liquid hydrocarbon-oxygen cells. Task F deals with work on establishing the basic methanol cell design, especially with regard to the operation of all components in a single cell. Task G is concerned with work on the development of methanol multicell systems. Finally, Task C describes exploratory studies aimed at new approaches to fuel cells.

SECTION 2

ABSTRACT

2.1 Task A, Hydrocarbon Electrode

Two general approaches were taken toward solution of the important catalyst cost problem. One involved studies aimed at understanding and improving the operation of noble metal catalysts. The other was to seek new, non-noble catalysts.

A comparative study of a number of platinum black catalysts prepared by different reduction procedures was made. The steady-state activity of these catalysts varied by a factor of one hundred, but all this variation could be attributed to structural features of the catalysts, rather than to their intrinsic catalytic properties. The abilities of the catalysts to electrochemically oxidize preadsorbed butane were all the same, as reported previously. It was shown that the rates at which they adsorbed butane, in the presence of electrolyte, were also essentially the same. Only the pore volume of the catalyst correlated with the steady-state performance, higher pore volumes resulting in better performance. Electron micrographs confirmed that the more porous catalyst structures were superior to the dense agglomerated structures.

The technique for measuring adsorption rates, mentioned above, was quite unique and led to some potentially valuable information about the action of platinum. The method involved flowing electrolyte, saturated with butane, through a porous metal frit on which the catalyst was mounted. At high flow rates mass transport limitations were overcome and fuel accumulation was adsorption rate limited. With this method it was found that the steady-state performance of static electrodes corresponded to that calculable on the basis of the adsorption rates. This indicates that the catalyst in the optimized electrode structures is functioning quite efficiently. Fuel transport is apparently not a problem in a properly compounded electrode. Secondly, a study of the effect of potential on the adsorption rate was carried out in the potential range of hydrogen adsorption. The rate of butane adsorption was proportional to the number of hydrogen sites of the "second kind" that were left uncovered. No adsorption would occur on the hydrogen sites of the "first kind," and butane desorption occurred when hydrogen of the first kind was forced onto the platinum by cathodization. This result indicates the importance of the two different types of platinum sites, as recognized by their characteristic hydrogen peaks in voltammetric scans, upon the oxidation of carbonaceous fuels. Many characteristics of the activity of various carbonaceous fuels, including voltage oscillations, could be explained on the basis of mechanisms involving the two sites. It has not been determined whether variations in the ratios or nature of the sites are possible. The effect of such variations on hydrocarbon oxidation is also unknown.

To further improve the utilization of platinum, the use of a carbon support was studied. Standard impregnated platinum-on-carbon matched platinum black in specific activity, giving limiting currents of 8 ma/mg of platinum on butane at 150°C. By using impregnation procedures designed to maximize adsorption and by treating the carbon with silica it was possible to double this activity. Similarly, by fabricating extremely thin electrodes it was possible to double the base level activity. Combination of these two beneficial effects is to be explored in the future. A study of the operation of these electrodes with liquid decane fuel was also begun, with promising initial results.

In the area of non-noble catalysts, both alloys and compounds of the transition metals have been studied. Attempts were made to prepare high surface area alloys by high temperature hydrogen reduction. The experimental technique proved to be difficult and the degree of alloying low. Other techniques, in particular using ternary Raney alloys, are to be emphasized in the future. The alloys were chosen on the basis of electronic structure, geometry, and chemical reactivity. Most interesting were alloys of gold with iron and cobalt, which showed activity on hydrogen in alkali. However, difficulty in maintaining activity and in making repeat preparations has prevented adequate checks for electrochemical corrosion stability.

Considerable effort has been spent making and testing mixed oxides of the perovskite lattice structure containing transition metals known to have catalytic properties. A wide variety of compositional and stoichiometric variations are possible with these compounds. The problem is to tailor them to meet the fuel cell requirements of conductivity and corrosion resistance. It was found that stoichiometric perovskites were quite acid resistant, but had very poor conductivities. The incorporation of lattice deficiencies, principally oxide ion vacancies, improved the conductivities markedly with some sacrifice in acid resistance. Within this broad generalization there was a wide variation in behavior. Nickel perovskites generally showed excellent acid resistance, actually coming to equilibrium with small quantities of nickel ion in the corroding acid. However, it was very difficult to make these compounds conductive. The best conductivities were achieved by doping with lanthanum. Cobalt compounds could be made very conductive by the incorporation of lattice deficiencies, but they then lost most of their acid resistance. With both nickel and cobalt the combined target properties could be approached but not met. Finally, it was found that conductivities imparted by oxide ion deficiencies were rapidly lost upon exposure to acid. Thus, it appears that the only satisfactory perovskites will be stoichiometric compounds with conductivities imparted by valence variations rather than by lattice defects. Perovskites containing manganese in the two, three, and four valence states have already shown some promise.

In still another approach to non-noble catalysts, a number of cyano and cyclopentadienyl complexes have been checked for catalytic activity. The results have not been promising so far. A uranyl salt has shown some activity with methanol, however, and is to be investigated further.

2.2 Task B, Hydrocarbon Fuel Cell

Total cell tests on liquid decane and oxygen were scaled-up to 4 inch electrodes to assess possible problems in an engineered cell. Performance equaled results from previous smaller laboratory cells, 20 mwatts/cm^2.

2.3 Task C, New Systems

A new electrolyte system, pyrophosphoric acid, has demonstrated adequate conductivity and buffer capacity at temperatures in excess of 200°C. Butane was highly active in this electrolyte on sintered platinum-Teflon electrodes, particularly when water vapor was added. Oxygen was also extremely active, with open-circuit polarizations approaching theoretical values. The oxygen performance was not sensitive to water vapor. Lower performance was obtained with low catalyst content electrodes, but the importance of electrode structural variables indicated that further improvements are possible. Other studies with concentrated buffer electrolytes have suggested that attainment of a steady-state pH in the presence of carbon dioxide is a rate controlled process, and with suitable operating conditions a pH level higher

than predicted from equilibrium considerations might be maintained. Performances of various reactants in carbon dioxide treated buffers was poorer than expected. The reason for this is not yet known. Cesium fluoride addition to less concentrated buffers did not impair methanol performance and allowed higher operating temperatures.

The dual structure cathode was analyzed in terms of the functions of each component. Only the sheet facing the air chamber was found capable of supporting appreciable currents. The sheet facing the electrolyte acted primarily as a barrier to help maintain an interface. Performances of platinum or silver dual electrodes were very poor in concentrated cesium di- and tribasic phosphate buffer and in cesium carbonate. However, in 6 M potassium carbonate, high activities were achieved, with the silver system equivalent to the platinum. In addition, the silver air electrode was insensitive to methanol, with no polarization debit or chemical oxidation occurring in the presence of fuel. A total cell test of the silver cathode with a P-type anode in 6 M potassium carbonate gave a net power output of 18 mwatts/cm^2.

Studies of inexpensive methanol catalysts were carried out with transition metal or gold alloys, as well as transition metal compounds. These were tested in potassium hydroxide and in potassium di- and tribasic phosphate buffer. Although a number of stable materials were found, none had satisfactory catalytic activity. Several unsuccessful attempts were also made to reduce metal oxides with decane in concentrated carbonate electrolyte. Finally, tests of slurried catalyzed carbon powders, suspended by bubbling decane through the electrolyte, showed no catalyst utilization advantages over static systems.

2.4 Task D, Methanol Electrode

Studies with the ruthenium modified P-type catalyst were extended to improve its overall performance in methanol-air batteries. The sensitivity to methanol concentration was determined to better define the fuel requirements which must be kept as low as possible to maximize fuel efficiency. The results showed that a minimum of 0.25 M methanol should be maintained in the expected operating range of current density to prevent significant performance loss at the anode. Sprayed Teflon coatings on one side of the anode were found to have no adverse effect on the performance of ruthenium modified P-type anodes. Resistance was increased only slightly. Such coatings could be useful as methanol diffusion barriers to minimize fuel loss through chemical oxidation at the cathode as described in Task F. Ruthenium modified P-type anodes were found to be only slightly sensitive to water purity. Use of distilled water instead of distilled and deionized water caused no performance debit. Even the use of tap water resulted in only a 0.04 volt loss at 50 ma/cm^2 in these short term tests. Effects on life have not been determined. Electrode vibration tests up to 100 cps with 0.375" displacements showed that the catalyst-electrode contact is tenacious and, therefore, catalyst attrition from the electrode should be minimal. Finally, storage and life tests have been extended to 4000 and 8000 hours, respectively. The ruthenium modified P-type catalyst has shown excellent stability at a variety of conditions in these tests.

Methanol electrode structure research has been extended to reduce noble metal costs in methanol-air cells. Studies with the present types of structures containing about 25 mg/cm^2 of ruthenium modified P-type catalyst showed that reducing catalyst loading by more than fifty percent could result in significant performance losses. These results agree with measurements on tantalum-diluted catalysts. Attempts to increase the availability of the catalyst and, therefore, its utilization by making two-layered electrodes or increasing porosity were not successful. Various reduction techniques were attempted to see if improvements in ruthenium modified P-type catalyst activity were possible. Reduction by the formaldehyde-sodium aluminate method, reported previously for

hydrocarbon platinum catalysts, gave the best results. However, this catalyst was inferior to the present hydrogen reduced form. Studies were also made of the effect of catalyst surface area on performance with methanol. The platinum black catalysts used in this work varied from 8 to 30 m^2/gm with the higher surface area material giving the best performance. As a result of these findings, studies of supported catalysts were initiated. Platinum on carbon electrodes with a tenfold reduction in catalyst loading were fabricated which give similar performance to unsupported platinum electrodes. Attempts were then made to reduce the more active ruthenium modified P-type catalyst on carbon. The resulting activity was strongly dependent on the reduction technique with the low temperature hydrogen reduction giving the best results, 10 ma/cm^2 at 0.35 volts polarization with 2 mg/cm^2 of noble metal. The performance showed that the catalytic advantage of ruthenium modified P-type catalyst could be obtained on supported electrodes but further activity improvements are required.

2.5 Task E, Air Electrode

Several tests have been carried out to assess the possibility of replacing the membrane backing at the cathode, used in methanol-air cells, with a coating applied directly to the electrode surface. With butyl latex, silastic, or Teflon coatings, the best performance was achieved with the coated side facing the air. In most cases, slightly higher polarizations were measured than for the membrane-clad electrode. Coating thickness did not affect performance, but did influence the leak rate. A scale-up debit was found for fabricating larger 9" x 5-3/4" electrodes, but the magnitude could not be accurately measured.

2.6 Task F, Methanol Fuel Cell

Efforts were directed toward eliminating the 0.1 to 0.2 volt performance debit associated with the use of tantalum screens in the large anodes. This voltage loss was essentially eliminated by gold coating the tantalum to prevent the formation of an insulating tantalum oxide film on the surface. Other studies were carried out to assess the operating characteristics and reliability of different sized cells. Partial immersion of the electrodes in 4" x 4" cells, which can result from upsets, storage, or tipping do not adversely affect their activity. In other tests 9" x 5-3/4" anodes were found to require higher methanol concentrations than smaller electrodes. This resulted in increased methanol diffusion and oxidation at the cathode.

Further testing was carried out on the development of a direct feed fuel cell. Porous diffusers were installed for adding methanol into the chamber, where the carbon dioxide evolved distributes the fuel. Power densities, voltages, and methanol chemical oxidation rates were comparable to those obtained with electrolyte circulation. In other tests, it was found that the rates of methanol oxidation at the cathode can be reduced to below 5 ma/cm^2 by using diffusion barriers, such as Dacron felt, between electrodes without impairing performance.

2.7 Task G, Prototype Development

Several sixteen cell multicell units were constructed to evaluate the operability of a methanol battery. One of these units, with a power output of about 100 watts, was packaged and delivered to Fort Monmouth. The second unit, containing several improvements, has been under test in the laboratory. Initial performance was 120 watts or about 25 $mwatts/cm^2$. After 275 hours on load during a four month period, the average cell voltage decline was only about 30 mv. Operation was stable with good fuel and air distribution. However, chemical oxidation at the cathode was somewhat higher than desired. Progress was also made on the development of a new methanol concentration controller and a low power electrolyte circulation pump.

SECTION 3

PUBLICATIONS, LECTURES, REPORTS, AND CONFERENCES

3.1 Lectures

Shropshire, J. A. - Theory of Redox Couples at Carbonaceous Fuel Electrodes--Second USAERDL Working Conference, Magnolia Manor, Magnolia, Massachusetts, May 2-4, 1965.

Epperly, W. R. - Direct Hydrocarbon Fuel Cell--Nineteenth Annual Power Sources Conference, Atlantic City, New Jersey, May 18, 1965.

Tarmy, B. L. - Methanol Fuel Cell Battery--Nineteenth Annual Power Sources Conference, Atlantic City, New Jersey, May 18, 1965.

Heath, C. E. - Fuel Cell Materials: Electrodes and Catalysts--AICHE Meeting, London, England, June 15, 1965.

Heath, C. E. - Methanol Fuel Cell Catalysis--Journees Internationales D'Etude Des Piles A Combustible, Brussels, Belgium, June 21-24, 1965.

3.2 Conferences

January 13, 1965 - Fort Monmouth, New Jersey

Organizations represented: United States Army Electronics Command
Esso Research and Engineering Company

The meeting was a review of progress and plans for the methanol-air and hydrocarbon-air fuel cells.

March 19, 1965 - Linden, New Jersey

Organizations represented: United States Army Electronics Command
Esso Research and Engineering Company

The meeting was a review of progress and plans for the methanol-air and hydrocarbon-air fuel cells.

May 4, 1965 - Linden, New Jersey

Organizations represented: United States Army Electronics Command
Esso Research and Engineering Company

The meeting was held to review specific questions related to the methanol-air fuel cell and hydrocarbon-air fuel cell programs.

3.3 Reports

This report is written in conformance with the detailed reporting requirements as presented in the Signal Corps Technical Requirement on Technical Reports

(SCL-2101P, 18 February 1963) under the terms of our contract; these requirements differ from the usual requirements for reports issued within Esso Research and Engineering Company.

3.4 Publications

Shropshire, J. A. and Tarmy, B. L. - The Nitric Acid-Oxygen Redox Electrode in Acid Electrolyte - Advances in Chemistry, No. 47, A.C.S., 153 (1965).

Shropshire, J. A. - The Catalysis of the Electrochemical Oxidation of Formaldehyde and Methanol by Molybdates - Journal of the Electrochemical Society, 112, 465 (1965)

Shropshire, J. A. - Flow Coulometry - Journal of Electroanalytical Chemistry, 9, 90 (1965)

SECTION 4

FACTUAL DATA

4.1 Task A, Hydrocarbon Electrode

Work on the hydrocarbon electrode has concentrated on reducing the catalyst cost. This is because even in favorable cases the catalyst cost is estimated to be about $5,000 per kilowatt of total fuel cell power. It is estimated that cost reductions of the order of a factor of one hundred will be required before low temperature hydrocarbon fuel cells can be used widely, although many specific applications will become possible with more modest improvements. Two basic approaches are being taken toward this goal. Considerable work is being done to improve the utilization of platinum, and attempts are being made to find non-noble systems that will catalyze the electrochemical oxidation of hydrocarbons.

Within the area of platinum utilization several approaches have been taken. At first, efforts were made to optimize theplatinum black catalysts. Various chemical reduction procedures were used to prepare the blacks, and correlations between their steady-state anodic activity and their physical and electrochemical properties were sought. In particular, the rates of adsorption of a saturated hydrocarbon, butane, on platinum black were measured under various conditions. Chemisorption often limits the performance of hydrocarbon electrodes. Any clues as to means of varying these rates could be valuable. Subsequently, carbon supports were investigated as means of improving platinum utilization. Previous work had indicated that platinum on carbon has a higher specific surface area than platinum black and, when activated properly, can yield electrodes of high specific current density. The present work concentrated on optimizing the structure of such electrodes, and on varying the chemical steps in the catalyst preparation. In addition, operation at temperatures above 150°C. has been considered and is discussed under Task C.

The search for non-noble catalysts was divided into three areas. In one, high surface area metal alloys were prepared by chemical methods, for testing in non-acidic electrolytes. Success in this program requires demonstration of alloy formation and not merely co-reduction, achievement of high surface areas, and choice of components whose geometric and electronic structure will provide catalytic activity and corrosion resistance. Secondly, considerable effort was spent on mixed metal oxides of the perovskite lattice structure, containing transition metal ions. Previous work had shown that some of these compounds are amazingly acid resistant, and that they can be rendered conductive by the incorporation of lattice deficiencies. Compounds combining these attributes were sought for electrochemical testing. Thirdly, a brief investigation was made of a few insoluble transition metal complexes, related to materials of known high electron transfer rates or to soluble hydrogenation catalysts.

Phase 1 - Hydrocarbon Adsorption Rates

In the previous report (6)catalyst studies using the voltage scan technique indicated that a wide variation in steady-state performance of a series of platinum catalysts was possible despite the fact that the catalysts were shown to possess comparable intrinsic electro-oxidation activity. Since the previous characterization, however, made no attempt to study adsorption rate limitations on the catalysts, an effort was made during this report period to define maximum fuel adsorption rates on representative platinum black samples. The variation of adsorption rate with potential was also measured. Since the adsorption was found to occur in the potential

range where adsorbed hydrogen is present in two characteristic forms on the surface, the relation between hydrocarbon and hydrogen adsorption was also investigated. Finally, the voltage scanning technique was applied to several other hydrocarbon fuels and catalysts, and an attempt was made to detect the refractory intermediates reported by other workers.

Part a - Flowing Electrolyte System for Measuring Butane Adsorption Rates

Hydrocarbon adsorption rates were measured using a flowing fuel-saturated electrolyte system to eliminate mass transport effects. Butane served as an ideal model fuel due to its high solubility and its structural similarity to the higher molecular weight hydrocarbons. The catalyst powder was mounted on the upper face of a porous, fritted tantalum sheet. Electrolyte, 3.7 molar sulfuric acid, was saturated with butane and flowed through the catalyst layer. The tantalum sheet and the catalyst were set up electrically to be the anode of a driven cell, and voltage scans were run to determine the amount of fuel adsorbed. Appendix A-1 gives a more detailed description of the set-up.

Three platinum black catalysts were chosen for the initial demonstration or feasibility runs on the system. These catalysts were: (1) Engelhard platinum black, (2) a sample prepared by HCHO reduction of aqueous H_2PtCl_6 in the presence of $Al(OH)_3$ and, (3) lithium reduced platinum black. The latter two catalysts were chosen for their wide variations in physical properties and measured steady state hydrocarbon performance, to be discussed in Phase 2. Fuel accumulation, i.e., the quantity of coulombs in the butane oxidation peak, was measured from continuous voltage scans on the three catalysts at a variety of accessible flow rates.

The applicability of the flow system concept to two of these catalysts was demonstrated by the existence of a plateau in fuel accumulation (during the fixed scan time) as flow rates increased. This indicated that at high flow rates mass transport limitations were overcome and adsorption rate became limiting.

Thus, both Engelhard and formaldehyde reduced platinum gave equivalent fuel accumulation rates independent of flow above 40 cc/min. Excellent reproducibility was also obtained at two widely different loadings of Engelhard platinum black. The lithium reduced catalyst, however, a material of low pore volume and relatively high bulk density, did not permit sufficient flow rates to reach the transport-independent plateau. However, even though it may not have reached the adsorption limited rate, this catalyst already showed two thirds the rate exhibited by the better catalysts. In contrast, the lithium reduced catalyst showed only 15 to 20 percent of the activity of the other two in steady state performance tests. Thus, the differences between the various catalysts are probably not related to their adsorption characteristics, but to their physical structure (Figure A-1).

Figure A-1

Butane Accumulation versus Flow Rate
95°C, 3.7 M H_2SO_4

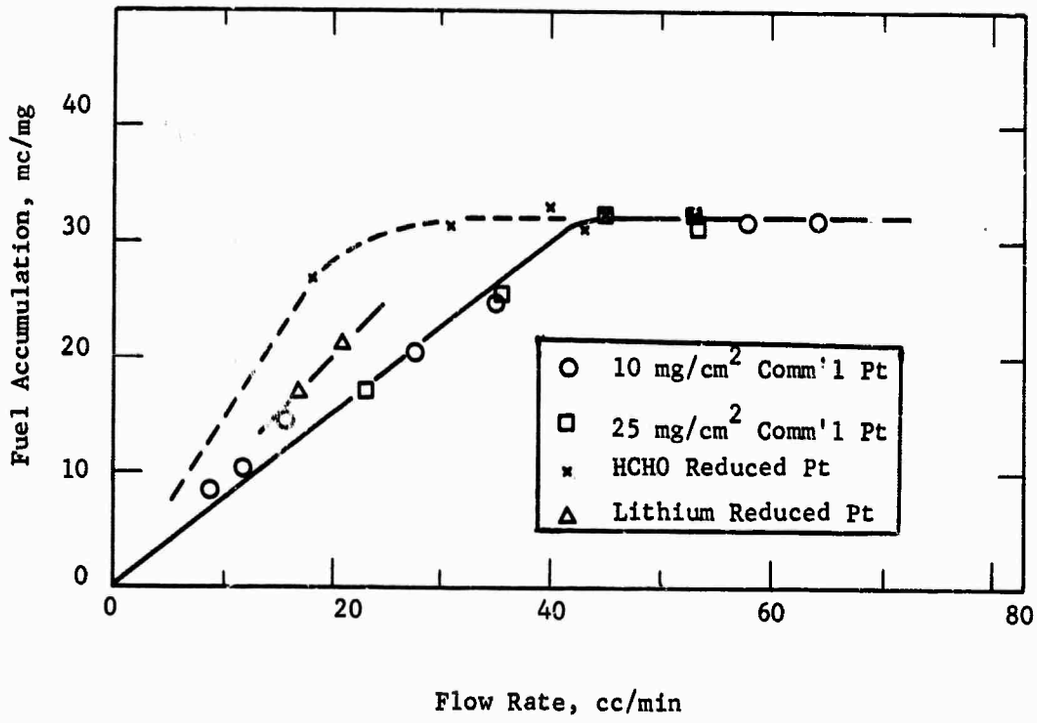

On the basis of these results and the similarity of values for the two platinum blacks used, further studies were restricted to Engelhard platinum black, at loadings of 10 mg/cm^2.

Further confirmation of the limitation of fuel accumulation by adsorption rather than mass transport was obtained from the temperature dependence of fuel accumulation at high flow rates. Thus, a value of 11 kcal/mole was calculated from the relative increase in accumulated coulombs from 80 to 100°C (Appendix A-2). This value, much too high to indicate transport limitation, agrees well with the values obtained previously (5) for the temperature dependence of limiting current for butane electrodes in sulfuric acid at 100°C.

Part b - Butane Adsorption Rate Versus Potential

Since continuous voltage scans do not give an unambiguous definition of adsorption time, the study of the effect of potential on adsorption rate was made using a potentiostatted sawtooth signal in conjunction with the flowing electrolyte system. The scan during the linearly rising part of the signal was used to measure accumulated fuel coulombs after a given wait period, by integration of the peak, while the step function collapse of the signal enabled the return to zero current (and

the start of the next fuel accumulation period) within about three seconds. Normally, six to eight measurements following various "wait" periods were enough to define the required coulombs accumulated vs time slope. This slope was generally quite linear in the time interval up to 50 seconds. The fuel accumulation during the scan and during the previous oxide reduction time period was evidenced as an intercept on the plot of coulombs versus wait time. A typical set of curves at various starting potentials is shown in Appendix A-3. The overall adsorption rate is the measured accumulation rate at a given potential plus a correction for the steady state burnoff rate, observed as a steady current during the adsorption period. Since this correction becomes larger as the potential moves positive and eventually renders readings unreliable, measurements were restricted to $\leq$ + 0.15 volts vs S.C.E. (See Appendix A-4 for detailed data)

The overall rates of butane adsorption varied significantly with potential in the range -0.05 to +0.15 volts vs S.C.E. as shown in Figure A-2. A maximum in adsorption rate appears to occur at +0.10 volts vs S.C.E. with decline as the potential moves more positive than that value. (See Appendix A-5) The maximum observed rate is about three times the steady state limiting current observed previously in these butane-sulfuric acid systems. For reference, the adsorption potential curve and typical steady state performance curve are shown superimposed in Figure A-2.

Figure A-2

Potential Dependence of Adsorption Rates
Butane, 3.7 M H_2SO_4, 95°C

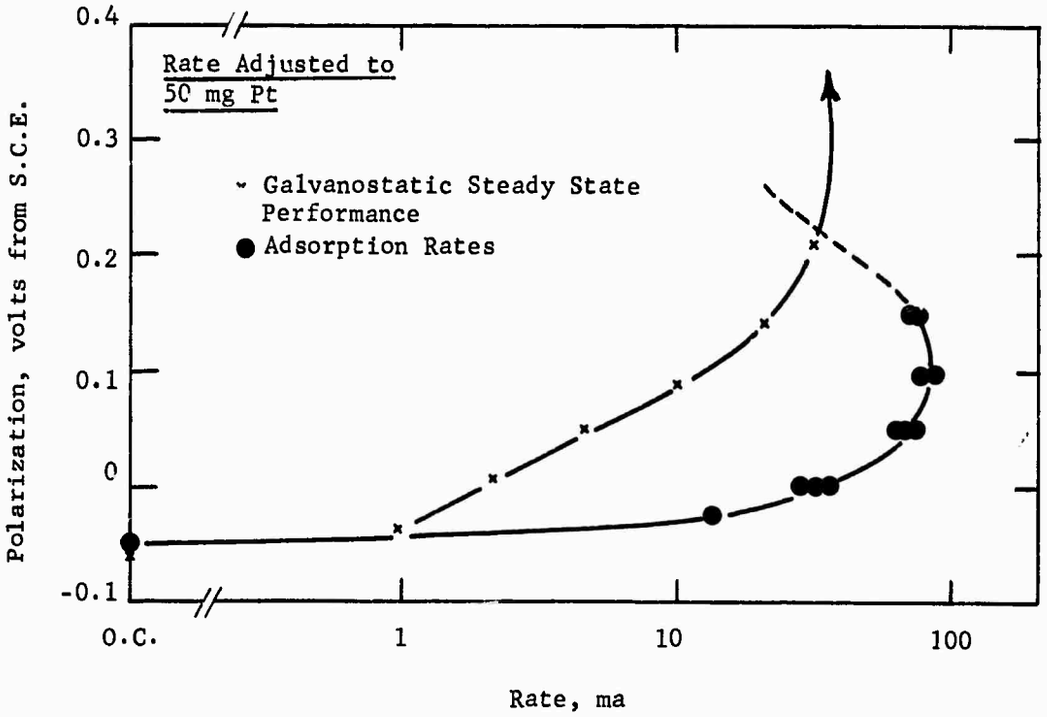

The point at which the extrapolated adsorption rate curve crosses the Tafel line of the electrode performance curve should correspond closely to the limiting current observed in galvanostatic steady state measurements. The fact that the observed limiting current falls in this region is significant since it indicates that the platinum in a compacted platinum-Teflon structure is being used as efficiently as that in the flow through system. Allusion will be made to this point in Appendix B-1 on electrode structure.

The potential range of increasing butane adsorption rate was noted to correspond to the known potential range of hydrogen coverage. As has been noted by many previous investigators (7, 8), the adsorbed H on platinum forms two distinct peaks in the voltage scan trace indicating that two distinct states or energy levels of adsorbed hydrogen atoms exist on the surface. This differentiation is clearly evident in the plot of fractional hydrogen coverage versus potential. Appendix A-6 gives these data along with surface areas or oxide coverages of Engelhard platinum black.

An explanation of the effect of potential on initial adsorption rates was finally obtained from a knowledge of the surface condition with respect to adsorbed hydrogen atoms. Thus, when initial adsorption rate was expressed as a function of hydrogen atom coverage for that potential, a linear relationship was obtained between rate and $1-\theta_H$ (Figure A-3).

Figure A-3

Effect of Hydrogen Coverage on Butane Adsorption Rate

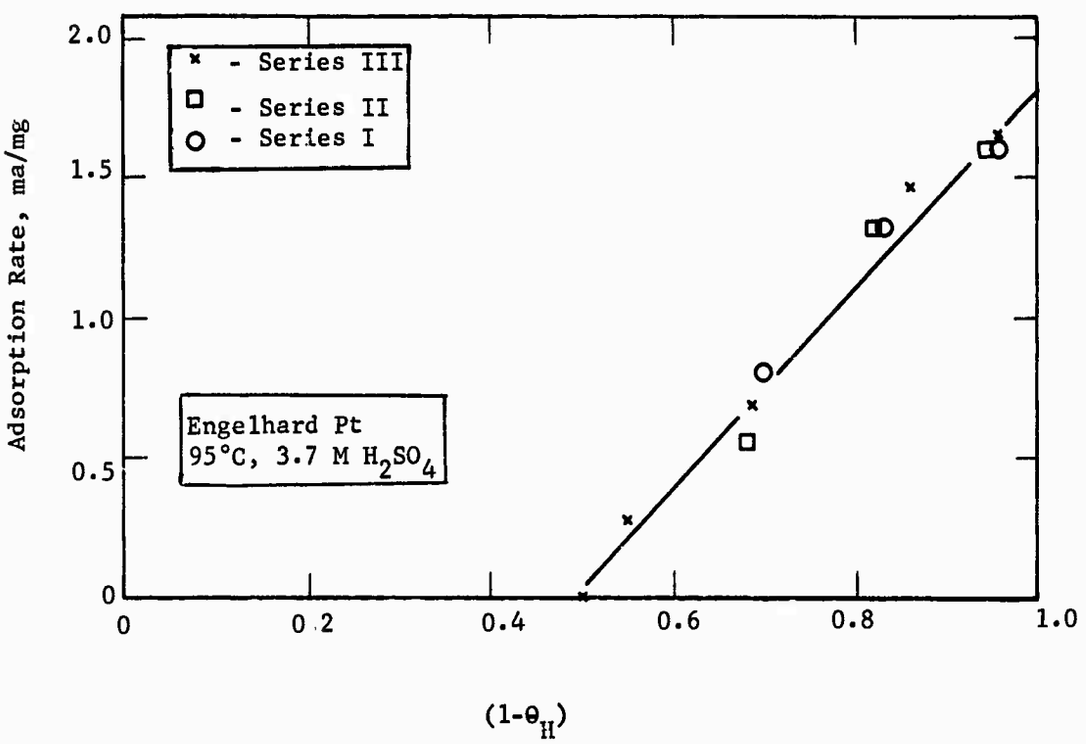

In addition to the linearity, the intercept of zero rate at $1-\theta_H \cong 0.5$ strongly suggests that the adsorption is occurring on only a single type of H· site (Type II, more anodic). Thus, as shown in Appendix Figure A-2, the potential of -0.05 volts vs S.C.E. corresponds closely to the inflection in the curve defining H· coverage and also defines the point of zero adsorption rate in Figure A-3. Linearity with $1-\theta_H$ also implies that the initial adsorption rate, exclusive of area considerations, probably does not vary appreciably over the potential range investigated.

Part c - Evidence in Support of
Adsorption on Type II Sites

Further evidence in support of adsorption on a single type of H· site was sought in measurements of equilibrium fuel adsorption. Previous studies (6, 9) on butane adsorption on platinum electrodes in sulfuric acid at 80°C indicated that saturation coverage corresponded to 1.58 ± 0.13 millicoulombs of butane per millicoulomb of oxide (oxide measured from 1.3 vs S.C.E.). Using the conversion in Appendix A-5, this corresponds to 3.3 millicoulombs butane per millicoulomb total H·, (Q_F^S/Q_H^S). If, however, adsorption of butane is restricted to Type II H· sites alone, then saturation of these sites, about 50% of the total, would correspond to $Q_F^S/Q_H^S(II) = 6.6$. This value corresponds closely to the expected 6.5 electrons per site for the complete oxidation of butane to CO_2 with occupancy of four platinum sites per butane molecule, and thus adds support to the postulated attachment on one type of site.

Additional support for the Type II adsorption was provided by the behavior of adsorbed butane in potential regions approaching hydrogen evolution. Pressed platinum-Teflon electrodes (10:1) saturated with preadsorbed butane showed no evidence of Type II H· oxidation in anodic scans from 0.0 volts vs S.C.E. Similar saturated electrodes subjected to cathodic scans showed gas evolution at potentials as positive as -0.02 volts vs S.C.E. (+0.13 vs reversible hydrogen) together with increased scan current in the region of Type I H· deposition (Appendix A-7). The excess coulombs contained in this increased current region over and above those normally associated with Type I H· deposition, were found to correspond to 3.87 and 3.94 electrons respectively per molecule of butane preadsorbed on the electrode surface, for two such cases. It appears, then, that preadsorbed butane, adsorbed to full coverage on Type II sites is desorbed rapidly as the potential region of Type I hydrogen deposition is reached, and subsequently the four missing hydrogen atoms are rapidly replaced on the surface with the passage of four electrons per original butane molecule.

The desorption of fuel from the saturated electrode is essentially a step function as the potential enters the region of initial Type I H· deposition. Thus, as shown in Appendix A-8, a surface containing saturation coverage of butane, stable at 0.0 volts vs S.C.E., desorbs about 80% of this fuel as the potential is moved negative by 40 millivolts.

Verification that the preponderance of desorbed gas was actually butane was obtained by vapor phase chromatography. A small trapped sample of desorbed gas indicated essentially 100% butane with traces of propane, ethane and methane.

Based on the preceding data, it appears that butane adsorption on platinum black in 3.7 M H_2SO_4 is restricted to Type II H· sites. The maximum initial adsorption rate is found at a potential of about +0.10 volts vs S.C.E., where H· coverage is about equal to zero. Positive to this potential, the adsorption rate appears to decline somewhat, possibly as a region of strong water orientation on the surface is reached.

The knowledge that fuel molecules occupy only Type II H· sites leads to an obvious question as to the occupancy of Type I sites in this potential range. Since it is probable that Type I sites contain adsorbed water or hydronium ions in this region, it is possible that fuel electro-oxidation is accomplished by interaction of the fuel molecules on Type II sites with water molecules on other, Type I, sites. This intriguing possibility suggests a two-site reaction scheme in which the electro-oxidation of a fuel is generally predictable from its adsorption behavior on the platinum. Such a scheme can be applied not only to saturate hydrocarbon fuels but to oxygenated fuels such as methanol, formaldehyde and to olefins as well. Some of the implications of a two site mechanism, including an explanation of oscillatory phenomena, are presented in Appendix A-9.

Part d - Adsorption-Oxidation of Butane on Rhodium

Subsequent to the discovery that butane adsorption on platinum was restricted to Type II H· sites, a brief study of butane adsorption-oxidation on rhodium was carried out. Rhodium was chosen since hydrogen atom deposition does not appear to involve two sites or energy levels as in the case of platinum, and thus rhodium may lack one of the necessary sites for simultaneous water and fuel adsorption. Butane adsorption exposures of pressed rhodium black electrodes ($NaBH_4$ precipitated) followed by voltage scans were carried out in sulfuric acid solution as well as phosphate and carbonate buffers and 85% phosphoric acid.

Rhodium showed very low activity for butane adsorption-electro-oxidation. Thus, at 80°C, no adsorption-oxidation was observed in buffer solutions, and only trace quantities of fuel adsorbed in 0.37 M H_2SO_4. (Appendix A-10) These observations are in qualitative agreement with the two-site postulate outlined previously. At 150°C in 85% H_3PO_4, adsorption-reaction of somewhat higher amounts of fuel occurred. However, since the characterization of platinum under those conditions is not available, no comparisons can be made at present.

Part e - Adsorption of Other Hydrocarbon Fuels on Platinum Black

The equilibrium adsorption of methane, ethane and propane on platinum black was also briefly studied in sulfuric and phosphoric acid electrolyte for comparison with butane. Adsorptions were carried out on pressed platinum electrodes using the technique described previously (6) and fuel adsorption determined by integrating the oxidation peak in the subsequent voltage scan.

In general, the quantity of coulombs obtained from the saturation coverage with fuel increased with increasing carbon number. Thus, in 3.7 M H_2SO_4, the maximum ratio of fuel coulombs to oxide coulombs (used as a normalizing factor) for the various fuels increased from 0.2 for methane to 1.58 for butane, as shown in Table A-1 below. At the same time, it appeared that ethane, propane and butane at saturation had displaced all the Type II H· as evidenced by the voltage scan from 0.0 volts vs S.C.E. Thus the possibility exists that the increasing coulombs obtained for higher carbon number fuels is simply a reflection of the larger number of electrons involved in the fuel oxidation to CO_2 and that ethane, propane and butane displace equal numbers of hydrogen atoms during adsorption. This situation would most reasonably arise only if the fuels adsorbed in an end-on attachment, displacing (as shown for butane) four hydrogen atoms per single fuel molecule. The relatively good agreement of observed fuel oxidation ratios (based on butane) to the calculated ratio of total electrons per molecule in Table A-1 suggests that this situation exists for ethane, propane and butane. Methane appears to be anomalous in this respect since even the maximum adsorption time did not result in removal of all the Type II hydrogen atoms. This may simply indicate a very slow adsorption of methane and achievement of less than saturation coverages in the time allowed.

Table A-1

Relative Adsorption of Lower Hydrocarbons on Platinum in H_2SO_4, 80°C

Fuel	Electrons, Oxidation to CO_2	Calc Electron Ratio, Based on Butane	Observed mc Fuel/mc Oxide	Observed Coulombic Ratio, Based on Butane
Methane	8	0.31	0.23	0.15
Ethane	14	0.54	0.83 (1)	0.53
Propane	20	0.77	1.24 (1)	0.79
Butane	26	1.00	1.58 (2)	1.00

(1) Average of longest exposures, two separate runs.
(2) Average obtained previously. Standard deviation equals $\pm$0.13.

Although fuel coulombs similarly increased with carbon number in experiments in 85% H_3PO_4 at 140°C, no simple relationship between the quantities was found. Thus, the adsorption behavior in this medium may differ from that in H_2SO_4. (Appendix A-8)

Part f - Oxidation of Adsorbed Butane as a Function of Potential

Some controversy exists as to the state of the platinum surface during hydrocarbon oxidation, certain investigators believing that refractory, partially oxidized materials occupy the surface, poisoning its activity to a greater or lesser degree [10]. A brief study was carried out, therefore, to see to what extent a preadsorbed quantity of butane was oxidized as a function of increasing positive potential. Wetted electrodes with butane saturation coverage adsorbed in vapor phase were therefore equilibrated at fixed potential levels in solution, where further accumulation of fuel is restricted by poor transport conditions. Following equilibration at a given potential, a voltage scan was obtained to ascertain the remaining coulombs of fuel on the electrode. Studies in 14.7 M phosphoric acid at 140°C indicated that over 90% of the fuel was removed by polarization to 0.4 volts (i.e. at +0.35 volts vs S.C.E.) with correspondingly lower values being obtained at lower temperatures in both phosphoric and sulfuric acid (Appendix A-8). Thus it does not appear that refractory surface species are a problem in operation at the higher temperature. After equilibration at +0.15 volts vs S.C.E., with over 50% of original fuel burned off, the ratio of anodic fuel coulombs to coulombs of hydrogen atoms displaced was still found to be 6.4, thus indicating that the remaining species were not partially oxygenated. Complete data are in Appendix A-8.

Part g - Adsorption of Butane on Non-Noble Metal Catalysts

A few brief tests were carried out to determine the butane adsorption and reaction on non-noble metal catalysts prepared in other phases of the program. Catalysts included Ni_2B, Ni-Au and Ni prepared by techniques discussed in Phase 5. Tests were carried out in NaOH (Ni_2B) and equimolar potassium mono, di, orthophosphate (all). Voltage scans after various periods of butane exposure indicated no detectable signs of activity for butane adsorption oxidation (Appendix A-10). No further studies were made.

Phase 2 - Studies of the Effects of the Physical Nature of Platinum Catalysts on Performance

The significance of electrode structure parameters such as thickness, wetproofing, catalyst dispersion, etc. on performance in the anodic oxidation of liquid and gaseous hydrocarbons has been discussed (4, 5, 6). These factors determine the macrostructure of the electrode which defines the nature of the critical fuel-catalyst-electrolyte contacting. This in turn establishes the capability of the electrode to achieve the maximum performance possible with the catalyst. While work has continued in all of these areas, studies have been made to differentiate between the various structural and catalytic effects. This has included not only the macrostructure of the electrode, described in Phase 4, but the physical properties or microstructure of the catalyst such as surface area and pore volume.

Part a - Electrochemical Evaluations

An understanding of the contributions of some of the electrocatalytic properties and catalyst microstructure to overall activity is important in seeking new, cheaper catalyst materials or improving catalyst utilization with present expensive noble metal materials. Therefore, studies of these various effects have been made.

In previously reported work (6 and Phase 1), techniques were described for establishing the intrinsic catalytic activity of a series of platinum catalysts by measuring the rate of adsorption of fuel under non-diffusion-limited conditions, and the rate of oxidation of the preadsorbed fuel. The results of these measurements for catalysts prepared by a variety of reduction techniques indicated that the intrinsic catalytic activity was similar for all of the platinum catalysts. This study was extended to an examination of steady-state performance of electrodes containing the catalysts. Each of the catalysts was formulated into a sintered platinum Teflon emulsion type electrode and tested on butane in 14.7 M phosphoric acid electrolyte from 80° to 150°C using the standard half cell testing procedure (6). This electrode formulation is not an optimum for butane gas since it is representative of the structures used for liquid decane. However, it was selected because of the need for good reproducibility. In this way variations in electrode macrostructure were minimized.

The results, in Table A-2 and Appendix A-11, show that the steady state performances varied by as much as 50 fold even though the intrinsic activities of the catalysts had been previously shown to be similar. The electrode performance variations did not correlate with the electrochemical surface areas as determined from measurement of the reduction of the oxide peak from voltage scans. These electrochemical surface areas varied by only a factor of 3--not nearly enough to account for the performance variation.

Table A-2

Electrode Performance of Various Platinum Black Catalysts

Butane, 14.7 M H_3PO_4, 150°C

Preparation of Platinum Black	Current Density at 0.4 volts Polarization, ma/cm^2	Electrochemical Surface Area, m^2/gm
A. Formaldehyde Reduced	2.5	8.9
B. Raney Pt from Co-reduced Pt-Ag	6.	22.5
C. Potassium Borohydride Reduced	15.	13.4
D. Lithium Reduced	19.	26.9
E. Commercial Platinum	90.	23.7
F. Formaldehyde Reduced in Presence of Sodium Aluminate	130.	21.8

Thus, in spite of the fact that catalysts of similar intrinsic activity were incorporated in similar electrode structures, the final steady-state electrode performances showed large variations.

Part b - Characterization of Catalyst Micro-Structure

Further studies to explain the large variations in electrode performance described in Part a were aimed at characterizing the physical state or microstructure of the catalyst. This included measurements of bulk density by gravimetri techniques, crystallite size(by X-Ray line broadening), BET surface area, and pore volume by N_2 capillary condensation. In addition, the appearance of the catalyst agglomerates in electron micrographs was noted. The results of these measurements are summarized in Table A-3.

Table A-3

Catalyst Structure Characterization

Butane Activity, (ma/cm^2)(1)	Bulk Density, gms/cm^3(2)	X-Ray Crystallite Size, Å	Surface Area, m^2/gm		Pore Volume, cm^3/gm
			Electrochemical(3)	BET	
A. 2.5	0.27	62	8.9	8	0.03
B. 6.	0.65	35	22.5	10	0.05
C. 15.	0.99	82	13.4	7	0.13
D. 19.	0.65	50	26.9	26	0.19
E. 90.	0.46	77	23.7	28	0.39
F. 130.	0.55	45	21.8	30	0.40

(1) Designations and activity as in Table A-2.
(2) From volume of fresh suspension settled through deionized water 24 hours.
(3) From coulombs in oxide reduction peak.

The BET surface areas ranged from 7 to $30 m^2/gm$, while pore volumes varied by more than a decade (0.03 to 0.4 cm^3/gm). Crystallite size was observed to extend from 32 to 82°A while agglomerate size (via electron microscope) ranged from 35 to 150°A.

Analysis of electron micrographs indicated that steady state performance could be correlated with the degree of aggregation of the catalyst particles. While quantitative comparisons were not possible it appeared that the more porous the catalyst agglomerates were the better the performance. There appeared to be a definite (and regular) difference in catalyst appearance. The higher activity catalysts were characterized by a lacy agglomerate structure with the individual crystallites forming a network of low coordination number, while the poorer catalysts showed much less lacy material, larger agglomerates and increasing amounts of large dense areas with well formed crystalline edges. Electron micrographs of the best (catalyst F) and worst (catalyst A) are compared in Figures A-4 and A-5. The trends observed in the electron micrographs can be placed on a quantitative basis by examining the effect of pore volume on the steady state butane performance of those catalysts. The correlation between butane current capability, ma/cm^2 at 0.4 volts polarized, and pore volume, shown in Figure A-6, is quite good.

Figure A-4

Electron Micrograph of
High Performance Catalyst

Pore Volume = 0.4 cm^3/gm

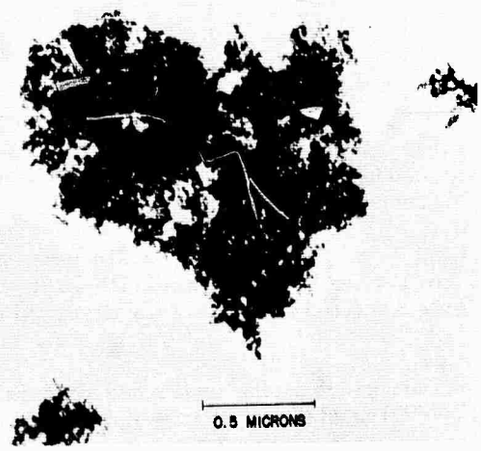

Figure A-5

Electron Micrograph of
Poor Catalyst

Pore Volume = 0.03 cm^3/gm

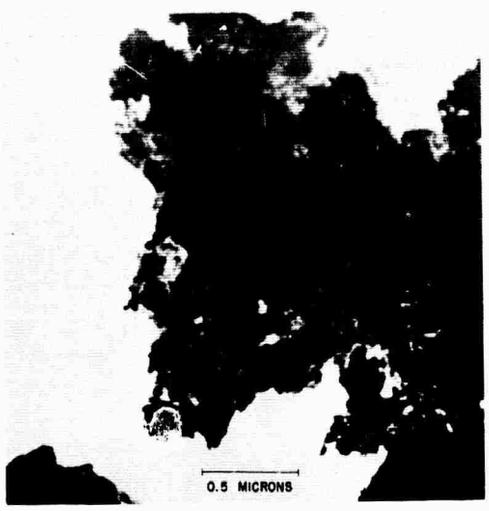

Figure A-6

Effect of Pore Volume on Performance

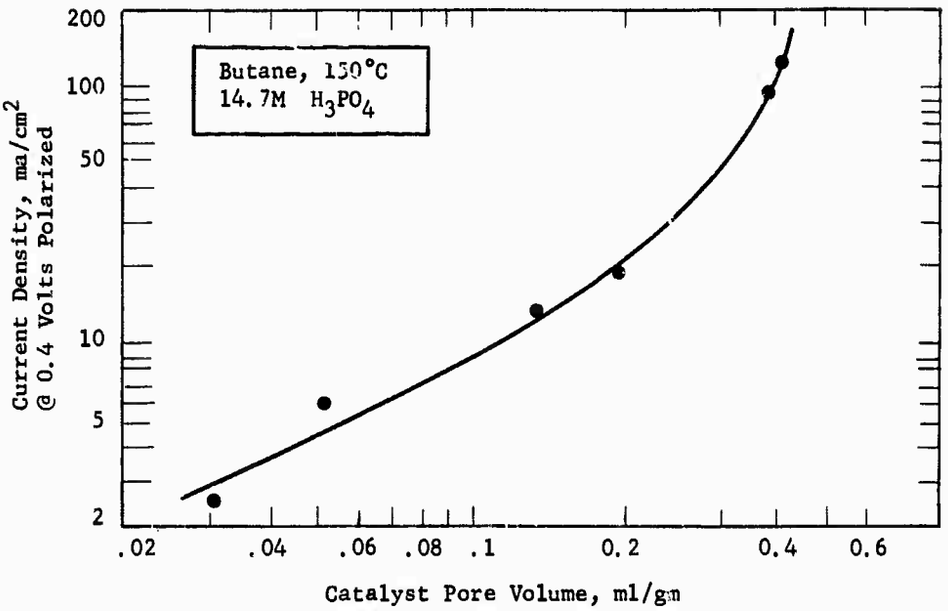

Examinations of the butane performance of these catalysts in 3.7 M sulfuric acid at 100°C, Appendix A-12, indicates that a correlation with pore volume also exists at this lower temperature. However, due to the lower reactivity, the physical factors are more readily masked by other chemical limitations, resulting in a poorer correlation.

These results lead to some important implications in electrocatalyst screening and development. First, it is clear that steady state performance testing alone will not necessarily detect catalysts of different intrinsic activity unless the catalyst microstructure is well defined. As a corollary it may not be possible to produce the correct micro-structure in a catalyst with superior intrinsic activity. Both properties are needed.

Part c - Studies of Hydrogen Performance

The performance of these previously prepared catalysts was examined using H_2 as the fuel in 14.7 M phosphoric acid at 100°C (Appendix A-13), to see if a correlation with butane performance existed. No correlation was obtained. The reason for this is unknown. It is noted, however, that the current density range is much higher with hydrogen, the voltage range is different (and therefore perhaps the wetting properties), and the electrochemical parameters are much different. In any case, while hydrogen may be useful for screening unknown materials for qualitative signs of electrochemical activity, it cannot be used for quantitative assessment of structure improvements in hydrocarbon electrodes.

Phase 3 - Increasing Platinum Utilization

While there is reason to expect that non-noble hydrocarbon catalysts can be found, at the present time the platinum metals are the only suitable materials known. With decreases in platinum loadings, it may be possible to prepare practical hydrocarbon fuel cells. A catalyst support appears to be necessary to achieve this aim. Without a support, platinum loadings of less than one mg/cm^2 could not provide the required electrode strength and electrical conductivity. It is also known that supports increase and stabilize catalyst surface areas. Carbon is being used as the support in this program. Aside from its conductivity and corrosion resistance, its high surface area and sorptive properties should promote maximum dispersion of the catalyst.

Part a - Preliminary Variables

For comparative evaluation of catalysts, a testing system was chosen involving a driven half cell unit, using gaseous butane fuel, thin electrodes of 4-5 cm^2 area, and 14.7 M H_3PO_4 @ 150°C. Under these conditions, the optimum utilization obtained for unsupported Pt black was 8 ma/mg. Attempts were made to follow structure improvements as closely as possible to guarantee that observed effects were applicable to a practical system.

Since a large number of variables were conceivably involved, a preliminary check was made to ascertain their importance relative to the desired target.

Minor effects were observed as a result of variation in catalyst washing procedures, and electrode formulation procedures (mixing and Teflon content variations). These results were then used to get an outside limit of the standard deviation from which significance of the more important effects could be judged (See Appendix A-14-I). It is recognized that the effects of the minor variables should be rechecked when new catalyst compositions are arrived at.

Two electrode structures were examined and found to be essentially the same in a 2 x 3 experiment. See Appendix A-14-II. With the elimination of this variable it was possible to obtain enough data to evaluate the effect of a catalyst activation technique. Use of this technique gave a statistically significant improvement. Most of the studies, therefore, included its use. See Appendix A-14-III.

With these preliminary factors disposed of, the principal methods of catalyst preparation may be considered. These involved the use of colloidal platinum sols and an auxiliary support, silica.

Part b - Colloidal Pt Catalysts

Most Pt on carbon catalysts previously studied have involved impregnation of a soluble Pt salt on carbon followed by reduction. A possible source of inefficient Pt utilization by this method is the relative inaccessibility of Pt deposited in the smaller pores of the carbon.

This possibility is avoided by adsorption of colloidal Pt onto carbon. Accordingly, Pt colloids prepared by several reduction techniques were examined. Use of sodium citrate, sodium borohydride and formaldehyde as reducing agents resulted in catalysts of relatively low activity (maximum limiting current = 5 ma/cm^2). Reduction with carbon monoxide at room temperature gave a catalyst with comparable performance on butane to the best impregnated catalyst previously obtained (See Table A-4 and Appendix A-15).

Table A-4

Variation of Butane Performance
with Carbon Supported Pt Catalysts

Catalysts	Reduction Method	Utilization, ma/mg @ η = 0.40 volts
Colloidal 6% Pt/C	Formaldehyde	1
" " "	Sodium Citrate	2
" " "	Carbon Monoxide	10
" 6% Pt-5Au/C	" "	7
" 6% Pt-10Ir/C	Borohydride	2
Impregnated " "	"	7(1), 10(2)

(1) Average of 5 Determinations
(2) Best Value

As can be seen from the above table, some loss in activity resulted from the inclusion of gold in the colloidal platinum on carbon catalyst. In compensation, catalyst stability appeared to be enhanced, as indicated by no loss in performance level after a 10 day period of intermittent operation. The straight platinum catalyst began to lose performance after three days. Further improvement may be obtainable by inclusion of other metals, e.g. Ir or Ru, or by inclusion of silica or other minerals in the support (see Part c).

Part c - Modification of Pt Deposition and Supports

Electron microscope studies have shown that platinum on carbon catalysts (both impregnated and colloidal) contain Pt deposited in the form of 25 to 200 Å aggregates. Since activity would be expected to increase with platinum surface area, attempts were made to improve the dispersion of platinum by adsorption of a Pt salt from dilute solution, and by inclusion of a more polar co-support. (For a discussion of the conductivity problem with mineral co-supports, see Phase 7, Part a.) The advantage of adsorption over the usual impregnation technique, in which all of a concentrated solution is soaked up by the powdered support, is that it eliminates the possibility of crystallization of trapped platinum salt during the drying operation. Ammonium chloroplatinate was found to be suitable for these adsorption studies.

An ideal co-support would be alumina, where monolayer Pt has already been achieved. While this material could be satisfactory for methanol in buffer solution, the need for acidic electrolytes in hydrocarbon cells precludes use of alumina as a permanent co-support. Silica was therefore examined. By adsorption of ammonium chloroplatinate (4-5% Pt) on freshly precipitated silicic acid gel (5% on carbon), followed by high temperature reduction, a catalyst was obtained with twice the previous utilization level. See Table A-5.

Table A-5

Effect of Silica on Platinum-on-Carbon Performance (1)

Catalyst	Avg. Performance, ma/mg, @ η = 0.40 volts	No.of Replicates
Adsorbed 4-5% Pt/C-5SiO_2	16	6
Impregnated 6% Pt-10Ir/C	7	5

(1) See Appendix A-15 for complete data.

With the number of replicates run and the known standard deviation, the advantage for the use of silica and its associated variables is certain at a greater than 99.5% confidence level. Other mineral supports and other forms of silica, e.g. layer silicates, are being examined in order to obtain further improvement.

Phase 4 - Electrode Structure Studies

The direct oxidation of liquid decane at 150°C and ambient pressure at rates as high as 140 ma/cm^2 has already been achieved (6). The research studies leading to this level of activity showed the structure of the electrode to be critical even at platinum loadings of 50 mg/cm^2. Therefore a program was undertaken to optimize the structure of the platinum-on-carbon electrodes. This was carried out in conjunction with the catalyst studies of Phase 3.

Part a - Preparation and Testing of Platinum-on-Carbon Electrodes

Several types of platinum-on-carbon preparations were used in these electrode structure studies as listed in Appendix A-16. However, the best in terms of mechanical stability, ease of preparation, and performance were sintered carbon-Teflon electrodes prepared similar to previous sintered platinum-Teflon electrodes (6). These electrodes were tested in half-cells at 150°C in 14.7M phosphoric acid electrolyte. Butane was generally used as the fuel in these initial studies since it has shown appreciable reactivity and the maintenance of the reaction interface on the electrode is less difficult with a vapor fuel than a liquid. The catalyst loading in these carbon-Teflon electrodes was generally less than 5 mg/cm^2, representing a reduction to one-tenth the loading in previous electrodes.

Initial measurements indicated that all of the platinized carbon electrode structures required some activation. Substantial improvements in current capability were obtained by oxygen treatment and polarizing to 0.8 to 0.9 volts relative to saturated calomel. Figure A-7 shows these effects on a carbon-Teflon electrode. The initial butane performance was 7 ma/cm^2 at 0.45 volts polarization. After cathodic operation as an oxygen electrode for 30 minutes, the current doubled to 14 ma/cm^2. Additional oxygen treatments did not give further significant improvements. However, driving the electrode to 0.8 to 0.9 volts vs. saturated calomel and allowing the butane to reduce the surface, produced performance increases. Several similar polarizations during 40 hours of testing increased the current to 40 ma/cm^2.

Figure A-7

Activation of Sintered Carbon-Teflon Electrodes

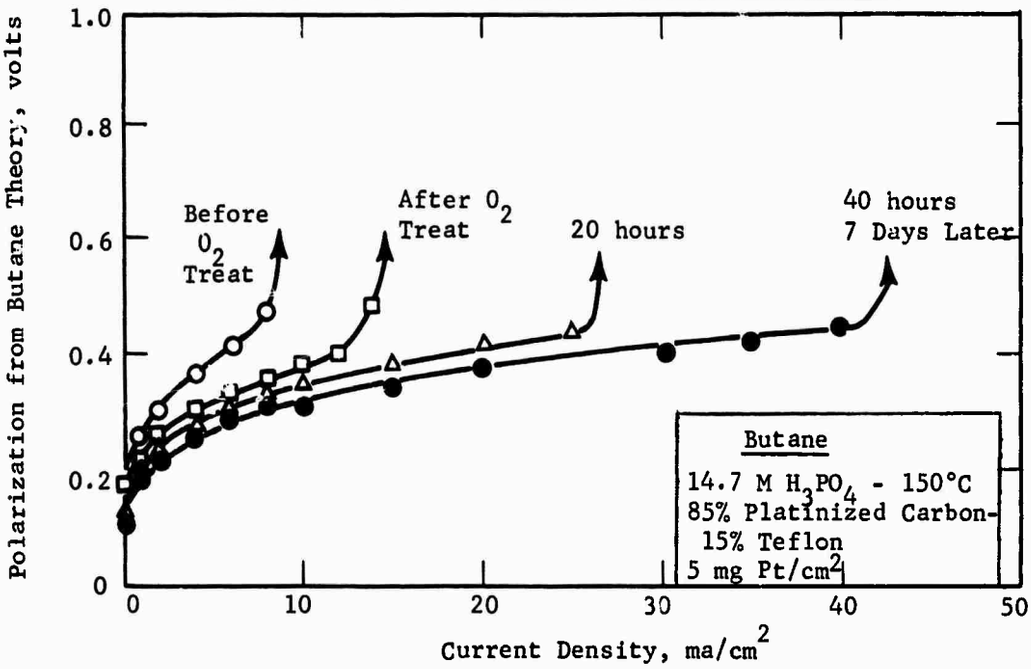

The mechanism of these activations has not been elucidated but it seems possible that they enable activation of the platinum catalyst by alternate oxidation and reduction and/or altering the wetting characteristics of the electrode surface. Reduction in the amount of Teflon and sintering in some electrodes, Appendix A-16, resulted in electrodes which equilibrated more rapidly at their maximum performance.

Once activated, the carbon supported catalysts gave typical performance characteristics as shown in Figure A-8. The Tafel slope of 0.11 and activation energy at limiting current of about 10 kcal/mole agree with the results for unsupported platinum discussed previously (6).

Figure A-8

Activation Energy on Sintered Carbon-Teflon Electrodes

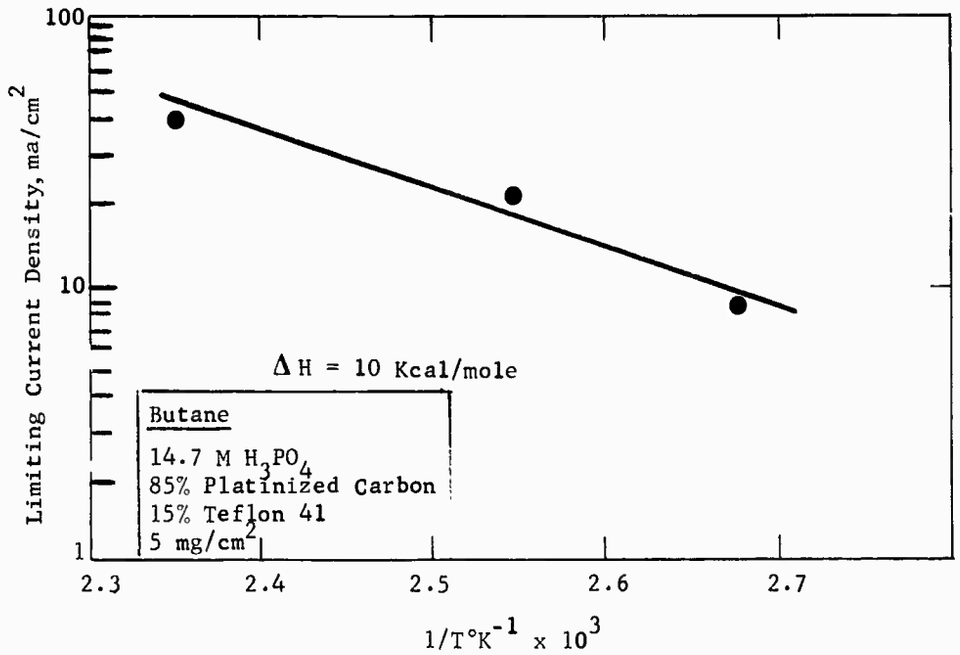

Part b - Electrode Fabrication Modifications

Some studies were made with the sintered carbon-Teflon electrode to determine the effect of the fabrication technique on performance. The variables considered in these tests were Teflon content, sintering pressure, and sintering time. The initial cold press or molding formulation and rate of gelling of the catalyst and Teflon emulsion were kept constant. The results of this preliminary variables study are shown in Table A-6.

Table A-6

Effect of Fabrication on Performance of Sintered Carbon-Teflon Electrodes

Fabrication Variable	Multiplies Current Density by
Sintering Pressure Increase from 1100 to 2200 psi	2.9
Teflon Increase from 15 to 30 wt%	0.14
from 10 to 15 wt%	1.15
Sintering Time from 1 min to 2 min	1.38

Increasing Teflon content from 15 to 30 percent resulted in a seven-fold reduction in current capability, while electrodes with 10% Teflon were only slightly worse than those with 15% Teflon. The optimum Teflon content must therefore be near 15%. Increased sintering pressure resulted in a three-fold increase in current density, while increased sintering time produced only about a forty percent improvement. In subsequent experiments it was found that the 15% Teflon (2200 psi -2 minutes) electrodes gave consistently better performance and these were used for further testing.

Part c - Catalyst Utilization

The sintered carbon-Teflon electrodes were used to evaluate the effect of catalyst loading, catalyst distribution, and electrode thickness on platinum utilization. Butane was used as the fuel in these tests at 150°C in 14.7M phosphoric acid electrolyte. The results of this study are summarized in Appendix A-17, and Figure A-9 shows a plot of current density at 0.45 volts polarization versus catalyst loading for the 3 and 6 wt % platinum-on-carbon preparations.

Figure A-9

Effect of Catalyst Loading - Sintered Carbon-Teflon Electrodes

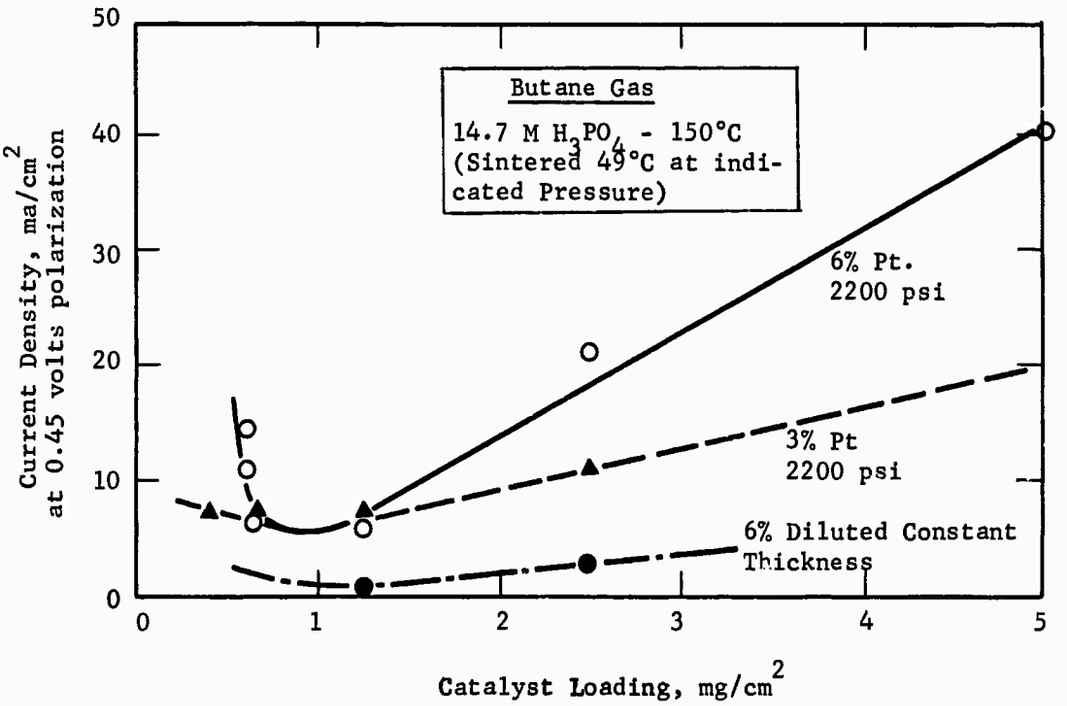

Current density increased with loading between 1 and 5 mg/cm^2, while reduction in the wt % Pt on carbon resulted in a flatter response. Dilution of the 6% platinum on carbon with nonreactive carbon to the 3% level also produced a marked reduction in performance.

At the lower loadings (< 1 mg Pt/cm^2) performance improvements were noted with decreases in platinum content. An analysis of these results indicates that this improved performance was due to a reduction in electrode thickness. The effect of thickness on catalyst utilization is shown in Figure A-10. Utilizations as high as 25 ma/mg of Pt have been obtained with electrodes whose catalyst layer thickness was 0.007 cm. The catalyst layer thickness was calculated from the measured electrode thickness by subtracting the equivalent thickness of the support screen.

Figure A-10

Catalyst Utilization - Sintered Carbon-Teflon Electrodes
(Butane, 14.7 M H_3PO_4 - 150°C)
(15 wt % Teflon)

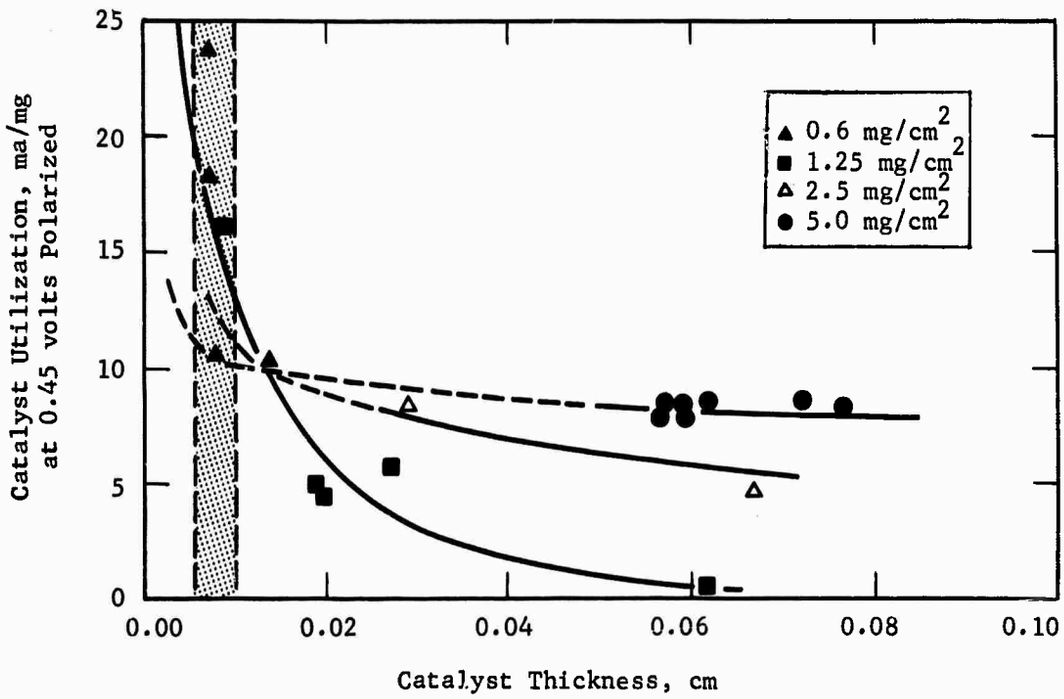

From these data it appears that electrodes with thinner catalyst layers are desirable in improving catalyst utilization. However, as noted in Figure A-10, there is a limit to the thickness reduction possible using our present support screens. Higher platinization levels and alternate physical structures (less than 0.001 cm) will be required to produce the desired levels of performance.

Some preliminary tests with these electrodes on liquid decane were obtained. Test results, shown in Figure A-11, indicate that 16 ma/cm^2 can be drawn at 0.5 volts polarized. This is comparable to the initial sintered platinum-Teflon electrode at a 50 mg/cm^2 loading. Table A-7 summarizes the status of the 5 mg Pt/cm^2 carbon electrode. Even at these initial stages of development, the carbon structure is giving somewhat better catalyst utilization on liquid decane.

Figure A-11

Decane Performance of Sintered Carbon-Teflon Electrodes

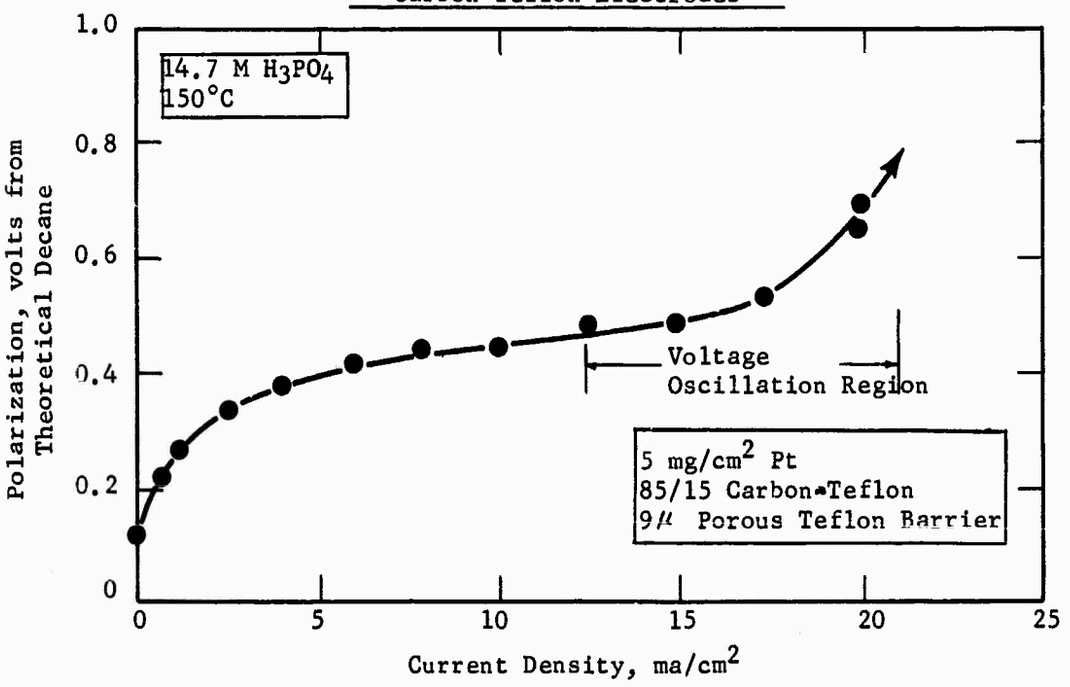

Table A-7

Comparison of Sintered Carbon-Teflon Electrodes and Sintered Platinum-Teflon Electrodes

Electrode	Catalyst Loading, mg/cm^2	Butane Data		Decane Utilization, ma/mg at 0.5 volts Polarized
		Activation Energy, kcal/mole	Pt Utilization, ma/mg, 0.45 Polarized	
Sintered Carbon-Teflon Electrode	5	10	8	3.2
Sintered Platinum-Teflon Electrode	50	12.4	2-8	2.0

Phase 5 - High Surface Area Alloys

Attempts have been made to replace the expensive electrode catalyst, platinum, with alloys of non-noble metals. Alloy compositions have been chosen so as to approach synthetically the d-band configuration and crystal lattice spacings of platinum, to prevent metal corrosion, and to mitigate the excessive oxide formation tendencies of some of the catalytic elements. An additional overall requirement has been set on all the alloys prepared in this program. That is, they must be of high surface area so that they can be readily evaluated for practical use in fuel cell anodes.

Initially, the decision to prepare binary alloys with the Group IB metals as one component of the alloy was made. These elements, copper, silver and gold, have a complete outer d-shell of electrons and one "fluid" electron in the outermost s-shell. This electron should be readily donated to other elements with d-electron deficiencies in alloy systems. With this in mind, particular attention was given to the preparation of alloys from the element iron, with one of Group IB elements, gold. Iron and gold, when alloyed together in an atomic ratio of approximately 1:1, has a calculated d-band vacancy similar to platinum - 0.6 Bohr magnetons. At this same atomic ratio of gold and iron the reported literature lattice spacings approach that of pure platinum.

Alloys of gold-nickel were also studied. It was thought that the catalytically active element nickel could be ennobled by alloying it with gold. The alloyed nickel might be stable to acidic media in which hydrocarbon activity has been found. In caustic medium, nickel is an active fuel cell catalyst only with hydrogen fuel.

The elements tungsten and molybdenum were also of interest as alloys with the Group IB elements. Both tungsten and molybdenum have a very strong tendency to adsorb hydrocarbons. However, the electron donating tendency is so strong that they form stable oxides. By alloying tungsten and molybdenum with gold or the other Group IB elements the strong oxide forming tendencies of the former might be mitigated.

In this phase of the program the alloys were prepared by coprecipitating salts of the desired elements. The metals were then reduced with hydrogen at high temperatures, 700-1000°C. Finally, the alloys were recovered and fabricated into electrodes and evaluated for electrochemical catalytic activity.

Samples of most of the preparations were analyzed by X-ray diffraction to gauge the extent of intermetallic interaction or alloying. Since most of the preparations included gold as a component, it was convenient to follow the change in lattice spacing from pure gold at 4.08Å. With gold as one component in most cases, the other binary metals have been nickel, cobalt, iron, tungsten and molybdenum. Several samples were prepared in which silver was employed as the Group IB donor element. (See Appendix A-18).

Particular attention was given to the preparation of alloys from the element iron for reasons outlined previously. In general it was found that with the above preparation technique only about 20% of the iron interacted with all the gold (see Table A-8) as judged by lattice spacing contraction from pure gold toward pure iron at 3.63Å. In the case of the nickel-gold samples, from the observed lattice spacing for the gold peak, it can be extrapolated that only about ten percent of the transition metal entered into the crystal structure of the noble metal. Cobalt failed to interact with gold, as judged by X-ray diffraction. Both the tungsten and molybdenum alloy preparations were obviously fused and unreduced. X-ray spectra on these materials were both ill-defined.

Table A-8

Summary of Alloy X-ray Data

Metal Composition	Gold Lattice Spacing (A°)	Calculated, % Transition Metal in Alloy
Au	4.08	0
Fe/40 Au	4.00	20
Ni/50 Au	4.05	10

The homogeneous unfused binary metal samples were evaluated for electrochemical catalytic activity. In the case of the Fe/40 Au material it was found that it was possible to draw substantial currents at fairly low polarization with electrodes fabricated from this catalyst. In 3M KOH electrolyte at 98°C with hydrogen as fuel, a current of 100 ma/cm^2 was obtained at a polarization of 0.08 volts. With Co/50 Au as the anode catalyst under the same operating conditions, 50 ma/cm^2 was obtained at a polarization of 0.13 volts. Table A-9 summarizes the runs with both iron and cobalt catalysts.

Table A-9

Activity of Gold Alloys

H_2 Fuel, 98°C, 3M KOH

Catalyst	Polarization (volts) at Indicated Current (ma/cm^2)					
	0	1	10	20	50	100
Fe/40 Au	0.02	0.02	0.03	0.03	0.04	0.08
Co/50 Au	0.02	0.02	0.04	0.12	0.13	--

The nickel-gold samples failed to yield even one ma/cm^2 at a stable potential.

It should be noted that the current obtained from the iron-gold and cobalt-gold electrodes was not reproducible. Poor current densities were obtained when the electrode was run a second time. In addition, it was found that the iron-gold electrode at the end of the run was rust colored. It is definitely possible that the current obtained was derived from the corrosion of the 80% of the iron unalloyed with the noble metal. To determine whether the observed currents were due to catalytic activity or to corrosion, a method for preparing reproducible, completely alloyed materials was sought.

Because of the incomplete metal-metal interactions of the samples, it was felt that reduction temperatures higher than 700°C would be needed to insure more extensive alloying. Higher reduction temperatures are also required to reduce molybdenum and tungsten salts. To attain more elevated reduction temperatures in the neighborhood of 1000°C, a change in furnace was required. The change in furnace also introduced a modification in hydrogen contacting with the unreduced alloy samples. In the lower temperature (below 700°C) work, a tubular reactor through which hydrogen flowed at a high rate was used. In this case intimate contacting of metal and hydrogen was possible. In the higher temperature studies the metal salts were in effect merely blanketed with an atmosphere of hydrogen. It was found in the higher temperature studies that the catalysts were both incompletely reduced and sintered. When a sample of 60 atom % iron, 40 atom % gold was reduced at 700°C under the blanket of hydrogen, an orange-brown looking sample was recovered which gave a positive thiocyanate test for ferric ion (Fe^{+3}) when contacted with water. When the same metal salt composition was treated at 700°C under a constant stream of hydrogen, a black, obviously reduced material was obtained. It thus appears that the more intimate contacting in the tabular reactor is required for successful reductions of the metal salts.

In several recent experiments adjustments have been made so that the temperature range of the tubular furnace has been extended. Even at 800°C the extent of alloying between gold and nickel or cobalt was still very low. These samples were essentially inactive as electrochemical fuel cell catalysts. Although it still may be possible to produce catalytically active alloys by the present coprecipitation-coreduction technique, other avenues for producing high surface area alloys starting with the metals in their reduced state are available. It is upon these approaches that considerable effort will be expended.

Phase 6 - Mixed Perovskites

The good acid corrosion resistance and conductivity of the mixed perovskites, described in the prior report of this series (6), indicated that these compounds offered promise for fuel cell use. However, in no case were both desirable properties incorporated into the same compound. The present studies covered a much wider range of elemental combinations and stoichiometric variations. Their purpose was to determine the compositional factors controlling corrosion and conductivity, and thereby to learn how to tailor these compounds to meet both fuel cell requirements at once.

Part a - Preparational Variables

To review briefly, the stoichiometric mixed perovskites have the formula $AB'_xB''_{1-x}O_3$, where A is a large spacing cation, B' is the catalytic element, and B'' is the acid resistant component. A number of elements have been used in each position as shown in Table A-10.

Table A-10

Elements Included in Perovskites

Position	I	II	III	IV	V	VI	VII	VIII
A	Li, Cs	Ca, Sr, Ba	La, Tl	Pb		Bi		
B'					V	Cr	Mn	Fe, Co, Ni, Ru, Rh, Ir, Pt
B''				Ti, Zr Sn, Hf	V, Nb Ta	Mo W		

Because of chemical differences, the perovskites containing a B'' ion in Group IV were worked on separately and are treated separately in Part d.

With many of the elemental combinations, variations in the stoichiometry or partial substitution (dopings) were made. Emphasis was placed on the incorporation of oxygen deficiencies to improve conductivity, but various combinations of lattice defects were tried, giving the following classes of compounds: stoichiometric, both undoped and doped; oxygen deficient; oxygen and B ion deficient, both undoped and doped; and A ion deficient. (See Appendix A-19 for a complete listing of the compounds prepared.)

The perovskites were prepared by firing pure, dried oxides or carbonates of the metals under various atmospheres at 1100 to 1500°C in zirconia boats in an alundum tube furnace. In the majority of cases the product formulas calculated from weight losses during firing agreed well with the nominal formulas chosen as the bases for preparing the mixtures. However, there were a number of exceptions. With acidic oxides, such as MoO_3, premature CO_2 release occurred. Easily oxidized metals such as Fe, Mn and Cr, when fired under nitrogen, appeared to be oxidized to

higher valence states by the CO_2 released from the carbonates. Copper, lead and silver compounds showed excessive weight losses due to reduction or volatilization. In all these cases only the nominal formula could be used to characterize the materials.

Perovskites with B" ions of Groups V and VI are discussed below in Parts b and c. Perovskites of Group IV are considered separately in Part d for reasons given in that section.

Part b - Acid Resistance

Acid corrosion data on perovskites containing nickel, cobalt, iron, manganese, copper and silver were obtained at 86°C with either 3.7M H_2SO_4 or with this acid containing a known concentration of the metal under study. The amount of catalytic metal lost from the perovskite was determined by analyzing the supernatant fluid polarographically. Appendix A-20 gives the detailed data. See reference (6) for the general experimental details and Appendix A-21 for the polarographic methods for managanese, copper and silver.

Stoichiometric perovskites containing Groups V and VI cations in the B" positions generally showed good corrosion resistance with a major portion of the B' cation being retained by the solid after at least one hundred test hours. Group V B" cations (Nb, Ta) generally gave more corrosion-resistant structures than the Group VI ones (Mo, W). Structures containing Group IV B" cations (Ti, Zr, Hf) had relatively poor acid resistance. See Part (d). Table A-11 gives typical data for nickel and cobalt compounds. Both strontium and barium compounds are included, as these proved to be about equal on the overall average.

Table A-11

Acid Resistance of Stoichiometric Nickel and Cobalt Perovskites

B'-Ion	B"-Ion	B"-Ion Group	Percent Metal Retained	Hours on Test(1) (86°C)
Ni	Ta	V	77-82(2)	240
Ni	W	VI	54	150
Co	Ta	V	79	195
Co	Mo	VI	34	190

(1) With 3.7 M H_2SO_4

(2) Range for three different preparations

Considering the catalytic metal ions, nickel gave more stable compounds than cobalt. Ferrous compounds appeared to be more stable than ferric ones. On the other hand, tetravalent manganese(Mn^{IV}) was more stable than bivalent manganese (Mn^{II}). Copper in a tantalum-based compound has good acid resistance (See Table A-12).

Table A-12

Acid Resistance of Stoichiometric Strontium Perovskites

B'-Ion	B''-Ion	Percent Metal Retained	Hours on Test
Ni	Ta	80 (avg)	240
Co_{II}	Ta	79	195
Fe_{III}	Ta	82	310
Fe_{II}	Ta	60	310
Mn_{IV}	Ta	40	125
Mn	Ti	95	125
Cu	Ta	80	150

Introduction of any type of non-stoichiometry greatly decreases acid resistance. Typical data are given in Table A-13.

Table A-13

Acid Resistance of Non-Stoichiometric Perovskites

Nominal Formula	Type of Ion Deficiency	Percent Metal Retained	Hours[1] on Test (86°C)
$SrNi_{0.33}^{II}Ta_{0.67}O_3$	None	80 (avg)	240
$Sr_{0.8}Ni_{0.33}^{II}Ta_{0.67}O_{2.80}$	A-ion	26	180
$SrNi_{0.75}^{II}Ta_{0.25}O_{2.38}$	O^{-2}-ion	22	180
$SrNi_{0.675}^{II}Ta_{0.25}O_{2.30}$	O^{-2}-ion; B'-ion	27	180

Nickel perovskites achieved good corrosion resistance apparently by equilibrating with nickel ions in the corroding solution. When partially depleted of nickel, most nickel-containing perovskites re absorbed nickel ion when the concentration of the latter in the acid phase was increased. The stoichiometric compounds showed this effect at nickel concentrations of 0.02-0.05 moles/liter, whereas higher concentrations (0.06-0.10 moles/liter) were necessary for the non-stoichiometric ones. The effect was not exhibited by cobalt and iron perovskites, even at quite high acid-phase ion concentrations (Table A-14).

Table A-14

Re-absorption of Metal Ions from Enriched Corroding Solutions

Nominal Formula	Period	B'^{+2} Concentration in Acid(moles/liter)		B' in Solid (% of original)	
		At Start	At End	At Start	At End
$SrNi^{II}_{0.33}Ta_{0.67}O_3$	7	0.0168	0.0148	75	79
	8	0.0284	0.0239	79	88
	11	0.0489	0.0461	95	101
$SrNi^{II}_{0.75}Ta_{0.25}O_{2.38}$	5	0.0703	0.0567	11	35
	6	0.0956	0.0819	35	60
$SrCo_{0.5}M_{0.5}O_3$	3	0.0319	0.0318	14	14.5
	6	0.0837	0.0881	11	10

However, high initial concentrations of cobalt ion in the acid did retard the rate of dissolution of this metal from stoichiometric perovskites (See Table A-15).

Table A-15

Comparison of Corrosion of Cobalt Perovskites by H_2SO_4-$CoSO_4$ Mixture

Nominal Formula	Corrosion with H_2SO_4 (1)		Corrosion with H_2SO_4-$CoSO_4$ (2)	
	Test Time(Hrs)	Percent Metal Retained	Test Time(Hrs)	Percent Metal Retained
$BaCo_{0.05}Mo_{0.5}O_3$	28	51	24	77
	210	39	265	67
			570	47
$SrCo_{0.5}Mo_{0.5}O_3$	28	39	24	51
	210	10	265	54
			570	42

(1) 3.7 M H_2SO_4
(2) 2.9 M H_2SO_4 - 0.8 M $CoSO_4$

Several non-stoichiometric cobalt-molybdenum and tantalum perovskites having conductivities in the range of interest for electrode fabrication ($>10^{-4}$ mho/cm) were tested with acid containing large amounts of cobalt. Unfortunately, this technique did not prevent virtually complete loss of the cobalt from these compounds (See Table A-16).

Table A-16

Corrosion of non-Stoichiometric Cobalt Perovskites by H_2SO_4-$CoSO_4$ Mixture

Nominal Formula	Conductivity ($ohm^{-1}cm^{-1}$)	Percent Cobalt Retained After Test Hours (1)			
		24	97	240	545
$SrCo^{II}_{0.75}Ta_{0.25}O_{2.38}$	3.8×10^{-4}	34	27	7	0
$SrCo^{II}_{0.9}Ta_{0.1}O_{2.15}$	2.9×10^{-3}	20	12	4	--
$SrCo^{II}_{0.67}Mo_{0.33}O_{2.66}$	1.6×10^{-4}	--	--	35	22
$SrCo^{II}_{0.75}Mo_{0.25}O_{2.50}$	2.2×10^{-2}	44	27	26	0
$SrCo^{II}_{0.675}Mo_{0.25}O_{2.43}$	3.3×10^{-2}	9	12	8	--

(1) 0.8 M $CoSO_4$ in 2.9 M H_2SO_4 at 86°C

Similarly, non-stoichiometric ferrous or ferric perovskites were not stable to acid.

To summarize, in general stoichiometric compounds are quite acid resistant. The corrosion of nickel perovskites can be stopped by equilibration with nickel salts added to the electrolyte. Cobalt compounds are stabilized considerably by adding large amounts of cobalt salts initially. When oxygen deficiencies are incorporated into the lattice, the corrosion of nickel compounds may still be stopped by equilibration, but cobalt cannot be held. Complete data on the other ions is not available yet but Mn^{IV} at least appears very promising from the corrosion standpoint. It appears overall that stoichiometric perovskites are the best prospect for the achievement of acid resistance.

Part c - Conductivities

A target conductivity of 10^{-4} mhos/cm was set, on the assumption that the particles could be ground down to one micron size and mixed with a conductive support, carbon, for electrode preparation. Essentially all of the stoichiometric perovskites showed conductivities of 10^{-7} to 10^{-11}. Furthermore doping of the stoichiometric compounds by substituting Li or La for ten percent of the A or B' ion did not help. Firing in air rather than under nitrogen also produced little improvement.

However, the introduction of oxygen deficiencies either alone or in combination with B ion deficiencies generally increased conductivity markedly. Target conductivities were reached with Cr, Mn, Fe and Co. However, perovskites containing nickel, which is of greatest interest because of its known catalytic properties, could not be improved by this means. (Table A-17)

Table A-17

Highest Conductivities Attained by Introduction on Non-Stoichiometry

B'-Ion	B" Ions Studied	Highest Conductivity mhos/cm
Cr	Ta, W	10^{-4}
Mn	Ta, W	10^{-3}
$Fe^{(II,III)}$	Ta, Mo, W	10^{-2}
Co^{II}	Ta, Mo, W	10^{-2}-10^{-3}
Ni	V, Nb, Ta, Mo, W	10^{-7}
Cu	Ta, Mo, W	10^{-5}
Ag	Ta	10^{-8}

A special effort was made to improve the conductivity of the nickel perovskites. The A ions Ca, Sr, Ba and Pb were tried with the B" ions Ta, Nb, V, W, and Mo in oxygen deficient structures both with and without added B ion deficiencies, all to no avail. However, doping with lanthanum, one of a number of dopants tried, definitely improved the conductivity of non-stoichiometric Sr-Ni-Ta compositions. Furthermore also in contrast with the stoichiometric oxides, the firing atmosphere proved to have an important effect, with an air atmosphere generally giving an order of magnitude improvement over a nitrogen atmosphere (Table A-18).

Table A-18

Effect of Doping and Firing Atmosphere on $SrNi_{0.675}Ta_{0.25}O_{2.30}$ Compositions

Added Ion	Replacing % of:		Conductivity (mhos/cm) when fired in: Nitrogen	Air
None	----------		$7.7 \cdot 10^{-8}$	$4.1 \cdot 10^{-6}$
La	10	Sr	$2.1 \cdot 10^{-6}$	$3.4 \cdot 10^{-5}$
La	50	Sr	$6.6 \cdot 10^{-4}$	$6.2 \cdot 10^{-3}$
La	10	Ni	$4.6 \cdot 10^{-7}$	$3.6 \cdot 10^{-5}$
Cs	10	Sr	$6.9 \cdot 10^{-7}$	$4.0 \cdot 10^{-6}$

The effect of air firing on the conductivity of oxygen deficient pervoskites appeared to be a very important lead. However, it was later discovered that conductivity arising from oxygen deficiency is extremely sensitive to acid. Conductivities are reduced to the level of the stoichmetric compounds when only a fraction of the material is corroded. (See Table A-19, and Appendix A-22 for details)

Table A-19

Effect of Acid Treatment on Conductivities of Non-Stoichiometric Perovskites

Nominal Formula	% B'-Ion Extracted	Conductivity	
		Before Acid Treatment	After Acid Treatment
$SrCo^{II}_{0.75}Mo_{0.25}O_{2.50}$	69.7	3.8×10^{-3}	2.6×10^{-12}
$SrCo^{II}_{0.6}Mo_{0.25}O_{2.35}$	58.0(1)	2.9×10^{-2}	1.9×10^{-10}
$BaNi^{II}_{0.75}Ta_{0.25}O_{2.38}$	51.3	2.8×10^{-7}	2.7×10^{-10}
$Sr(Ni^{II}_{0.61}La_{0.068})Ta_{0.25}O_{2.34}$(2)	36.3	3.6×10^{-5}	4.4×10^{-9}

(1) Value probably low
(2) Fired under air; others fired under nitrogen

The better conducting non-stoichiometric materials show definite gas evolution during the early stages of acid treatment. The stoichiometric ones do not show gas evolution and neither do they show much of a conductivity loss on acid treatment. The nature of the gas has not been determined, but by analogy with the high valence cobalt compounds in reference (6), the gas may be oxygen.

This result indicates that the non-stoichiometric perovskites may be acquiring their conductivity in the same way that lithiated nickel oxide does. Incorportion of Li_2O into the 1:1 NiO lattice leaves oxygen deficiencies. At high temperatures the crystals pick up molecular oxygen in an attempt to restore stoichiometry. The oxygen goes into the lattice as oxide ions, the electrons required being extracted from the crystal's valence bands leaving "holes" or Ni^{+3} ions. The movement of the holes accounts for the increased conductivity. This may be a satisfactory means of incorporating conductivity into perovskites, but apparently Ni^{+3}, Co^{+3}, or Co^{+4} are too powerful as oxidants to be stable in aqueous acid. They apparently react to form oxygen, losing their "holes" and their conductivity. It appears that near stoichiometric compounds are required having mixed valence states which are stable to acid. Di- and tetra-valent manganese and tungsten^{+4} and $^{+6}$, which show acid stability in the tungsten "bronzes", may be suitable.

Part d - Group IV Perovskites

Perovskites based on the Group IV elements, (Ti, Zr, Hf) along with Ba or Sr as the A ion are being considered separately, since they cannot be classified along with the Group V and VI compounds for two reasons. Firstly, the catalytic metal, Cr, Mn, Fe, or Co must be in the tetravalent state. Secondly, there is no "stoichiometric" value of x, and compositions were fired in which x varied from 0.1 to 0.75. A series of Group IV-based perovskites have also been prepared in which the A ion was trivalent La. In these compounds the catalytic ions were divalent Mn, Fe, Co, Ni and Cu and x was 0.5. It was thought that the incorporation of these metals into the perovskite lattice in their divalent states would render the perovskites more stable to acid.

X-ray powder patterns were obtained on most of the fired materials and used as a criterion of completeness of the reaction and confirmation of the perovskite structure. The homogeneity of the product was found to be effected by the composition and the firing conditions. Materials with the composition $AB'_{0.33}B''_{0.67}O_3$ had X-ray patterns fitting the pseudo-cubic perovskite structure, while compositions with different B'/B'' ratios did not always yield a product of single phase. In those cases where B' was Fe, and also those where the A ion was La, the only compositions fired had the B'/B'' ratio equal to unity and these were found to show the typical perovskite X-ray pattern. The firing conditions, i.e., atmosphere, temperature and time, were found to influence the homogeneity of the product and had to be ascertained for the various types of perovskites. The perovskites of composition $LaB'_{0.5}B''_{0.5}O_3$ were especially sensitive to firing conditions and it was found that, generally, homogeneous phases were more likely for firings in air, at longer times, at higher temperature (within the range 1100-1250°C), and with periodic regrinding of the material during the firing procedure. The X-ray data are presented in Appendix A-23.

The electrical conductivities of the Group IV based perovskites showed a wide range of values, varying over a range of ten orders of magnitude. The target conductivity value (10^{-4}mhos/cm) has been achieved in the Co and Fe containing perovskites. Those perovskites containing Mn or Ni had better conductivities when La was the A ion rather than Sr or Ba and in this case Ni containing compounds reached the target value. In those Group IV perovskites containing Sr or Ba the conductivities have been found to be controlled by the catalytic ion, whereas, the B'' ion exhibits a negligible effect. The conductivity order is Co > Fe>> Mn. Increasing the B'/B'' ratio also favors the conductivity of these compounds; that is, the greater the amount of catalytic element the greater the conductivity.

The acid resistance of the Group IV based perovskites is quite poor with the notable exception of those containing Mn as the catalytic element. Perovskites containing tetravalent cobalt and iron show complete dissolution of these metals after about 24 hours in 3.7 M H_2SO_4 at 86°C. Also, they show no tendency to reabsorb the respective metal ion when the concentration of the metal in solution is increased. The increased acid stability of the manganese compounds compared to the cobalt or iron perovskites is probably a reflection of the greater stability of the tetravalent state for Mn. Lanthanum containing compounds also showed very poor acid stability where the catalytic elements were divalent Fe, Co, Ni and Cu.

Although the perovskites did not exhibit satisfactory acid resistance for use as electrodes in acid electrolytes, a number of them were tested for activity with H_2 and O_2 in alkali in order to get some indication as to whether the perovskites possessed electrochemical activity. Due to the relatively low conductivity of the perovskites, electrodes contained carbon as the conducting support. Carbon is known to possess catalytic activity for O_2 but is not active for H_2.

All tests were carried out in 3 M KOH at 100°C. The results of evaluations of perovskites for oxygen activity are presented in Appendix A-24.

The perovskites have shown no appreciable electrochemical activity as oxygen electrodes. In no case was the activity of perovskites greater than

that of a blank electrode containing carbon, a known oxygen catalyst. However, perovskite on carbon electrodes have shown ability to retard the deactivation of carbon by overpolarization. The carbon support material could sustain currents of greater than 200ma/cm^2. However, when allowed to polarize beyond the limiting current, to 0.8 volt versus the reversible oxygen potential, the carbon electrodes lost most of their activity. When the perovskites were included, the effects of overpolarization were much less severe, possibly due to some wetting effect of the hydrophilic oxides. The effects of overpolarization on a perovskite and carbon blank electrode are shown in Table A-20.

Table A-20

Perovskite Stabilization of Carbon Electrodes
3 M KOH, 100°C

Electrode	Polarization From Oxygen Theory At Indicated ma/cm^2, volts					
	1	5	10	50	100	300
Carbon Blank,(1) Run 1	0.395	0.400	0.445	0.490	0.520	0.580
Carbon Blank,(1) Run 3	0.420	0.660	--	--	--	--
$SnFe^{IV}_{0.5}H_{0.5}O_3$(2) Run 2	0.410	0.450	0.465	0.515	0.550	0.640
$SnFe^{IV}_{0.5}H_{0.5}O_3$(2) Run 3	0.410	0.460	0.490	0.640	--	--

(1) 50 wt % Carbon
(2) 25 wt % Carbon, 25 wt % Perovskite

The perovskite electrodes tabulated in Appendix A-24 were also tested for activity for hydrogen. They showed no activity other than that attributable to the carbon, being 0.6 to 0.7 volts polarized at open circuit.

Thus, in summary, the Group IV based perovskites have sufficient electrical conductivities but the acid resistance is not satisfactory and they have shown no electrochemical activity for either hydrogen or oxygen in alkali.

Phase 7 - Transition Metal Complexes and Redox Catalysts

A number of metal complexes have been examined as anode catalysts in the hope that bonding with a ligand might provide unusual redox or adsorption properties. These included cyano complexes, cyclopentadienyl complexes and uranium oxy complexes.

Part a - Cyano Complexes

Cyano complexes of transition metals meet several requirements of a potential hydrocarbon fuel cell catalyst:

- Stability and insolubility in acid for a large number of complexes.
- Reversible redox couple--large range of E_o's available.
- Rapid transfer of electrons between reduced and oxidized forms.
- Presence of d-band vacancies.

With regard to the conductivity requirement, enhancement of conductivity is possible by use of charge transfer complexes e.g. cupric ferrocyanide or thallium (I) ferricyanide(11). This conductivity problem may be further lessened by preparation of the catalyst as a thin film on a conductive support such as carbon. According to W. A. Weyl (12), a film of an insulator of less than 100 Å thickness acts as a semiconductor, allowing the passage of electrons.

Because of their ready availability and high stability, the ferro- and ferricyanides were initially chosen for examination: $Fe(CN)_6^{-4} \leftrightarrow Fe(CN)_6^{-3} + e$, $E_o = -0.48$. Methanol was chosen as a fuel for screening tests, since electrode structure problems are minimized thereby. Most of the insoluble complexes examined were prepared by impregnation of a soluble complex, e.g. potassium ferrocyanide, on carbon, formulation into a flag electrode and then immersion of the electrode into a solution containing a transition metal cation, e.g. Cu^{++}. The impregnated soluble salts were also evaluated as catalysts. None of the compounds showed activity on carbon alone. See Appendix A-25. When examined as cocatalysts with Pt the best result was obtained with cupric ferrocyanide, which gave the same limiting current and Tafel slope as Pt alone, but with increased polarization of 0.3 volts throughout.

Similarly, the prussides (pentacyanoaquoferrate (II)) were examined as cocatalysts with Pt.

$$Fe(CN)_5 (H_2O)^{-3} \leftrightarrow Fe(CN)_5 (H_2O)^{-2} + e, \quad E_o = -0.49$$

Possible advantages of this system are:

- The readily replaceable H_2O group which favors fuel chemisorption.
- The known oxidizing ability of the pentacyanoaquoferrate (III) form for methanol (13).

However, as before, there was an extra polarization above that of platinum itself of about 0.35 volts. It is concluded that an unfavorable E_o for electrochemical conversion of the Fe (II) to Fe (III) form is responsible for this additional polarization, a consequence of the greater stability of the Fe (II) form. Choice of complexes where the oxidized form has higher stability, e.g. the cobalticyanide system, may result in lowering of the polarization normally obtained with platinum.

Part b - Cyclopentadienyl Systems

Because the cyclopentadienyl complexes of many of the transition metals have properties similar to the cyano complexes, the former were also screened for catalytic activity. The complexes such as dicyclopentadienyl iron (ferrocene), (a) below, and cyclopentadienyl-molybdenum tricarbonyl dimer, (b) below, were all impregnated onto activated carbon or onto 6% Pt

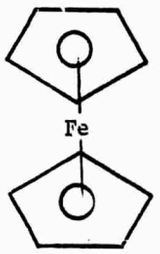

(a)

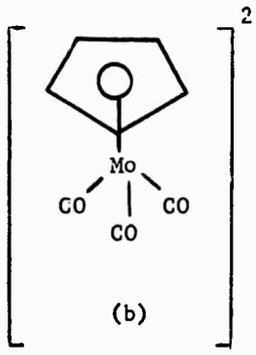

(b)

on carbon. Sintered Teflon emulsion electrodes were prepared from the complex samples and evaluated mainly in 3 M KOH at 97°C with hydrogen as fuel. In all cases the cyclopentadienyl complexes listed in Table A-21 failed to act as catalysts. It was not possible to draw even 1 ma/cm^2 from electrodes prepared from these materials.

Table A-21

Cyclopentadienyl Complexes Tested

Compound	Formula
Dicyclopentadienyl iron	C_5H_5-Fe-C_5H_5
Dicyclopentadienyl nickel	C_5H_5-Ni-C_5H_5
Dicyclopentadienyl cobalt	C_5H_5-Co-C_5H_5
Acetylferrocene	CH_3-CO-C_5H_5-Fe-C_5H_5
Chloromercuri-ferrocene	Cl-C_5H_5-Fe-C_5H_5
Cyclopentadienyl-iron dicarbonyl dimer	$(C_5H_5$-Fe-$(CO)_2)_2$
Cyclopentadienyl-molybdenum tricarbonyl dimer	$(C_5H_5$-Mo-$(CO)_3)_2$

These complexes also wiped out the catalytic activity of platinum when impregnated onto carbon containing 6% platinum. The total lack of activity from the complexes may be a manifestation of their very low conductivity (about 10^{-11} - 10^{-12} mhos/cm). No further work is planned with these complexes, unless compounds of this type with more interesting electronic properties are uncovered in the literature.

Part c - Studies on the Uranyl Redox System

Uranyl compounds were of interest as possible heterogeneous redox catalysts involving U (IV) and/or U (V)$\rightleftharpoons$U (VI):

$$UO_2^{+} \rightleftharpoons UO_2^{++} + e \ (1M\ H^{+}), \quad E_o = -0.063 \text{ volts}$$

$$U^{++} + 2H_2O \rightleftharpoons UO_2^{++} + 4H^{+} + 2e, \quad E_o = -0.334 \text{ volts}$$

It was determined that the uranyl acid phosphate, UO_2HPO_4, was insoluble in a NaH_2PO_4/H_3PO_4 buffer (pH~2), but dissolved in more acidic solutions. However, using this acidic buffer electrolyte with an active platinum catalyst, a limiting current of only 0.5 ma/cm^2 was obtained on butane at 100°C. Therefore, for a more valid evaluation of the potential value of the uranyl system, methanol was used as a fuel. With a flag electrode (4 cm^2) containing 10% UO_2HPO_4 on carbon, a limiting current of 8 ma was obtained despite the fact that due to mechanical problems ~90% of the catalyst had fallen off the electrode at the beginning of the run. See Appendix A-25. Estimated limiting performance accordingly was 10 ma/mg of UO_2HPO_4 or 15 ma/mg based on uranium content, which appears to be quite promising.

The uranyl system may be adaptable to a more acidic electrolyte for hydrocarbon catalysis in the form of an acid-insoluble complex. The uranyl ferrocyanide complex was considered, but it undergoes reaction with both sulfuric and phosphoric acids.

An additional experiment was carried out to determine whether molybdic oxide could function as a redox catalyst with decane. Decane vapor was passed over MoO_3 at temperatures up to 450°C, in the hope that the conductive MoO_2 would be formed. However, no reaction occurred as evidenced by lack of CO_2 formation and lack of any change in the X-ray diffraction pattern of the MoO_3.

4.2 Task B, Hydrocarbon Fuel Cell

While electrode catalysis and structure research to reduce catalyst cost have been emphasized, some engineering research studies have been initiated in more compact total cells to assess problems in liquid hydrocarbon-air fuel cell operation. These tests were made with the best present anodes, sintered platinum-Teflon electrodes with 50 mg/cm^2 of catalyst. The results of these tests were used in designing a hydrocarbon test facility. Construction of the new test equipment has been initiated.

Phase 1 - Studies in Hydrocarbon Fuel Cells

Performances with liquid decane and oxygen in total cells were determined to explore possible interactions and other operating problems. These tests were made in more compact 10 cm diameter glass cells as a preliminary to design of cells for more extensive engineering evaluations. These glass cells were similar to previous cells (6) except that the interelectrode space was reduced from 7 cm to 1 cm and the active electrode surface area was increased from 6.5 cm^2 to 63 cm^2. The sintered platinum-Teflon anode included a 9 micron thick, porous Teflon barrier on the fuel side as described previously (6). The cathode was also a sintered platinum-Teflon electrode.

The performance of the cell compared favorably with previous performances in smaller cells as shown in Figure B-1. Peak power, excluding ohmic resistive losses, was 21 mw/cm^2 at 0.3 volts at 150°C in 14.7 M phosphoric acid.

Figure B-1

IR-Free Performance of Decane-Oxygen Cell

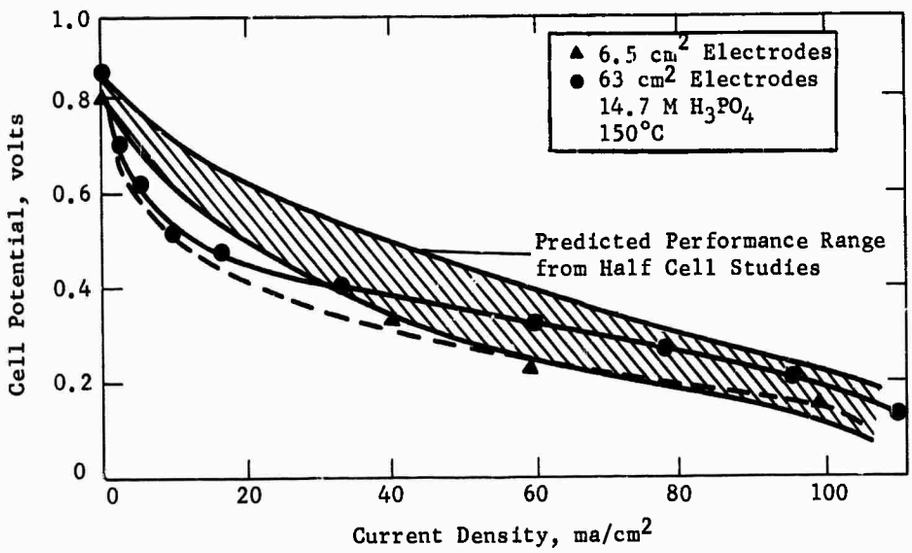

These tests also showed that separation of the porous Teflon barrier from the anode is still a problem. After 3 days of testing with temperature varying between 25°C and 150°C, the barrier pulled away from the anode and fuel flooding resulted. Performance decreased to 0.14 volts at 80 ma/cm^2. Other aspects of scale-up of the electrodes in this more compact cell appeared satisfactory.

One operating problem in these tests resulted from the accumulation of decane in the interelectrode space. This apparently resulted from transport of decane through the anode. This occurred at open circuit as well as under load. Since the solubility of decane in the electrolyte is low, the mechanism of this transport is not clear. Considerable gas evolution was noticed from the anode surface in this space and an immiscible decane layer formed on top of the electrolyte. Thus, the transport might involve vaporization of the fuel in the electrode, followed by recondensation and accumulation in the interelectrode space. The promotion of the vaporization of decane in the electrode due to the hydrophobicity of the surface is described in Appendix B-1.

Phase 2 - Hydrocarbon Cell Design

As a result of the work discussed in Phase 1, a hydrocarbon total cell test facility was designed. A schematic of this facility is shown in Figure B-2. The fuel transport problem described in Phase 1 has been considered in the design of the cell in two ways. The interelectrode space has been provided to permit adequate disengagement of the hydrocarbon from the electrolyte and a recycle system for recirculating the fuel to the anode has been provided. In addition, overly porous cathodes must be avoided to prevent excessive contacting of the hydrocarbon and oxygen at the catalytic surface of the cathode.

It is anticipated that these cells, as designed, can be constructed of Teflon. However, other suitable structural materials are desirable, particularly at temperatures above 150°C. Ceramic filled Teflons offer potential improvements in mechanical stability and chemical inertness. One such material, Rulon(1), has been tested and gave encouraging results. Samples of Rulon gave no evidence of creep or other dimensional changes after one week of continuous exposure to 14.7 M phosphoric acid at 150°C. In addition, after 24 hours at 250 to 260°C in pyrophosphoric acid, the samples were unchanged. No weight gain was detectable in either test.

Further tests of structural materials are planned and construction of the hydrocarbon cell test facility has been initiated.

(1) Commercially available from the Dixon Corporation, Bristol, Rhode Island.

Figure B-2

Schematic of Hydrocarbon Total Cell Test Facility

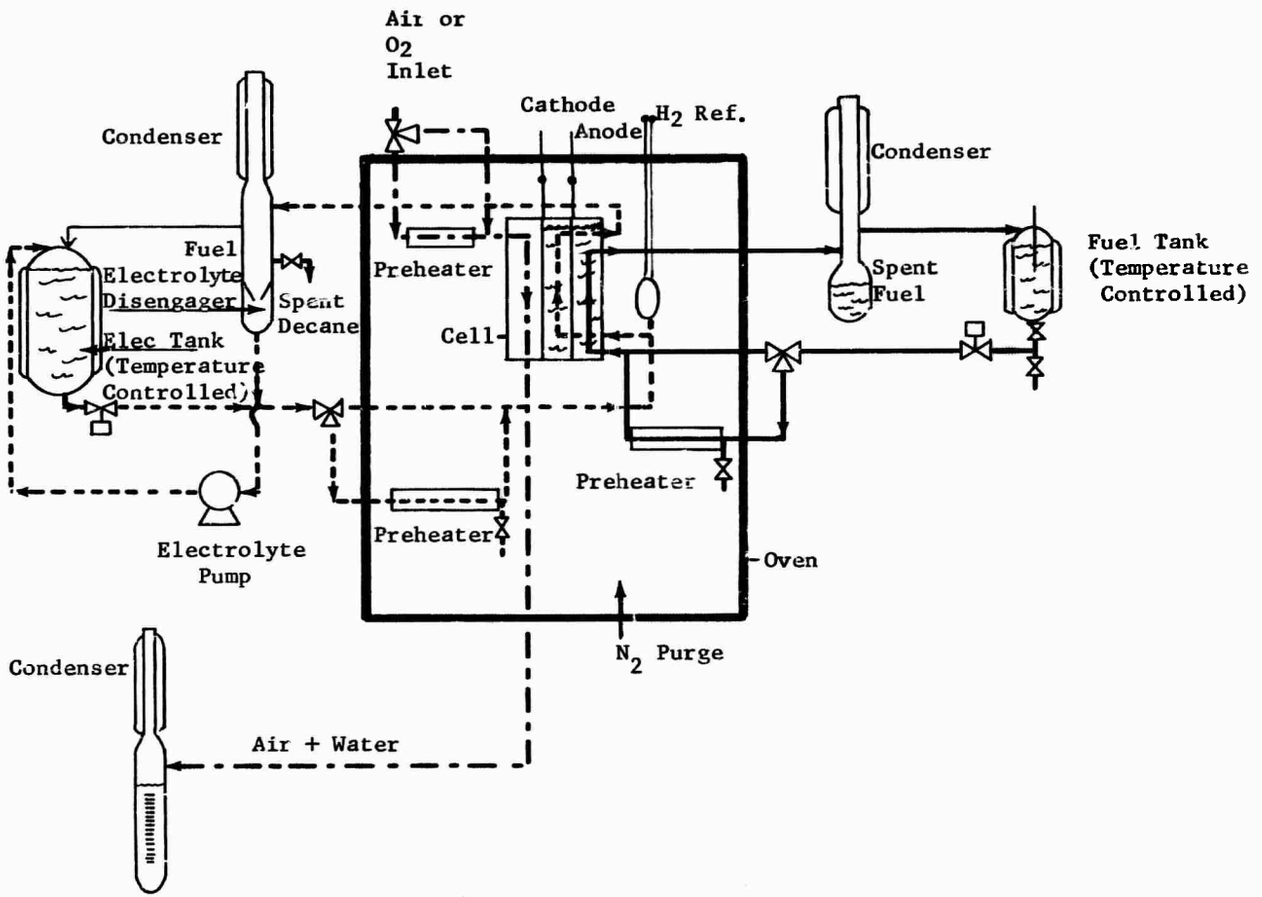

4.3 Task C, New Systems

Studies in the New Systems area have continued to stress those investigations falling outside conventional fuel cell approaches. Previous investigations have examined buffer electrolytes, electrode structures and catalysts for these electrolytes, and dynamic electrodes, among other topics. These areas have been further examined, as well as a new intermediate temperature electrolyte, pyrophosphoric acid.

Phase 1 - Pyrophosphoric Acid Electrolytes

One approach which can be used to increase the utilization of platinum catalyst is operation at higher temperatures. Results from butane adsorption studies have indicated that a performance level of 100 ma/cm^2 at 0.3 volts polarization might be reached with only 0.5 mg/cm^2 of catalyst in the vicinity of 300°C (6). This temperature region is beyond the limit of aqueous electrolytes but below the area in which molten oxide-carbonate systems operate. In order to test catalyst utilization in this region, it is necessary to find a suitable electrolyte. One candidate for this purpose is pyrophosphoric acid, which is liquid between 60 and 427°C, and is thermally stable. Several other requirements must be met by any electrolyte however, and so the conductivity and buffering capacity of this acid were first determined. Performance tests with hydrocarbons, oxygen, and air were also run.

Part a - Conductivity of Pyrophosphoric Acid

Solid pyrophosphoric acid is composed of the pure phase $H_4P_2O_7$. Upon melting, it converts to a complex equilibrium mixture of various acids ranging from ortho- and pyro- to penta- and even higher molecular weight phosphoric acids. Since little free water is present, self-dissociation is required to produce electrolytic conductivity. Measurements were made in a standard conductivity cell with an AC bridge over the range of 100 to 250°C. No differences were observed between the values obtained at 60 or 1000 cps. Figure C-1 illustrates the results, with the specific resistance falling from 15 ohm cm at 100°C to about 2.5 at 250°C. For comparison, 3.7 M sulfuric acid at 25°C has a specific resistance of about 1.3 ohm cm. It appears then that in the temperature region of interest, pyrophosphoric acid is sufficiently conductive for fuel cell use.

Figure B-2

Schematic of Hydrocarbon Total Cell Test Facility

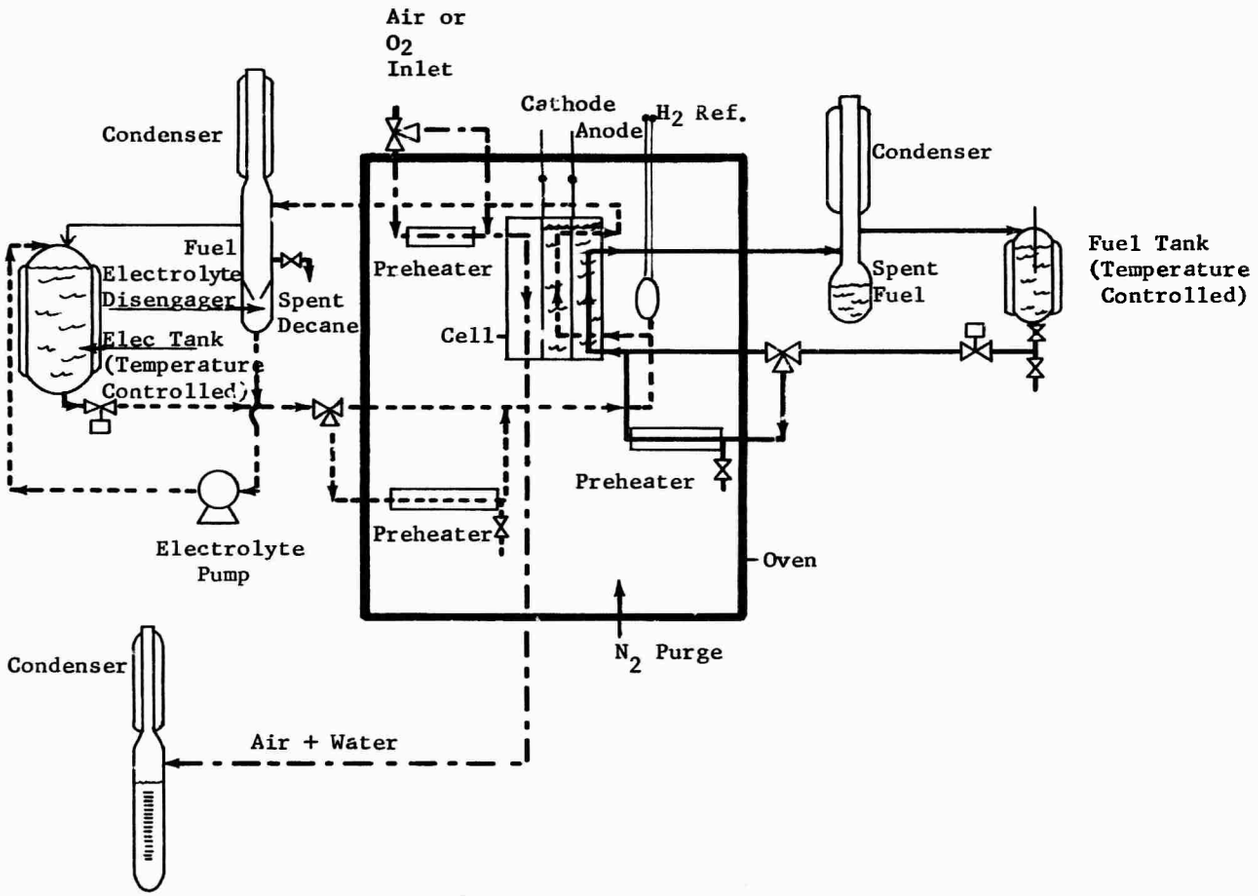

Figure C-1

Conductance of Pyrophosphoric Acid

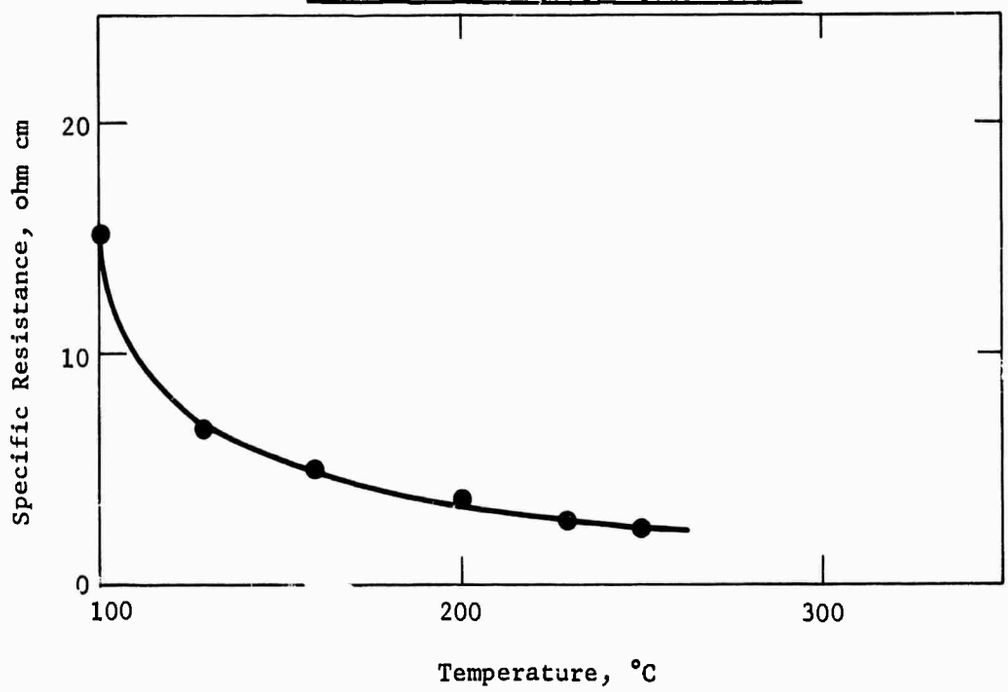

Part b - Buffer Behavior of Pyrophosphoric Acid

The ability of pyrophosphoric acid to minimize ionic concentration polarization at fuel cell electrodes was tested at 200 to 250°C. At the anode, hydrogen, which would be expected to exhibit no activation polarization, was reacted on a sintered platinum-Teflon electrode. No polarization was measured at current densities up to 1000 ma/cm^2. Cathodic ionic concentration polarization was measured by evolving hydrogen from the platinum-Teflon structure. As at the anode, no polarization was found at up to 1000 ma/cm^2. These results indicate that in pyrophosphoric acid at over 200°C there is essentially no ionic concentration polarization at either electrode with this relatively non-porous structure. In view of this behavior, it is not expected that much additional polarization would be encountered even with more porous electrode structures.

Part c - Effect of Water Vapor on Hydrocarbon Performance

Tests of hydrocarbon activity in pyrophosphoric acid were carried out, primarily with butane at 250°C. A few tests were also run with other fuels, and at other temperatures. The electrodes were sintered platinum-Teflon structures containing 50 mg/cm^2 of catalyst. The electrolyte, corrosive to both tantalum and glass, necessitated the use of platinum screen supports for the electrodes

and the periodic replacement of the test cells. A Kordesch-Marko bridge was used to eliminate the effect of ohmic polarization from the measured performance.

The butane performance was found to be quite sensitive to the partial pressure of water in the fuel feed. This was controlled by passing the fuel through a water reservoir prior to entering the cell. Figure C-2 shows the activity of butane as a function of this parameter. It is seen that the polarization at moderate current densities decreases with increasing water temperature up to 95°C, reversing the trend as the boiling point is approached.

Figure C-2

Water Vapor Influence on Butane Activity

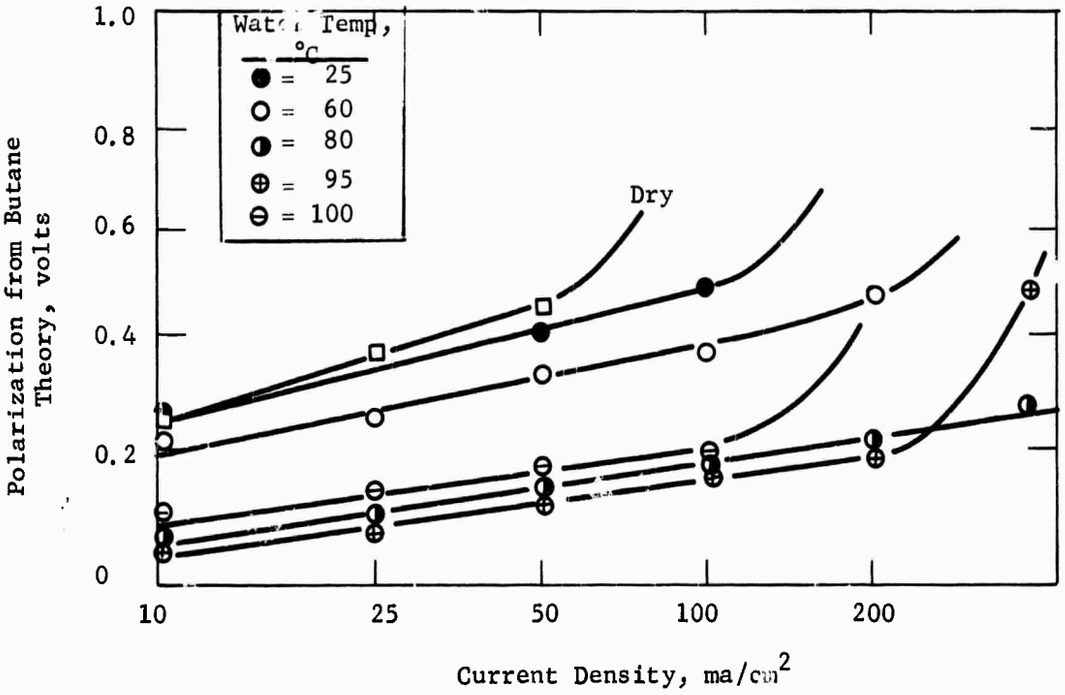

The lowest polarization recorded at 100 ma/cm^2 is 0.18 volts. The limiting current also increases, up to a maximum of about 400 ma/cm^2 at a water temperature of 80°C, falling off above this temperature. This is shown in Figure C-3, where the limiting current is plotted against the water vapor pressure.

Figure C-3

Effect of Water Vapor on Butane Limiting Current

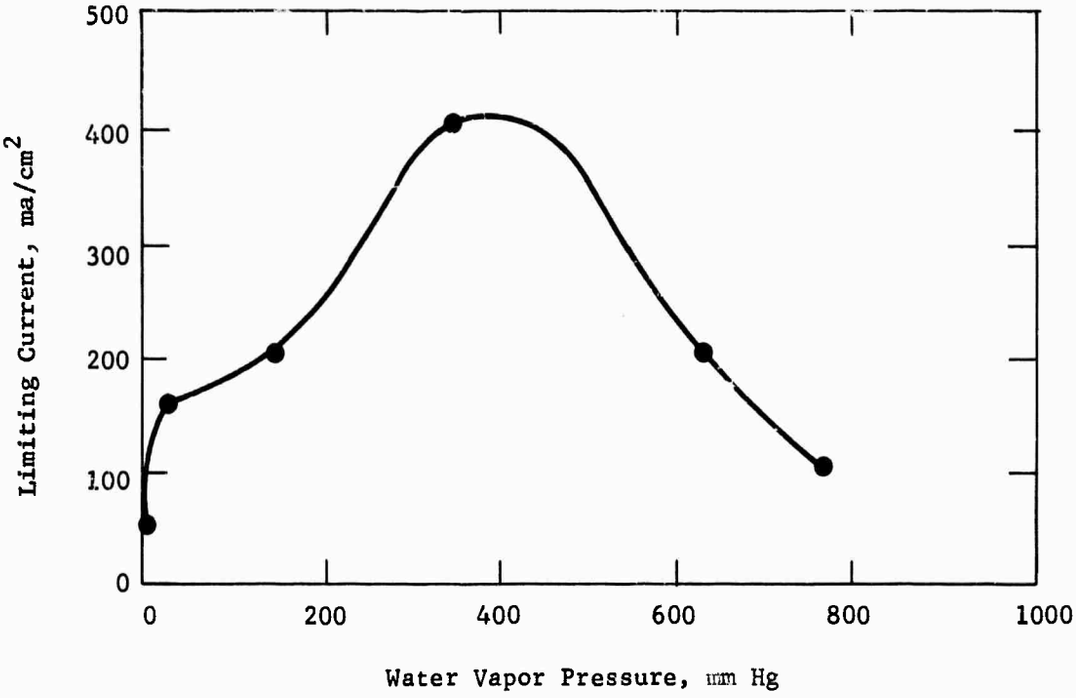

These effects, plus the poor performance of dry butane, clearly indicate the importance of a proper supply of water in this system. If there is insufficient water, the butane reactivity is hindered; if too much, the electrode becomes butane concentration limited. In this connection, it should be noted from Figure C-2 that the Tafel slope also changes with water vapor pressure, reaching a constant value of about 0.13 when the reservoir temperature reached 80°C or higher. This suggests that not only is the butane reaction hindered with insufficient water present, but it may also proceed via a different mechanism.

Additional runs were also carried out with hydrocarbons in pyrophosphoric acid. Butane was reacted at 275°C with little change in polarization from 250°C, although the limiting current was doubled. Ethane, at 230°C was slightly less active than butane is at 250°C. Based upon the negligible effect of temperature on polarization just discussed, this lower activity of ethane compared to butane appears to be real. Performance was improved by water addition to the feed stream, although no systematic study was made with ethane. Decane was also studied, at 275°C, by steam distillation to the platinum-Teflon electrode. No attempt was made to optimize the fuel feed conditions. At 50 ma/cm^2, the polarization was 0.24 volts, and the limiting current about 150 ma/cm^2. Finally, a number of six-carbon fuels were run at 275°C, by passing a nitrogen carrier stream through the liquids, followed by a water reservoir at 80°C. Again, no attempt was made to optimize these

conditions. Normal hexane, the most active of this group, was polarized 0.34 volts at 50 ma/cm^2. The others tested, in order of decreasing activity, were 2 -methylpentane, cyclohexane, hexene-1, and benzene. This same group of fuels was also tested in phosphoric and sulfuric acids, showing lower performance than in pyrophosphoric. Complete details of these and all other tests discussed in Part c are given in Appendix C-1.

Part d - Low Catalyst Content Butane Electrodes

Having established the conductivity, buffering capacity, and suitability for hydrocarbon reactivity of pyrophosphoric acid, attention was turned to the primary purpose of this investigation, increasing the catalyst utilization. Electrodes composed of catalyzed carbon and a binder, and similar to the thin carbon structures previously described (5), were tested with butane at 275°C, the fuel generally humidified by a water reservoir at 80°C. These electrodes, which contained 5 mg/cm^2 of catalyst, were prepared with several carbon to binder ratios, porosities, and thicknesses.

Performance of butane was found to vary considerably with the electrode structure. However, repeat runs with the same electrodes, or replicated runs, were not reproducible, preventing a rational correlation of performance changes with specific factors. Thus at each of the three thickness levels tested, using 6, 12, or 18 wt % of catalyst on carbon, a different combination of carbon to binder ratio and porosity gave the highest performance. Performance was improved with these electrodes by operating the water reservoir at 95°C instead of 80°C. For example, a low porosity electrode made up of a 2:1 ratio of 18 wt % catalyst on carbon powder to binder, had its limiting current increased from 25 to 75 ma/cm^2 by increasing the water temperature. No improvement in catalyst utilization was obtained over the level of sintered platinum-Teflon electrodes at 275°C however, the value at the limiting currents being 15 ma/mg for each system. Further work is necessary to improve the reliability of these measurements and to optimize the performance and catalyst utilization levels. Details of all carbon supported electrodes are found in Appendix C-2, as well as several other different, but inactive structures.

Part e - Oxygen Performance in Pyrophosphoric Acid

The performance of oxygen was determined in pyrophosphoric acid over a temperature range of 200 to 250°C, using primarily the sintered platinum-Teflon electrode. Several runs were also made with low catalyst content (5 mg/cm^2) carbon electrodes at 275°C. Activity variations were quite large on the platinum-Teflon electrodes, even though they were nominally identical. For example, at 230°C, the most active electrode was polarized only 0.08 volts at 100 ma/cm^2, while the least active was polarized 0.28 volts. These variations may have been due to difficulties in maintaining the sintering temperature constant. In all cases, the limiting currents were in excess of 750 ma/cm^2. When air was substituted for oxygen, little performance change occurred up to about 25 ma/cm^2. Beyond this level, polarization increased, by 40 mv at 50 ma/cm^2, and 90 mv at 100 ma/cm^2. Activity was still higher than with oxygen on similar electrodes in 14.7 M phosphoric acid at 150°C however. Figure C-4 shows that at 100 ma/cm^2, air performed 140 mv better at 230°C than oxygen at 150°C. The direct oxygen comparison shows a 230 mv difference between typical performances in these two electrolytes. Several runs were also carried out in which the gas feed was pre-humidified. No effects on performance were detected.

Figure C-4

Performance of Platinum-Teflon Electrodes
in Phosphoric and Pyrophosphoric Acids

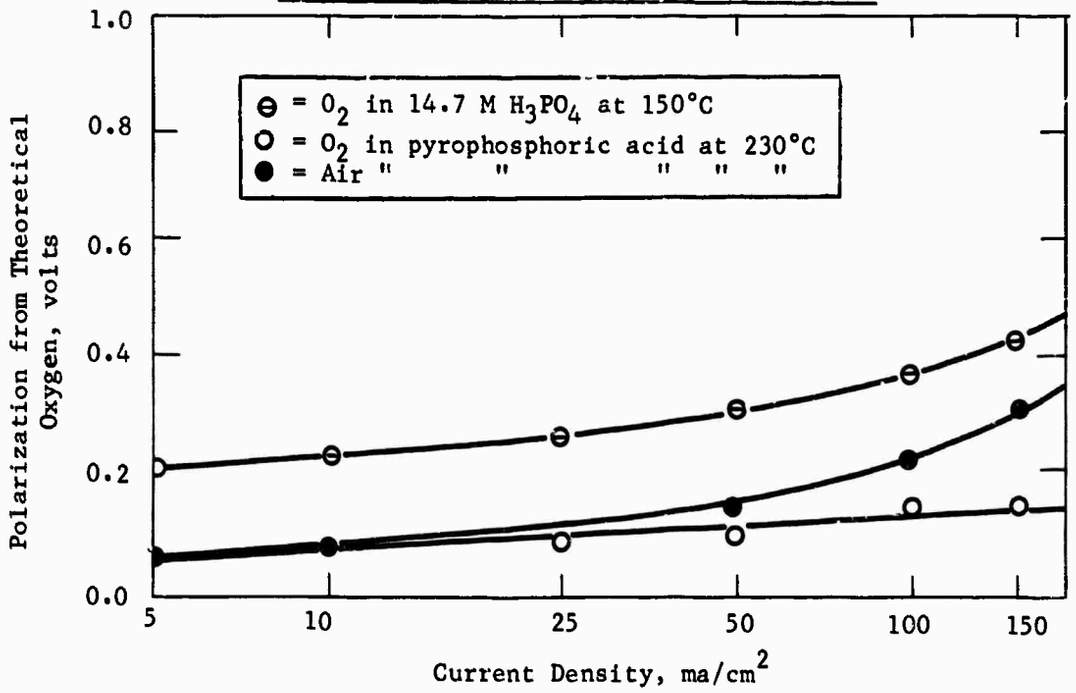

With the reactivity of oxygen in pyrophosphoric acid established, further work aimed at improving catalyst utilization. Initial tests with the catalyzed carbon electrodes described in Part d were made at 250 or 275°C. As with butane, a variation of performance with structure was noted. In the absence of replicates, however, it is not yet known if these represent random errors or true structural effects. In any event, the highest activity obtained showed a polarization of 0.40 volts at 100 ma/cm^2 and a limiting current of over 300 ma/cm^2. Details of all these runs are found in Appendix C-3. It is evident that oxygen shows a large activity increase at the higher temperatures possible in pyrophosphoric acid, in contrast to butane. Further work will concentrate on improving the catalyst utilization with the carbon electrodes and study the efficient use of air in place of oxygen.

Phase 2 - Buffer Electrolytes

Buffer electrolytes are of interest because they are less corrosive than acids and increase the number of potential catalysts applicable to systems utilizing carbonaceous fuels. The continued investigation of buffer electrolytes has concentrated on the carbon dioxide rejection of and reactant performance in high pH, concentrated solutions. The addition of inert salts as a means of raising operating temperatures has also been studied. Finally, further tests of the pyrophosphate salt buffer system, as distinguished from pyrophosphoric acid, were carried out.

Part a - Concentrated Buffer Electrolytes

Concentrated buffer systems have been investigated because they have relatively high boiling points and, therefore, can be used at elevated temperatures. The highest concentrations reached with buffer solutions at room temperatures have been with the cesium di- and tribasic phosphate system. Solutions containing up to 3.5 moles/liter of each component have boiled as high as 145°C, and allowed high activity with methanol on platinum catalysts at 130°C. However, they are not initially carbon dioxide rejecting, and when sparged with this gas, fall several pH units (6). Subsequent tests have indicated, however, that at a given temperature, the final pH is dependent on the carbon dioxide flow rate. This suggest that at the lower flow rates, the solution is not saturated with carbon dioxide, and further suggests that an electrolyte may be operated at higher than its equilibrium pH by proper design. Additional discussion of this point is found in Phase 3 of this Task. It was also found that these "equilibrated" solutions, containing mono- and dibasic phosphate, carbonate, and bicarbonate anions, could not be restored to their original pH by heating in the absence of carbon dioxide. Further work will be carried out to explain these results.

Tests have now been carried out on the activity of methanol, hydrogen, and oxygen with platinum catalyst in this "equilibrated" electrolyte. At 130°C, using a dual platinum-Teflon electrode having 25 mg/cm^2 of platinum sandwiched between the two electrode sheets, poor methanol activity was obtained. Part of this was traced to difficulties in maintaining an adequate supply of fuel at the anode. As shown in Figure C-5, the polarization at 100 ma/cm^2 decreased from 0.54 to 0.47 to 0.40 volts versus a reference hydrogen electrode as the fuel was first fed as a vapor, then by syringe directly on the electrode, and finally with the fuel chamber dead-ended.

Figure C-5

Effect of Methanol Feed on Performance

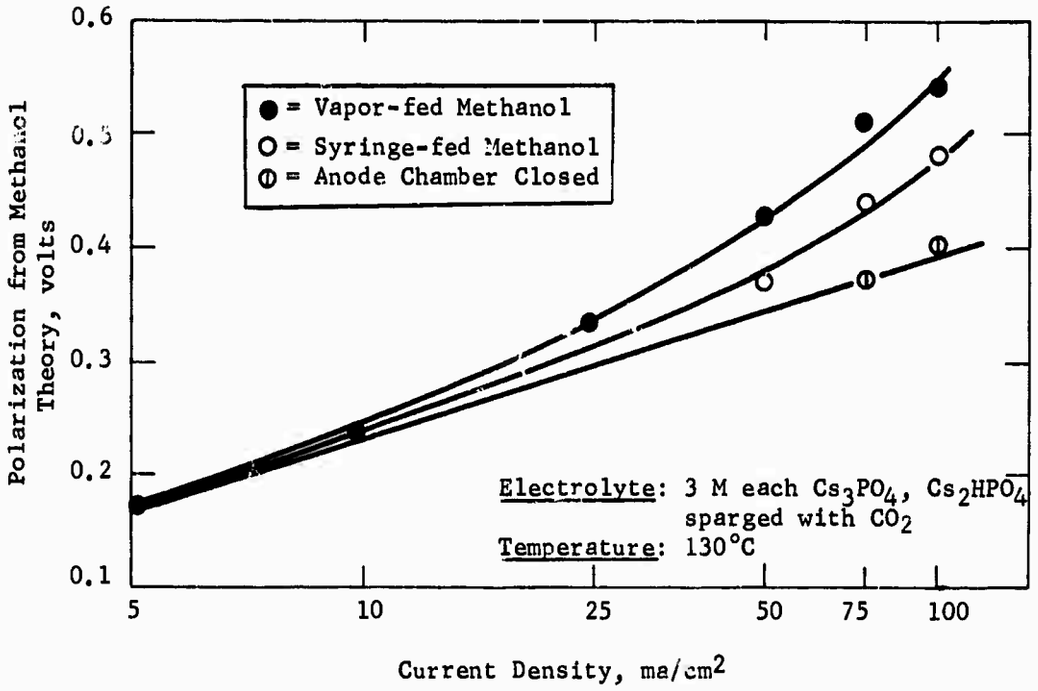

In contrast, the unequilibrated electrolyte had previously given only 0.21 volts polarization at 100 ma/cm^2 and 130°C (6). In addition, at 5 ma/cm^2, where fuel concentration polarization is not a factor, the unequilibrated solution still gave about 90 mv less polarization than the "equilibrated" electrolyte. Therefore, some factor arising from the latter solution must be the cause of the lowered performance. Ionic concentration polarization, which could be present if the "equilibrated" electrolyte did not have sufficient buffering capacity, was also ruled out by running a flag electrode with dissolved methanol. Stirring the system had no effect upon performance up to about 100 ma/cm^2, indicating that the solution was functioning as a buffer, at least for anodic reactions.

Poor activities were also obtained with hydrogen and oxygen on the dual platinum-Teflon electrode at 130°C, the former was polarized 0.14 volts at 50 ma/cm^2, with the limiting current only 75 ma/cm^2. The best oxygen performance was a polarization of 0.37 volts at 10 ma/cm^2, with a limiting current of about 25 ma/cm^2. Additional cathode runs in unequilibrated electrolyte are discussed in Phase 3 of this Task.

To check the possibility of the electrolyte not functioning as a buffer when operated as a catholyte, hydrogen was evolved from the dual electrode. At 100 ma/cm^2, only 70 mv polarization was measured, indicating satisfactory buffer capacity. These gases were also tested with diluted samples of the equilibrated electrolyte, showing greatly improved performance. When sufficient water was added to give a composition nominally 1 M each in the di- and tribasic phosphates, polarizations of only 0.12 and 0.42 volts at 100 ma/cm^2 were obtained for hydrogen and oxygen respectively, even though the operating temperature was lowered to 80°C. Details of all the runs in the equilibrated electrolyte are given in Appendix C-4.

The lowered performance of methanol in the carbon dioxide treated solution, compared to fresh electrolyte, and the poor activity of hydrogen and oxygen, require further work for explanation. Several possibilities exist, including a known chloride ion level of several hundred ppm in the salts used to prepare the "equilibrated" electrolyte, low solubilities of the gaseous reactants, and wetting difficulties. Additional experiments will be carried out to clarify these points.

Part b - Addition of Cesium Fluoride to Buffer Solutions

Temperatures of up to 145°C have been achieved with concentrated buffer electrolytes, as described in Part a. Experiments have been initiated to extend this level by addition of a neutral salt to the concentrated solution. Cesium fluoride was chosen as the salt because of its high solubility and presumed lack of effect on electrochemical reactions. This latter consideration was tested by adding one mole/liter of the salt to buffer solutions composed of 1 M each potassium mono- and dibasic phosphate or 1 M each carbonate and bicarbonate. These solutions were run with methanol and oxygen on platinum electrodes at 60°C. Table C-1 shows that no performance loss was encountered with methanol.

Table C-1

Methanol Performance in Presence and Absence of Fluoride Ions

Platinum Catalyst, 1 M CH_3OH, 60°C

Current Density, ma/cm^2	Polarization from Methanol Theory, volts			
	1 M KH_2PO_4 1 M K_2HPO_4	1 M KH_2PO_4 1 M K_2HPO_4 1 M C_sF	1 M $KHCO_3$ 1 M K_2CO_3	1 M $KHCO_3$ 1 M K_2CO_3 1 M C_sF
5	0.37(1)	0.32	0.27(1)	0.25
10	0.39	0.35	0.30	0.32
50	0.47	0.43(1)	0.38	0.38
100	0.51	0.48	0.42	0.42
200	0.58	0.55	0.47	0.49(1)

(1) Onset of carbon dioxide evolution.

The only anomaly was the higher current densities required for carbon dioxide evolution in the presence of fluoride, since the neutral salt should have little effect on the pH. Oxygen performance was slightly impaired. In the carbonate-bicarbonate buffer, using the dual platinum-Teflon structure, the polarization at all current densities was about 80 mv higher in the presence of fluoride.

The addition of cesium fluoride to raise the operating temperature of the concentrated buffer system was investigated with a solution 3.3 M each in cesium di- and tribasic phosphate. It was possible to add about 3 moles/liter of the fluoride to this solution at room tempersture. Although some cloudiness occurred, there was no precipitation and the boiling point was raised from the original 135°C to 150°C. By concentrating the system further through evaporation the boiling point was further increased to 180°C, although room temperature solubility was sacrificed. Additional combinations will be tested, and reactant performance, particularly of hydrocarbons, will be determined at the higher temperatures.

Part c - Pyrophosphate Buffers

Buffer solutions prepared from salts of pyrophosphoric acid have previously shown favorable properties as fuel cell electrolytes (6). Tests have now been conducted of their hydrolysis behavior by maintaining them at 80°C for periods up to 90 hours at the pH range, 6-9, in which they function as buffers. Addition of a silver salt showed, by formation of a characteristically yellow silver orthophosphate precipitate, that considersble hydrolysis had occurred. Only at a pH level of 11 or higher, well outside the buffering region, was the hydrolysis reaction suppressed. Because of this instability, no further work is planned with these systems.

Phase 3 - Air Electrodes for Buffer Electrolytes

Development of sir electrodes for use in buffer electrolytes has continued, with emphasis on the use of silver catalyst and the dual electrode structure (6). Tests have been carried out to enhance activity and to better understand the function of each component of the dual structure. In addition, studies in concentrsted buffer solutions hsve been carried out at temperatures up to about 130°C.

Part a - Dual Electrode Structures

Previous studies have established that the dual electrode structure, composed of two platinum-Teflon sheets, gave high performance with air in buffer electrolytes (5). Furthermore, one of these sheets could be replaced by a silver-Teflon sheet, with no loss of performance under certain conditions (6). Initial attempts to evaluate the function and activity of each sheet independently, by electrically insulating them, were not successful. However, further work has made progress in this area. The dual platinum-Teflon electrode was tested in a 1 M each carbonate-bicarbonate buffer of pH 10.6 at 60°C with air. Teflon-ring spacers were positioned between the two sheets of this structure, and by careful pressure adjustment a leakproof seal was obtained, with the sheets electrically insulated from each other. Although the geometrical arrangement of the dual electrode system was disturbed, it was possible, by measuring the performance of each component independently, to obtain a clear picture of their relative activities. As shown in Table C-2, the two performances were similar at 1 ma/cm^2. At 50 ma/cm^2 however, the inner, electrolyte-facing sheet, failed, due to air starvation. The outer sheet, although inferior to standard dual electrode performance, did not fail. When a single platinum-Teflon sheet was backed on the electrolyte side by a porous Teflon sheet, it was only slightly inferior to the standard performance. This confirms that the inner sheet is functioning primarily as a barrier. Any metal present in its structure is not significantly active catalytically, although it may influence the porosity and hydrophobicity of the sheet.

Table C-2

Effect of Dual Electrode Arrangement on Performance

Electrode	Electrically Connected Component	Polarization from Oxygen Theory at Indicated ma/cm^2, volts		
		1	10	50
Dual Platinum-Teflon	Both	0.20	0.28	0.43
" " "	Air-side	0.25	0.35	0.62
" " "	Electrolyte-side	0.25	0.50	1.27
Single Platinum-Teflon with Porous Teflon Sheet Facing Electrolyte	--	0.23	0.29	0.47

Other tests involving nickel-Teflon sheets were also made. A dual nickel-Teflon electrode was inactive, and a nickel-Teflon sheet backed by a platinum-Teflon sheet showed only the activity of the air starved platinum. Thus nickel has no catalytic activity in this system. The reverse configuration was less active than, for example, simply a porous Teflon sheet backing a platinum-Teflon electrode. Finally, a triple silver-Teflon electrode showed no advantage over a dual electrode. Details of all tests discussed in Part a appear in Appendix C-5 .

Part b - Concentrated Buffer Electrolyte

The concentrated solution composed of cesium di- and tribasic phosphates has been discussed previously (6). In addition, its behavior with carbon dioxide has been described in Phase 2 of this report, where the poor air electrode performance obtained in "equilibrated" electrolyte is mentioned. Tests have also been carried out of air electrode activity in fresh electrolyte, not contacted with carbon dioxide. These have been conducted primarily in 3.3 M each di- and tribasic phosphate, with dual silver- or platinum-Teflon electrodes at about 130°C. Runs have also been carried out with single sheet electrodes and under several operating and structural conditions.

All electrodes in the concentrated buffer showed very poor activity at 125 or 130°C. Humidification of the air stream did not help, but application of 2-1/2 inches of pressure improved the polarization about 100 mv at 100 ma/cm^2. Also of some benefit was the use of a more porous silver-Teflon sheet on the electrolyte side, or dilution of the buffer to 0.7 M in each component. This latter change helped even though the operating temperature was lowered to 80°C. None of these activity changes was sufficient, however, to bring the performance to a satisfactory level. Appendix C-6 contains the data for these runs.

Since very poor cathode activity has been obtained in both the carbon dioxide treated and fresh concentrated buffers, the debit does not appear to be associated with the composition changes which occur during equilibration. Rather, it is probably due to one or more of the factors discussed in Phase 2, high chloride ion concentration, low gas solubility, or wetting problems. Further work will seek to verify these possibilities and improve air electrode performance, particularly with the silver-catalyzed system.

Part c - Comparison of Cesium and Potassium Carbonates

Because of the poor activity obtained with air electrodes in concentrated cesium phosphate buffer, a study was initiated to compare cesium salts with potassium salts. It was hoped to determine the presence of any specific cation effects. Performance tests were carried out with air and dual silver-Teflon electrodes in 6 M cesium carbonate, 6 M potassium carbonate, and a 4 M potassium and 2 M cesium carbonate solution at 112 to 118°C. Table C-3 illustrates that the potassium solution was superior to the cesium solution, especially at higher current densities. In fact, the performance in the former system represents the best activity yet observed for silver catalysts in buffer electrolytes. The mixed solution was equivalent to this level. Further data is presented in pendix C-6 .

Table C-3

Performance of Silver Cathodes
in Cesium and Potassium Solutions

Dual Silver-Teflon Electrode ; Air

Electrolyte	Temp, °C	Polarization from Oxygen Theory at Indicated ma/cm^2, volts			
		1	10	20	50
6 M Cesium Carbonate	118	0.36	0.44	0.48	--
6 M Potassium Carbonate	112	0.32	0.39	0.41	0.45
4 M Potassium Carbonate + 2 M Cesium Carbonate	112	0.32	0.38	0.40	0.45

The cesium carbonate solution allowed better performance than the concentrated cesium phosphate buffer. Since the former material contained a much higher chloride content than the latter, it appears that this impurity may not be influencing the activity. The mixed solution, which matches the potassium solution in activity, tends to confirm this. These results may mean, rather, that the cesium ion concentration is important. The alkali metals vary with atomic number in their activity coefficients, the direction of change being dependent on the anion (14). With a proton accepting anion such as carbonate or phosphate, the larger cation, cesium, will have a larger activity coefficient than a smaller cation, potassium. This effect explains the higher boiling point of a 6 M cesium carbonate solution, 129°C, compared to 117°C for 6 M potassium carbonate, and may be related to the poor cathode performance in cesium solutions. However, satisfactory oxygen activity has been reported in concentrated cesium carbonate, using platinum-Teflon electrodes (15). This suggests that catalytic or structural factors may overcome any debits inherent in cesium solutions. Further work is planned to define more definitely the influence of impurities and investigate the specific effects of cesium ions, particularly their interactions with cathode catalyst and structure variables.

Part d - Interaction of Methanol with Silver Cathode

Two problems which can arise at the cathode when using soluble fuels are chemical oxidation of the fuel and also increased polarization. The silver-6 M potassium carbonate system, having demonstrated high performance levels, also offered the possibility of reducing methanol interactions because of the negligible anodic activity of silver. Earlier work, with a less active system, has suggested this to be the case (6), but more extensive tests at practical polarization levels were needed for confirmation. These have now been carried out, with dual silver-Teflon electrodes in 6 M potassium carbonate at 105°C. Not only was the effect of methanol on polarization measured, but also the oxygen and carbon dioxide contents of the exhaust air stream were determined.

These experiments have demonstrated that methanol has no effect on the silver cathode polarization. For example, the polarization at 100 ma/cm^2 did not change from the original 0.62 volts with successive additions of methanol, the final concentration reaching 6.3 vol %. The original, methanol-free value was about 100 mv higher than reported in Part c, primarily due to a porous Teflon sheet placed on the air side of the dual electrode to restrict leakage which developed during the run. Simultaneously with the polarization measurements, the oxygen and carbon dioxide contents of the exit air stream were being monitored, using a Beckman F-3 oxygen analyzer and a Beckman IR315 carbon dioxide analyzer. Within

the sensitivity of these instruments, corresponding to about 5 ma/cm^2, no change in the content of these gases was detected. Therefore, if chemical oxidation was occurring, it was at a rate equivalent to less than 5 ma/cm^2. Similar runs at other current densities gave comparable results, as shown in Appendix C-7.

Phase 4 - Buffer Electrolyte Total Cells

The high activity exhibited by the dual silver-Teflon cathode in 6 M potassium carbonate electrolyte, coupled with its insensitivity towards methanol, prompted a brief look at its performance in a total cell.

Part a - Total Cell Performance

A cell was assembled using a dual silver-Teflon air electrode and the 6 M potassium carbonate electrolyte. The anode was made up from a screen containing P-type catalyst, backed by two AA-1 platinum-Teflon sheets. With this interface-maintaining structure, methanol was fed as a vapor in a nitrogen stream. At 105°C with air the cell had a maximum power output at the terminals of about [illegible] mwatts/cm^2. No effort was made to minimize ohmic polarization, and with the [illegible] of 100 and 200 mv at 50 and 100 ma/cm^2 subtracted out, the power densities rose to 23 and 37 mwatts/cm^2 at these currents. Substituting oxygen for air further improved the output to an IR free value of 51 mwatts/cm^2 at 100 ma/cm^2. The cathode performance was very close to that obtained in half-cell tests, 0.48 volts with air at 50 ma/cm^2. These results, details of which are shown in Appendix C-8 , demonstrate that the dual silver-Teflon air electrode can be operated satisfactorily in a total cell. Further work with total cells will determine if potassium carbonate can reject carbon dioxide under practical operating conditions.

Phase 5 - Non-noble Catalysts for Methanol Oxidation

A number of different types of non-noble metal catalysts have been prepared and evaluated for methanol activity. These include compounds of transition metals which have shown activity in hydrocarbon reactions. Also, a number of metal alloys were prepared by co-reduction of their salts. Both of these types of catalysts were prepared on carbon supports. Other unsupported alloys were made by melting the metals together in an arc furnace. Tests were run in the 1 M each potassium di- and tribasic phosphate buffer of pH 12, and also in potassium hydroxide. The latter electrolyte was used to avoid missing catalysts which might be active only at the higher pH, but, with some modification, could be made active in buffer. Finally, some experiments were carried out in concentrated buffer in an attempt to chemically reduce metal oxides with decane as the first step in a possible redox system.

Part a - Transition Metal Compounds

Several compounds of transition metals which are active in hydrocarbon reactions were prepared on carbon as a conductive support. These consisted of tungsten and nickel-tungsten sulfides and cobalt and nickel molybdates. They were evaluated at 80 and 90°C in pH 12 phosphate buffer containing 1 M methanol. None of these were active catalysts under these operating conditions. A catalyst which consisted of 30 wt % of cobalt molybdate on carbon was evaluated in 6.9 M potassium hydroxide and would sustain currents of about 10 ma/cm^2, with a polarization of about 0.4 volts at open circuit. The data indicate that these catalysts require temperatures higher than can be achieved in practical methanol fuel cells to be effective. The performance of these catalysts is listed in Appendix C-9.

Part b - Crystal Lattice Parameters and Catalyst Activity

Platinum and its alloys are the most active catalysts for the anodic oxidation of methanol. To evaluate the relation between crystal lattice parameters and catalyst activity a number of non-noble metal alloys having lattice parameters similar to platinum were prepared and evaluated as methanol catalysts. The alloys were prepared by co-reduction of their salts adsorbed on carbon in an amount leaving 10 percent metal on the support. Some compositions prepared were Sb-48Ni, Au-35Ni, Co-43Sb, 38Au-23Ag-39Cu and Cu-25Au. None of these alloys had activity for oxidation of methanol at 80 to 90°C in pH 12 phosphate buffer. The data is listed in Appendix C-9 . Thus, attempts to prepare active catalysts based upon the criterion of lattice spacing have not been successful.

Part c - Gold and Gold Alloys as Methanol Catalysts

Gold and several alloys of gold have been evaluated as methanol catalysts. These catalysts were prepared by melting the metals in an arc furnace. The buttons formed were inverted and remelted five times to assure homogeneity. The buttons were then pulverized to less than 325 mesh powder and fabricated into porous electrodes by use of a binder. Of the metals alloyed with gold, nickel, copper, silver, and iridium all decreased its catalytic activity while zirconium and titanium had little effect on it. Current densities of 100 ma/cm^2 could be drawn from gold or gold-zirconium catalysts when oxidizing methanol in 6.9 M potassium hydroxide at 90°C. However, these electrodes were polarized about 0.6 volts from theory at 5-10 ma/cm^2. This high polarization at low current densities makes them unacceptable as practical catalysts. None of these catalysts had activity in a buffer electrolyte of 1 M each potassium di- and tribasic phosphate. The performance of these electrodes is shown in Appendix C-9 .

Part d - Unsupported Transition Metal Alloys

About 20 transition metal alloys were prepared in which one metal was from the group composed of molybdenum, nickel, chromium, cobalt, copper, iron, or manganese, all of which have shown catalytic activity for certain hydrocarbon reactions. The other metal was from the group made up of titanium, zirconium, tantalum, or tungsten, which was added to increase the corrosion resistance. These alloys were prepared by melting the metals together in an arc furnace and then remelting five times to ensure homogeneity. The metal buttons were next pulverized to less than 325 mesh particles and pressed into porous disc electrodes by use of a binder. The electrodes were evaluated at 80 and 90°C in a pH 12 phosphate buffer electrolyte and in 6.9 M potassium hydroxide, each containing 1 M methanol. None of the alloys were effective catalysts in the pH 12 buffer electrolyte. In base, a current density of 100 ma/cm^2 could be maintained with only one of the alloys, Ti-33Ni. However, the polarization was 0.7-0.8 volts at this current. Nearly all of the alloys prepared did not corrode chemically or anodically during evaluation. This was shown by spectrographic analysis of the electrolyte after running.

This study has shown that it is possible to protect non-noble metal catalysts from anodic corrosion in base or buffer and that it may be possible to utilize the catalytic activity of these transition metals at the same time. Additional alloys will be prepared and evaluated as catalysts based upon these experiments. The performance of these alloys as anodes is shown in Appendix C-9 .

Part e - Comparison of Non-noble Catalyst Activity in Buffer and Base

Many of the non-noble metal catalysts prepared have been evaluated in a pH 12 phosphate buffer electrolyte and in 6.9 M potassium hydroxide. The performance in buffer has been consistently poorer than in the strong alkaline electrolyte. A comparison of the activity of four catalysts in these two electrolytes is included in Table C-4 and shows current densities 5 to 100 times greater in potassium hydroxide than in the phosphate buffer.

Table C-4

Catalyst Activity in Strong Alkali and Phosphate Buffer Electrolyte
90°C, 1 M Methanol

Catalyst Composition	Electrolyte	Current Density at Indicated Polarization from Theory, ma/cm^2	
		0.5 Volts	0.7 Volts
Co-5Ru	6.9 M KOH	10.6	14.5
	1 M K_2HPO_4 + 1 M K_3PO_4	0.4	1.6
$CoMoO_4$ on C	6.9 M KOH	0.8	2.3
	1 M K_2HPO_4 + 1 M K_3PO_4	.09	0.53
Ti-33Ni	6.9 M KOH	6.8	22.0
	1 M K_2HPO_4 + 1 M K_3PO_4	0.25	1.5
Au-25%	6.9 M KOH	1.0	13.0
	1 M K_2HPO_4 + 1 M K_3PO_4	.01	.06

The reason for this very large difference in activity is not known certainly it is not a reflection of the difference in conductivity of the two electrolytes as the currents are too small for this to be a factor. In addition, it has been amply demonstrated previously that the active noble metal catalysts retain their activity in buffer.

Part f - Reactions of Redox Agents in Carbonate Electrolyte

Although certain metal oxides, such as rhenium heptoxide and molybdenum trioxide can be reduced by decane when slurried in concentrated acid, it has not been possible to carry out the electrochemical re-oxidation step efficiently. In the molybdenum case, a soluble reduction product is formed in the acid, which can be re-oxidized at low current densities with favorable potentials. However, higher currents cannot be reached, due apparently to the formation of molybdenum polyanions in the acid electrolyte. With the development of concentrated buffers, it became feasible to attain the higher temperatures believed necessary for the decane-oxide chemical reaction at a high enough pH to minimize polyanion formation.

Tests were carried out with 10 gram portions of sodium molybdate, ammonium tungstate, and rhenium heptoxide, each dissolved in a 50 ml portion of 6 M potassium carbonate and refluxed under decane at 117°C. No reactions occurred, however, even when nickel or platinum powders were added as possible catalysts. These three reagents were also tested with 1 M methanol in the carbonate solution at 110°C, but again no reaction took place. Further tests will be made at higher temperatures and with other oxides and catalysts.

Phase 6 - Slurry Catalyst Systems

Previous slurry catalyst studies have been conducted with a rotating electrode providing the turbulence for maintaining the catalyst suspension (5,6). An alternative method, requiring less energy, would involve utilizing the immiscibility and lower density of decane in aqueous electrolyte. Thus if this fuel is sparged through the electrolyte, sufficient turbulence may be produced to maintain a catalyst suspension.

Part a - Catalyst Suspensions with Bubbling Decane

Tests of the bubbling concept were run with a 15 mm diameter glass chamber, with exit and entrance tubes. A glass frit, through which decane could be sparged, was placed in the entrance tube, and glass wool in the exit tube to prevent catalyst loss. The electrode was simply a stationary platinum gauze in the chamber. Initial runs were made with platinum and rhodium powders in 3.7 M sulfuric acid. The rhodium agglomerated at the bottom of the chamber almost immediately and could not be suspended. The platinum was suspended at first, but as its potential approached to within a few hundred millivolts of the decane theoretical open circuit potential, it also agglomerated. It was found, however, that powdered carbon could be suspended without difficulty. Accordingly, carbon-supported catalyst was used for the remainder of the investigation.

The catalyzed carbon was used in a variety of systems, by itself and ballmilled with Teflon powder, with and without added surfactant, and in 3.7 M sulfuric or 14.7 M phosphoric acids. In addition to the suspension experiments, several runs were also performed with the catalyst pressed onto the gauze current collector. It was observed in all cases that the carbon slurry was easily flooded by fuel, necessitating periodic interruptions in the decane flow. This in turn resulted in less turbulence and less energetic movement of the particles. Performance improvements resulting from the intermittent supply of fuel were primarily obtained at or near the limiting current region. In fact all improvements, whether obtained by the use of surfactants, higher temperature electrolyte, or increase in catalyst particle density, occurred mainly in this region. For example, the addition of 0.04 wt % of FC-95 surfactant to the sulfuric acid electrolyte produced only a 50 mv improvement at 1 ma, but the limiting current was increased from just over 1 to 5 ma. Full details of these runs are in Appendix C-10. The best performance and catalyst utilization values were obtained in phosphoric acid at 150°C. At a polarization of 0.60 volts, 5 ma could be drawn, giving a utilization of 0.8 ma/mg. This is considerably poorer than has been obtained with static electrodes, apparently due to the poor contacting between catalyst particles and the current collector. Improvements appear to require the use of other substrates, less easily flooded by decane, which would allow increased turbulence in the system.

4.4 Task D, Methanol Electrode

Studies of the methanol electrode in sulfuric acid electrolyte have concentrated on improving various aspects of ruthenium modified P-type catalyst performance in the methanol-air battery and developing electrode structures to improve catalyst utilization so as to reduce noble metal costs. Research for new methanol catalysts has been aimed at cheaper non-noble metal materials for use in less corrosive buffer electrolytes as described in Task C.

Phase 1 - Studies of Ruthenium Modified P-type Catalyst

Several studies have been carried out to improve the performance of ruthenium modified P-type anodes in the methanol-air battery. These have covered a variety of performance characteristics such as sensitivity to methanol concentration, effects of anode coatings and water purity on performance, mechanical stability, storage, and life.

Part a - Effect of Methanol Concentration on Ruthenium Modified P-type Catalyst Performance

Quantitative data on the response of anodes to changes in methanol concentration are necessary in selecting proper concentration levels for cell operation. In the present study, the performance of the hydrogen reduced ruthenium modified P-type catalyst was determined at various methanol concentrations. The tests were made in a well-stirred half cell described previously (5). The resulting performance curves are shown in Figure D-1 and the data are tabulated in Appendix D-1.

Figure D-1

Methanol Concentration Dependence of Ruthenium Modified P-type Catalyst

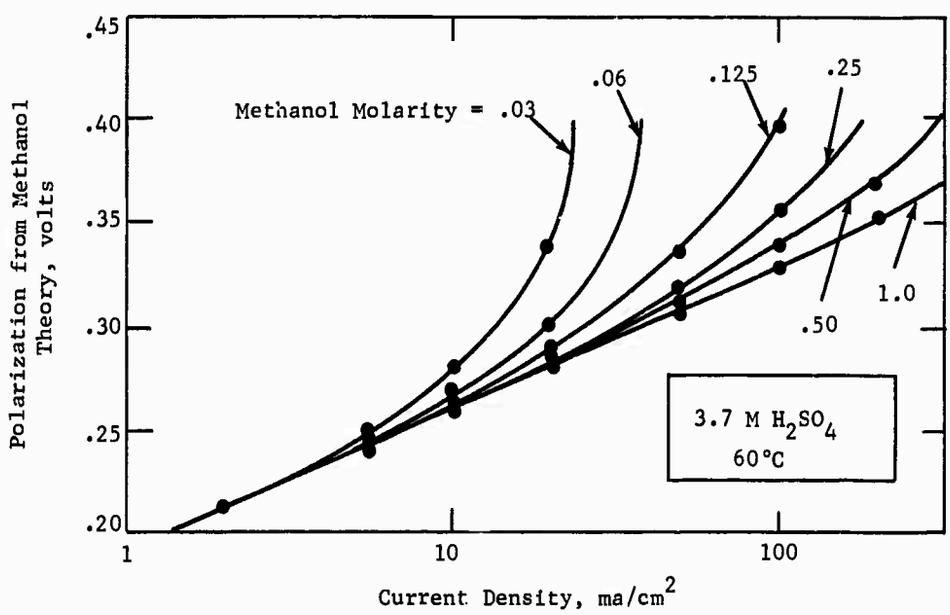

At low current density and/or high methanol concentration, a single Tafel line is approached for all performance curves. This indicates that the inherent electrocatalytic rate is not concentration dependent. However, at high currents or low methanol concentrations, it appears that mass transport limitations become effective and deviation from Tafel behavior occurs. Thus, some of the catalyst sites become fuel deficient and the concentration dependence is determined by the electrode structure.

Concentration dependence has sometimes been measured by potentiostatting the anode and measuring current density. In the present case, such a measurement would give relationships which are strongly dependent on the chosen potential and which do not differentiate between catalytic and transport phenomena. Limiting currents can be measured with such a technique by potentiostatting the anode at a sufficiently high polarization to insure diffusion control of the reaction. These measurements were made on ruthenium modified P-type anodes at 0.8 volts from methanol theory in 3.7 M sulfuric acid electrolyte with various methanol concentrations. The results are tabulated in Appendix D-1 and are presented in Figure D-2.

Figure D-2

Effect of Methanol
Concentration on Limiting Current

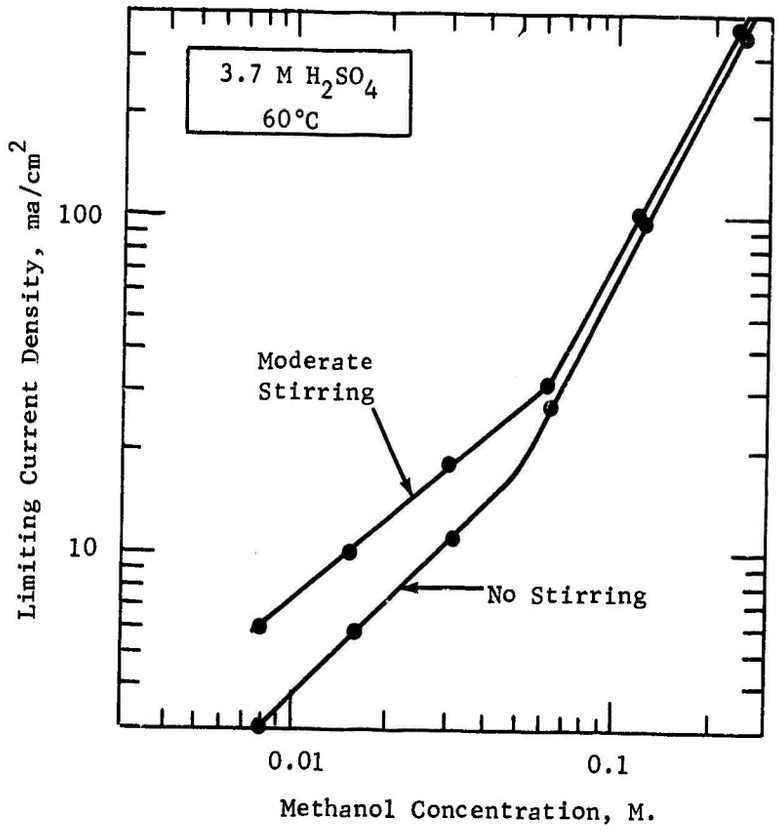

At low current densities, the limiting current density is proportional to concentration and mechanical stirring in the bulk electrolyte has a significant effect. This agrees with the usual model of Fick's law diffusion across a stagnant layer of constant thickness. At higher current densities, the limiting current for a given concentration is increased and mechanical stirring in the bulk electrolyte solution has little effect. In this regime the evolution of carbon dioxide at the electrode surface appears to increase mass transport to the catalyst surface, probably by reducing the diffusion layer thickness as described previously (1).

Thus, high limiting currents are possible at fairly low methanol concentrations, for example 350 ma/cm^2 for 0.25 M methanol. However, in order to minimize polarization losses to about 20 mv, the current density for 0.25 M methanol must be limited to about 100 ma/cm^2.

Part b - Methanol Electrode Coatings

Studies in methanol-air cells, Task F, have shown that loss of fuel due to chemical oxidation at the cathode is directly proportional to the concentration of methanol in the electrolyte chamber adjacent to the membrane side of the cathode. Thus, improved performance and efficiency can be achieved by limiting the amount of methanol that diffuses from the anolyte chamber through the anode into the electrolyte chamber. Although the methanol electrode itself acts as a barrier (1), the methanol flux could be further reduced by providing an additional diffusion barrier. Therefore, a brief study was made of the effect on anode performance of a hydrophobic coating on the electrolyte chamber side of a methanol electrode.

A coating of about 5 mg/cm^2 Teflon 41-BX was sprayed on a small conventional ruthenium modified P-type anode. The latter was tested in a glass half cell at 60°C, with 1 M methanol in 3.7 M sulfuric acid in the anolyte chamber and acid only in the counter-electrode chamber. As shown in Table D-1, anode performance at 50 ma/cm^2 was not affected by the presence of the Teflon barrier. However, ohmic losses through the electrode structure increased somewhat from 0.005 volts to 0.020 volts at 100 ma/cm^2. Complete data are listed in Appendix D-2.

Table D-1

Effect of Teflon Coating on Methanol Electrode Performance

Coating	Polarization from Methanol Theory at Indicated ma/cm^2, volts(1)		Ohmic Loss at 100 ma/cm^2, volts
	50	100	
Teflon	0.28	0.52	0.020
None	0.28	0.31	0.005

(1) 60°C, 1 M CH_3OH in 3.7 M H_2SO_4.

Thus, anode performance was not seriously impaired by the coated barrier. Previous studies with cells of this configuration showed that, very little methanol diffuses through the electrode during the 1-2 hours required to perform these tests (6). However, further tests are required in total cells to establish the overall benefit of this barrier for reducing methanol diffusion to the cathode.

Part c - Effect of Water Purity on Electrode Performance

An experiment was carried out to determine the effect of using less pure water on the performance of the present anodes and cathodes. The work was carried out in the 1" diameter half cell unit (5) at 60°C using electrolyte mixtures prepared with the following types of processed water: distilled and deionized water, distilled water, refluxed tap water, and tap water. All solutions were prepared with 1 M methanol and 3.7 M sulfuric acid.

The standard Cyanamid AA-1 electrode, with a pressed Permion 1010 membrane, displayed no noticeable change in polarization when tested with solutions prepared using the four types of water described above. The anodes showed a slight increase in polarization as the quality of water was reduced, but the maximum degradation was only 40 mv. It is important to note, however, that the initial performance of the anode in the distilled-dionized water was relatively poor, the polarization at 50 ma/cm^2 being about 20 to 30 mv higher than the best anodes that have been previously tested. Thus, it may be possible that the deleterious effects of the low purity water were masked by previous contamination of the electrode. These results are summarized in Table D-2.

Table D-2

Effect of Water Purity on Performance

Electrode	Type of Water Processing	Polarization from Theory at 50 ma/cm^2	Polarization from Theory at 100 ma/cm^2
Cyanamid AA-1 Cathode	Distilled - D.I. H_2O	0.45	0.47
	Distilled H_2O	0.44	0.46
	Refluxed Tap H_2O	0.45	0.49
	Tap H_2O	0.46	0.48
Ru Mod P-type Anode	Distilled - D.I. H_2O	0.31	0.35
	Distilled H_2O	0.31	0.35
	Refluxed Tap H_2O	0.33	0.36
	Tap H_2O	0.35	0.38

Part d - Electrode Vibration Tests

A small polypropylene test cell was constructed for testing the tolerance of various electrode construction techniques to vibration. The cell had two separate chambers each containing 1-1/6" diameter electrodes immersed in electrolyte. The assembly was mounted on an MB Type "C" vibrator with a force capacity of 0 to 50 lbs for frequencies of 5 to 200 cps and displacements of 0 to 1/2".

A variety of electrodes were tested, including anodes made with no binders and several containing Teflon or an EPR latex. Electrodes were evaluated in this cell at 18, 23, and 100 cps with displacements of 0.375", 0.25", and 0.01", respectively. Vibration tests were also made in which the electrolyte level was lowered to the center line of the electrode. This resulted in violent agitation when vibrated at the higher amplitudes. In addition, a 240 mg lead ball was attached to the center of the electrodes to increase the stress on the electrode. No appreciable catalyst loss was evident in any of the tests, showing that the catalyst-electrode contact was tenacious.

Part e - Storage Tests with Ruthenium Modified P-type Catalyst

Previous testing indicated that no significant change in activity occurred as a result of storing catalyst powder in either water or 3.7 M sulfuric acid that contained 1 M methanol (6). These tests have been continuing with no change in performance having occurred after 160 days. The complete tabulation is presented in Appendix D-3.

The performance debits resulting from long term storage of anodes in sulfuric acid were also evaluated as a function of the methanol concentration in the electrolyte. These results are needed to assess the types of shutdown and storage procedures that will be required. Methanol concentrations of up to 1 M were employed.

These tests showed that electrodes stored in acid under open circuit conditions lost of the order of 10 mv when stored in electrolyte containing less than 0.01 M methanol. However, under the same conditions, about 50 mv was lost with methanol concentrations above 0.1 M. Most of this loss occurred after a relatively short storage period, remaining fairly stable thereafter. This is illustrated in Table D-3 with the more detailed performance data presented in Appendix D-3.

Table D-3

Effect of Methanol Concentration in Storage on Anode Performance

Methanol Conc, M	Performance Debit at 50 ma/cm^2, mv After Indicated No. of Storage Days			
	1	7	14	30
0	0	15	10	15
0.01	0	15	20	0
0.1	5	55	25	50
1.0	10	25	50	50

Further work is required to define the effect of storage conditions more completely. However, based on the data above and past work (6), there appear to be no serious problems.

Part f - Life Tests with Ruthenium Modified P-type Catalyst

Half cell life tests as previously reported (6) have been continued. The data are summarized in Appendix D-4. These cells are operated continuously except for a daily 15 minute open circuit, and polarization readings are recorded 30 minutes after the cell is put back on circuit. In addition, the cells are occasionally reactivated by flushing and overpolarizing in methanol-free acid.

Indications are that, operating in properly purified solutions without sustained overpolarization, these catalysts suffer a mild activity loss with time, which can be regained with the activations described. Five replicate runs of borohydride-reduced catalyst lost an average of only .005 v in life tests ranging from 5400 to 8000 hours. The two best of these are still in operation at 8000 hours and show an average improvement of .012 v. More recent tests on the hydrogen reduced catalyst, now favored for the methanol-air battery, show an average gain of .005 volts on two cells at 1100 hours, thus indicating that these more active catalysts are as good as the borohydride catalysts in terms of activity maintenance.

It is thought that trace amounts of impurities such as halides are responsible for some performance loss. The daily open circuiting of electrodes regains about .02 to .04 volts which is thought to be due to desorption of poisoning anions. Two of the three cells run with calomel reference electrodes (numbers III, IV, V) showed very substantial activity decline attributed to leakage from the reference electrode.

It seems likely that trace amounts of partial oxidation products such as aldehydes, ketones, etc, may also cause performance losses and that the activation procedure serves to burn these off of the electrode. Addition of .03 wt % of acetone and propionaldehyde caused a performance loss of .12 volts. This was recovered by the activation procedure.

Some total cell life testing has also been done. The equipment and general procedure for small, total-cell life tests was described in (6). A summary of the data is presented in Appendix D-4, and the highlights are in Table D-4.

Table D-4

Total Cell Life Tests

Cell	Current, ma/cm^2	Temp, °C	Cell Voltage			Present Life, hours
			Start	1000 hrs	Present	
1	43	60	0.44	0.43	0.39	3800
2	46	60	0.43	0.42	0.42	3800
3	85	80	0.39	0.36	0.29*	2300
4	83	80	0.43	0.40	0.25*	2800

* At 25 ma/cm^2--could not support higher current.

The cells were occasionally reactivated by washing and overpolarizing in methanol-free electrolyte, but no reactivations had been undertaken at the 1000 hour mark.

At 1000 hours, the performance of cells 1 and 2 confirms the conclusion reached previously (6), that significant deactivation does not result merely from long term operation. The substantial losses in cells 1, 3, and 4 after 1000 hours resulted from serious upsets in the normal mode of cell operation. For instance, these cells were driven for a long time during an electrolyte flow stoppage, which caused severe polarization increases. This situation occurred in the laboratory tests where the cells were driven by a constant current power supply. Cell 2 also suffered minor flow interruptions, with less serious consequences.

Phase 2 - Studies of Methanol Electrode Structure

Work has been extended to reduce the amount of noble metal catalyst in methanol electrodes for use in sulfuric acid electrolyte. Some effects of catalyst loading were determined in structures with and without non-catalytic, conductive diluent materials. Several attempts were made to increase the accessibility of the catalyst to the fuel through structural modificationsin both the catalyst and electrode. In addition, preparations of supported catalysts with low noble metal loadings on carbon were made using various reduction techniques.

Part a - Effects of Non-Catalytic Diluents

Previous studies of catalyst loading with ruthenium modified P-type catalyst showed that performance was insensitive to catalyst loading over a wide range at relatively high loadings. A minimum of 12 mg/cm^2 was required to achieve complete coverage of the electrode surface. In order to fabricate electrodes with lower catalyst loadings, non-catalytic tantalum particles were incorporated into the catalyst paste to insure enough bulk volume for full coverage and conductivity. A linear relationship between performance and catalyst content was then found down to 1 mg/cm^2 (6).

The studies with conductive fillers have been extended to include eight other materials. These were finely divided gold, tungsten, graphite, carbon, and the carbides of boron, tungsten, zirconium, and tantalum. They were chosen for their inertness and conductivity and were intimately mixed with dry, hydrogen reduced ruthenium modified P-type catalyst at levels of 5, 7, and 10 mg/cm^2 catalyst loading depending on bulk volume. Electrodes were stabilized with 0.5 wt % of 41 BX Teflon emulsion which was added to the moistened mixture. Performance of these electrodes was measured in 3.7 M sulfuric acid, 1.0 M methanol, at 60°C. Results showed large differences between the various diluents. The extreme cases were 65 ma/cm^2 for gold and 0.1 ma/cm^2 for tantalum carbide, with gold-tantalum (60 ma/cm^2) and tantalum (45 ma/cm^2) the next best, and zirconium carbide near tantalum carbide with 0.9 ma/cm^2. When using catalyst utilization as a measure, gold or gold-tantalum were best, with 6.5 and 6.0 ma/mg, respectively. Next was finely ground graphite with 5.4 ma/mg.

These results are tabulated in Table D-5 and Appendix D-7.

Table D-5

Effects of Various Diluents on Ruthenium Modified P-type Catalyst Performance

3.7 M sulfuric acid, 1 M methanol, 60°C

Diluent	Catalyst Loading, mg/cm^2	Current Density at 0.35 volts Polarization, ma/cm^2	Catalyst Utilization at 0.35 volts Polarization, ma/mg
Graphite, 50%	5	27	5.4
Carbon, 50%	5	14	2.8
Au, 80%	10	65	6.5
Ta, 80%	10	45	4.5
Au, 40%Ta, 40%	10	60	6.0
W, 80%	10	27	2.7
WC, 90%	10	17	1.7
B_4C, 90%	10	9	0.9
TaC, 90%	10	0.1	0.01
ZrC, 90%	7	0.9	0.13
None (standard)	20	120	6.0

These results show some carbides to be reactive and influencing electrode performance negatively, while most others proved to be inert. These latter show a similar utilization range to undiluted catalyst but reflect the lower performance typical for the lower catalyst content.

Part b - Effects of Two-Layer Electrodes and Various Binders

Several attempts were made to increase the available catalyst in gold or tantalum diluted electrodes by placing most of the catalyst into the upper layer of a two-layer electrode, or by using different types of binder and creating voids in the structure. Several two-layer electrodes were fabricated with loadings of 5 and 10 mg/cm^2 catalyst on top of tantalum or gold. The diluent was first pressed onto the electrode support to prepare a continuous smooth layer. Then the catalyst was spread thinly over it and the whole structure pressed again at increased pressure. In one electrode, a fraction of the catalyst was also incorporated into the bottom layer such that the catalyst content in this layer was 10 wt % with 50 wt % in the top layer.

Performances varied linearly with the amount of catalyst present, regardless of distribution throughout the structure. Data obtained with well mixed diluted electrodes and undiluted catalyst at similar loading levels were similar, indicating that no additional catalyst had been made accessible to the fuel. Values measured in 3.7 M sulfuric acid and 1.0 M methanol at 60°C were 45 and 50 ma/cm^2 at 0.35 volts polarization when 10 mg/cm^2 catalyst was used and 25 ma/cm^2 with 5 mg/cm^2 catalyst on top of a gold layer. Only 3 ma/cm^2 was obtained with 5 mg/cm^2 catalyst on top of a tantalum layer. These results are listed in Table D-6 and Appendix D-7.

Table D-6

Effect of Two-Layered Electrode Structure

3.7 M sulfuric acid, 1.0 M methanol, 60°C

Electrode Composition, wt %	Catalyst Loading, mg/cm^2	Current Density at 0.35 volts Polarization, ma/cm^2	Catalyst Utilization at 0.35 volts Polarization, ma/mg
20% cat-80% Ta (all catalyst in top layer)	10	50	5.0
10% cat-90% Ta (all catalyst in top layer)	5	3	0.6
10% cat-90% Au	5	25	5.0
20% cat-80% Ta	10	45	4.5

In another series of experiments to influence the structure and properties of electrodes, Kynar, Teflon, and Saran at levels of 3 and 5 wt % were used as binders. Some of these electrodes were also prepared with porosities between 20 and 40%. As shown in Table D-7 and Appendix D-7, all plastic additions at these levels, as well as increased porosity, caused performance debits of between 50 and 100 mv. Thus, the current density of 50 ma/cm^2 at 0.35 volts polarization in a binder free electrode dropped to 28 ma/cm^2 with 5% Saran, to 18 ma/cm^2 with 5% Kynar, and to 5 ma/cm^2 with 5% Teflon. Structures with increased porosity showed some debits, but generally

reflected the influence of the binder used. Thus, a structure with 20% porosity without Teflon showed 35 ma/cm^2, which dropped to 28 ma/cm^2 with 1% Teflon and to 1 ma/cm^2 with 5% Teflon.

Table D-7

Effect of Binder and Porosity
in Tantalum Diluted Electrodes

3.7 M sulfuric acid, 1.0 M methanol, 60°C
10 mg catalyst/cm^2, 30 and 50 mg/cm^2 total loading

Binder, wt %	Porosity Increase, vol %	Current Density at 0.35 volts Polarization, ma/cm^2
None	0	50
5% Saran	0	28
5% Kynar	0	18
5% Teflon	0	5
None	20	35
1% Teflon	20	28
5% Teflon	30	1
3% Kynar	30	4

Thus, these attempts to place more of the catalyst on the surface of the electrode or to make the structure more open to increase fuel accessibility to the catalyst were not successful.

Part c - Effects of Catalyst Loading with
Ruthenium Modified P-type Catalyst

Since previous studies of loading effect with undiluted catalysts were limited to a minimum of 12 mg/cm^2, conclusions concerning catalyst utilization limitations in present electrode structures were based on results with diluted catalyst which indicated significant performance loss at lower loadings. Special techniques were sought for preparing low loaded, undiluted catalyst loadings to assess the effect of reducing catalyst quantity in present methanol electrodes. These electrodes were prepared without binders on roughened platinum flags. The ruthenium modified P-type catalyst was dried in vacuum and spread on the flag at loadings of 4 to 40 mg/cm^2. Performances were measured at 60°C on 1 M methanol in 3.7 M sulfuric acid electrolyte.

The results were similar to those for diluted catalyst with a linear relationship between current density at 0.35 volts polarization and catalyst loading in the range 0 to 20 mg/cm^2. Performance increases leveled out at higher loadings with constant performance above 40 mg/cm^2. Polarization values ranged from 0.32 to 0.46 volts at 100 ma/cm^2 and 0.46 to 0.62 volts at 500 ma/cm^2. These results are tabulated in Table D-8 and Appendix D-8 and are plotted in Figure D-3. The values for tantalum diluted electrodes in this figure were taken from previous measurements for comparison (6).

Table D-8

Effects of Catalyst Loading with
Ruthenium Modified P-type Catalyst

Catalyst Loading, mg/cm^2	Polarization from Methanol Theory at Indicated ma/cm^2, volts					Current Density at 0.35 volts Polarization, ma/cm^2	Catalyst Utilization at 0.35 volts Polarization, ma/mg
	0	1	10	100	500		
50	0.13	0.18	0.24	0.32	0.46	170	3.4
40	0.05	0.16	0.24	0.32	0.46	160	4.0
20	0.14	0.19	0.26	0.34	0.49	120	6.0
18	0.06	0.20	0.26	0.35	0.55	100	5.4
14	0.08	0.19	0.20	0.36	0.56	80	5.7
10	0.17	0.21	0.28	0.39	--	50	5.0
6	0.16	0.23	0.31	0.42	--	25	4.3
5	0.15	0.22	0.30	0.41	0.62	32	6.8
4	0.22	0.26	0.33	0.46	--	13	3.2

Figure D-3

Effect of Catalyst Loading of
Ruthenium Modified P-type Catalyst

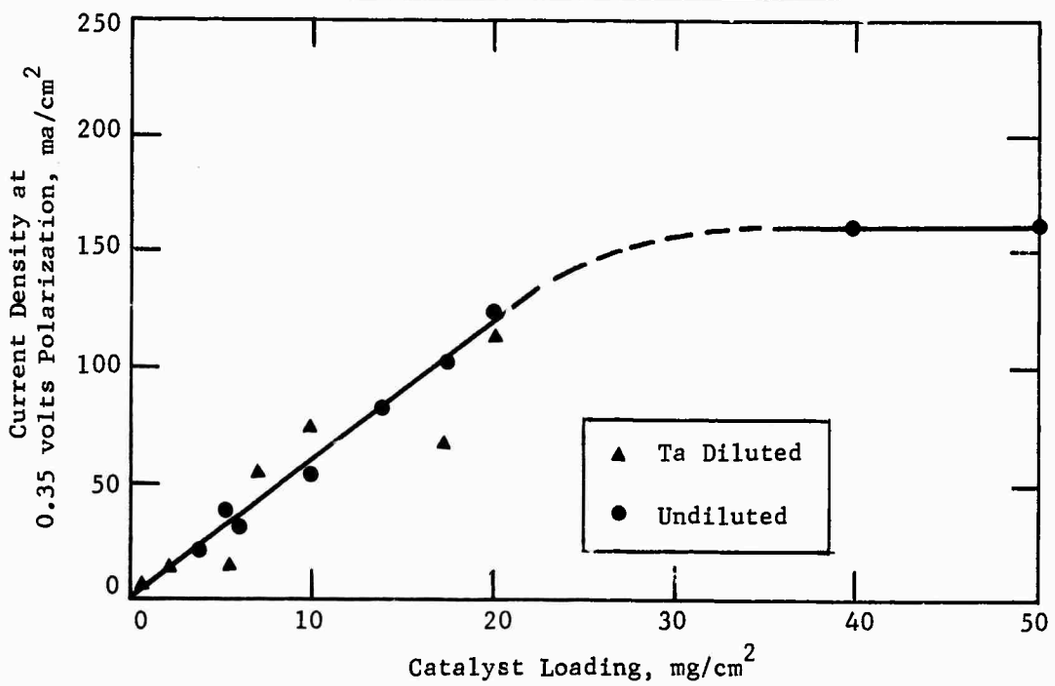

These data show that the use of tantalum had no effect upon electrode performance. They also demonstrate that the present methanol electrode with 20-25 mg/cm^2 of catalyst can be reduced by no more than one-half without an appreciable performance debit. There is a fairly constant catalyst utilization of between 4 and 6.8 ma/mg over the range from 40 to 5 mg/cm^2.

Part d - Effects of Reduction Techniques on
Activity of Ruthenium Modified P-type Catalyst

To study the influence of different reducing methods on the activity of the presently used methanol catalyst, a metal salt solution of standard composition was reduced with formaldehyde in presence of 1 M sodium aluminate, with a radical anion reagent formed from lithium and biphenyl, or with carbon monoxide in 0.0025 and 1 wt % aqueous solution. All were carried out at moderate temperatures between 25° and 70°C. In the formaldehyde reduction the effects of pH of the reaction solution and the wash solution on activity were also tested. Results indicated somewhat improved performance when the pH was adjusted to 11 instead of 8 as in previous preparations. Also, the aluminate was more completely removed after the reduction with 6 N potassium hydroxide than with 3 M sulfuric acid, which led to 50 mv higher performance at 100 ma/cm^2.

When the reduction was carried out by sparging carbon monoxide into a highly dilute solution of metal salts (0.0025 wt %), a colloidal catalyst dispersion was formed which was completely adsorbed on carbon after 12 hours. In this case, a potassium hydroxide treatment, followed by 5% sulfuric acid, gave an 80 mv debit compared to a sulfuric acid wash only.

Tests of all these compounds were made on Pt flag electrodes with a loading of 20 mg/cm^2 in 3.7 M sulfuric acid with 1.0 M methanol at 60°C. Results were compared with results from the most active catalyst prepared by hydrogen reduction Results showed almost equal performance for the two preparations. Debits of 30-40 mv with the radical anion treated material and another 100 mv debit with the carbon monoxide reduced catalyst were observed. Some typical data were 0.30 volts polarization at 100 ma/cm^2 for hydrogen reduction to 0.45 volts for carbon monoxide reduction, which corresponded to a 24 fold decrease of current density at 0.35 volts. These data are listed in Table D-9 and Appendix D-8. They show that present methods are superior to any of the other three techniques. The performance of hydrogen reduced ruthenium modified P-type catalyst has been discussed previously (6) and recent data are presented in Appendices D-5 and D-6.

Table D-9

Effect of Reducing Agents on
Ruthenium Modified P-type Catalyst

20 mg/cm^2, 3.7 M H_2SO_4, 1.0 M CH_3OH, 60°C

Catalyst Preparation	Polarization at Indicated ma/cm^2, volts					Current at 0.35 volts Polarization, ma/cm^2	Catalyst Utilization at 0.35 volts Polarization, ma/mg
	0	1	10	100	500		
H_2	0.09	0.16	0.23	0.30	0.41	240	12.0
HCHO on $NaAlO_2$, pH 8	0.09	0.20	0.26	0.33	0.48	170	8.5
HCHO on $NaAlO_2$, pH 11	0.04	0.20	0.26	0.32	0.41	210	10.5
Radical Anion Reduction	0.08	0.17	0.25	0.36	0.49	80	4.0
CO reduced in solution	0.20	0.27	0.35	0.45	0.57	10	0.5

Part e - Effect of Surface Area on Methanol
Activity for Platinum Black Catalysts

Several electrodes were fabricated with platinum blacks of known surface area, pore volume, and bulk density to determine a correlation between these parameters and catalyst activity for methanol. These catalysts had been made with formaldehyde-sodium aluminate, radical anion, hydrogen, and formaldehyde reduction. Catalyst loading varied between 20 and 70 mg/cm^2 according to bulk density. Test results obtained in 3.7 M sulfuric acid, 1.0 M methanol, at 60°C showed the highest catalyst utilization of 3.5 ma/mg at 0.45 volts polarization for catalyst reduced with formaldehyde on sodium aluminate, the lowest of 0.7 ma/mg for formaldehyde reduction in solution. These two catalysts represent the highest and lowest values of surface area and pore volume as shown in Figure D-4 and Table D-10. Appendix D-9 lists the performance of these platinum catalysts.

Figure D-4

Area Effects in Platinum Blacks

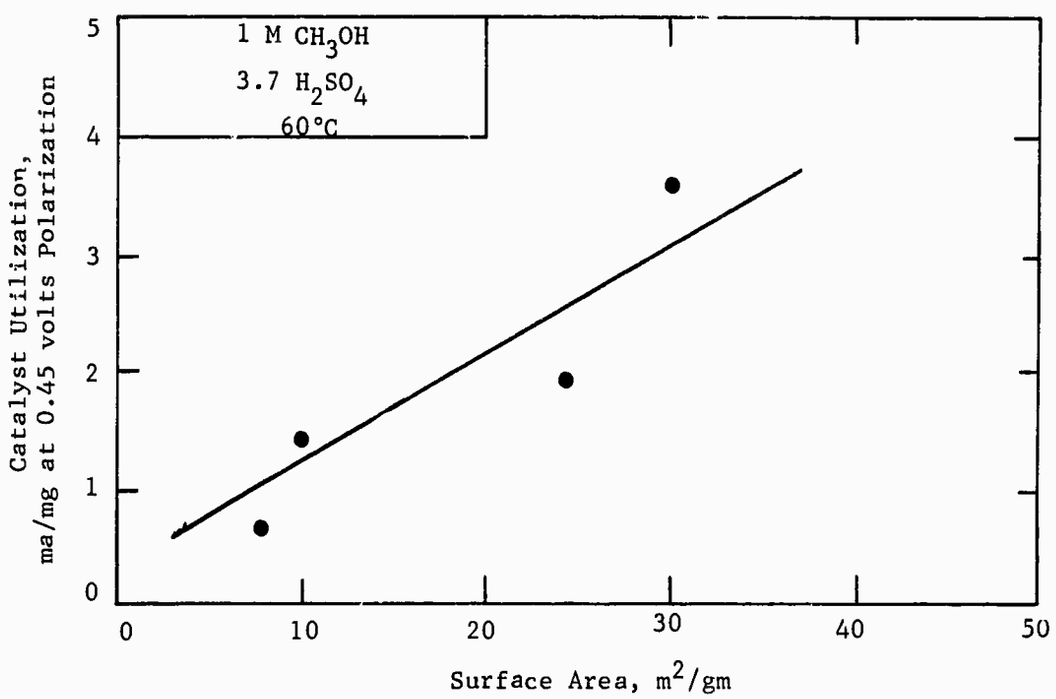

Thus, the microstructure of the catalyst is important in obtaining good utilization as in the case of hydrocarbons discussed in Task A.

Table D-10

Correlation Between Surface Area and Activity of Platinum Blacks

Catalyst Preparation	Catalyst Loading, mg/cm^2	Surface Area, m^2/gm	Pore Volume, cm^3/gm	Bulk Density, gm/cm^3	Catalyst Utilization at 0.45 volts Polarization, ma/mg
HCHO on $NaAlO_2$	20	30	0.40	0.55	3.5
Li/Biphenyl Radical Anion	38	26	0.19	0.65	1.7
Alloyed with Ag, then Ag Removed	70	10	0.05	0.65	1.4
HCHO	20	8	0.03	0.27	0.7

Part f - Performance of Supported Methanol Catalysts

After the completion of the tests with low loadings of undiluted or diluted catalyst which had shown a linear performance drop with decreasing catalyst content, experiments were conducted with supported catalyst on high surface area materials in order to disperse it in a more finely divided form. These experiments were encouraged by results with platinum catalyzed carbon where catalyst loading had been reduced by one tenth to 1.2 mg/cm^2 and performance debits of less than 40 mv were measured. This work was extended with attempts to reduce the higher performing ruthenium modified P-type catalyst on carbon. Several reducing techniques were used on impregnated carbon that had been carefully dried at 110°C before and after the impregnation with aqueous metal salt solutions. In one case, the impregnation and reduction was carried out separately for each component. In another, the carbon was preactivated with Pt. Structural changes were limited to the use of different amounts of Teflon or latex binder, vacuum drying the catalyst, and the use of boron carbide and coal as supports.

The most active catalyst was prepared by a hydrogen reduction between 130 and 250°C at metal loadings of 20 and 30% followed by a treatment with 0.01 N potassium hydroxide and sulfuric acid. This catalyst gave 0.35 volts at 10 ma/cm^2, 0.42 volts at 50 and 0.46 volts at 100 ma/cm^2 at catalyst loadings of 2 mg/cm^2. The catalyst utilization at 0.35 volts was 5 ma/mg which is the same as with 20 mg/cm^2 unsupported catalyst. These electrodes gave identical values at 1 and 2 M methanol concentration. IR-measurements using a Kordesch-Marko bridge device showed IR-values below 20 mv at 100 ma/cm^2 and around 80 to 100 mv at 500 ma/cm^2. Continuous operation at 50 ma/cm^2 of one such electrode showed a 30 mv decline after four hours and no loss in the next 20 hours. The standard electrode preparation was made with 0.5 wt % Teflon 41 BX emulsion. Larger additions of Teflon or the use of uncured butyl latex as binder at concentrations of 1 and 5% gave debits of 50 to 100 mv. Also, reductions with potassium borohydride solution, at high temperatures, or in a stepwise fashion were detrimental. Using a ballmilled coal of low conductivity as support gave large debits of 200 mv. However, boron carbide of 800 mesh particle size showed an improved open circuit of 0.03 volts polarization from theory, which is in the range of unsupported catalyst and 200 mv better than all the carbon supported compounds. All these results are listed in Appendix D-10 and Table D-11 and the effects of reduction techniques plotted in Figure D-5.

Table D-11

Performance of Supported Methanol Catalyst

3.7 M sulfuric acid, 1.0 M methanol, 60°C,
2 mg catalyst/cm^2, 0.5% Teflon emulsion

Catalyst Preparation (Reduction)	Polarization from Methanol Theory at Indicated ma/cm^2, volts					Catalyst Utilization at 0.35 volts Polarization, ma/mg
	0	1	10	50	100	
H_2 on Carbon at 125°C	0.21	0.27	0.35	0.42	0.46	5.0
Same, Vacuum Dried	0.17	0.27	0.35	0.42	0.44	5.0
KBH_4 30°C on Carbon	0.22	0.26	0.38	0.50	--	3.0
High temp reduction on Carbon	0.34	0.56	--	--	--	--
H_2 on Carbon, Stepwise Impregnation	0.19	0.27	0.39	0.51	--	2.3
Same with 2% Teflon	0.22	0.30	0.46	0.59	--	1.0
H_2 on Carbon 120°C 5% Butyl Latex	0.26	0.32	0.43	0.58	0.68	1.0
H_2 on Boron Carbide	0.03	0.25	0.35	0.47	--	5.0

Figure D-5

Effect of Reducing Technique on Activity of
Carbon Supported Ruthenium Modified P-type Catalyst

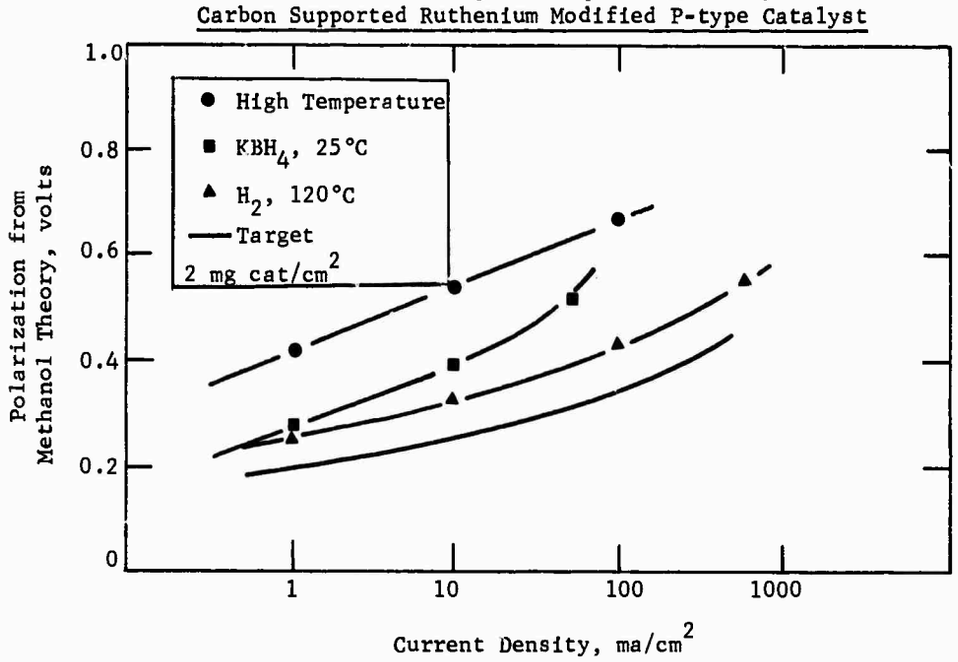

Thus, while catalyst utilization at 0.35 volts polarization has not been significantly increased as yet, these supported catalysts appear to offer a promising technique for decreasing noble metal loading.

4.5 Task E, Air Electrode

Studies have been carried out aimed at developing cathode structures which do not require the use of membrane backings. Tests have been made on several coatings, applied directly to the surface of American Cyanamid AA-1 platinum-Teflon electrodes. Additional air electrode studies, carried out in connection with the anode catalyst, buffer electrolyte, and methanol chemical oxidation programs are presented in Tasks A, C, and F.

Phase 1 - Membrane-free Electrode

The air electrode used in multicell engineering work consists of a Permion 1010 membrane carefully pressed to the electrolyte-facing surface of a Cyanamid AA-1 platinum-Teflon electrode. However, fabrication is difficult and the membrane used to prevent gross water flow is fragile, easily detachable, and expensive. Because of these difficulties, studies were initiated on methods of fabricating membrane-free air electrodes.

Part a - Preparation of Membrane-free Electrodes

The basic technique used in preparing a membrane-free electrode consisted of applying a porous, hydrophobic, acid resistant coating to the surface of a Cyanamid AA-1 electrode. Both spraying and painting techniques were used to apply Teflon, silicone, and butyl rubber coatings to the substrate electrode. The chief criteria used to evaluate these electrodes were performance and leak resistance under battery operating conditions.

Part b - Peformance Evaluations in the Absence of Methanol

Fabricated electrode polarization measurements were made in a 1" diameter half-cell test apparatus, equipped with a reflux condenser and a standard calomel electrode. The test cell arrangement and instrumentation were described in a previous report (5). Several experimental cathode coatings were tested in methanol-free 3.7 M sulfuric acid at 60 °C. These included sulfur-containing and sulfur-free butyl latexes, Silastic, and Teflon.

These electrodes were tested with their coated side in contact with the air. However, several were also tested with the coated face of the electrodes in contact with the electrolyte. In all cases, the electrode, of a given configuration, performed better when the coated side directly faced the air stream. The general level of the polarization values of the coated electrodes was somewhat higher, about 50 mv, than the average electrode fabricated with a pressed Permion membrane (when tested in methanol-free electrolyte). These results are illustrated in Table E-1, and detailed data are shown in Appendix E-1.

Table E-1

Polarization Studies of Coated Cathodes

3.7 M Sulfuric Acid - 60°C

Coating	Polarization At Indicated Current Density, volts	
	50	100
Sulfur-containing Butyl Rubber Latex	0.45	0.55
Silastic Diluted in Decane	0.47	0.51
Sulfur-free Butyl Rubber Latex	0.45	0.49
Teflon #1 3X Emulsion	0.42	0.46
Membrane Electrode	0.40	0.43

Part c - Effect of Methanol Concentration

Tests were conducted to evaluate the performance of coated electrodes in electrolyte containing different concentrations of methanol. These experiments were again carried out with the 1" diameter half-cell apparatus at 60°C.

It was found that both the Silastic-coated and Teflon-coated electrodes performed comparably to the membrane electrode. At 50 ma/cm^2 with 1 M methanol present the Silastic-coated electrode polarization was only 20 mv higher and the Teflon-coated electrode 50 mv higher than the membrane electrode. The difference in polarization was even smaller at lower concentrations of methanol as shown in Table E-2 and detailed in Appendix E-2.

Table E-2

Effect of Methanol Concentration

Electrode Description	Polarization, volts, at 50 ma/cm^2 and Indicated Methanol Concentration, M		
	0.5	0.75	1.0
Teflon-coated Cyanamid AA-1	0.51	0.54	0.56
Silastic-coated Cyanamid AA-1	0.49	0.51	0.53
Permion membrane Cyanamid AA-1	0.49	0.48	0.51

Part d - Effects of Coating Thickness

Experiments were conducted to determine the effect of coating thickness on the performance of these electrodes. A few Cyanamid AA-1 electrodes, 1" in diameter, were spray coated with "Fluoroglide" Teflon emulsion using an aerosol can while a few others were drip coated with decane-diluted Silastic using a medicine dropper. These electrodes were tested in the small 1" diameter half-cell apparatus, previously described, using electrolyte containing 1 M methanol in the Teflon series and no fuel in the testing of the Silastic series.

The results of these tests implied that the electrochemical performance of the above electrodes was relatively insensitive to changes in coating thickness. The polarization varied only by 50 mv for a 100-fold change in Teflon coating and hardly at all for a fourfold change in Silastic coating thickness. These results are presented in Appendix E-3.

On the other hand, the leak rate of electrolyte into the air chamber has been found to depend on the coating thickness. The Teflon spray coated electrodes using this "Fluoroglide" aerosol, displayed a decrease in leak rate with an increase in coating thickness whereas the reverse trend was observed with the Silastic-coated electrodes. This can be understood by referring to the photographs of the coating structure taken through a 60 power microscope. These photographs are presented in Appendix E-3, Figure E-1. They distinctly show that the sprayed Teflon deposits on the surface of the electrode in bundles of agglomerated materials. On the other hand, the Silastic coating forms a continuous film which becomes more susceptible to cracking as the coating becomes thicker. The leak rate data, presented in Table E-3, illustrate this effect.

Table E-3

Effect of Coating Thickness on the Leak Rate of Electrolyte

Coating Type	Relative Coating Thickness	Leak Rate Under a 6" Head of 3.7 M Sulfuric Acid, cm^3/min
Teflon ("Fluoroglide")	1	2
	10	1.4
	100	
Silastic	1	2.2
	4	>10

Part e - Scale-up Debit

A Silastic-coated cathode was fabricated with a 4" x 4" Cyanamid AA-1 electrode to determine the problems involved in preparing larger electrodes. This electrode and a conventional anode were assembled into a total cell assembly. The cell was tested at 60°C, using an electrolyte consisting of 0.75 M methanol in a 3.7 M sulfuric acid solution. After reaching steady state, cell voltages of 0.26 volts at 50 ma/cm^2 were attained.

Open Circuit Potential	- 0.54 volts
Total Cell Potential at 50 ma/cm^2	- 0.26 volts
Anode Polarization	- 0.28 volts
IR Loss	- 0.04 volts
Calculated Cathode Polarization	- 0.62 volts

The cathode polarization calculated by difference, was about 100 mv higher than that measured for a similar Silastic electrode when tested in the 1" half-cell. However, a 1" diameter portion of the 4" x 4" electrode tested in a smaller unit, gave a polarization of 0.57 volts, indicating that the true scale-up debit was 50 mv. The poor absolute polarization of the 4" x 4" electrode, as compared with Silastic-coated electrodes tested earlier was probably a result of the difficulty experienced in coating the large electrode.

A spray coated Teflon cathode was also scaled-up to the larger 9" x 5-3/4" size and incorporated into a total cell assembly. The cell was tested at 60°C using 0.75 M methanol in 3.7 M sulfuric acid with air and pure oxygen as the oxidizing agents. The detailed results are presented in Appendix E-4. At 40 ma/cm^2, the total cell potential was only 0.04 volts, with anode and cathode polarizations of 0.36 and 0.72 volts respectively.

It is difficult to estimate a true scale-up debit of the Teflon spray coated electrode since the emulsion used to coat the large electrode (Teflon 41 BX) differed from that used to fabricate the 1" diameter electrodes previously tested.

4.6 Task F, Methanol Fuel Cell

Further experience in testing of single and multicell assemblies has revealed a number of problems requiring further understanding or solution. Particular attention was directed toward improved multicell operation and cell design. In addition, work was continued on the development of a direct feed fuel cell.

Phase 1 - Total Cell Operation

Major efforts were centered on eliminating the ohmic loss associated with the use of tantalum screens as the anode structure, evaluating the potential performance debits of using partially immersed electrodes, and of having insufficient electrode response to methanol.

Part a - Ohmic Losses in Anode Screen Structure

The previous report (6) indicated that the use of a tantalum screen as the basic structure caused significant ohmic losses amounting to more than 0.1 volt at 100 ma/cm^2. Tests were, therefore, carried out to determine whether increasing the conductance of the paths from the catalyst to the current collector would significantly reduce this debit.

The initial experiments were carried out using the 5.7 cm^2 electrodes containing 25 mg/cm^2 of catalyst. Tantalum, gold, and gold-coated tantalum screens were employed. In some of the tests, the catalyst was diluted with 25 mg/cm^2 of gold. Measurements were made of both polarization and ohmic losses within the structure for current densities up to 1000 ma/cm^2. The results are detailed in Appendix F-1. The high current densities were employed to maintain high currents on an absolute basis in these small electrodes, comparable to the current flowing along the surface of large sized electrodes.

It was found that increasing electrical conductivity of the structure improved electrode performance and decreased internal ohmic losses. Gold coating the tantalum screen resulted in a 120 mv decrease in polarization and a 90 mv decrease in ohmic losses at 1000 ma/cm^2. The use of the gold diluent also decreased electrode polarization and the ohmic loss. However, it offered little advantage over coating the screens alone. This is illustrated in Table F-1. The problem apparently overcome was the resistance of the tantalum oxide coating on the wire surface.

Table F-1

Effect of Increased Conductivity on Performance

Screen/Gold Diluent	Polarization, volts (1)		Ohmic Loss, mv (1)	
	No	Yes	No	Yes
Tantalum	0.62	0.56	155	100
Gold Coated Tantalum	0.50	0.05	45	60
Gold	0.50	--	30	--

(1) At 1000 ma/cm^2.

These results were further confirmed in tests using electrodes 9" x 5-3/4" in size. The polarization at 50 ma/cm^2 decreased from 0.47 volts with the tantalum screen to 0.36 volt with the gold coated screens. Similarly, the ohmic loss decreased by 105 mv. These gold-coated tantalum screens proved to be only 40 mv worse in polarization and 10 mv worse in ohmic loss than platinum screens, indicating that the very thin gold coating has eliminated the contacting problem between the wire mesh and the catalyst. These data are presented in Appendix F-2.

Part b - Performance of Partially Immersed Anodes and Cathodes

In practical fuel cell applications the electrode occasionally will not be completely covered by electrolyte as a result of either changes in orientation of the battery or of leakage of electrolyte. Therefore, half cell experiments were run to determine the performance characteristics of partially exposed anodes. A normal performance curve was determined with the electrode surface completely covered with electrolyte. After part of the electrolyte was drained from the cell so that the anode was half immersed in the electrolyte, the performance was remeasured. The cell was then completely drained and allowed to stand overnight, after which it was refilled and the performance again determined. The resulting performances are shown in Figure F-1.

Figure F-1

Effect of Anode Exposure on Performance of Ruthenium-Modified P-type Catalyst

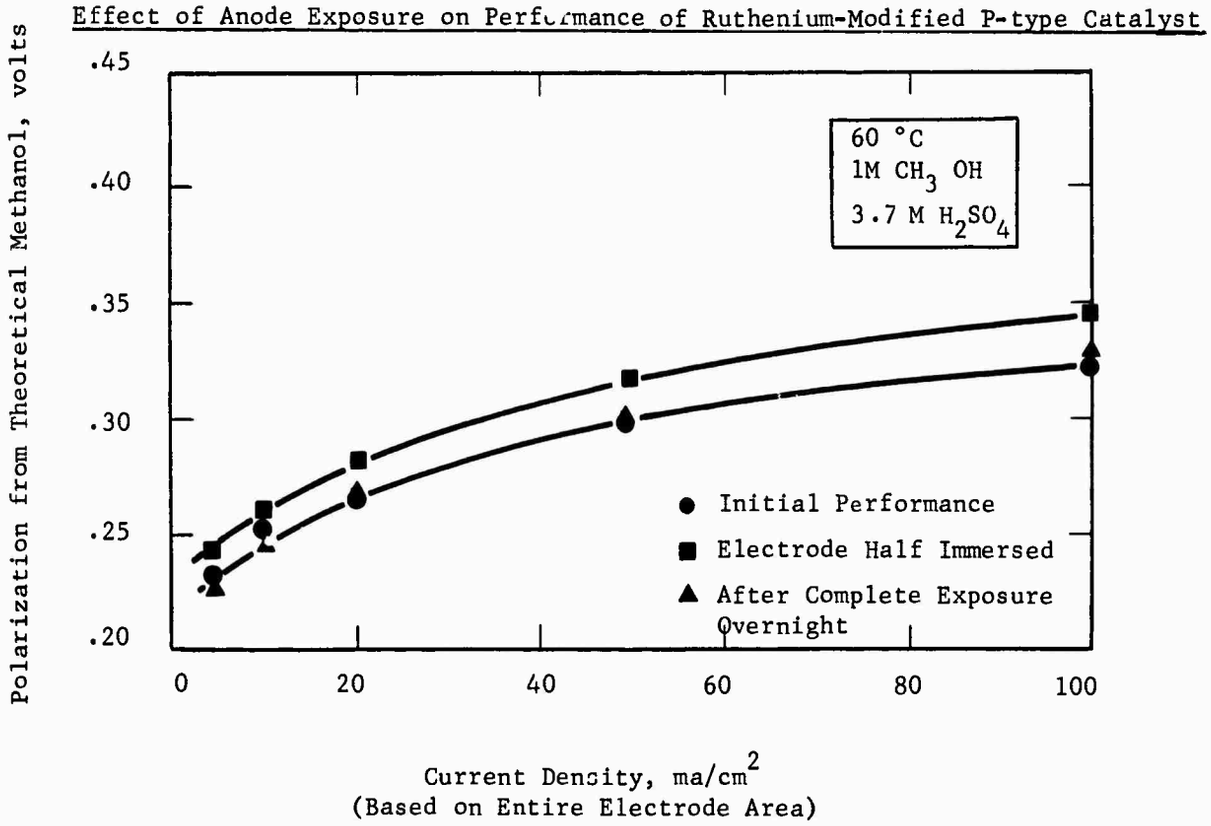

Partial immersion resulted in about a 20 mv loss in performance. This loss appears directly attributable to the loss in surface area. The resultant performance was found to be in agreement with previous results when based on the area remaining submerged in the electrolyte. Overnight exposure to the humid atmosphere of the cell caused no performance loss. Thus, it is seen that the effects of partial exposure would be proportional to the lost area, and even total exposure for moderate lengths of time causes no evident damage to the catalyst.

As part of this study, the same performance evaluations were made on an American Cyanamid AA-1 air electrode clad with the Permion 1010 membrane. These are shown in Figure F-2. Partial immersion gave performances directly predictable from the increased working current density of the immersed portion. Overnight exposure caused no serious change in performance.

Figure F-2

Effect of Cathode Exposure on Performance

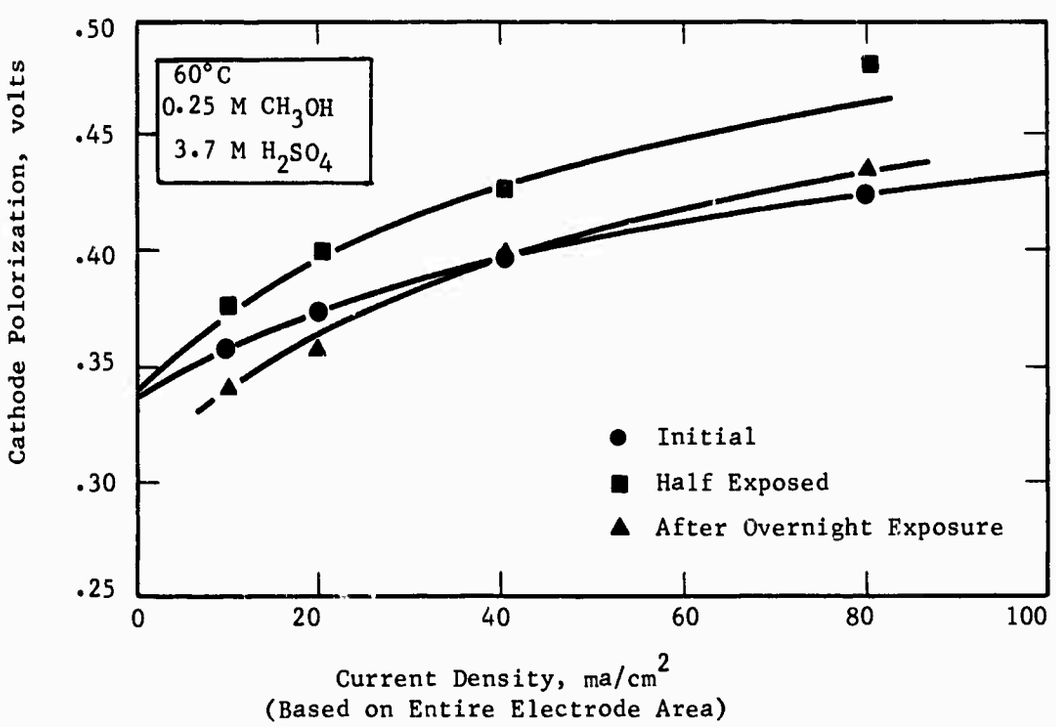

Thus, the cell components appear able to withstand upsets in electrolyte level with moderate performance declines, depending on the amount of exposed surface area.

Part c - Methanol Concentration
Dependency of 9" x 5-3/4" Anodes

Comparisons were made of the effect of methanol concentration on performance of large 9" x 5-3/4" and small 1 inch diameter electrodes. This was prompted by the fact that anodes in the sixteen cell stack required higher methanol concentrations than expected. Tests were therefore carried out using well stirred fuel chambers in half cell tests to determine whether this debit was associated with scale-up of the electrodes or with poor fuel distribution within a cell of the multicell unit. The half-cell facilities employed were described in previous reports (5, 6).

Comparable results were found in the performance of the 9" x 5-3/4" anodes in the well-stirred half-cell and in the sixteen cell multicell units. Using 1 M methanol, both systems were polarized about 0.31 volts at 40 ma/cm^2, compared with only 0.30 volts for the small 1 inch diameter anodes. However, when the methanol concentrations were reduced to 0.25 M, the larger anodes in both systems were polarized 0.45 volts compared with only 0.32 volts for the small electrodes. These data are shown in Figure F-3 and detailed in Appendices D-1, F-3, and G-10.

Figure F-3

Effect of Methanol Concentration on Anode Performance

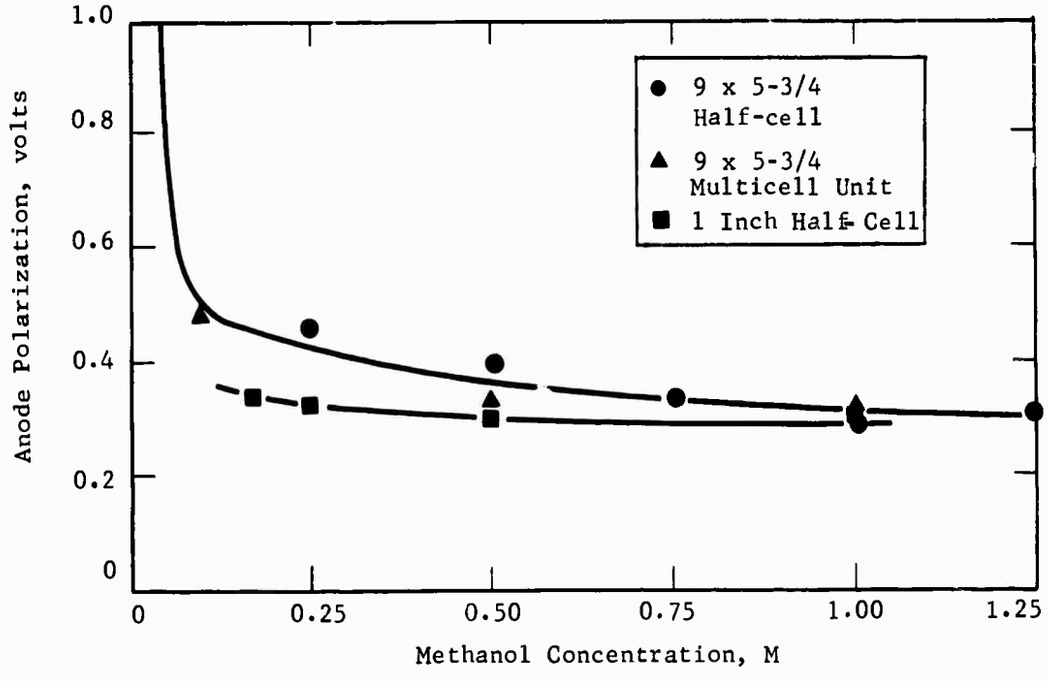

These data indicate that contacting of methanol with the catalyst is impaired in the large electrodes, perhaps as a result of the larger carbon dioxide evolution and hydrostatic heads, and that improved structures are required to make better use of methanol at the anodes.

Part d - Effects of Methanol at the Cathode

The diffusion of methanol to the cathode and its subsequent consumption has been a recurring problem in using the soluble fuel (1 to 6). This results in reduction of cell voltage and coulombic efficiency. Therefore a study of this reaction was made with the present methanol fuel cell components in order to determine its basic characteristics. These tests were made in a well-stirred half cell assembly similar to cells described previously (5). A constant, uniform methanol concentration was maintained in the stirred anolyte adjacent to a Permion 1010 membrane clad cathode. The performance of the cathode was measured and the conversion of methanol to carbon dioxide was determined.

The effect of methanol concentration in the stirred anolyte between the anode and cathode on the performance of the cathode is shown in Figure F-4. Low methanol concentrations of 0.125 M or less result in less than a 25 mv polarization increase at 40 ma/cm^2. However, higher concentrations can result in substantial losses, for example 120 mv for 1 M methanol. These results are tabulated in Appendix F-4.

Figure F-4

Effect of Methanol on Cathode Performance

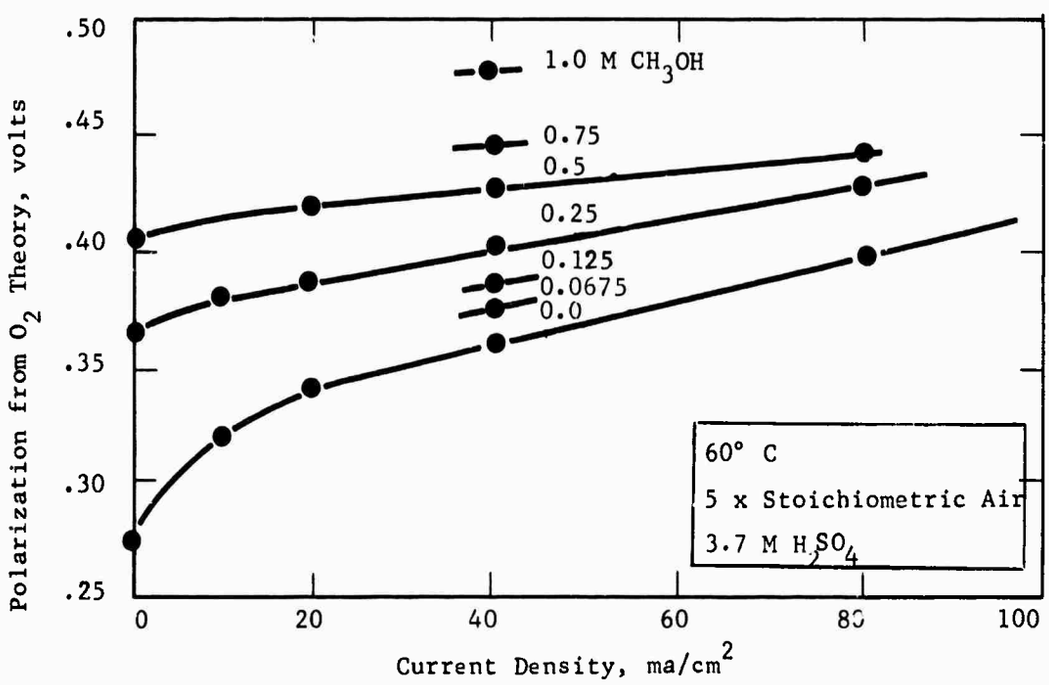

The loss of fuel due to direct oxidation of methanol at the cathode was also determined by measuring the oxygen and carbon dioxide contents of the effluent air stream as described in Appendix F-5. Figure F-5 shows that the rate of direct methanol oxidation increases linearly with the methanol concentration in the well-stirred anolyte. The rate is expressed in terms of the current density that would be produced if the same methanol consumption went to produce useful electrical energy by electrochemical oxidation at the anode.

Figure F-5

Effect of Methanol Concentration on Direct Oxidation at the Cathode

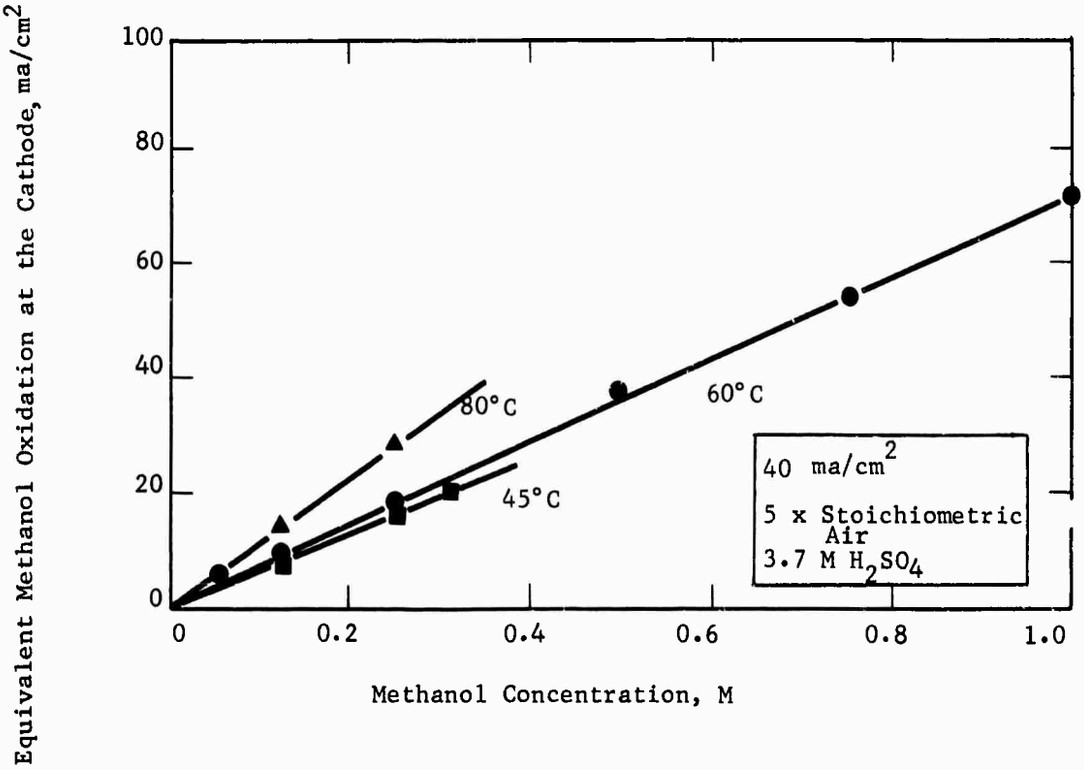

This linear dependence of rate on concentration suggests that the overall reaction rate is controlled by diffusion of methanol through the interface maintaining membrane which is pressed against the cathode.

The effect of current density on the direct oxidation of methanol at the cathode was found to be negligible over the range 0 to 80 ma/cm^2 as shown in Figure F-6. This also shows that the rate is not potential dependent over this range of operation of the electrode, 0.79 to 0.85 volt from hydrogen.

Figure F-6

Effect of Current Density on Direct Oxidation of Methanol at the Cathode

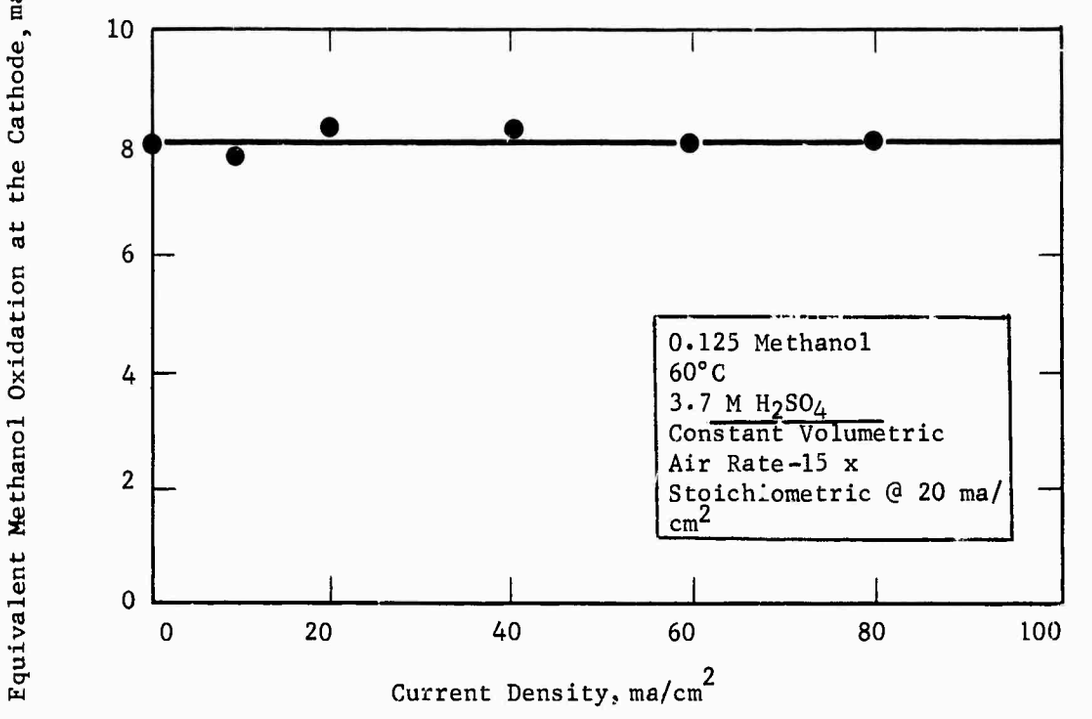

However, increased volumetric air flow at a given current density did result in increased rates of methanol oxidation as shown in Figure F-7.

Figure F-7

Effect of Air Rate on Direct Methanol Oxidation

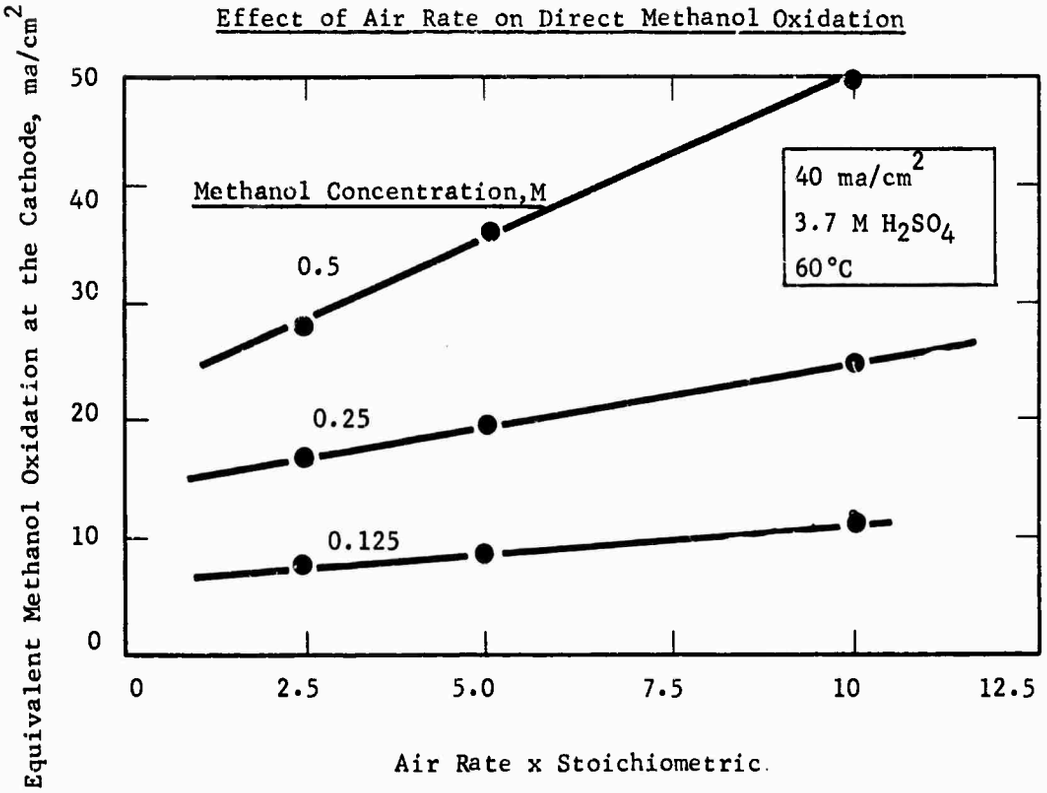

While this does not agree with the simple diffusion mechanism of methanol through the membrane, it is possible that the other factors affecting methanol and electrolyte transport in the cell are affecting this simplified picture.

Nevertheless, these half cell studies do confirm the findings in total cells that excessive transport of methanol to the cathode can cause substantial losses in methanol-air fuel cell performance. Effective control of methanol concentration in the anolyte and reduction in diffusion rates appear to be the best means for controlling this reaction.

Part e - Effect of Using Surfactants on Total Cell Performance

A small performance decline after three to four hours of operation occasionally occurred during the initial testing of the sixteen cell methanol battery. Normal performance was regained after open-circuiting the battery for about one hour. The suspected cause of this decline was holdup of carbon dioxide bubbles within the cell chambers. These bubbles probably covered a portion of the electrode surface thus restricting the access of electrolyte. One possible remedy tested was to reduce electrolyte surface tension to allow release of smaller, more mobile gas bubbles from the anode surface. Therefore, a study was made to determine the effect of FC-95 surfactant on the operation of a methanol cell.

The tests were run in a glass cell using 5.7 cm^2 electrodes and 1 M methanol in 3.7 M sulfuric acid at 60°C. The cell design is shown in Appendix F-6. As shown in Table F-2, adding 0.05 wt % FC-95 reduced cell voltage by 20 mv due to decreased cathode performance. Lowering the electrolyte surface tension adversely affected the position of the gas-liquid interface within the cathode. Consequently, surfactant studies were not carried out in the sixteen cell stack. Complete data are given in Appendix F-7.

Table F-2

Effect of Surfactant on Methanol Cell Performance

FC-95 Surfactant Concentration, wt %	Performance, ex IR, at 50 ma/cm^2, volts(1)		
	Cell Voltage	Electrode Polarization from Respective Theory at 50 ma/cm^2	
		Anode	Cathode
0	0.40	0.30	0.47
0.05	0.38	0.30	0.50

(1) 1 M CH_3OH in 3.7 M H_2SO_4 in anolyte chamber at 60°C. 5 times stoichiometric air rate.

Phase 2 - Direct Feed Methanol Cell

An alternative method of operating a methanol-air fuel cell is by direct addition of methanol fuel to the anolyte in the cell. This is in contrast to the present mode of operation in which the fuel-electrolyte solution is circulated between the cell and an external sump. Direct fuel addition to the cell would eliminate the need for an electrolyte pump and represents a potentially simpler type of operation, particularly for low power units. While research to develop an effective electrolyte pump has been encouraging, studies of direct feed have continued to assess its utility in methanol cell operation.

Part a - Comparison of Direct Feed with Circulating Fuel-Electrolyte

A key requirement in a direct feed cell is the avoidance of large methanol concentration gradients in the anolyte. Uniform concentration, such as that achieved in the circulating cell is necessary to produce good anode performance and minimize methanol loss to the cathode. The initial studies of this problem were reported previously (6). The 4" Teflon direct feed cell used in the present work was designed as a result of these studies and is shown in Figure F-8. It utilizes two porous Teflon diffuser elements for methanol fuel injection while minimizing back flow of water and electrolyte. These elements are carefully sealed in the cell wall to prevent leakage. This cell is equipped with an external circulating system so that it can be switched from direct feed to circulating fuel-electrolyte operation. In this way, a convenient comparison between the two modes is possible.

Figure F-8

Direct Feed Methanol Cell

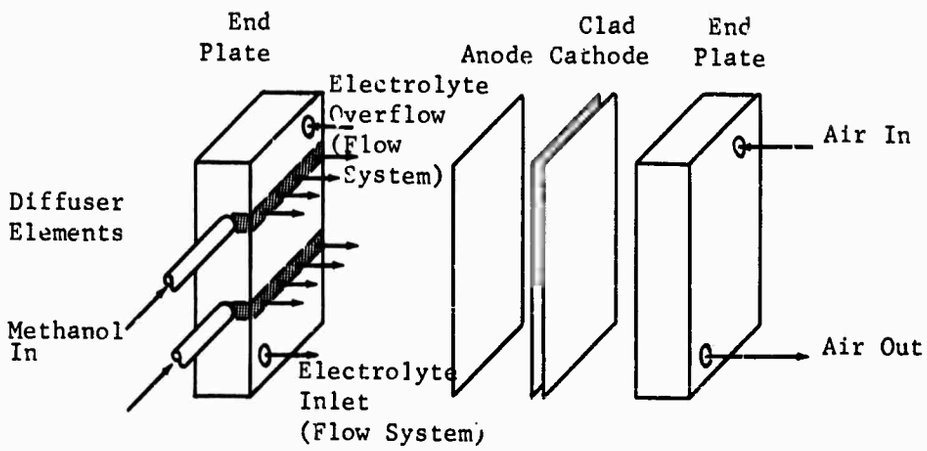

With this cell, several comparisons were made between direct feed and circulating operation. Cell voltage, anode polarization, and methanol oxidation at the cathode were determined. These data are presented in Appendix F-8. Both types of operation generally performed at similar levels in all of these comparisons. However, methanol loss through oxidation at the cathode remained high for both modes of operation. Thus, chemical oxidation varied from 20 to 100% of the electrochemical oxidation depending on the sample of Permion 1010 membrane used. The best performances in the same cell assembly are compared in Table F-3.

Table F-3

Comparisons of Direct Feed and Circulating Fuel-Electrolyte

60°C, 3.7 M H_2SO_4

	Direct Feed	Circulating
Current Density, ma/cm^2	40	40
Cell Potential, volts	0.47	0.45
Anode Polarization from Theory, volts	0.31	0.33
Cathode Polarization from Theory, volts	0.40	0.39
Chemical Oxidation of Methanol at the Cathode, equivalent ma/cm^2	10	8
Feed Rate	1.2 x stoichiometric	0.5 M methanol in 3.7 M H_2SO_4 50% electro-chemical conv. per pass

Part b - Studies with Methanol Diffusion Barriers

As a result of the half cell studies on methanol oxidation at the cathode discussed in Phase 1, Part d, two types of methanol diffusion barriers were tested in this cell in preliminary experiments aimed at reducing the fuel loss. These barriers were placed in the interelectrode space between the anode and membrane clad cathode. One of the barriers used was a Dacron felt, about 60 mils thick, which was intended to eliminate convective currents and thereby effectively lengthen the methanol diffusion path. The alternate approach was to use an immobilized electrolyte in the interelectrode space. This electrolyte was a gel made from 3.7 M sulfuric acid and polyethylene oxide, Polyox.

Both techniques were successful in reducing methanol oxidation at the cathode. The Dacron felt cut fuel loss to an equivalent 4.4 ma/cm^2, about one-half that observed in the best previous direct feed test. Excellent anode performance was obtained indicating good methanol distribution, 0.28 volts polarization at 40 ma/cm^2. However, cell performance was somewhat lower than expected, 0.43 volts at 40 ma/cm^2. The immobilized electrolyte in circulating fuel-electrolyte was even more effective in reducing methanol loss to as little as an equivalent 1.5 ma/cm^2 with similar anode and cell performance. However, the gelled electrolyte was not stable and performance declined with time. These data are compared in Table F-4 and summarized in Appendix F-3.

Table F-4

Effect of Diffusion Barriers
on Methanol Cell Performance

60°C, 3.7 M H_2SO_4

	Dacron Felt	Polyox Gel
Current Density, ma/cm^2	40	40
Cell Potential, volts	0.42	0.43
Anode Polarization from Theory, volts	0.28	0.29
Chemical Oxidation of Methanol at the Cathode, equivalent ma/cm^2	4.4	1.5

Thus, a direct feed cell can give comparable performance to the circulating cell, even at low levels of methanol oxidation at the cathode. As such, it represents a potential alternative approach to methanol-air fuel cell operation.

Part c - Natural Air Convection Methanol Cells

A further simplification in methanol cell operation would result from the elimination of the forced air system. Therefore, a test was made to evaluate the performance of a methanol-air cell operating with natural convective air flow. The test was made with direct methanol feed in a standard cell assembly except that the air chamber was removed to permit easy access for diffusion of oxygen to the cathode surface. Thus, this cell was operating with no auxiliaries. Cell performance is shown in Figure F-9 and the data are summarized in Appendix F-8.

Figure F-9

Performance of Natural Air Convection Methanol Cell

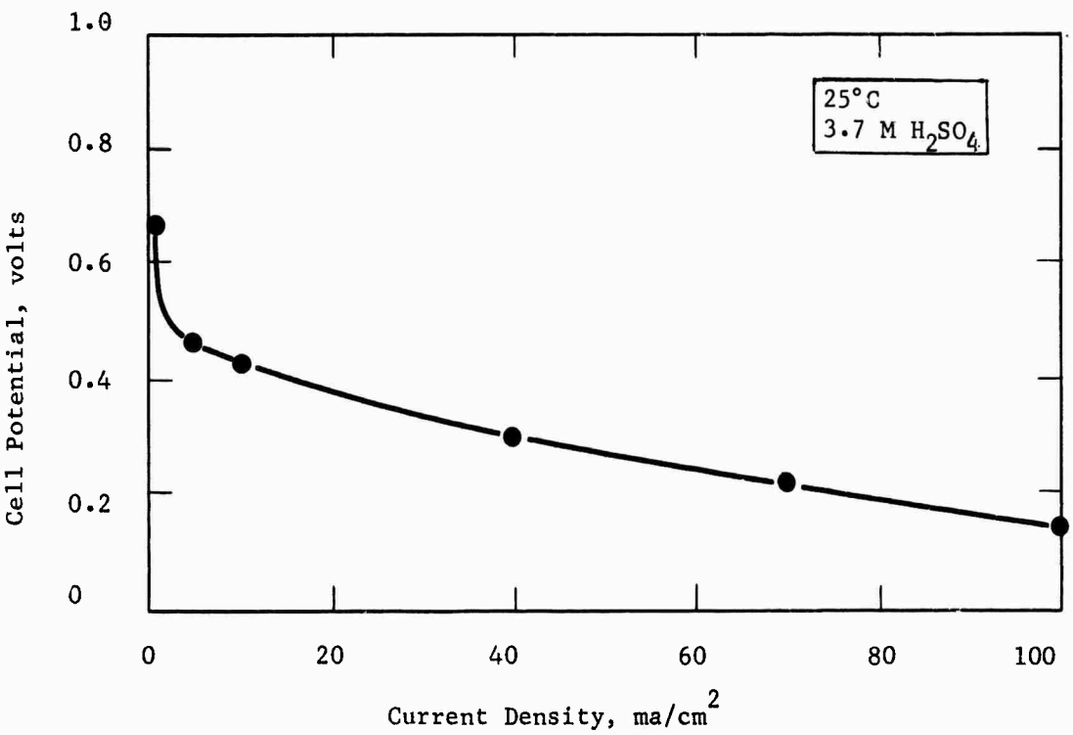

While this performance is poorer than in previous studies at about 25°C with forced air circulating, this cell was able to generate up to 14 $mwatt/cm^2$. It shows that substantial current densities, up to 100 ma/cm^2, can be sustained without auxiliary power. This type of operation might prove useful in aiding startup.

4.7 Task G, Prototype Development

Engineering research has continued on the development of a methanol-air prototype fuel cell stack, its auxiliaries, and controls. Emphasis has been placed on improving the operation of multicell units containing sixteen cells.

Phase 1 - Self-Contained Methanol Multicell Unit

A sixteen cell methanol multicell unit was constructed, its performance evaluated, and then delivered to the U.S. Army Electronics Command in January, 1965. The technology leading to the designs of the individual components and the operating procedures is discussed in this and previous semi-annual and final reports (1 through 6).

Part a - Description of the Multicell Assembly

The unit, as delivered, consisted of two parts, a Multicell Assembly and an Auxiliary Rack. The Multicell Assembly, shown in Figure G-1, was a finished piece of hardware, 11-1/4" wide x 12" high x 11-1/2" deep. It housed the sixteen cells and the air blower. These components were engineered into the unit. They occupied about sixty percent of the available volume.

Figure G-1

Methanol Multicell Assembly

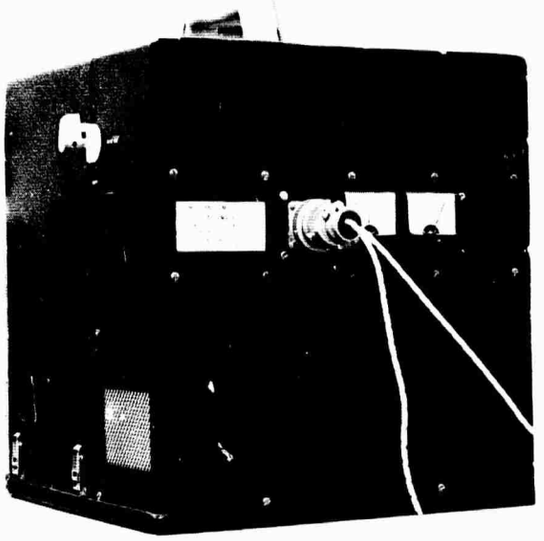

The remaining empty volume served to represent space that will be required by the methanol feed and water balancing systems. These have not yet been engineered into the assembly. Their components were mounted on the Auxiliary Rack. Descriptions of the Multicell Assembly, the Auxiliary Rack, and their operation are presented in greater detail in Appendices G-1 and G-2.

Part b - Components of the Methanol Multicell Unit

Several modified components and procedures were used in the assembly of the Methanol Multicell Unit. The sixteen 9" x 5-3/4" anodes were loaded with 25 mg/cm^2 of the ruthenium modified P-type catalyst pressed at 3000 psi, without a binder, into gold-plated tantalum screens. Half-cell data, discussed previously in Task F, showed that gold plating considerably reduced the ohmic losses usually obtained with plain tantalum screens. Previous studies showed that no significant advantages in anode performance or life were obtained by using higher catalyst loadings, lower pressing pressures, or Teflon binding agent (6). American Cyanamid AA-1 electrodes were used as cathodes. Electrolyte-equilibrated Permion 1010 membranes were pressed carefully to the cathodes at 1500 psi. Sheets of 20 mil thick filter paper were used as platen-facing to equalize the pressure distribution, thus preventing membrane rupture by the cathode screen structure. To further insure against membrane damage, the current collectors were not pressed together with the membranes and cathodes. Instead, they were attached to an additional polypropylene spacer placed in the cathode compactment. These spacers were also used in the anode compartments and served to distribute more equally the pressure of the rib-type polypropylene springs on to the current collector. Thus, better contact was obtained between the electrodes and the current collectors.

Finally, the carbon dioxide escape slots on top of the anodes were raised above the electrolyte level. This prevented methanol-containing electrolyte from circulating between the anode fuel chamber and the inter-electrode space, where methanol might contact the cathode and be consumed.

Part c - Performance of the Methanol Multicell Unit

The performance of the Methanol Multicell Unit was determined prior to delivery to the U.S. Army Electronics Command. The unit delivered 50 watts output immediately upon startup from ambient conditions. After 50 minutes of operation, power outputs of close to 100 watts were sustained. The performance characteristics during these tests is shown in Figure G-2.

Figure G-2

Performance of Multicell Unit

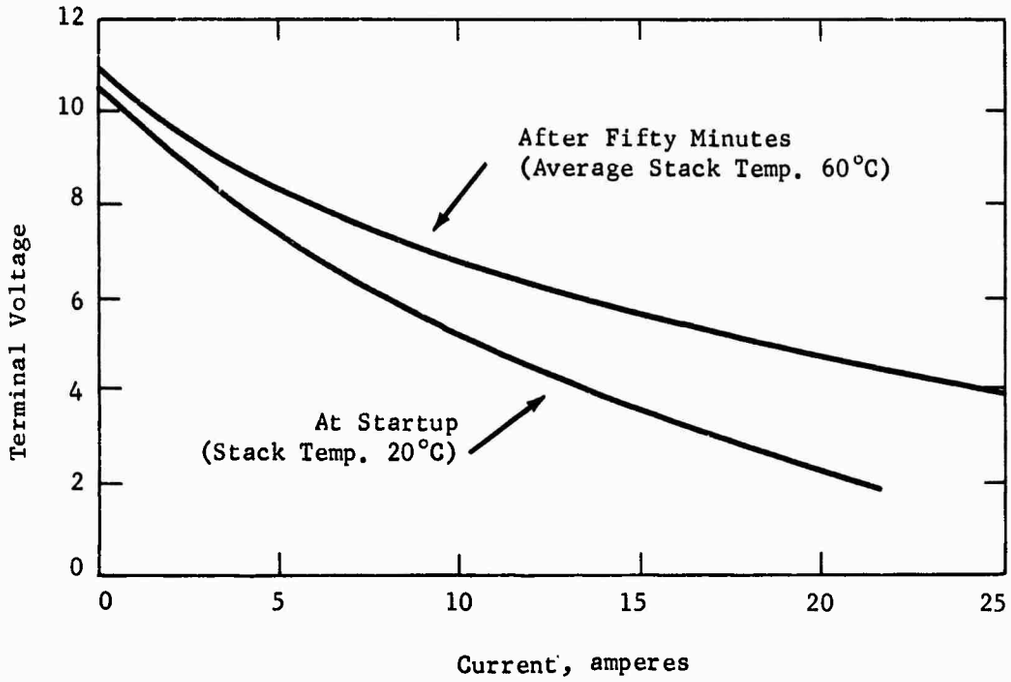

The substantial improvement in performance over that obtained in prior units is attributed to the improved anode structures. As shown in Figure G-3, average cell voltage at 50 ma/cm^2 increased from 0.19 volts to 0.35 volts upon substitution of gold-plated tantalum screens for the conventional tantalum screens. About 70% of this increase resulted from the reduced ohmic losses in the anode, as discussed in Task F, Phase I. Additional data are given in Appendices G-3 and G-4.

Figure G-3

Effect of Gold-Plated Tantalum Screens on Performance of Multicell Unit

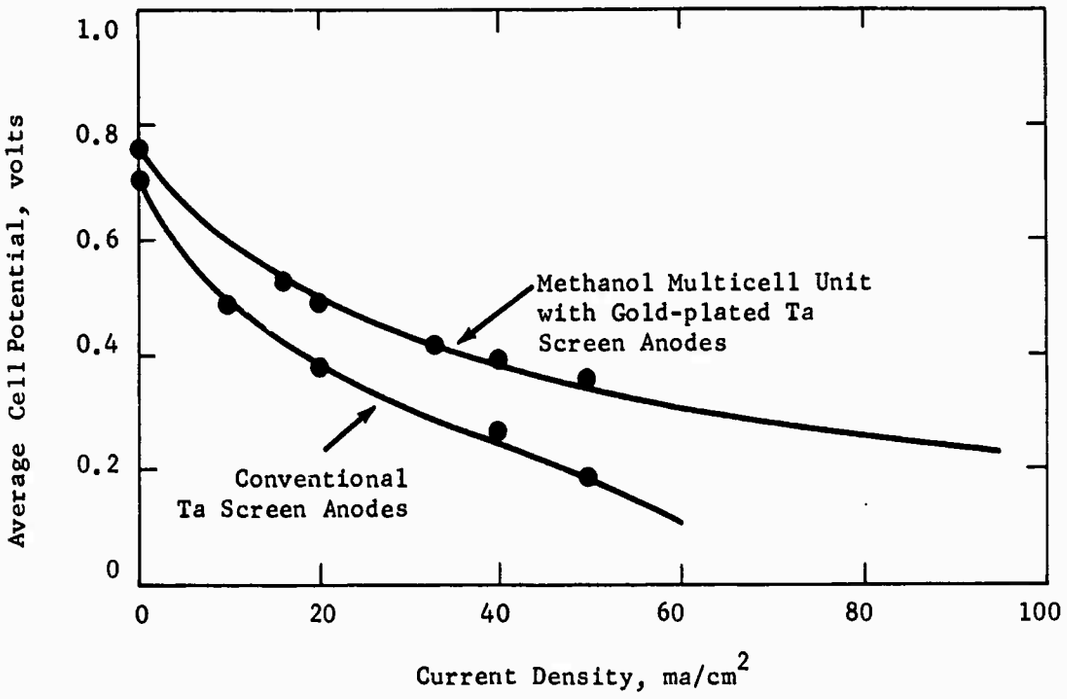

Phase 2 - Operating Characteristics of Sixteen Cell Stack

A second sixteen cell stack containing 9" x 5-3/4" electrodes was assembled to test more fully the performance, and the effects of the major operating variables on the operating characteristics of larger units.

Part a - Performance of Sixteen Cell Stack

The assembly procedures and modified components used in this unit were substantially the same as those employed for the Methanol Multicell Unit described in Phase 1. One exception was the use of a more thoroughly washed ruthenium modified P-type anode catalyst prepared with hydrogen reducing agent. The average performance of this catalyst at 50 ma/cm^2 was 0.29 volts polarized compared with 0.31 volts for the catalyst used previously.

The new stack performed significantly better than the assembly described in Phase 1. Initial testing showed that average cell voltage at 50 ma/cm2 was 0.41 volts, compared with 0.46 and 0.50 volts, the best results obtained previously in single 9" x 5-3/4" and 4" x 4" cells, respectively. These data are illustrated in Figure G-4. Additional details are given in Appendix G-5.

Figure G-4

Comparative Performances of Methanol Fuel Cells

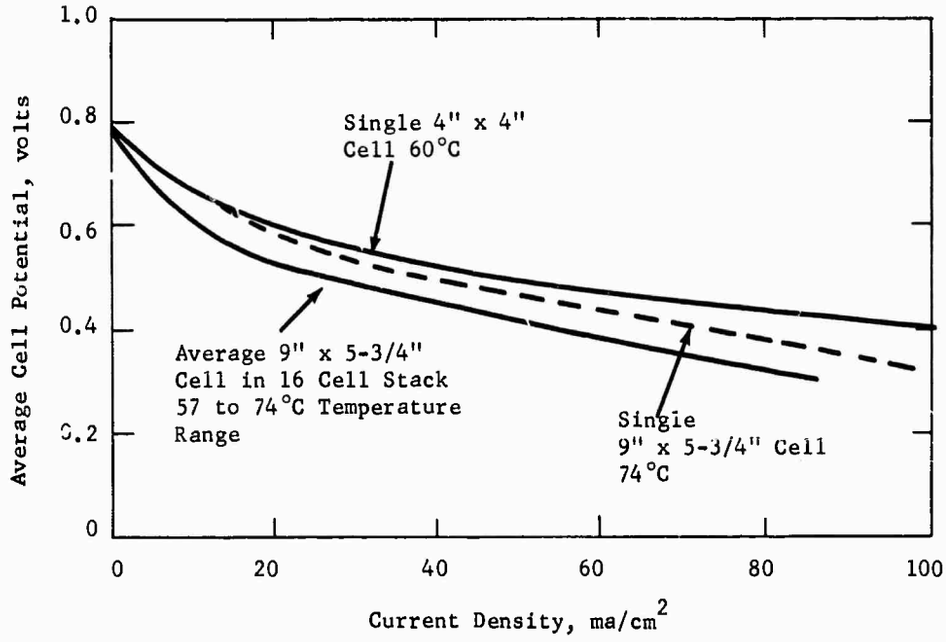

In terms of practical output, the battery delivered 120 watts maximum power at about 5 volts, as shown in Figure G-5. This is equivalent to a power density of about 25 mwatts/cm^2. For comparison, maximum power levels of 40 mwatts/cm^2 have been reached in single 4" x 4" cells.

Figure G-5

Power Output of Sixteen Cell Stack

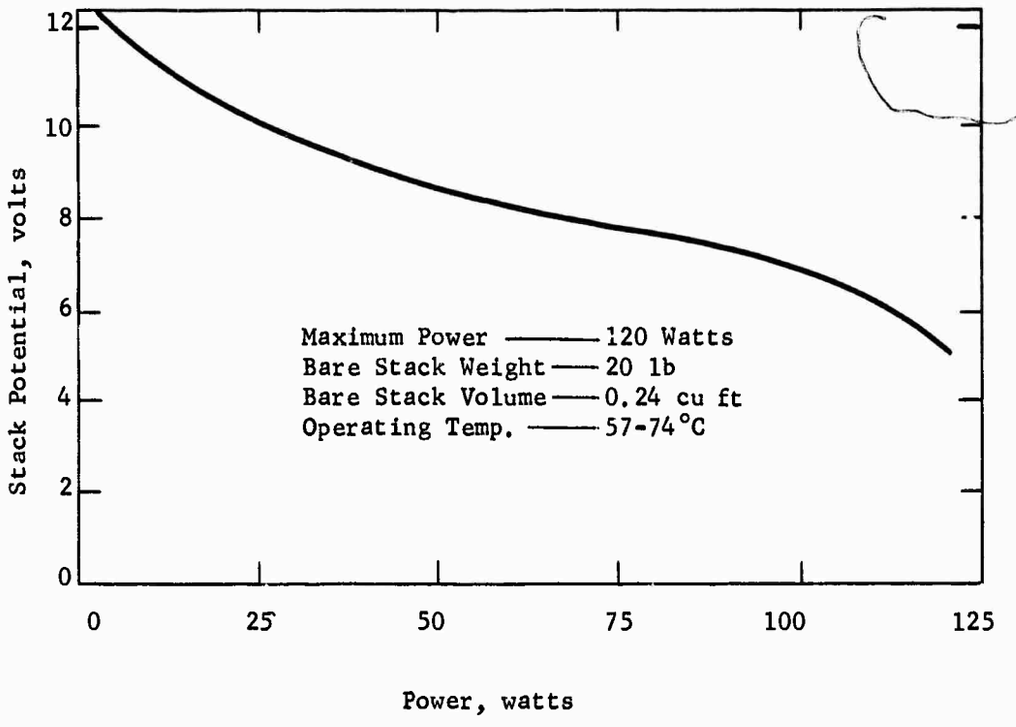

Electrode polarization was the major source of performance loss within the methanol stack. For example, at 50 amps/ft^2, ten times stoichiometric air rate, 0.25 M methanol feed, and 50% conversion per pass, an average cell in the sixteen cell stack produced 0.41 terminal volts. At these conditions, typical electrode polarization losses were 0.31 volts for the anode and 0.42 volts for the cathode. An ohmic loss of 0.06 volts also existed. Figure G-6 shows the distribution of cell voltage losses as a function of current density.

Figure G-6

Distribution of Losses in Sixteen Cell Stack Performance

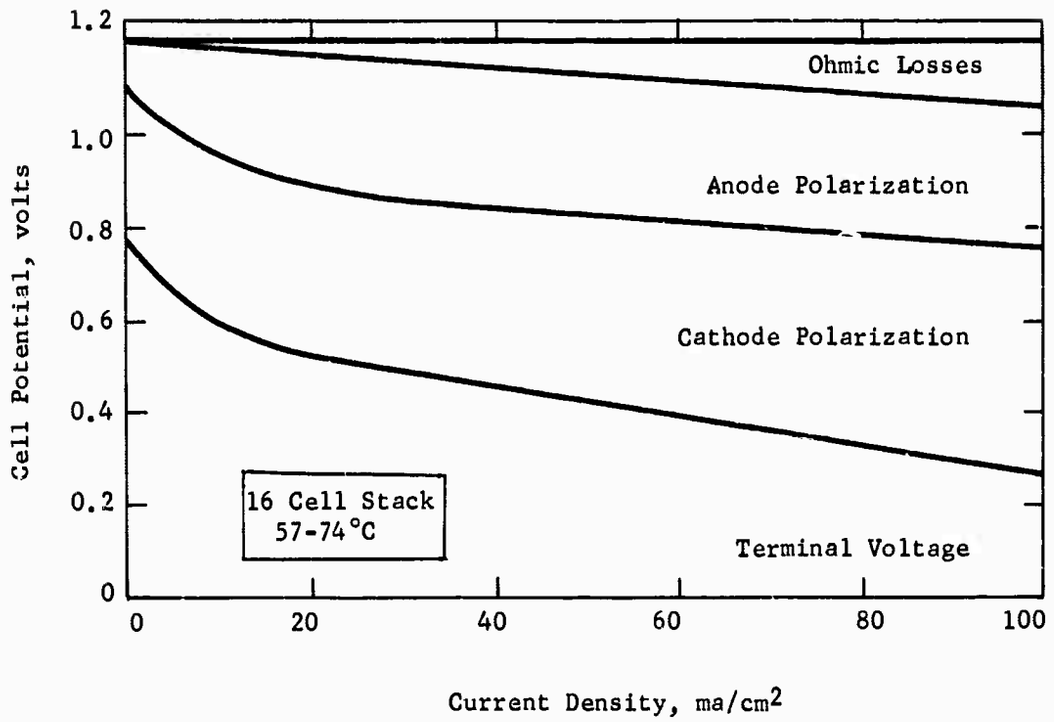

Battery performance was stable with time. As shown in Figure G-7, average cell voltages declined only 30 mv after 275 hours on current load, or a total stack life of four months. Stack behavior was studied intensively during this period and occasionally the stack was operated under severe conditions of methanol and air starvation. Nevertheless, maximum power after these tests averaged 111 watts, about 6 percent lower than initially. Detailed data are given in Appendix G-6.

Figure G-7

Performance Stability with Time

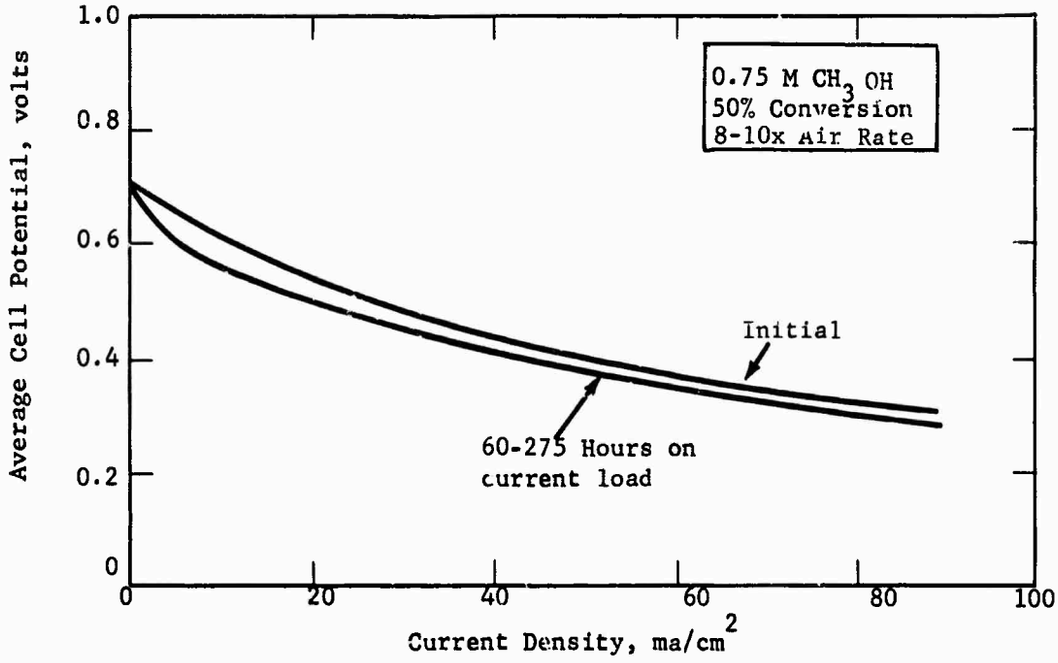

Stable anode structures were probably responsible for the low performance decline of the sixteen cell stack observed during this period. Fifteen of the 9" x 5-3/4" anodes were found to be essentially intact upon inspection when the stack was disassembled after 213 hours on current. Catalyst retention was excellent; only one anode showed signs of catalyst loss.

The gold-plating on the tantalum screens was also examined and found to be intact. This probably contributed to the rather stable ohmic losses obtained in the stack and shown in Table G-1. Previous data with a stack containing anodes prepared with plain tantalum screens showed increases in ohmic losses of 30 mv at 100 ma/cm^2 during the first 94 hours on current (6). Complete ohmic loss data are given in Appendix G-7.

Table G-1

Ohmic Loss Data for Sixteen Cell Stack

Stack Operation on Current, hours	Average Ohmic Loss per Cell at 100 ma/cm^2, mv
1	114
20	117
45 to 213	126

Part b - Effect of Major Variables on Performance

The methanol fuel cell battery must be able to provide stable performance, that is, be insensitive to large changes in key operating variables such as electrolyte, methanol, and air flow rates. This, in turn, will minimize requirements for adequate battery control. Therefore, tests were made to determine the effect of major process variables on the performance of the sixteen cell unit.

Inlet methanol concentrations to the sixteen cell stack were varied in once-through operation from 0.25 to 1.25 M methanol in 3.7 M sulfuric acid. Electrolyte flow rates were varied to give 25 to 75 vol % nominal methanol conversion per pass through the cell. Wide ranges of methanol conversion rates and inlet methanol concentrations were tolerated without seriously impairing stack performance. Figure G-8 shows that maximum performance was maintained over a twofold change in inlet methanol concentration, from 0.5 to 1.0 M, and a threefold change in methanol conversion rate, from 20 to 60 vol % per pass, through the stack.

Figure G-8

Effect of Methanol Concentration and Conversion Rate on Stack Performance

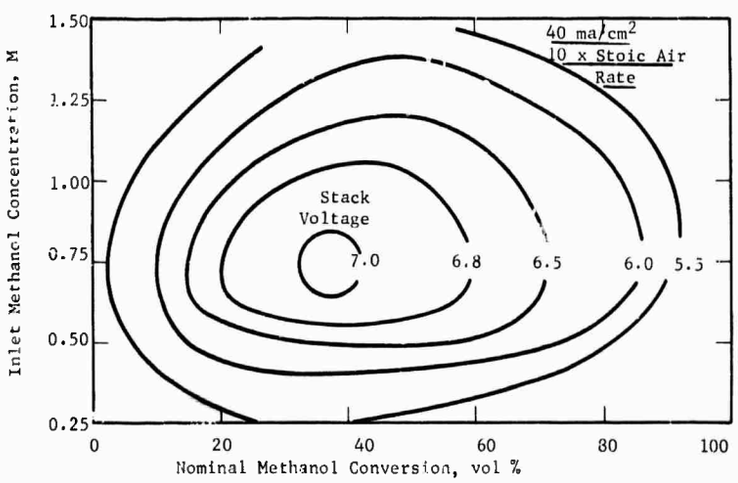

At low methanol concentrations and high conversion levels, the methanol electrodes showed signs of fuel starvation. For example, at a conversion level of 50 vol %, average anode polarization increased from 0.30 volts at 1.0 M inlet methanol concentration to 0.44 volts loss at 0.25 M methanol. On the other hand, reducing methanol concentration improved cathode performance by limiting the amount of methanol that reached the cathode by diffusion through the anode. As a result of these self-compensating effects, the performance of the sixteen cell stack was optimum at about 0.75 M inlet methanol concentration, as shown in Figure G-9. Complete data are given in Appendices G-8 to G-10. The effect of methanol concentration on electrode performance is also discussed in Task F.

Figure G-9

Effect of Methanol Concentration on Cell and Electrode Performance

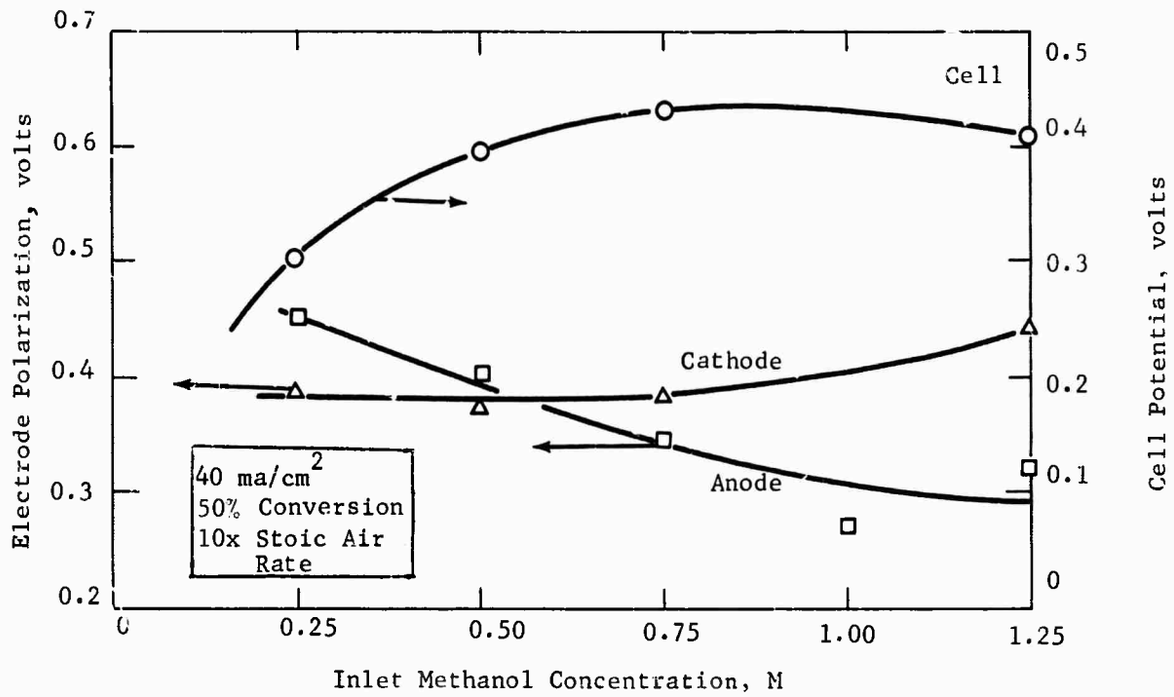

Part c - Fuel Distribution in Sixteen Cell Stack

Uniform supply of fuel to each of the cells in the stacked assembly is important for maximum stack performance. Previous studies indicated that fuel maldistribution might be a problem. However, these data were confounded with possible anode composition effects (6). Therefore, the possible existence of fuel maldistribution was restudied using the present sixteen cell stack.

Anode polarization data showed that significant maldistribution problems did not exist. This is shown in Figure G-10, where the equivalent anode polarizations at 60°C are plotted versus cell position for two runs at 40 ma/cm^2, 50 vol %

conversion, and 0.25 M or 0.75 M methanol inlet concentration, respectively. The low concentration data are particularly important, because minor maldistribution problems should be magnified during operation with methanol deficient concentrations. Complete data are listed in Appendix G-8 to G-10. Details of the procedure used to calculate equivalent anode polarization values are given in Appendix G-8 .

These data, together with the corresponding cathode performance distribution data presented previously (6), indicate that large-scale fuel distribution problems are absent in the sixteen cell stack assembly. However, the present studies were made using an intermittent-action adjustable-diaphragm Mace pump to deliver the feed solution and any changes in pump type could alter this conclusion.

Figure G-10

Distribution of Anode Polarizations in Sixteen Cell Stack

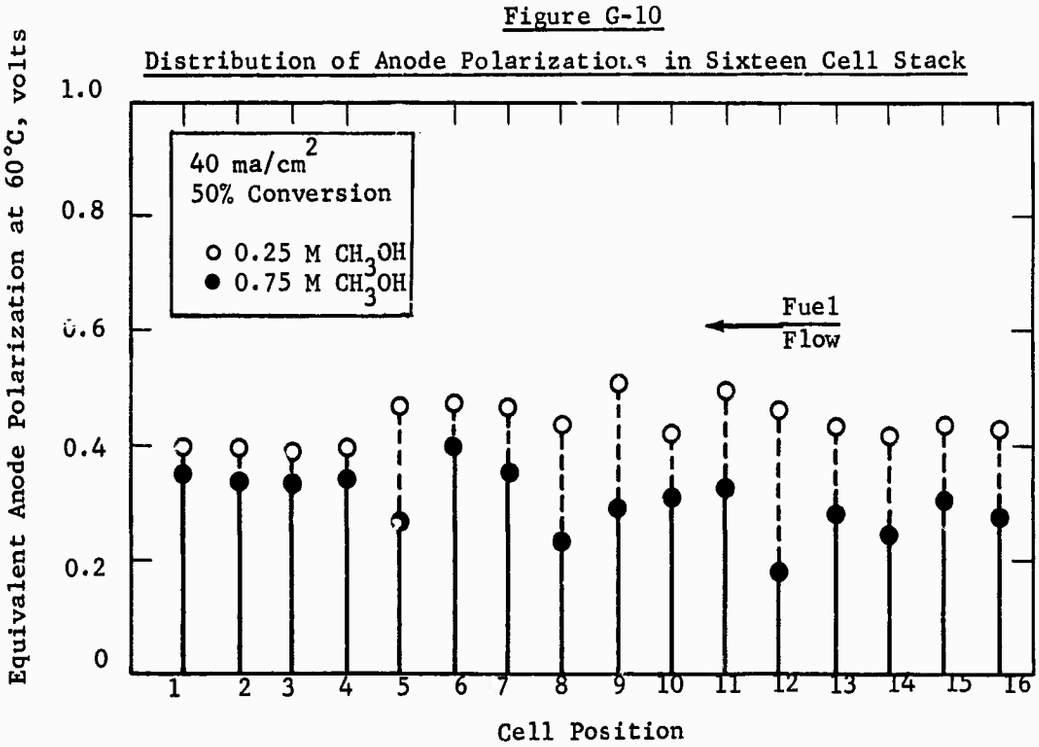

Part d - Effect of Air Rate on Performance

The effect of changes in air rate on the performance of the sixteen cell stack was also determined. The air flow rate is a key variable in the overall operation of a self-contained methanol battery. Air flow may be used to control electrolyte temperature by adjusting the rate of water removal from the stack. Therefore, it is important that stack performance be stable over a wide range of air flow rates. As shown in Figure G-11, performance of the sixteen cell battery was insensitive to changes in the air flow rate, above about three times the stoichiometric requirement. Complete data are given in Appendix G-8 to G-10.

Figure G-11

Effect of Air Rate on Performance

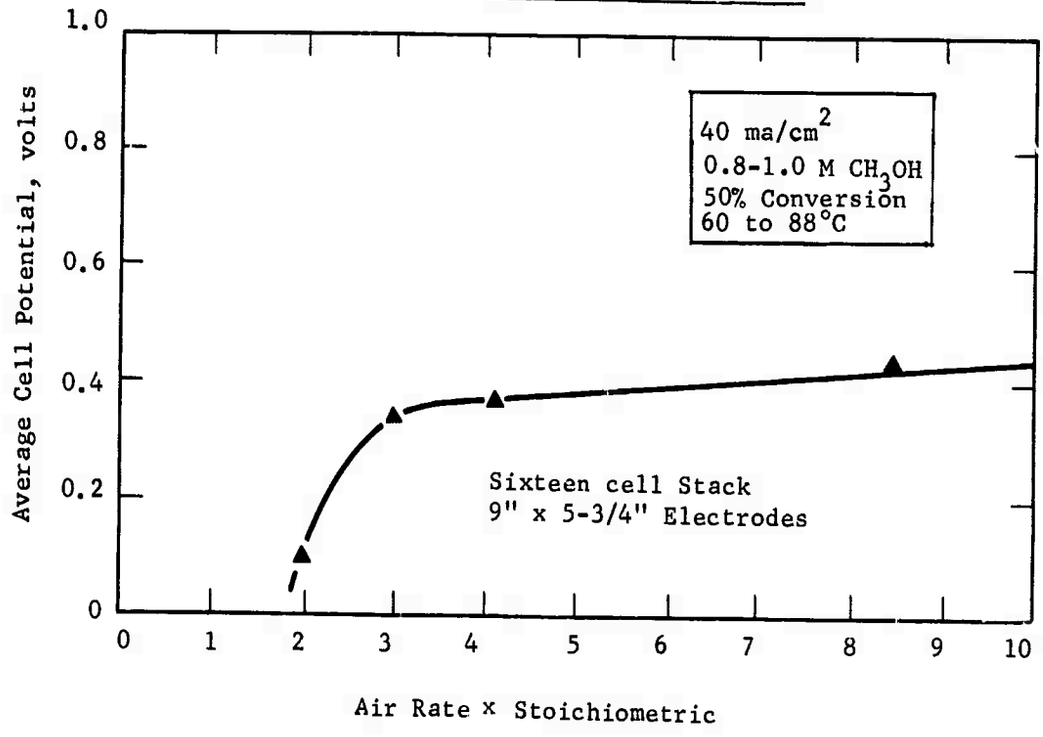

Part e - Thermal Characteristics of Sixteen Cell Stack

Temperatures within the stack must be kept below about 90°C. At higher temperatures, performance suffers due to malfunctioning of the cathodes, and loss of fuel via vaporization. Furthermore, the polypropylene cells, themselves, become distorted through thermal creep.

Therefore, temperature distributions within the sixteen cell battery were measured. As illustrated in Figure G-12, individual cell temperatures ranged from 57 to 74°C under typical operating conditions. This wide temperature distribution resulted from the introduction of cool air and electrolyte into either side of the battery through the manifold system. No attempt was made to equalize this temperature distribution by heat conservation techniques or by altering the flow patterns through the battery. Nevertheless, the data in Figure G-12 show that cell voltages were not greatly affected, although the effect of the imposed temperature was evident. Complete data are given in Appendix G-8 to G-10.

Figure G-12

Effect of Temperature Profile on Distribution of Cell Voltage

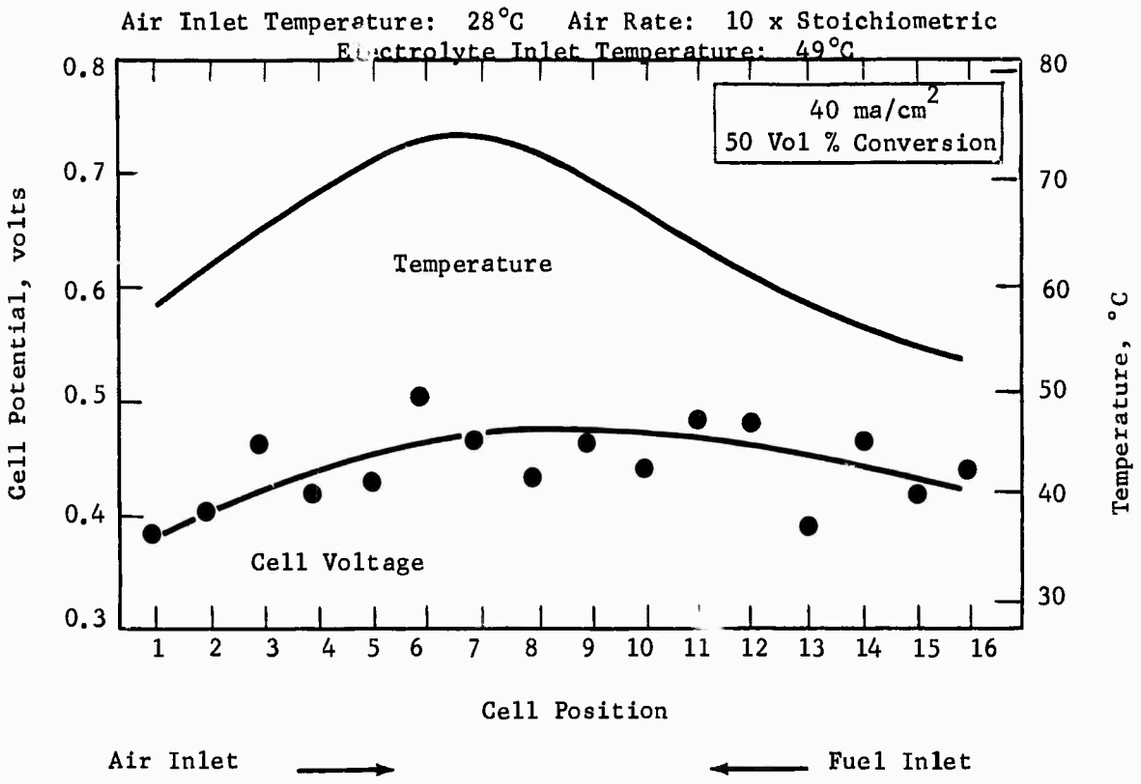

The fact that the cells delivered useful power at lower temperatures is of considerable importance in achieving rapid startup. As an example, the data illustrated in Figure G-13 show that the battery delivered 5 volts or 12 mw/cm^2 at a current density of 40 ma/cm^2 immediately after startup at a normal laboratory temperature of 27°C. Steady-state performance was attained in about 20 minutes.

Figure G-13

Typical Startup Characteristics From Ambient Conditions

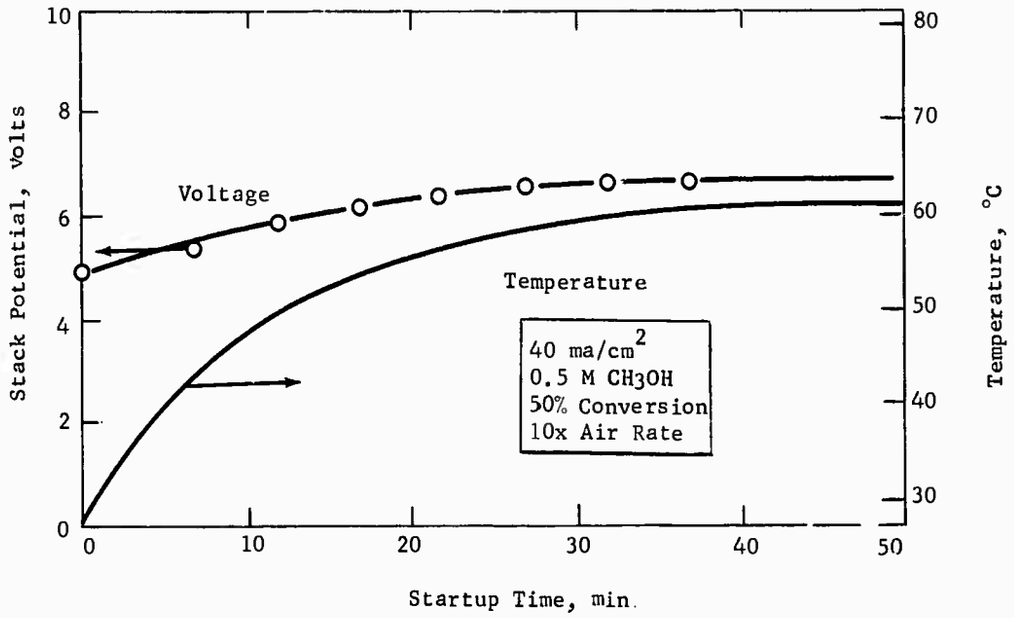

The stack also exhibited considerable latitude in its ability to reject heat. This heat dissipation is accomplished in large measure by vaporizing additional quantities of water from the surfaces of the cathodes into the effluent air stream. The sensible heat of the stack components and contents is thereby reduced.

As an example, a series of runs was made at widely differing conditions. These ranged from 26 to 62°C inlet air temperature and 27 to 52°C inlet electrolyte temperature. In addition, several runs were made with saturated air streams. As shown in Table G-2, these variations in inlet conditions resulted in only a 9°C variation in maximum cell temperature within the battery, from 77 to 86°C. This corresponded to a change in average cell temperature from 67 to 73°C. Furthermore, average cell performance was not affected, averaging 0.40 volts at 40 ma/cm^2 with a standard deviation of $\pm$ 0.02 volts (one sigma limit). This is well within the normal precision limits of battery data.

Table G-2

Effect of Varying Inlet Temperatures
on Thermal Stability of Methanol Stack

Current Density: 40 ma/cm^2
Methanol Concentration: 0.75 M
Conversion per pass: 50 vol %

Air Inlet		Electrolyte Inlet	Maximum Cell	Average Battery	Average Cell
Temp, °C	Humidity	Temp, °C	Temp, °C	Temp, °C	Voltage
26	Dry	27	77	67	0.40
52	Dry	36	77	68	0.41
51	Dry	52	83	72	0.38
52	Dry	51	77	67	0.39
48	Saturated	27	78	69	0.42
51	Saturated	27	79	69	0.37
52	Saturated	38	83	71	0.42
51	Saturated	49	78	65	0.41
52	Saturated	49	86	73	0.43
62	Saturated	50	84	72	0.39

Part f - Water Loss Rates from the Sixteen Cell Stack

A self-contained methanol fuel cell system must have a device for recovering water from the exhaust air stream. Although the cell reactions produce net water, excess water is lost from the electrolyte by means of vaporization from the cathode surface. This water loss mechanism helps to control cell temperature, because the required heat of vaporization is obtained by decreasing the sensible heat of the electrolyte and cell components. Therefore, experiments were carried out to establish the range of water loss rates from the sixteen cell stack during operation over a range and electrolyte inlet temperatures and inlet air humidities. These data are needed for proper sizing of a water recovery device.

Measured total water loss rates were about 2 to 3 cc/min for stack operation with dry inlet air, compared with maximum values of 5 to 6 cc/min obtained with hot, humid air. The water production rate during these tests was about 1.1 cc/min, from both the electrochemical and chemical oxidation of methanol. As shown in Figure G-14, water loss rates with humid air leveled off at inlet air temperatures above 40°C. This means that the net water loss rate decreased. The net loss rate is the difference between the total loss rate and the rate of water input from the humid air stream. Of course, decreasing the net water loss rate also decreased the rate at which heat is removed from the stack. However, as shown in Part e, the temperatures within the stack never exceeded the maximum allowable temperature of 90°C. Complete data are given in Appendices G-8 to G-10.

Figure G-14

Effect of Inlet Air Conditions on Water Loss Rate

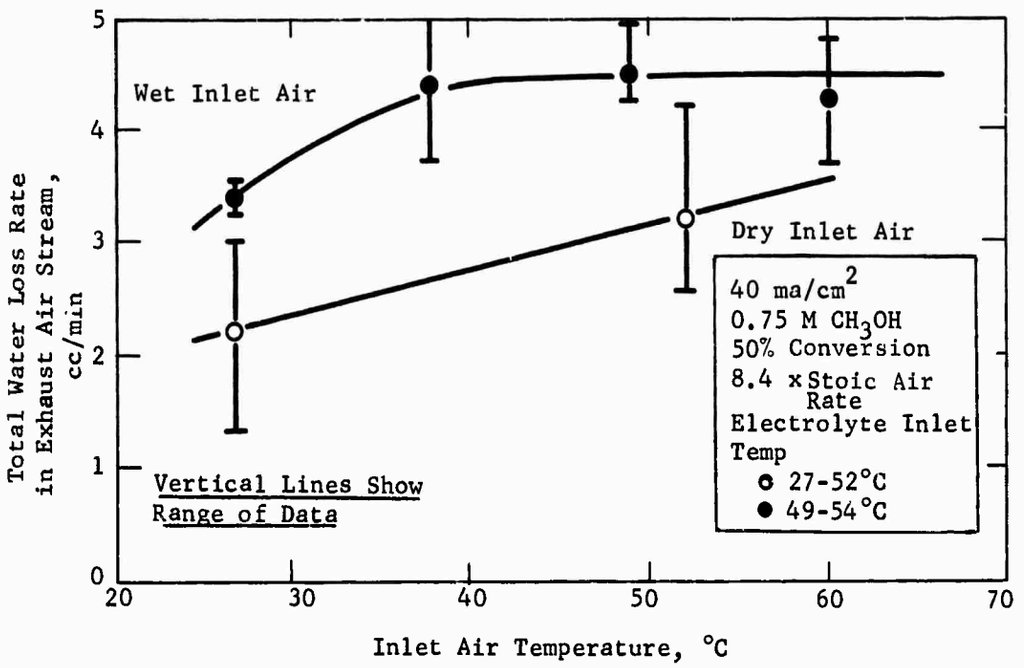

A very close correlation was found between the measured total rate of water loss and the water loss rate calculated on the assumption that the exhaust gas was saturated with water at the measured temperature in the exit air manifold. This is shown in Figure G-15. Hence, it may be possible to control water removal rates by monitoring the exhaust gas temperature.

Figure G-15

Comparison of Measured With
Calculated Water Loss Rates

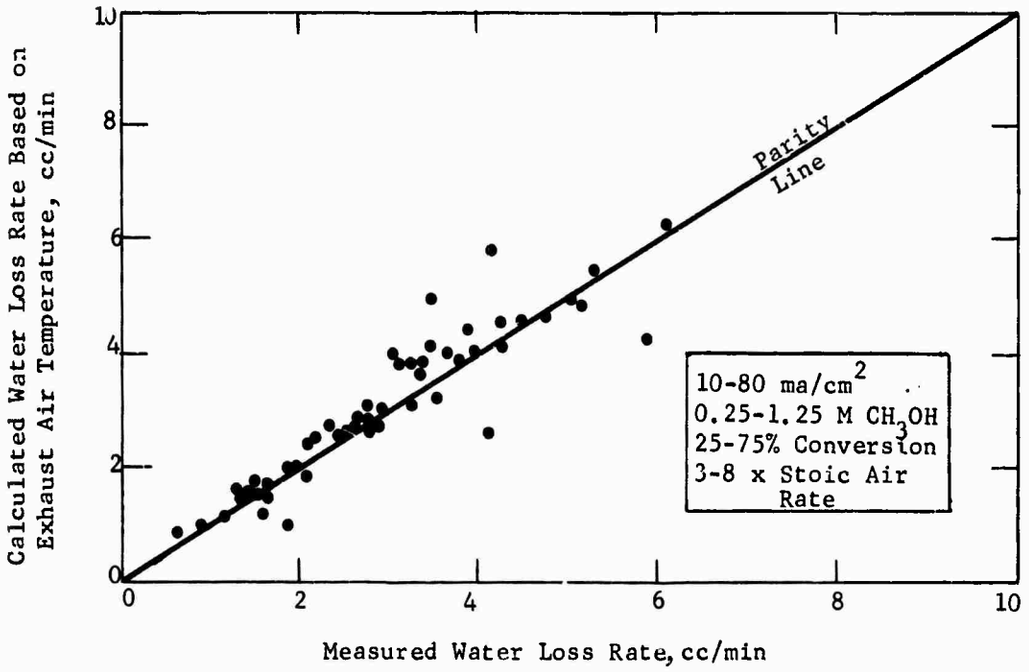

Part g - Chemical Oxidation in
the Sixteen Cell Stack

The parasitic consumption of dissolved methanol at the fuel cell cathode, in addition to reducing cathode performance and contributing to decreased overall fuel utilization, generates heat and thereby produces additional temperature control problems. Therefore, studies were made to define the effect of stack operating variables on the extent of chemical oxidation.

As expected, these studies showed that chemical oxidation was minimized when operating at low methanol inventories within the stack. As shown in Figure G-16, low inlet methanol concentrations of about 0.25 M, and high methanol conversion rates of 60 to 80% gave chemical oxidation rates of about 5 ma/cm^2, when expressed on the basis of equivalent methanol consumption. However, these levels of methanol concentration and conversion do not correspond to the levels required for maximum stack performance. The dotted curve in Figure G-16 shows that chemical oxidation values of about 15 ma/cm^2 can be reached by operating at 70 vol % conversion level and 0.75 M methanol. Complete data are given in Appendices G-8 to G-10.

Figure G-16

Effect of Operating Variables on Chemical Oxidation

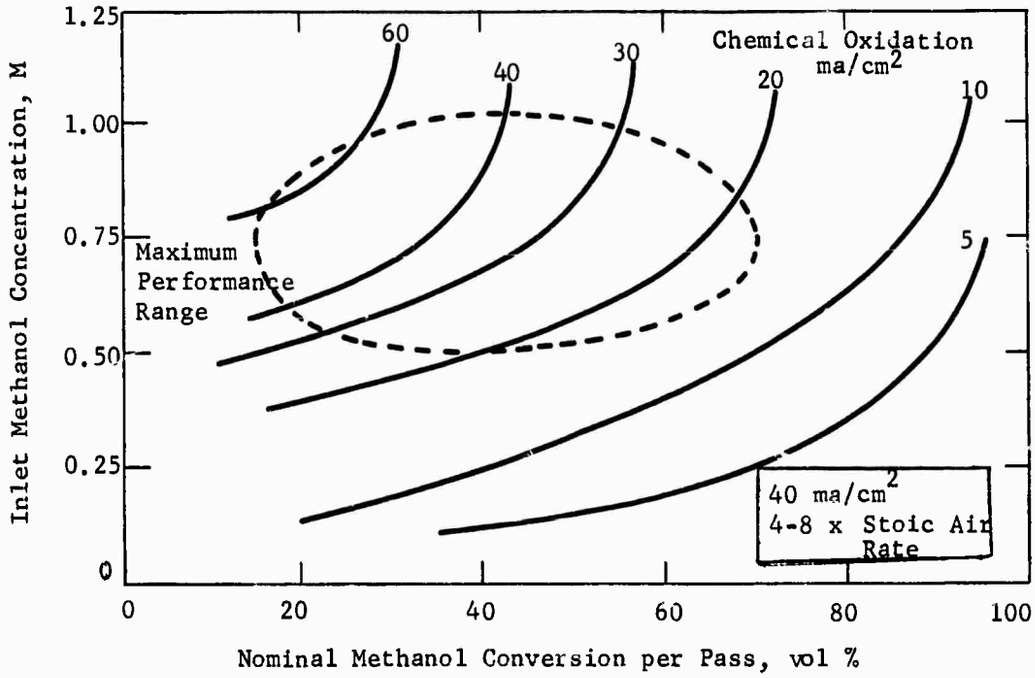

Tests in the multicell unit confirm the result in smaller single cells that the rate at which methanol reaches the cathode is controlled by diffusion from the anolyte chamber. This is shown by the data plotted in Figure G-17. Here chemical oxidation rates are plotted against a variety of methanol concentrations: cell inlet concentration; cell outlet concentration, calculated from the rates of chemical and electrochemical methanol consumption; average anolyte chamber concentration, calculated from the inlet and outlet values; and true concentration adjacent to the cathode membrane. The latter values were obtained from well-stirred half cell studies reported in Task F, Phase 1.

Figure G-17

Effect of Methanol Concentration on Chemical Oxidation

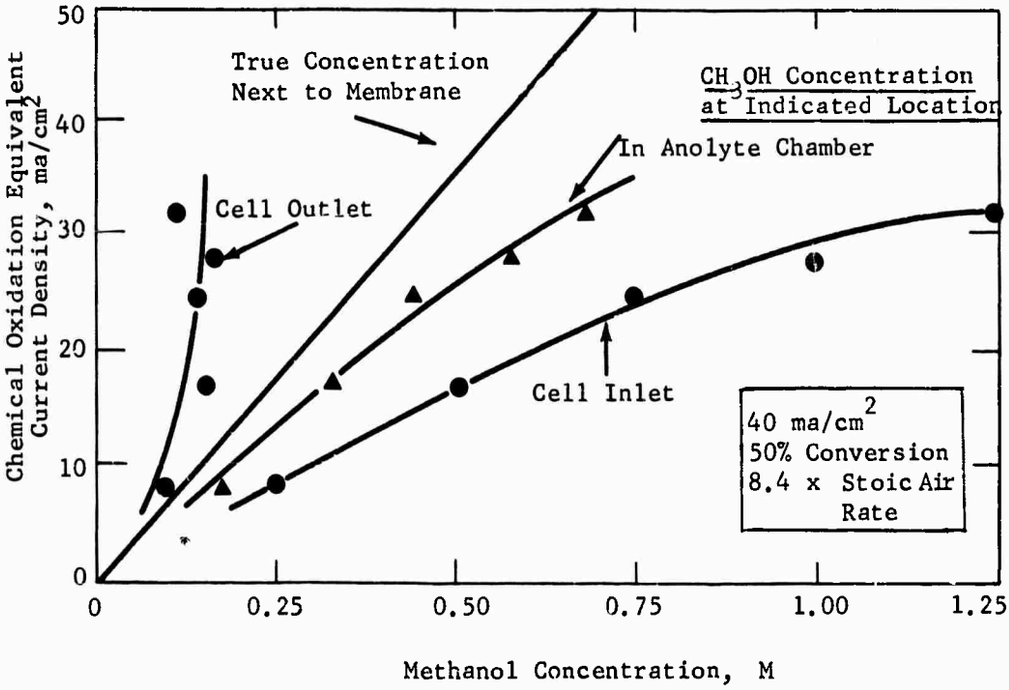

The cell inlet methanol concentration line underpredicts the "true" data line, suggesting that inlet electrolyte does not by-pass around the anode directly into the chamber adjacent to the cathode membrane. Also, the cell outlet concentration line considerably overpredicts the extent of chemical oxidation. This means that the cell is not acting as a well-mixed vessel with considerable back flow of exiting electrolyte over the top of the anode. On the other hand, the line corresponding to the average anolyte composition appears to give the best fit. This would be expected on the basis of an increased driving force for methanol diffusion through the anode into the center chamber of the cell.

The effect on chemical oxidation of water flux rate through the cathode was also evaluated. A possible mechanism for increased methanol transport to the cathode is the "drag-along" phenomenon, wherein the net water flux from the center chamber through the cathode acts to pull along more methanol molecules than expected from the diffusional concentration gradient alone. A range of water flux rates was obtained by operating the sixteen cell stack at various inlet air temperatures and humidity. Net water loss rates were thereby varied from essentially zero to about 4 cc/min.

As shown in Figure G-18, there was no effect on the rate of chemical oxidation. Thus, diffusion alone appears to be the mechanism controlling methanol transport to the cathode.

Figure G-18

Effect of Water Transport Rate on Chemical Oxidation

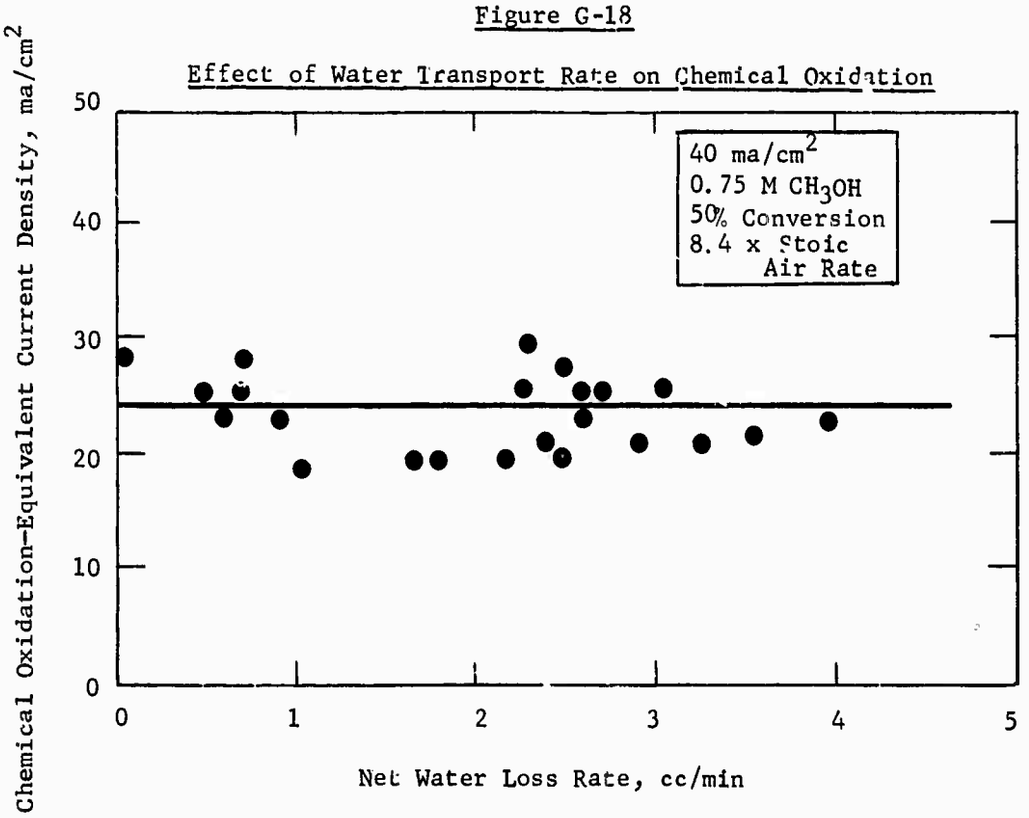

Part h - Performance of Methanol Fuel Cell Stack Using Formaldehyde

A possible approach to improving the startup capabilities is the use of trioxane. Trioxane is a stable, white solid, which presents no special handling or toxicological problems. It sublimes at 46°C, melts at 64°C, and boils at 116°C without decomposing. When added to concentrated sulfuric acid, it catalytically depolymerizes to form its monomer, formaldehyde. A formaldehyde-air cell has a greater theoretical voltage than a methanol air cell, 1.30 volts. Furthermore, it is somewhat more reactive than methanol. Therefore, greater heating rates should be possible.

To demonstrate this, the performance of the 16 cell stack was evaluated substituting 1 M formaldehyde for methanol at normal ambient conditions. No effort was made to modify stack operation to accomodate the change. The power output from the stack increased to 174 watts at 5.1 volts. Furthermore, it was necessary to chill the circulating electrolyte to 16°C to keep the temperature from rising above 88°C inside the stack. As shown in Figure G-19, the average cell voltage was

about 0.1 volts greater than that obtained using methanol. This should also be true at lower temperatures and therefore should permit more rapid startup at lower temperatures. However, further information in low temperature tests is still needed. Complete data for operation with formaldehyde fuel are given in Appendix G-11.

Figure G-19

Effect of Formaldehyde
on Sixteen Cell Stack Performance

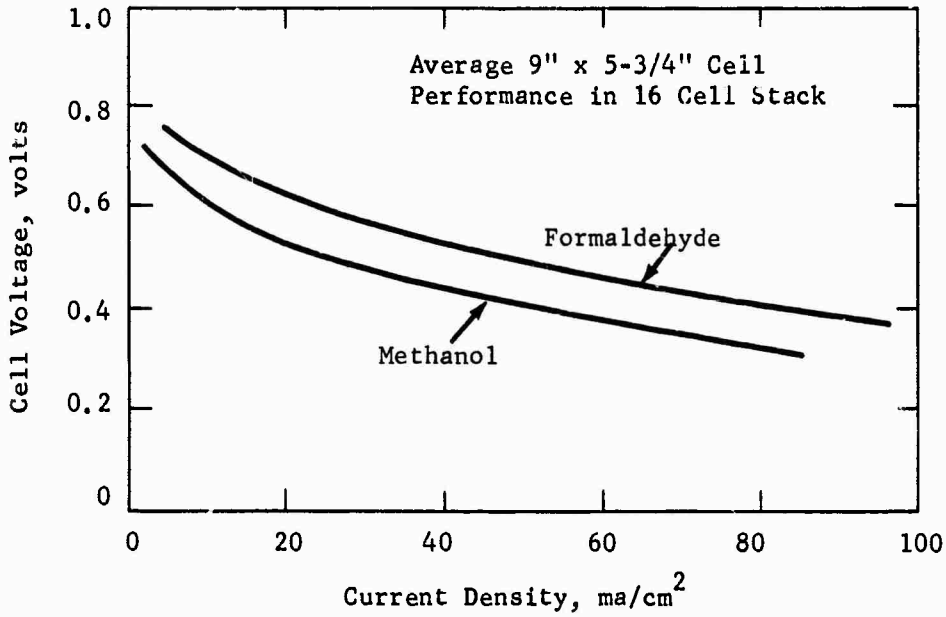

Phase 3 - Auxiliaries and Controls

Additional efforts have been centered on developing the necessary compact auxiliary equipment required for the operation of a self-contained battery. Of particular importance is the development of a reliable methanol concentration controller and a low power electrolyte circulating pump.

Part a - Methanol Analyzer System

The development and operation of a current-scanning, methanol analyzer for use with multicell units has been discussed in previous reports (3, 4, 5, 6). It has become apparent, however, that the methanol response and life characteristics of the platinized electrodes under scanning conditions, especially in the presence of soluble, cell contaminants, are too variable for use as a controller. Studies were carried out to test the applicability of a new analyzer concept. This technique, in essence, measures the limiting current of an electrode under conditions where methanol flow to the electrode is limited by a membrane rather than the variable nature of the catalyst.

The basic analyzer element consists of a diffusion-restricting membrane pressed tightly to the surface of a platinum black electrode. Permion 1010 membrane and Cyanamid AA-1 electrodes pressed together at 1000 psig have been found suitable for the purpose. In operation, the element is arranged in the container of fuel-electrolyte solution so that methanol diffuses through the membrane at a slow rate and contacts the electrode. The potential of the electrode is maintained at about 0.85 volts versus a hydrogen evolving electrode, a level where methanol oxidation is diffusion limited. Under these conditions, all the fuel reaching the electrode is oxidized to CO_2 and the current in the system is directly proportional to the methanol arrival rate, which in turn is linearly proportional to the fuel concentration on the other side of the membrane, providing temperature is held constant. Current response of the system to changes in fuel concentration can then be used to control fuel input circuits.

Part b - Laboratory Testing of the Methanol Analyzer

Feasibility studies were carried out in the unit shown in Appendix G-12 For convenience, membrane-electrode circlets were mounted in a modified polypropylene 3/8" tubing connector. The methanol-3.7 M sulfuric acid solutions were stirred by means of a magnetic stirrer in the cell, and a slow nitrogen sparge at the external side of the membrane on the analyzer element.

All studies indicated a linear relationship between current output and methanol concentration. This is illustrated in Figure G-20.

Figure G-20

Analyzer Response to Methanol Concentration

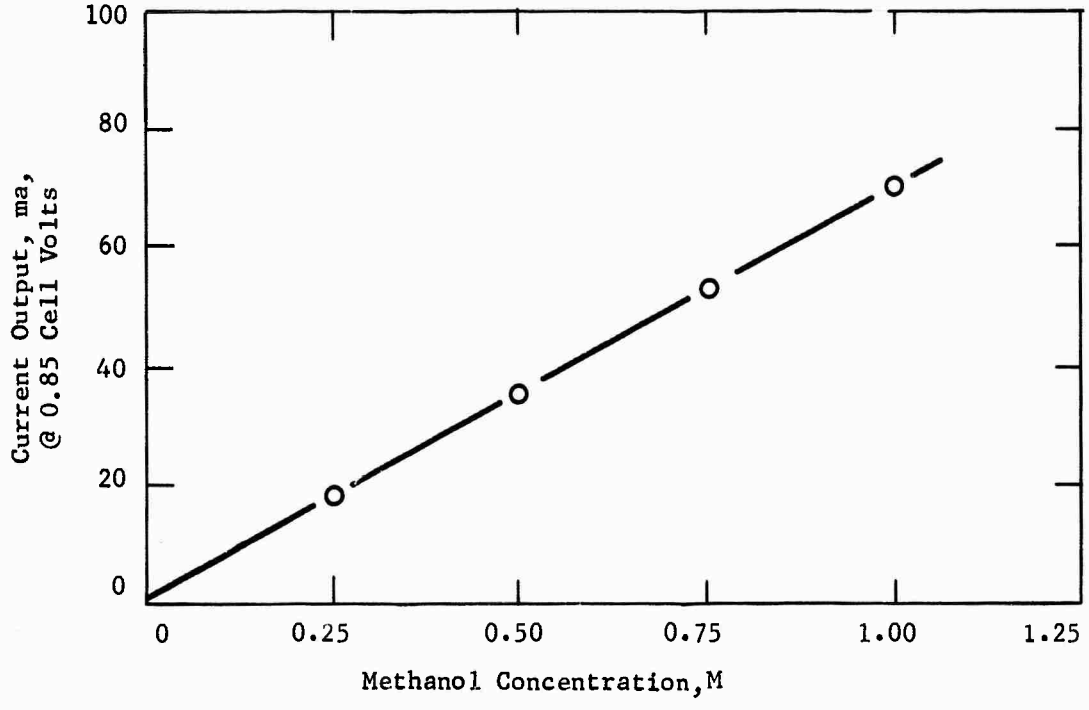

Measurements of the temperature dependence of current at a fixed fuel concentration indicated an activation energy of about 4.8 to 5.0 kcal/mole in several studies. This low value is in accord with the transport limited conditions imposed. Complete data are contained in Appendix G-13.

Part c - Effect of Impurities and Life

Under transport limiting conditions, the quantity of catalyst on the analyzer element is far in excess of that necessary to effectively oxidize the arriving fuel. In this case, soluble electrode contaminants would not be expected to seriously affect the cell operation. This was confirmed in tests in which several impurities were added to the electrolyte. For example, the addition of 28 ppm of soluble ruthenium produced no effect on an operating unit.

These preliminary studies indicate performance is stable with time. The unit used for impurity testing was operating in excess of one thousand hours before it was shut down with no change in performance. Complete data are contained in Appendix G-13.

Part d - Methanol Analyzer Temperature Compensation

The response of the methanol analyzer current to changes in temperature corresponds to an apparent activation energy of 4.9 kcal/mole. This is equivalent to about 2.4% change per °C at a fixed methanol concentration. A temperature correction arrangement is required to incorporate the analyzer in a control system where the electrolyte stream through the analyzer cell is changing temperature. A temperature correction circuit was therefore designed and tested. The design is shown in Figure G-21.

The correction method is based on adding two voltages in the proper ratio so as to cancel the temperature effect on current measurements from the analyzer cell. One voltage is an adjustable fraction of the voltage drop across a small resistor in series with the analyzer cell. This voltage increased 2.4% for each degree centigrade of temperature change. The second voltage is also a fraction of the voltage drop across a small resistor in series with the analyzer cell. However, the level of this voltage is a function of the resistance of a thermistor in the stream being analyzed. This voltage decreases about 3.5% for each °C temperature rise. The proper ratio of the two voltages for good temperature compensation is chosen by adjusting the slider position on a potentiometer connected between the uncompensated and overcompensated voltage supply points. Typical data are shown in Table G-3.

Figure G-21

Diffusion-Type Methanol Analyzer
Temperature Correction Circuit

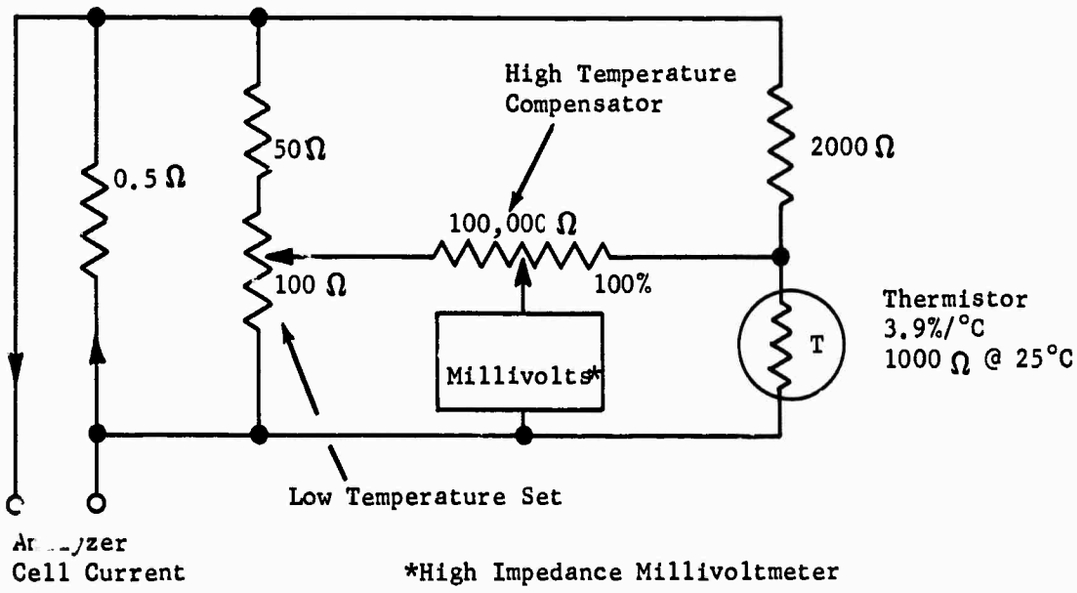

*High Impedance Millivoltmeter

Table G-3

Methanol Analyzer Temperature Correction

0.5 M CH_3OH in 3.7 M H_2SO_4

Temperature, °C	Indicated Methanol Concentration, M	
	Calculated	Measured
25	0.495	--
30	0.498	--
35	0.502	0.500
40	0.500	0.500 (1)
45	0.500	0.500
60	0.500	0.500 (2)

(1) By definition
(2) By calibration

This correction arrangement will be redesigned to work at lower voltage and resistance levels and will be incorporated in a transistorized fuel cell control system.

Part e - Electrolyte Circulating Pump

A prototype model of a compact, low-power, electrolyte-circulating pump was designed and constructed. The pump is a gear pump mounted in a cubical polypropylene case measuring 1-3/4" per side, with 5/8" diameter gears and bearings of Teflon. Alternate shafts were used made of polypropylene and tantalum sealed with a viton gasket. The pump is pictured in Figure G-22.

Figure G-22

Electrolyte Gear Pump

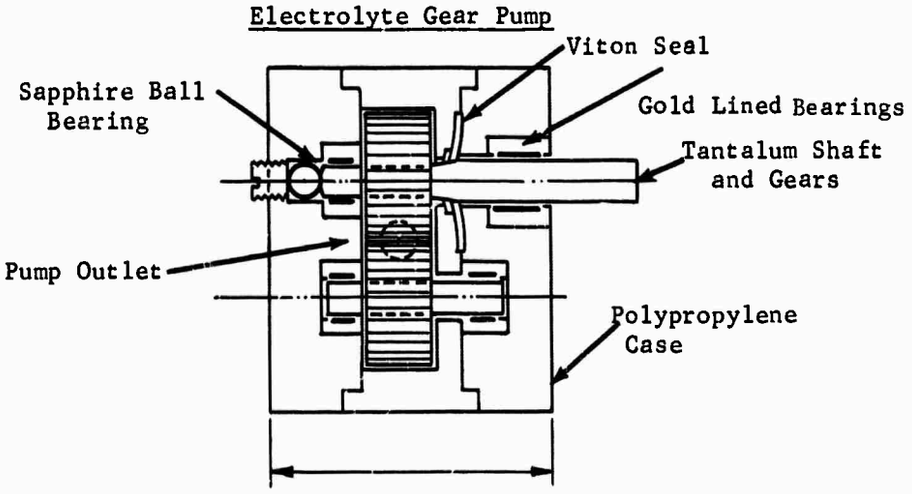

The pump delivered the target flow rate, 20 liters per hour, against a 12" head with a power expenditure of only 0.75 volts. Altnough only 2% efficient, its power requirement is significantly less than any commercially available pump. However, the low power requirements and the limited materials of construction made sealing around the shaft difficult and bearing wear was a problem. These materials all have a high coefficient of friction on each other and on Teflon, and have shown evidence of rapid wear. Therefore, the pump was modified to operate submerged in the electrolyte reservoir tank to eliminate the leak problem. In addition, the bearings have been lined with 6-mil gold foil to reduce bearing wear. The pump is presently undergoing extensive life testing.

SECTION 5

CONCLUSIONS

5.1 Task A, Hydrocarbon Electrode

Phase 1 - Hydrocarbon Adsorption Rates

A successful method was developed for measuring hydrocarbon adsorption rates, free of mass transport effects. This will aid future catalyst research. It was possible to calculate approximately correct values of the limiting current of operating electrodes, from measured adsorption rates. This indicates that platinum surface area in Teflon-bonded porous-diffusion electrodes is being utilized effectively. Thus, significant catalyst improvements can be made only by altering chemical or microstructural properties. It was also found that hydrocarbons are adsorbed only on half of the available platinum sites. The active sites correspond to the "Type II" hydrogen sites, long recognized in chronopotentiometric or voltammetric studies on platinum. However, the Type I hydrogen sites are also involved in the adsorption process, since the placing of adsorbed hydrogen atoms on these sites causes desorption of the fuel. The Type I sites may be occupied normally by water molecules, which are necessary for the adsorption process. The two-site hypothesis should help explain many phenomena observed in the electro-oxidation of organic fuels. Studies are underway to alter the ratio or the nature of the two types of sites and to determine the consequent effect on hydrocarbon performance.

Phase 2 - Studies of the Effects of the Physical Nature of Platinum Catalysts on Performance

Micro-structure, rather than chemical properties, has controlled the performance of platinum black catalysts. The activity of platinum catalysts prepared by a number of chemical procedures was correlated with the pore volume of the platinum black and with the apparent openness of structure, based on electron microscope studies. The rates of adsorption or electro-oxidation of fuel were essentially the same and surface area was not a significant variable. Thus, future catalyst preparations should aim at maximum structural openness, where the crystallites are arranged in networks of low-coordination number.

Phases 3 and 4 - Increasing Platinum Utilization-Electrode Structure Studies

The use of a carbon support has significantly increased platinum utilization with hydrocarbon fuels, thus lowering catalyst costs. The base level of 8 ma/mg for unsupported platinum was raised to about 16 ma/mg by the simultaneous use of an improved impregnation procedure and a silica co-support. In addition, separate electrode structure optimization studies showed that very thin electrodes gave improved performances, about 25 ma/mg. The successful combination of these two effects will lead to a practical hydrocarbon electrode.

Phase 5 - High Surface Area Alloys

It is still necessary to study prospective alloy catalysts in a high surface area form. The performance obtained with smooth metals cannot be extrapolated to predict the operation of practical catalysts. In particular, the distinction between corrosion and catalytic activity is difficult when the surface area is low. However, the preparation of high surface area alloys by chemical reduction has so

far proven difficult. The extent of alloying has been low and the electrochemical activity has not been stable or reproducible enough to allow for meaningful interpretation. However, the principles for the choice of alloys still appear to be valid, so that more work with better preparation procedures is warranted. The use of ternary Raney alloys followed by controlled leaching appears to be a promising route to follow.

Phase 6 - Mixed Perovskites

The acid resistance of the perovskites, their ability to be tailored into relatively conductive forms, plus their ability to incorporate prospective catalytic metals, makes them very promising for use in fuel cells. However, the technique of incorporating oxide ion deficiencies in the lattice to improve conductivity has not proven satisfactory. This approach usually results in compounds which fail to meet the conductivity and corrosion resistance requirements simultaneously. It was also shown that acid corrosion of oxide deficient crystals caused the loss of all conductivity improvement generated by the deficiency. However, it is known that oxides of this type can be made conductive by the inclusion of multiple valence states of the metal in the lattice. Therefore, stoichiometric perovskites containing the full complement of oxide ions and multiple valence states to provide conductivity look most promising in this area. Some of the partially tetravalent manganese compounds listed in the appendix tables have already shown favorable properties.

Phase 7 - Transition Metal Complexes and Redox Catalysts

None of the cyano and cyclopentadienyl complexes so far examined have shown any significant activity or co-activity with platinum. However, application of the principles of homogeneous catalysis to the fuel cell problem should still be possible and promising complexes are to be evaluated as uncovered. The uranyl system also appears to be a promising redox-couple worthy of further examination.

5.2 Task B, Hydrocarbon Fuel Cell

Phases 1 and 2 - Studies in Hydrocarbon Fuel Cells-Hydrocarbon Cell Design

Performance of liquid decane and oxygen in realistically sized cells has reached 20 mwatts/cm^2 in short term tests at 150°C, the same level observed in smaller cells. Although the separation of the porous Teflon barrier previously noticed at the anode remains a problem, other aspects of scale-up seemed satisfactory. Transport of decane through the anode with resulting accumulation in the interelectrode space was a problem. The mechanism of this transport is not known. Additional test facilities to study this problem have been designed.

5.3 Task C, New Systems

Phase 1 - Pyrophosphoric Acid Electrolytes

Pyrophosphoric acid is capable of supporting high performance levels with hydrocarbon fuels and oxygen at temperatures in excess of 200°C. Butane has a much higher limiting current at 200°C, although at lower current densities it is not significantly more active compared with performance in phosphoric acid at 150°C. Water vapor addition to hydrocarbon fuels is required for maximum activity. On the other hand, oxygen performance at the higher temperature is greatly improved at all levels of current density. Carbon electrodes containing as little as 5 mg/cm^2 of catalyst were found less active than sintered platinum-Teflon electrodes, but

optimization of structural variables should help to minimize this loss. Although pyrophosphoric acid has demonstrated sufficient conductivity and buffering capacity for fuel cell use, it is highly corrosive, and suitable materials will have to be found before it can be used extensively. A filled Teflon-type material known as Rulon has already indicated chemical and structural stability in pyrophosphoric acid as described in Task B.

Phase 2 - Buffer Electrolytes

The steady state pH achieved by concentrated buffers may not correspond to that expected from equilibrium considerations if cell configuration and operating temperature allow rapid escape of carbon dioxide. Further work is required to clarify this point. Methanol, hydrogen, and oxygen perform poorly in carbon dioxide-treated concentrated buffers. The limitation is not related to buffer capcity, but may reflect impurities in the salts or anomalous wetting and solubility effects. Cesium fluoride can be added to dilute buffers to raise the operating temperature, without affecting methanol performance. Finally, pyrophosphate salt buffers hydrolyze too readily for fuel cell applications.

Phase 3 - Air Electrodes for Buffer Electrolytes

In the dual electrode structure, only the sheet facing the air supply is active. The inner sheet maintains the interface, and therfore it requires no catalyst. Nickel is not an active cathode catalyst in buffer electrolyte. The dual structure electrode, with either silver or platinum catalyst is not active in concentrated buffer solutions, probably for reasons similar to those discussed in Phase 2. However, in 6 M potassium carbonate, both catalysts are equally active, demonstrating for the first time that a non-noble catalyst can match the performance of platinum in a buffer electrolyte. In addition to cost, the silver electrode has the further advantage of insensitivity to methanol. No polarization debit or chemical oxidation is observed in the presence of the fuel.

Phase 4 - Buffer Electrolyte Total Cells

The advantages demonstrated by the silver cathode in half cell tests were confirmed in total cells. Using 6 M potassium carbonate electrolyte and a P-type anode, 18 mwatts/cm^2 were achieved with the non-noble air electrode.

Phase 5 - Non-noble Catalysts for Methanol Oxidation

No non-noble active anode catalysts have yet been prepared, although several alloys and transition metal compounds have been found stable in buffer or potassium hydroxide. Lattice spacing is apparently not a critical parameter in these studies. In those cases where some performance has been observed, the level is higher in potassium hydroxide than in buffer electrolyte. The reason for this is not clear.

Phase 6 - Slurry Catalyst Systems

The use of slurried, catalyzed-carbon particles, supported by the turbulence of bubbling decane through the electrolyte, offers no performance or catalyst utilization advantages over static systems.

5.4 Task D, Methanol Electrode

Phase 1 - Studies of Ruthenium Modified P-type Catalyst

Studies with ruthenium modified P-type anodes have been carried out to provide additional information concerning various aspects of performance in methanol-air batteries. The effect of methanol concentration has been established. In battery applications, at current densities up to 100 ma/cm^2, the methanol concentration should be maintained above 0.25 M methanol to prevent significant performance losses. Better control over methanol diffusion and chemical oxidation at the cathode should be possible through the use of barriers, as discussed in Task F. A feasible debit-free barrier was formed by spraying Teflon on the anode. The present ruthenium modified P-type anodes continue to give evidence of good chemical and mechanical stability in life tests and as shown in studies with various types of water and at several vibration levels.

Phase 2 - Studies of Methanol Electrode Structure

Research has continued to reduce catalyst cost in methanol electrodes by improving noble metal catalyst utilization in acid electrolyte. Studies of electrode structures similar to those currently employed showed that performance varies linearly with catalyst loading in the range 1 to 20 mg/cm^2. Thus, a reduction by more than one-half from the present 25 mg/cm^2 noble metal level would cause significant performance losses. The same result was found in a number of diluted catalysts containing various non-catalytic, conductive materials. Because of the similar performance in these studies, it is concluded that present electrode structures cannot be significantly improved with respect to catalyst utilization. However, the initial results with catalyst supported on conductive substrates are promising. These supported catalysts offer a technique for effectively distributing small amounts of noble metal uniformly on the electrode surface. In addition, the supported catalysts should tend to provide better microstructure, for example higher surface area and pore volume. This was shown by the results obtained with 1.2 mg/cm^2 of platinum on carbon. In addition, improved catalytic activity of ruthenium modified P-type catalyst has been demonstrated on supported structures containing only 2 mg/cm^2 of noble metal. The sensitivity of catalyst performance to variations in preparative procedures suggests that further improvements in performance are possible.

5.5 Task E, Air Electrode

Phase 1 - Membrane-free Electrode

Interface-maintaining electrodes, backed by a hydrophobic coating applied directly to the air side of the electrode, can be prepared and operated successfully. However, a scale-up debit exists and further work is necessary to minimize this factor.

5.6 Task F, Methanol Fuel Cell

Phase 1 - Total Cell Operation

The anode performance debit for the 9" x 5-3/4" electrodes resulting from the poor conductivity of tantalum screens was corrected by gold-coating the screens. Slight additional improvement was found possible by adding equal amounts of gold to the catalyst. Other tests showed that temporary partial immersion of electrodes does not impair catalytic activity with performance remaining proportional to the fraction of the electrode still immersed in the electrolyte. The large 9" x 5-3/4" anodes were

found to require greater methanol concentrations than expected, as a result of poorer contacting of the catalyst with methanol. The consequent higher methanol concentrations also result in higher than desired rates of chemical oxidation of methanol.

Phase 2 - Comparison of Direct Feed with Circulating Fuel-Electrolyte

Performance equivalent to that of the electrolyte-circulating system can be obtained by using porous diffusers for feeding methanol directly to a cell chamber. Comparable power densities, voltages, and chemical oxidation rates at the cathode were found. Substantial reduction in the rates of chemical oxidation of methanol, to satisfactory levels, is attainable using Dacron felt diffusion barriers, or alternatively, a gelled electrolyte. In addition, natural convection, rather than blowers, can be used to supply air to individual cells at currents as high as 100 ma/cm^2.

5.7 Task G, Prototype Development

Phases 1 and 2 - Self-Contained Methanol Multicell Unit-Operating Characteristics of Sixteen Cell Stack

The operation of the sixteen cell multicell unit demonstrates the feasibility of constructing and operating a stable, self-sustained, methanol battery that responds quickly to load changes. Power outputs could be further increased to 120 watts with the use of improved catalyst preparative techniques, the gold-coated tantalum screen structures, and some design changes in the unit. This corresponds to about 25 $mwatts/cm^2$. Most of the voltage debits were attributed to polarization at the two electrodes. Fuel and air distribution to the cells were good. The average cell temperature and temperature distributions at steady state attained the levels expected; the average temperature was about 70°C for a wide range of operating conditions. Water loss from the stack was somewhat higher than expected and was found to correlate with the exhaust gas temperature. Chemical oxidation rates at optimum conditions were high, about 15 ma/cm^2. This rate can be reduced to 5 ma/cm^2 with about a 20% performance loss. Tests with formaldehyde substituted for methanol as fuel resulted in power outputs of 35 $mwatts/cm^2$, indicating that trioxane, a solid polymer of formaldehyde, could be useful during cold startup as a methanol unit.

Phase 3 - Auxiliaries and Controls

A new diffusion controlled analyzer has demonstrated linear response to methanol concentration, insensitivity to impurities, and long life. With the successful testing of a temperature compensation circuit it is now ready for further development as a controller. A small, low power pump, constructed for circulating electrolyte, has demonstrated an ability to operate on less than 1 watt.

SECTION 6

PROGRAM FOR NEXT INTERVAL

Catalyst cost is the primary factor presently limiting the use of the hydrocarbon-air fuel cell. Since the latter part of 1964, when high performance with liquid hydrocarbons was achieved, attention has been focused on the problem of catalysis. A number of technically valid ideas on how to formulate inexpensive, non-noble metal catalysts have been generated, and these approaches will be investigated in the next program period. In addition, progress has been made on increasing the utilization of noble metal catalysts using conductive supports, and this work will be continued to determine the extent to which utilization can be improved.

The successful operation of a multicell methanol stack has been achieved. Future work will emphasize the development of a self-contained methanol battery with an integrated process and electrical system. A program of testing and evaluation of the components will be undertaken to improve the reliability of the unit. In addition, research on methanol cells will continue with the main objectives of reducing catalyst cost and improving electrode performance.

The past and projected distributions of effort on each of these tasks are as follows. The emphasis will depend on the rates of progress in each area.

		Effort Expended in 1965, %	
Task	Title	Actual January-June	Projected July-December
A	Hydrocarbon Electrode	35	37
B	Hydrocarbon Fuel Cell	2	3
C	New Systems	15	13
D	Methanol Electrode	15	16
E	Air Electrode	2	1
F	Methanol Fuel Cell	7	5
G	Prototype Development	24	25

Research and development is expected to concentrate, during the second half of the year, on the areas discussed below.

6.1 Task A, Hydrocarbon Electrode

Catalysis will continue to receive the most attention in future research efforts. The work will continue to be directed toward the use of liquid hydrocarbons in the jet fuel boiling range. Emphasis will be placed on investigations of non-noble metal catalysts. However, in order to maintain a balanced effort, further work will be undertaken to improve the utilization of platinum. The goal of this work will be reduction of platinum loading to less than one mg/cm^2 and the use of the lowest possible temperatures consonant with adequate performance will be emphasized. Operation at temperatures up to 200-300°C will be studied to define the optimum level. The program on non-noble catalysts will continue to develop two approaches. First, catalytically active metals of Groups VII and VIII will be incorporated into compounds stable enough for use in acid electrolyte. Second, alloys of non-noble metals and other compounds with poor acid stability will be prepared and evaluated in buffer electrolytes. The demonstrated activity of noble metal catalysts justifies their further development only if catalyst loading can be

substantially reduced. The approach will continue to be to disperse the catalyst on conductive supports as well as to explore techniques for increasing intrinsic activity.

Research on acid resistant, non-noble metal compounds will continue on the mixed oxides and will expand into the mixed interstitial carbides of transition elements. The working principles leading to acid stability and conductivity will continue to be defined prior to the determination of catalytic activity.

The catalytic properties of non-noble metal alloys and of mixed oxides with poor corrosion resistance will be evaluated in buffer electrolytes. Alloys will be chosen on the basis of average d-band vacancies and adsorption tendencies.

Carbon and other conductive refractories will be examined as supports for noble metal catalysts. Techniques for increasing the activity of supported catalyst such as the use of silicates and molecular sieves as ancillary substrates with carbon, will be explored. The possibility of using some of the interstitial compounds of this program as supports will be considered. Since thin electrodes increase catalyst utilization, further development of electrode structures is planned.

If warranted by catalyst developments, studies will be initiated to modify or develop particular electrode structures using new catalysts. In all of the catalyst studies, gaseous hydrocarbons will be used as model fuels in preliminary tests. Attractive catalysts will be tested with liquid hydrocarbons, generally at 100 to 200°C.

The feasibility of a liquid-phase steam reforming process for hydrogen generation will be assessed. A successful liquid phase operation could remove a major disadvantage of steam reforming, the low thermal efficiency. Work will be carried out to determine the rate of reaction and hydrogen reductivity with liquid phase operation at 150 to 250°C using an active, non-noble metal catalyst.

6.2 Task B, Hydrocarbon Fuel Cell

Engineering research on total cells operating at 150°C will be extended to produce an operable design with existing electrodes. Emphasis in this program will be on development of components.

6.3 Task C, New Systems

Discovery of a new electrolyte, pyrophosphoric acid, which can be operated at 250-300°C, has raised the possibility of using operating temperatures higher than previously possible. The capability of this system has now been defined for massive platinum electrodes. Work will be continued to determine the extent to which platinum loading can be reduced in this system. Limited studies on materials of construction will be continued in order to assess the corrosion problems inherent in this system.

The capabilities of low temperature buffer electrolyte systems have been demonstrated in half-cells. Further work will be carried out to assess the performance of a total cell operating with potassium carbonate electrolyte. Establishment of a suitable means for rejecting carbon dioxide from the system will be of prime importance since cathode performance is sensitive to pH. Further work will also be carried out on the concentrated, high temperature buffer systems to determine whether air electrode performance can be improved.

Other areas to be investigated include the dynamic electrode and exploratory electrolytes. Work on the dynamic electrode will be undertaken to define the extent to which catalyst utilization can be improved. Exploratory work on electrolytes for use at 250 to 300°C will be carried out.

6.4 Task D, Methanol Electrode

Incentives still exist for research on the methanol electrode, although active catalysts were developed in 1964. About 25% of the total efficiency loss in the methanol-air cell can be attributed to the anode catalyst. Therefore, promising catalysts prepared in the program of Task A will be evaluated for methanol activity. In addition, studies will be made to reduce catalyst loading consistent with performance, stability, attrition, and fabrication requirements by using conductive supports such as carbon.

6.5 Task E, Air Electrode

Effective structures for air electrodes in acid and buffer electrolytes are now available. However, the initial polarization of oxygen catalysts remains an unsolved problem and continued catalyst research is planned. This program will be integrated with the anode catalyst studies and promising compositions will be evaluated for oxygen reduction activity. Further work on membrane-less air electrode will also be undertaken since this could reduce the cost and improve reliability.

6.6 Task F, Methanol Fuel Cell

Large methanol fuel cells, alone and in multicell units, have demonstrated good performance. However, further definition of chemical oxidation and the mass and energy flow in these cells is needed for advanced cell and battery design. Work to reduce chemical oxidation by reducing the rate of transport of methanol to the cathode will be undertaken. The use of barriers in the interelectrode space and immobilized electrolyte will be investigated. A study of systems which could be used for heat and water balancing will be made. Also, alternate anode designs will be considered to improve methanol contacting with larger electrodes.

6.7 Task G, Prototype Development

The major goal of the program on prototype development will be the design and construction of a self-contained methanol battery which will deliver at least 60 watts. The battery package will contain a multicell stack, a fuel supply, and an integrated process and electrical system. The cell stack is already essentially developed, and most of the effort will be directed toward features required to integrate the system fully. Methanol and acid concentration controllers will be tested for reliability. These and the electrolyte circulation pump will be incorporated into the system. In addition, a water economy unit will be developed for the system.

SECTION 7

IDENTIFICATION OF PERSONNEL AND DISTRIBUTION OF HOURS

7.1 Background of New Personnel

William R. Epperly (M.S., Chemical Engineering, Virginia Polytechnic Institute) is currently section head responsible for all fuel cell research activities. He was formerly section head of separations research. He has been with Esso Research since 1957 and during most of his career has been involved in research and development of separations processes. In addition, he has worked on hydrocarbon conversion processes such as steam reforming, hydrogen treating, and pyrolysis. He has four U.S. patents, thirteen patents pending, and one publication.

Herbert H. Vickers (Mechanical Engineering Degree, Southampton University, England) has a total of 38 years experience in various areas of construction and research. He has spent 28 years with Esso Research on a variety of special assignments including design and construction of process equipment, developing testing procedures, and fuel cells. He holds over 20 patents and has published 5 technical papers.

Martin Lieberman (M.S., Chemical Engineering, The Polytechnic Institute of Brooklyn) joined Esso Research in April, 1965. He has been engaged in studies of various problems relating to the methanol battery. Prior to his employment with Esso, he spent 5 years in various aspects of semiconductor development where he worked on transistors and thermoelectric power plants. He has also studied heat recovery and air pollution systems. He has one patent which is pending.

7.2 Distribution of Hours

The following are the technical personnel who have contributed to the work during the reporting period 1 Jan. 1965 - 30 June 1965 and the approximate number of hours of work performed by each:

Morton Beltzer	928
George Ciprios	822
William R. Epperly	718.5
I-Ming Feng	826
Carl E. Heath	120
Eugene L. Holt	834
Hugh H. Horowitz	871.5
Donald E. LeClair	536
Duane G. Levine	870
Martin Lieberman	440
John M. Matsen	956
Andreas W. Moerikofer	850
Charles E. Morrell	880
Eugene H. Okrent	804
Robert K. Resnik	762
Joseph A. Shropshire	928
Barry L. Tarmy	849
Charles E. Thompson	932
Herbert H. Vickers	688
Elliot A. Vogelfanger	888
James A. Wilson	740
Abraham A. Zimmerman	900
Total	17,143

SECTION 8

REFERENCES

(1) Heath, C. E., Tarmy, B. L., et al, Soluble Carbonaceous Fuel-Air Fuel Cell, Report No. 1, Contract DA 36-039 SC-89156, 1 Jan. 1962 - 30 June 1962.

(2) Tarmy, B. L., et al, Soluble Carbonaceous Fuel-Air Fuel Cell, Report No. 2, Contract DA 36-039 SC-89156, 1 Jan. 1962 - 31 Dec. 1962.

(3) Tarmy, B. L., et al, Soluble Carbonaceous Fuel-Air Fuel Cell, Report No. 3, Contract DA 36-039 AMC-00134(E), 1 Jan. 1963 - 30 June 1963.

(4) Tarmy, B. L., et al, Soluble Carbonaceous Fuel-Air Fuel Cell, Report No. 4, Contract DA 36-039 AMC-00134(E), 1 Jan. 1963 - 31 Dec. 1963.

(5) Heath, C. E., Holt, E. L., Horowitz, H. H., Levine, D. G., Tarmy, B. L., et al, Hydrocarbon-Air Fuel Cell, Report No. 5, Contract DA 36-039 AMC-03743(E), 1 Jan. 1964 - 30 June 1964.

(6) Heath, C. E., Holt, E. L., Horowitz, H. H., Levine, D. G., Tarmy, B. L., et al, Hydrocarbon-Air Fuel Cell, Report No. 6, Contract DA 36-039 AMC-03743(E), 1 July 1964 - 31 Dec. 1964.

(7) Breiter, M., Knorr, C. A., and Volkl, W., Z. Elektrochem, 59, 681 (1955).

(8) Will, F. G., J. Electrochem Soc., 112, 451 (1965).

(9) Shropshire, J. A., Okrent, E. H., and Horowitz, H. H., Presentation at Symposium on Fuel Cells, Div. of Fuel Chemistry, 149th Mtg., ACS, Atlantic City, Sept. 1965.

(10) Brummer, S. B., Reports Nos. 2 and 3, Contract No. DA 44-009 AMC-410(T) Tyco Laboratories, October 30, 1964, March 31, 1965.

(11) Jorgensen, K., Inorganic Complexes, Academic Press, New York, 1963, p. 172-3.

(12) Weyl, W. A., A New Approach to Surface Chemistry and to Heterogeneous Catalysis Penn State College Bulletin, XLV, No. 25, p. 31 (1951).

(13) Hofmann, K. A., Ann. Chem., Liebigs, 312, 1 (1900).

(14) Harned, H. S., and Owen, B. B., The Physical Chemistry of Electrolytic Solutions Reinhold Publishing Co., New York, 1958.

(15) Cairns, E. J., and Bartosik, D. C., J. Electrochem Soc., 111, No. 11, 1205 (1964).

(16) Brummer, S. B., and Ford, J. I., J. Phys. Chem., 69, 1355 (1965).

(17) Pliskin, W. A., and Eischens, R. P., Z. Phys. Chem., 24, 11 (1960).

(18) Presbey, C. H., Jr., and Schuldiner, S., J. Electrochem Soc., 108, 985 (1961).

(19) Eucken, A., and Weblus, B., Z. Elektrochem, 55, 114 (1951).

(20) Franklin, T. C., and McClelland, D. H., J. Phys. Chem., 67, 2436 (1963).

(21) Shropshire, J. A., J. Electrochem Soc., 112, 465 (1965).

(22) Gileadi, E., Rubin, B. T., Bockris, J. O'M., J. Phys. Chem., in press.

(23) Niedrach, L. W., J. Electrochem Soc., 111, 1309 (1964).

(24) Wroblowa, H., Piersma, B. J., and Bockris, J. O'M., J. Electroanal. Chem., 6, 401 (1963).

APPENDIX A-1

EQUIPMENT USED FOR BUTANE ADSORPTION RATE MEASUREMENTS

The apparatus used for the flowing electrolyte experiments is shown in Figure A-1.

The platinum black powder was held at the upper face of an 18 mil porous tantalum sheet by the downward flow of electrolyte. The two liter flask containing 3.7 M H_2SO_4 was briskly stirred and saturated with Instrument Grade butane. Electrical connections were made to the porous tantalum plate (via a gold current collector), an auxilliary electrode in the flask, and a saturated calomel electrode with Luggin capillary about 1/4 inch above the surface of the tantalum plate. The tantalum was cleaned by gentle wire brushing and a once-through application of aqueous HF followed by deionized water prior to each use.

Potentiostatted triangular or sawtooth voltage signals were applied to the working electrode from a modified Anotrol Model (4101) Research Controller fed by the output of a Servomex LF 51 function generator. The resultant I-V(t) functions were recorded on a Moseley Model 135 x-y plotter and coulombic quantities of fuel oxidized were obtained by integration of the desired peaks using a planimeter.

The parts of the flow system shown in Figure A-1 are identified as follows:

A - Teflon Stopcock
B - Gold Current Collector
C - Porous Tantalum Plate
D - Powdered Platinum Black
E - Clamp
F - Insulation (over tape heaters)
G - 2-Liter Flask
H - Luggin Capillary
I - Counterelectrode
J - Butane Sparges
K - Thermometer, with Therm-O-Watch Relay
L - Saturated Calomel Electrode
M - Condenser
N - Make-up Addition Bottle

Figure A-1

Flow System for Butane Adsorption Measurements

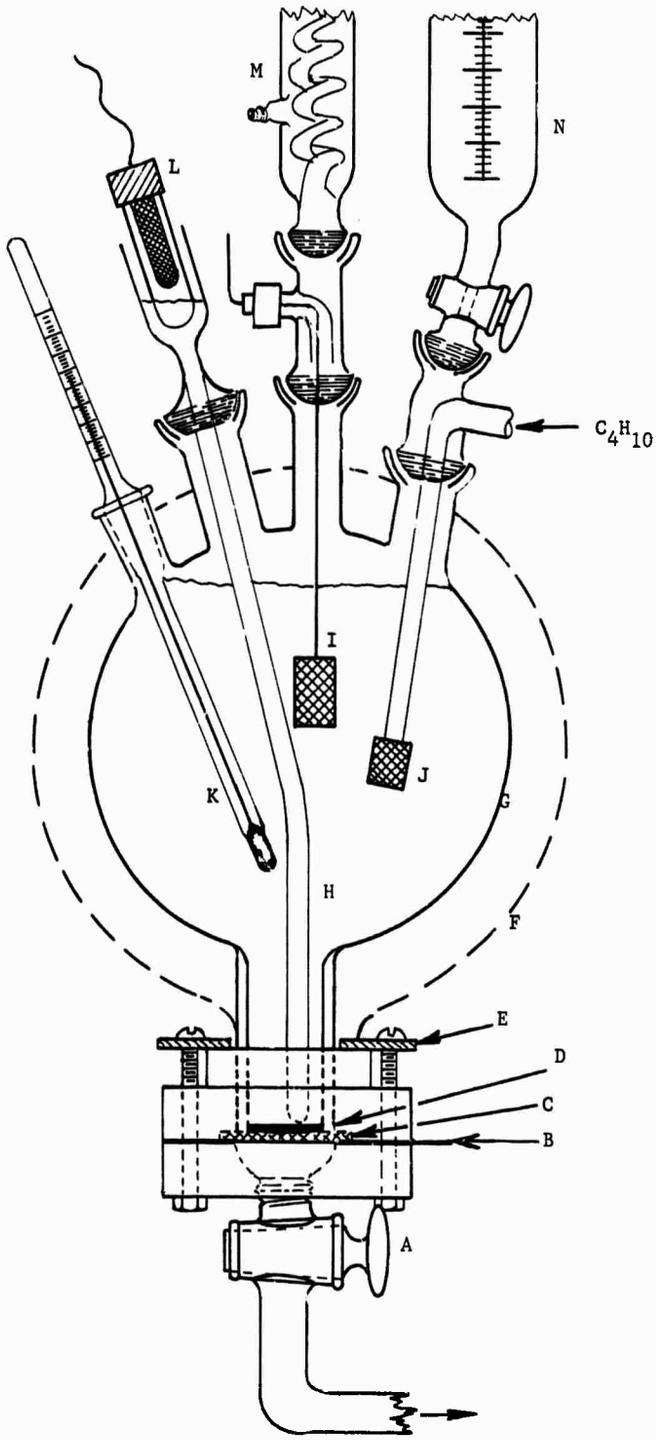

APPENDIX A-2

SUMMARY OF BUTANE ADSORPTION RATE MEASUREMENTS ON PLATINUM - CONTINUOUS SCAN

Platinum Black, 3.7 M H_2SO_4, Scan 0-1.12 Volts Versus S.C.E.

Temperature, °C	Flow Rate, cc/min	Butane Accumulated, mc/mg	Catalyst Loading, mg/cm^2	Continuous Scan Rate, volts/sec	Remarks
95	23.5	16.7	25	0.022	3.8 cm^2 total area, Engelhard Pt black
	36	25.5	-	-	
	45	32.7	-	-	
	53	32.8	-	-	
	54	32.4	-	-	
95	9	8.76	10	0.022	Engelhard Pt black - variation in catalyst loading. Same scan as above.
	12	10.1	-	-	
	16	14.1	-	-	
	28	20.4	-	-	
	35.5	24.7	-	-	
	58	31.5	-	-	
	64	32.1	-	-	
95	21 (1)	21.6	25	0.022	Lithium - Reduced Pt
	17	16.6			
95	18	26.6	10	0.022	Formaldehyde - Reduced Platinum
	31	31.3	-	-	
	40	33.0	-	-	
	43	31.0	-	-	
100	64	43.2	10	0.028	Temp Study Δ E* $\simeq$ 10 k cal/mole
90	64	28.2	10	0.028	Engelhard Pt black
80	64	21.8	10	0.028	
95	64	15.6	10	0.055	Scan Rate Study
	64	22.2	-	0.036	Engelhard Pt black
	64	32.9	-	0.022	
	64	45.9	-	0.016	

(1) Did not reach flow-independence levels.

Figure A-2

Expected Butane Adsorption During Scan

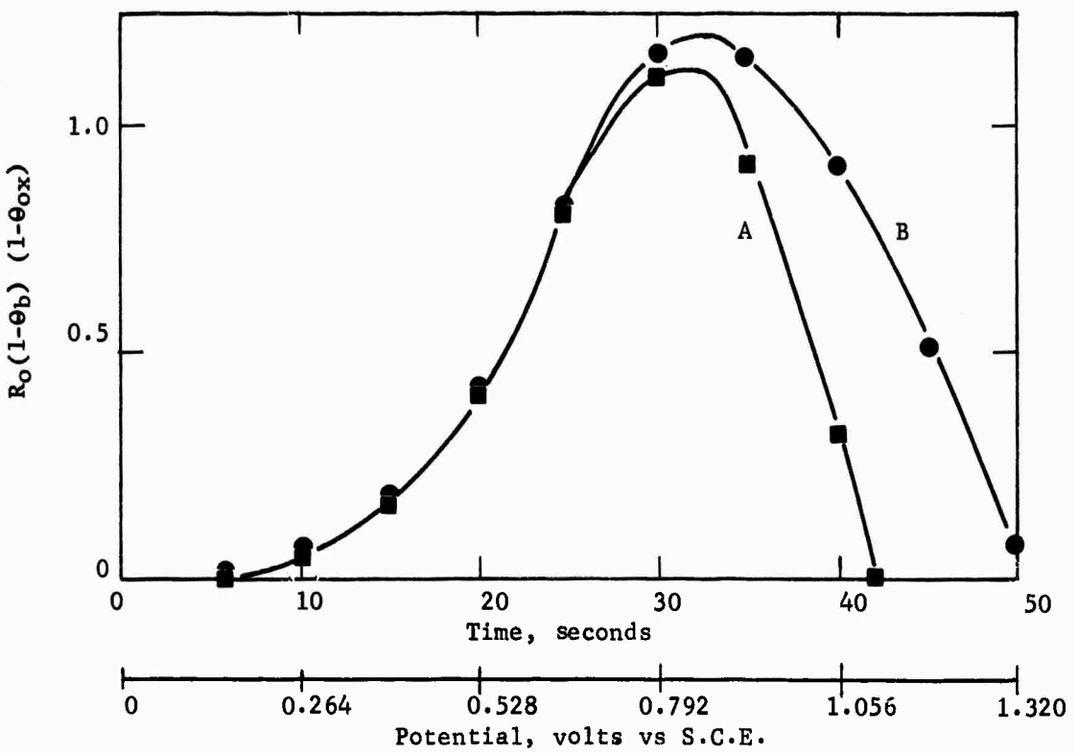

APPENDIX A-3
TYPICAL BUTANE ADSORPTION RATE CURVES

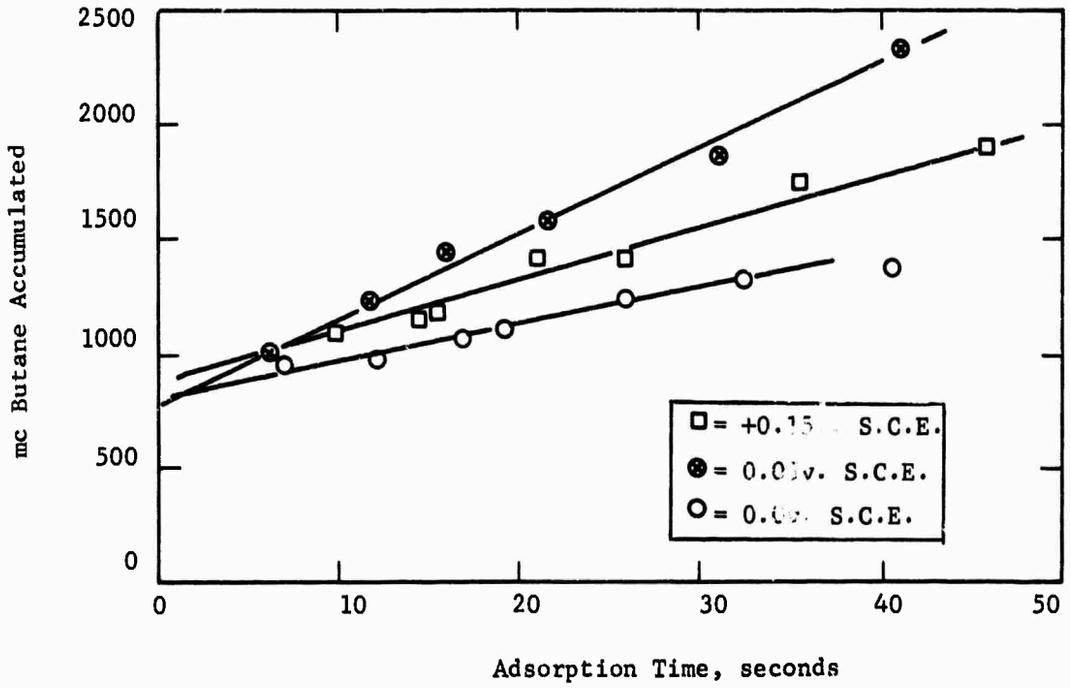

APPENDIX A-4

SUMMARY OF BUTANE ADSORPTION RATE MEASUREMENTS ON PLATINUM - SAWTOOTH SCAN

38 mg Engelhard platinum black, 95°C, 3.7M H_2SO_4, Scan to 1.12 volts versus S.C.E.

Potential, volts vs S.C.E.	Adsorption Time, sec	Butane Accumulated, millicoulombs	Observed Adsorption Rate, ma/mg	Steady State Current Correction, ma/mg	Remarks
+0.15	6.2	911	0.71	0.82	Series I.
	11.0	1172			$\theta_H = 0$
	15.4	1211			
	17.1	1347			Total Adsorption
	20.6	1501			Rate = 1.54 ma/mg
	28.3	1723			
	33.6	1782			
	41.2	2005			
	53.3	2225			
+0.15	5.4	814	0.59	0.82	Series II,
	10.5	1104			$\theta_H = 0.02$
	14.8	1152			
	15.6	1172			Total Adsorption
	21.0	1413			Rate = 1.41 ma/mg
	26.1	1413			
	35.6	1752			
	46.0	1883			
+0.10	6.2	1047	1.02	0.58	Series I,
	7.5	1038			$\theta_H = 0.041$
	9.8	1299			
	13.5	1472			Total Adsorption
	22.5	1821			Rate = 1.59 ma/mg
	24.6	1929			
	30.2	1938			
	40.3	2441			
	51.7	2643			
+0.10	6.3	1007	1.00	0.58	Series II,
	9.7	1132			$\theta_H = 0.056$
	14.1	1269			
	15.5	1289			Total Adsorption
	21.4	1675			Rate = 1.58 ma/mg
	29.3	1937			
	40.3	2257			
+0.10	6.7	1270	1.05	0.58	Series III,
	10.8	1502			$\theta_H = 0.041$
	15.5	1598			
	21.0	1909			Total Adsorption
	28.3	2132			Rate = 1.63 ma/mg
	42.0	2537			
+0.05	5.4	824	0.99	0.33	Series I
	8.1	1066			$\theta_H = 0.173$
	13.6	1338			
	18.4	1569			Total Adsorption
	27.4	1976			Rate = 1.32 ma/mg
	42.0	2450			
	54.2	2655			
+0.05	6.6	1007	0.98	0.33	Series II,
	11.8	1230			$\theta_H = 0.178$
	16.0	1442			
	21.8	1579			Total Adsorption
	31.1	1850			Rate = 1.31 ma/mg
	40.9	2315			

APPENDIX A-4 (Cont'd)

SUMMARY OF BUTANE ADSORPTION RATE MEASUREMENTS ON PLATINUM - SAWTOOTH SCAN

38 mg Engelhard platinum black, 95°C, 3.7M H_2SO_4, Scan to 1.12 volts versus S.C.E.

Potential, volts vs S.C.E.	Adsorption Time, sec	Butane Accumulated, millicoulombs	Observed Adsorption Rate, ma/mg	Steady State Current Correction, ma/mg	Remarks
+0.05	8.5	1485	1.14	0.33	Series III,
	11.8	1629			θ_H = 0.142
	16.7	1821			
	22.3	2172			Total Adsorption
	27.0	2247			Rate = 1.47 ma/mg
	37.5	2770			
0.0	5.8	736	0.67	0.13	Series I,
	7.9	834			θ_H = 0.296
	10.6	853			
	18.2	1057			
	26.0	1318			Total Adsorption
	38.0	1550			Rate = 0.80 ma/mg
0.0	7.2	936	0.42	0.13	Series II,
	12.2	988			θ_H = 0.316
	13.9	940			
	16.9	1075			Total Adsorption
	17.3	1018			Rate = 0.55 ma/mg
	19.1	1114			
	25.6	1114			
	25.9	1230			
	23.5	1318			
0.0	8.4	1231	0.55	0.13	Series III,
	8.4	1189			θ_H = 0.311
	12.3	1250			
	18.6	1375			Total Adsorption
	20.1	1482			Rate = 0.38 ma/mg
	30.7	1628			
	38.8	1880			
-0.025	12.3	1066	0.28	0.0	Series III,
	16.8	1066			θ_H = 0.449
	23.2	1142			
	30.3	1220			Total Adsorption
					Rate = 0.28 ma/mg
-0.05	9.8	950	~0.0	0.0	Series III,
	15.6	1056			θ_H = 0.495
	19.9	950			
	22.6	1115			Total Adsorption
	31.8	989			Rate = 0.0 ma/mg
	38.5	1027			

APPENDIX A-5

ESTIMATION OF EXPECTED BUTANE ADSORPTION DURING VOLTAGE SCAN IN FLOWING ELECTROLYTE SYSTEM

One further evidence of the decline in butane adsorption rate as potential moves positive to +0.15 volts vs S.C.E. was obtained from the maximum butane adsorption on platinum black under flow conditions. This value, millicoulombs fuel/millicoulombs oxide (1.3 volts) = 1.61, was about equal to that observed previously in stagnant systems (1.58). Since under high flow conditions a significant contribution to the observed coulombs is expected as oxidized fuel is replaced during the time of the scan, this observation suggests that fuel adsorption rates are very low in the middle potential region prior to the onset of oxide formation.

The expected fuel contribution during the scan was estimated from:

$$\Delta Q = \int_{t_1(V_1)}^{t_2(V_2)} R_o\,(1-\theta_b)(1-\theta_{ox})\,dt$$

where θ_b represents the coverage with butane and a θ_{oxide} term was included to accommodate the fact that surface oxide formation will undoubtedly interfere with fuel adsorption. R_o is the maximum butane rate of adsorption, the value 1.6 ma/mg taken at +0.10 volts vs S.C.E.

Values of θ_b and θ_{ox} were obtained from the scan curves for saturated and blank electrodes as a function of potential (time) during the scans at 26 mv/sec. Two θ_{oxide} functions were assumed: (1) one with θ_{oxide} equal to unity at one-half the total coulombs required for 2 electron PtO formation. This would be the case if PtOH were formed first or if PtO were formed on half the sites: and (2) θ_{oxide} equal to one at full 2 electron oxide level.

The combined function is shown in Figure A-2, plotted against time. The two integrals correspond to additional butane contributions of 10 and 15% respectively expected during the course of the scan. Since the observed contribution is essentially negligible, it is concluded that butane adsorption rate must fall to essentially zero in the potential range of the scan where re-adsorption of fuel is possible.

APPENDIX A-6

ELECTROCHEMICAL CHARACTERIZATION OF PLATINUM BLACK

The commercial (Engelhard) platinum black used in the study of butane adsorption was electrochemically characterized using the voltage scanning technique. Measurements were made using the pressed electrodes described previously, immersed in argon-sparged 3.7 M H_2SO_4 at 80°C. Adsorption-discharge of protons to form H· in the region negative to + 0.2 volts vs S.C.E. was defined as a function of potential from anodic scans. The coulombs required to reduce the oxide formed by anodization to a fixed potential of 1.3 volts vs S.C.E. was measured. A summary of this data is given in Table A-1, and fractional H· coverage plotted against potential in Figure A-3.

The quantity of coulombs required for the maximum deposition of H· the surface is seen to correspond closely to one half the number required for oxide reduction from 1.3 volts vs S.C.E. On the usual assumption of one hydrogen atom per platinum atom, the surface at 1.3 volts vs S.C.E. is thus believed to consist essentially of a completed layer of PtO. The quantity of coulombs required for hydrogen deposition was also used to calculate a rough value for the electrochemical surface area of the catalyst. Using a value of 210 μ coul/cm^2 as the value for H. deposition on one true cm^2 (8,15), a total surface area of about 23 m^2/gm was calculated. This value agrees fairly well with the 28 m^2/gm found by the nitrogen B.E.T. method.

Table A-1

Hydrogen Deposition on Platinum As a Function of Potential

Equilibration Potential, volts vs S.C.E.	Total H., mc/mg	Fraction of Max H.
+0.05	6.54	0.14
+0.02	12.0	0.25
0.0	15.4	0.32
-0.02	17.2	0.36
-0.04	19.7	0.41
-0.06	22.8	0.48
-0.08	29.1	0.61
-0.10	37.2	0.78
-0.12	42.6	0.89
-0.14_4	47.8	1.00

48 mg sample of Engelhard Pt black; total oxide reduction from 1.3 volts vs S.C.E., Q_o (1.3) = 100 mc/mg.

Figure Ā-3

Hydrogen Coverage versus Potential

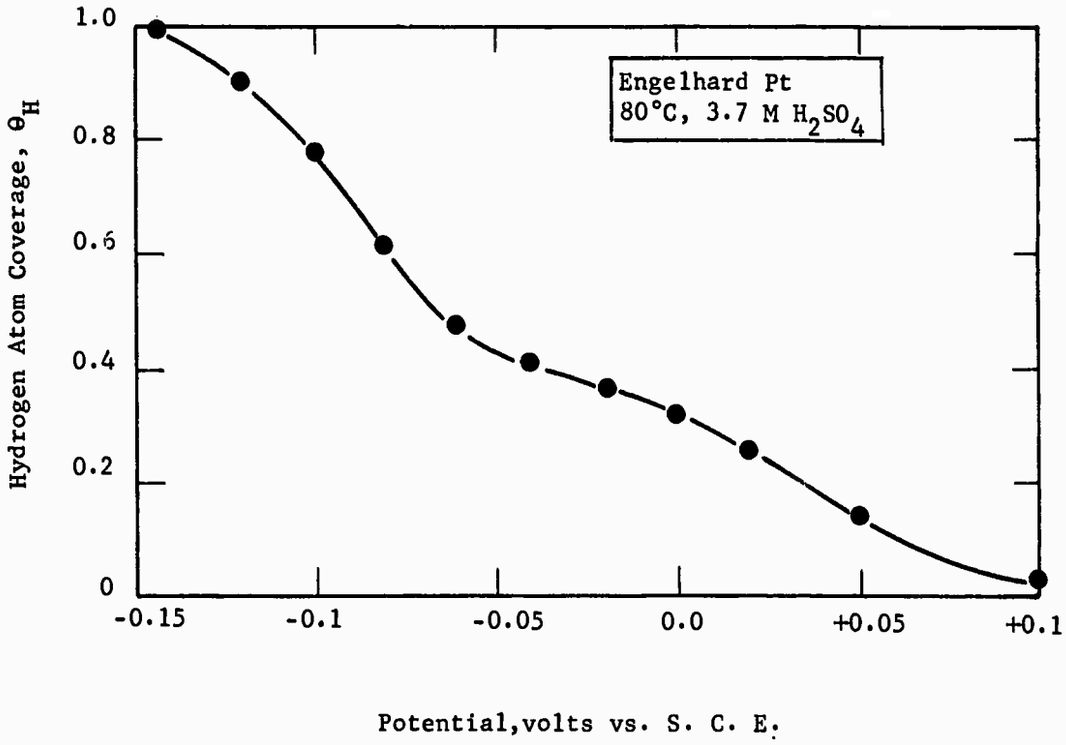

APPENDIX A-7

REPLACEMENT OF ADSORBED BUTANE WITH HYDROGEN

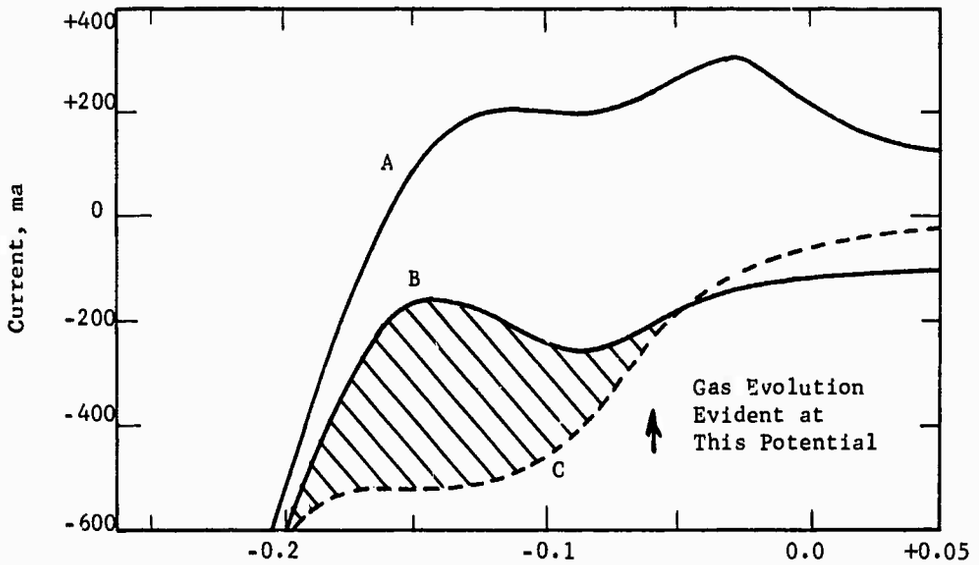

Curve A: anodic scan, no adsorbed butane.

Curve B: cathodic scan, no adsorbed butane.

Curve C: cathodic scan, with adsorbed butane.

APPENDIX A-8

EQUILIBRIUM HYDROCARBON ADSORPTION MEASUREMENTS

Voltage Scan Technique - Engelhard Platinum Black[1]

Fuel	Electrolyte	Temperature, °C	Adsorption Time, Min	Potential of Adsorption, volts vs S.C.E.	Equilibration Potential after Adsorption, volts vs S.C.E.	Accumulated Fuels, Millicoulombs	Millicoulombs Fuel / Millicoulombs Oxide[2]	Remarks
Methane	3.7 M H_2SO_4	80	60	+0.05	-	496	0.11	
	3.7 M H_2SO_4	80	120	+0.05	-	961	0.23*	
	14.7 M H_3PO_4	140	60	+0.05	-	587	0.34	
	14.7 M H_3PO_4	140	120	+0.05	-	758	0.46*	
Ethane	3.7 M H_2SO_4	80	60	+0.05	-	3030	0.73	Replicates
	3.7 M H_2SO_4	80	120	+0.05	-	3139	0.74*	
	3.7 M H_2SO_4	80	60	+0.05	-	-	0.81	
	3.7 M H_2SO_4	80	120	+0.05	-	-	0.91*	
	14.7 M H_3PO_4	140	60	+0.05	-	1279	0.71	
	14.7 M H_3PO_4	140	120	+0.05	-	1329	0.75*	
Propane	3.7 M H_2SO_4	80	60	+0.05	-	4898	1.03	Replicates
	3.7 M H_2SO_4	80	120	+0.05	-	5448	1.19*	
	3.7 M H_2SO_4	80	60	+0.05	-	-	1.35	
	3.7 M H_2SO_4	80	120	+0.05	-	-	1.28*	
	14.7 M H_3PO_4	140	60	+0.05	-	2334	0.94*	
	14.7 M H_3PO_4	140	120	+0.05	-	2667	0.91	
Butane	3.7 M H_2SO_4	80	Max	+0.05	-	-	1.58 ± 0.13	Standard from Report No 6.
	14.7 M H_3PO_4	150	60	+0.05	-	1263	0.48	Note drastic effect of 10°C temp change. (see below)
	14.7 M H_3PO_4	150	120	+0.05	-	1309	0.57	
	14.7 M H_3PO_4	140	60	+0.05	-	3514	1.63*	
	14.7 M H_3PO_4	140	60	+0.05	-	6075	2.14*	
	14.7 M H_3PO_4	135	30	0.00	-	4910	1.70*	
	14.7 M H_3PO_4	135	180	0.00	-	4760	1.66*	
	14.7 M H_3PO_4	140	60	+0.05	-	6866	1.76*	
	14.7 M H_3PO_4	140	120	+0.05	-	6340	1.80*	
Butane	14.7 M H_3PO_4	140	60	+0.05	+0.15	1872	0.69	$\frac{\text{Coulombs Fuel}}{\text{Coulombs [H]}} = 6.4$
	14.7 M H_3PO_4	140	60	+0.05	+0.25	566	0.20	
	14.7 M H_3PO_4	140	60	+0.05	+0.35	353	0.14	
	14.7 M H_3PO_4	140	60	+0.05	+0.45	154	0.07	

APPENDIX A-8 (CONTINUED)

EQUILIBRIUM HYDROCARBON ADSORPTION MEASUREMENTS

Voltage Scan Technique - Engelhard Platinum Black[1]

Fuel	Electrolyte	Temperature, °C	Adsorption Time, Min	Potential of Adsorption, volts vs S.C.E.	Equilibration Potential after Adsorption, volts vs S.C.E.	Accumulated Fuels, Millicoulombs	Millicoulombs Fuel / Millicoulombs Oxide[2]	Remarks
Butane	14.7 M H_3PO_4	100	60	+0.05	+0.05	2624	1.75	
	14.7 M H_3PO_4	100	60	+0.05	.15	2981	2.08	
	14.7 M H_3PO_4	100	60	+0.05	.25	2666	1.88	
	14.7 M H_3PO_4	100	60	+0.05	+0.35	1866	1.28	
	14.7 M H_3PO_4	100	60	+0.05	+0.45	866	0.59	
	14.7 M H_3PO_4	100	60	+0.05	+0.55	534	0.36	
Butane	3.7 M H_2SO_4	80	60	+0.05	+0.05	-	1.58 ± .13	Standard, Report No 6
	3.7 M H_2SO_4	80	60	+0.05	+0.15	7767	1.38	
	3.7 M H_2SO_4	80	60	+0.05	+0.25	5786	1.16	Study of surface coverage vs equilibrium potential
	3.7 M H_2SO_4	80	60	+0.05	+0.35	2549	0.51	
	3.7 M H_2SO_4	80	60	+0.05	+0.45	1626	0.36	
	3.7 M H_2SO_4	80	60	+0.05	+0.55	799	0.17	
	3.7 M H_2SO_4	80	60	+0.05	+0.65	655	0.14	
Butane	3.7 M H_2SO_4	80	30	+0.05	0.00	9250	1.66*	Check on "Standard"
	3.7 M H_2SO_4	80	30	+0.05	-0.02	4390	-	
	3.7 M H_2SO_4	80	30	+0.05	-0.04	2015	-	Study of Fuel Desorption vs Potential
	3.7 M H_2SO_4	80	30	+0.05	-0.06	906	-	
	3.7 M H_2SO_4	80	30	+0.05	-0.08	732	-	
	3.7 M H_2SO_4	80	30	+0.05	-0.10	674	-	
	3.7 M H_2SO_4	80	30	+0.05	-0.12	515	-	
	3.7 M H_2SO_4	80	30	+0.05	-0.14	376	-	
Butane	14.7 M H_3PO_4	80	60	0.0	-	-	1.46	
	14.7 M H_3PO_4	80	180	0.0	-	-	1.84*	
Butane	1 M K_2SO_4	80	10	-0.30	-	2150	-	Oxide Reduction Poorly Defined.
	1 M K_2SO_4	80	30	-0.30	-	4620	-	
	1 M K_2SO_4	80	60	-0.30	-	5340	-	
Butane	1 M KH_2PO_4 + 1 M K_2HPO_4	80	30	-0.41	-	1045	0.30	

APPENDIX A-8 (CONTINUED)

EQUILIBRIUM HYDROCARBON ADSORPTION MEASUREMENTS

Voltage Scan Technique - Engelhard Platinum Black[1]

Fuel	Electrolyte	Temperature, °C	Adsorption Time, Min	Potential of Adsorption, volts vs S.C.E.	Equilibration Potential after Adsorption, volts vs S.C.E.	Accumulated Fuels, Millicoulombs	Millicoulombs Fuel / Millicoulombs Oxide[2]	Remarks
Butane	1 M KH_2PO_4 1 M K_2HPO_4	80	60	-0.41	-	1230	0.31	
	1 M KH_2PO_4 1 M K_2HPO_4	80	180	-0.41	-	1975	0.51	
	1 M KH_2PO_4 1 M K_2HPO_4	80	60	-0.41	-	1410	0.44	
	1 M KH_2PO_4 1 M K_2HPO_4	80	60	-0.31	-	1353	0.43	
	1 M KH_2PO_4 1 M K_2HPO_4	80	60	-0.21	-	1260	0.46	
Butane	1 N NaOH	80	30	-0.83	-	nd[3]	-	
	1 N NaOH	80	60	-0.83	-	nd	-	
	1 N NaOH	80	900	-0.83	-	nd	-	
Butane	1 M Na_2CO_3 1 M $NaHCO_3$	80	10	-0.70	-	Carbonate Reduction - Reoxidation		
	1 M Na_2CO_3 1 M $NaHCO_3$	80	30	-0.70	-	Carbonate Reduction - Reoxidation		
	1 M Na_2CO_3 1 M $NaHCO_3$	80	60	-0.70	-	Carbonate Reduction - Reoxidation		

* Value taken as maximum coverage for the specific run conditions or used in average.

(1) Except as noted. Fifty milligrams of black mixed with five milligrams (DuPont) Teflon 41BX.

(2) From voltage scan reduction peak from 1.3 volts vs S.C.E.

(3) None detected.

APPENDIX A-9

IMPLICATIONS OF A TWO-SITE INTERACTION IN THE OXIDATION OF CARBONACEOUS FUELS

The differentiation of the platinum surface with respect to adsorption of two different "types" of hydrogen is well known, and has been the subject of numerous investigations in recent years. (7,17-20). As indicated in phase 1, part b, it is now apparent that the surface of platinum can also be differentiated with respect to butane adsorption. Franklin and McClelland(20) have also noted relationships between H_2O_2 decomposition and quantity of Type II (more anodic) hydrogen on the platinum surface. If it is assumed that this surface differentiation extends to water as well as fuel interactions, a reaction scheme emerges which is applicable to oxygenated and olefinic as well as saturate fuels.

Basic Postulates

The generalized scheme of fuel reaction is assumed to be:

(1) $H_2O \longrightarrow H_2O^*$ adsorbed

(2) Fuel $\longrightarrow$ Fuel* (adsorbed)

(3) $M + H_2O^* \longrightarrow M\text{-}OH + H^+ + e$

(4) $M\text{-}OH + Fuel^* \longrightarrow CO_2 + H_2O + M$ (etc)

The basic postulate to be advanced here is that the platinum surface is differentiated into two types of sites with respect to water interaction as well as fuel adsorption. Thus, in a general way, if a fuel adsorbs strongly enough to block those water sites which normally are active at the most negative potentials, it will require high polarization for its oxidation, i.e. by interaction with those water sites active at more positive potentials.

We will define:

1. A Type A water site is related in existence to the Type I H site, the $M + H_2O \longrightarrow M\text{-}OH + H^+ + e$ reaction being slow on these sites and occurring at the most negative potentials.

2. A Type B water site is related in existence to the Type II H site, the $M + H_2O \longrightarrow M\text{-}OH + H^+ + e$ reaction essentially a fast, equilibrium function of potential at more positive levels.

In addition to these postulates it is assumed that all carbonaceous fuels will be oxidized to CO_2 if the electrode is severely polarized to significant platinum oxide formation. With these assumptions the electrochemical behavior of each fuel is thereafter determined by its adsorption behavior. Butane, formaldehyde and ethylene will be discussed as representative of the various classes.

Adsorption-Reaction of Butane

Butane, as discussed previously, adsorbs only on Type II sites. As a result, interaction with "A" water sites can occur at the most negative potentials.

This leads to:

$$(5)\quad H_2O \rightleftharpoons H_2O^*(A)\ \text{(equil)}$$

$$(6)\quad C_4H_{10} \rightleftharpoons C_4H_{10}{}^*(II)\ \text{(equil in Tafel)}$$

$$(7)\quad M + H_2O^*A \longrightarrow M\text{-}OH(A) + H^+ + e\ \text{(R.D.S.)}$$

$$(8)\quad M\text{-}OH(A) + C_4H_{10}{}^*(II) \longrightarrow M + CO_2 + H_2O\ \text{(fast)}$$

In the Tafel region, equilibration of reaction (6) produces an electron discharge limitation with expectation of 2 RT/F behavior starting at low polarizations. This agrees well with previous observations on the butane system in 3.7 M sulfuric acid at 100°C (5,6). The limiting current, as discussed previously, is dictated by Reaction 6. The observed characteristics of butane as well as HCHO and ethylene reaction are summarized in Table A-2.

Adsorption-Oxidation of Formaldehyde

The single carbon oxygenated fuels adsorb strongly on both Type I and II sites at equilibrium. (1,21). The fuel adsorption on Type I sites precludes the adsorption of water and type "A" metal-water intereaction. Thus the potential equilibrates at the more positive levels of type "B" metal water interaction, an increase in potential of 0.2-0.3 volts. Interaction of fuel on Type I sites with the fast M, MOH reaction on "B" sites would produce a limitation by Reaction 4 with resultant RT/F behavior at low currents. This behavior is characteristic of the oxygenated single carbon fuels on platinum in acid. (1,2) Thus:

$$(9)\quad HCHO \rightleftharpoons HCHO^*\ \text{(I and II) equil}$$

$$(10)\quad M + H_2O(B) \rightleftharpoons M\text{-}OH(B) + H^+ + e\ \text{(equil)}$$

$$(11)\quad M\text{-}OH(B) + HCHO^*(I) \longrightarrow M + CO_2 + H_2O\ \text{(R.D.S.)}$$

For comparison typical performance curves (E-log I) for butane and formaldehyde are shown in Figure A-4.

Table A-2

Oxidation Characteristics Of Various Fuels In Sulfuric Acid Electrolyte

Observed Characteristic	Fuel		
	Butane	HCHO	C_2H_4
Adsorption — Type I	None	Complete	Some
Adsorption — Type II	Complete	Complete	Complete
Initial Polarization, mv versus N.H.E.	100	450, Initial Transient at 100	350≠
Tafel Slope	2 RT/F	RT/F	2 RT/F≠
Fuel Conc Dependence, Tafel Region	0	0	<0≠
Fuel Conc Dependence, Limiting Region	<1/2	(~1/2, CH_3OH)	1*

≠ Data of Wroblowa et al, see reference (24).

* Diffusion limited, under conditions employed.

Figure A-4

Comparison of Butane and Formaldehyde Performance

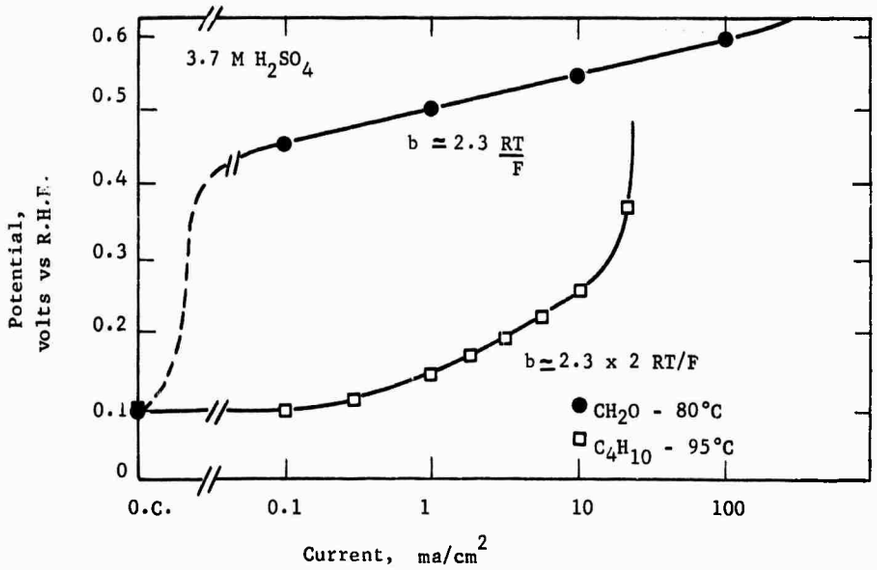

Application to Oscillations

The two site postulate lends itself well to explanation of oscillatory phenomena. Consider the formaldehyde system under galvanostatic operation. At high currents an adsorption limit of fuel on Type I sites occurs while fuel remains on Type II sites. Adsorption of water than on "A" sites (related to type I) allows a low potential interaction of M, MOH on "A" sites with fuel on Type II sites. Polarization then decreases until "A" sites are blocked by continued fuel readsorption or formation of a refractory A-II product. The resultant oscillation of potential would be expected to closely resemble the now-familar oscillations observed with oxygenated fuels in acid solution. (1,2)

Behavior related to these oscillations is often exhibited immediately after the open circuit immersion of a freshly prepared oxided platinum electrode in formaldehyde-sulfuric acid solution. In this case an immediate very low polarization is achieved by A-II interaction, followed by gradual increase in polarization as fuel readsorbs on Type I sites, blocking this reaction. This behavior is indicated by the dotted line in Figure A- 4.

Similarly, in the case of a low polarization saturate fuel reaction, the formation of a stable oxygenated intermediate would be expected to block "A" sites as discussed previously. This would lead to increasing polarization until the oxygenated species is removed by B-I interaction, the potential then returning to its original levels. Such oscillations are common with the saturate fuels.

Adsorption-Oxidation of Ethylene

Ethylene is believed to represent the middle ground between reaction of saturates and oxygenated fuels. At atmospheric pressure the relatively high coverages (22,23) indicate adsorption on some Type I as well as Type II sites. With the olefin, the adsorption on Type I sites is believed to the sufficiently incomplete as to allow the A-II interaction to occur. This leads to the observed (24) 2RT/F behavior with polarization increased by the low number of "A" sites available. Since the adsorption of ethylene on Type I sites appears to be reversible (22) the reaction would be expected to have a negative pressure dependence i.e., $(di/dp)_\eta < 0$ in the Tafel region as increased coverage blocks "A" sites. These predictions agree well with the behavior observed by Wroblowa et al. (24). It would seem probable that ethylene reaction would tend to approach that of oxygenated fuels at higher pressures, as blocking of "A" sites approaches completion.

Summary

In addition to organization of the reaction of carbonaceous fuels, the two-site postulate lends itself well to other aspects of reaction on platinum black. Thus the controversial water versus peroxide production upon oxygen reduction might very well be considered in a similar light.

The proposed two-site scheme is not intended to present a thoroughly complete and satisfying description of these complex reactions. It does appear, however, to bring together a wide variety of observations on seemingly unrelated phenomena.

APPENDIX A-10

BUTANE ADSORPTION - NON-PLATINUM CATALYSTS

Voltage Scans Covering 1.3 Volts

Catalyst	Electrolyte	Temp. °C	Adsorption Time, min	Potential of Adsorption, Volts vs S.C.E.	Accumulated Fuel, millicoulombs milligram	Remarks
Ni_2B	1 M NaOH	80	10	-0.83	nd (1)	Oxide reduction - O_2 evolution seem fairly reversible.
	1 M NaOH	80	30	-0.83	nd	
	1 M NaOH	80	60	-0.83	nd	
Ni_2B	1 M KH_2PO_4 1 M K_2HPO_4	80	30	-0.60	nd	Anodic oxidation (dissolution) peaks @ -0.4 - 0.5 volts vs S.C.E.
	1 M KH_2PO_4 1 M K_2HPO_4	80	60	-0.60	nd	
Ni·Au	1 M KH_2PO_4 1 M K_2HPO_4	95	30	-0.60	nd	Character of both components visible in voltage scan.
	1 M KH_2PO_4 1 M K_2HPO_4	95	60	-0.60	nd	
Ni	1 M KH_2PO_4 1 M K_2HPO_4	80	10	-0.60	nd	Blank to check oxide.
Rh	0.37 M H_2SO_4	80	60	+0.0	19.8	Oxidizes very high polarization.
	0.37 M H_2SO_4	80	100	+0.12	18.5	Q Fuel/Q Oxide = 0.41
	1 M Na_2CO_3 1 M $NaHCO_3$	80	60	-0.55	nd	Carbonate Reduction-Reoxidation
	1 M Na_2CO_3 1 M $NaHCO_3$	80	105	-0.55	nd	Carbonate Reduction-Reoxidation
	1 M K_2HPO_4 1 M KH_2PO_4	80	30	-0.4	nd	
	1 M K_2HPO_4 1 M KH_2PO_4	80	60	-0.4	nd	
	1 M K_2HPO_4 1 M KH_2PO_4	80	100	-0.5	Trece	Oxidizes at very high polarization
	14.7 M H_3PO_4	150	60	+0.05	7.7	Q Fuel/Q Oxide = 0.18
	14.7 M H_3PO_4	150	120	+0.05	16.0	Q Fuel/Q Oxide = 0.43
Ir	3.7 M H_2SO_4	80	60	+0.05	26	Oxide poorly defined.
	14.7 M H_3PO_4	150	60	+0.16	22.4	
	14.7 M H_3PO_4	150	120	+0.16	27	Note similar value, H_2SO_4 80°C

(1) None detected.

APPENDIX A-11

CATALYST STRUCTURE STUDIES--SINTERED PLATINUM TEFLON ELECTRODES

(14.7 M H_3PO_4, Butane, 85% Pt/15% Teflon Electrodes)
(50 mg catalyst/cm^2)

Catalyst Description	Temp, °C	Polarization from Theoretical Butane at Indicated ma/cm^2, volt												Remarks
		0	0.10	0.5	1.0	5.0	10	20	40	60	80	100	150	200	
2918-31-1 H_2 reduced (1)	100	0.09	0.13	0.54	Dead	--	--	--	--	--	--	--	--	--	
	125	0.12	0.24	0.31	0.56	--	--	--	--	--	--	--	--	--	0.72 at 2 ma/cm^2.
	150	0.15	--	0.5	0.52	0.64	--	--	--	--	--	--	--	--	7.5 ma/cm^2 = 0.84.
2918-35 HCHO reduced	100	0.07	0.21	--	Dead	--	--	--	--	--	--	--	--	--	
	150	0.09	--	--	0.28	---------- 2.5 ma/cm^2 at 0.40 volts ----------									
2918-39 Co. reduced with Ag by H_2, Ag leached (1)	100	0.14	0.17	0.34	0.40	Dead	--	--	--	--	--	--	--	--	
	115	0.13	0.26	0.34	0.42	---------- 2 ma/cm^2 at 0.4d, 3 at 0.52 ----------									
	125	--	0.20	0.2[illegible]	0.34	0.52	--	--	--	--	--	--	--	--	
	150	0.17	0.17	0.19	0.22	0.36	0.55	---------- 0.37 at 15 ----------							
2918-34-1 Potassium Borohydride reduced	100	0.10	0.15	--	0.31	0.48	---------- 0.58 at 7.5 ma/cm^2 ----------								
	125	0.15	--	--	0.28	0.37	0.46	---------- 0.54 at 15 ma/cm^2 ----------							
	150	0.07	--	--	0.22	0.20	0.33	0.46	----- 0.62 at 30 ma/cm^2 -----						
2918-38 Lithium Reduced	100	0.09	0.16	0.24	0.30	0.41	0.66	--	--	--	--	--	--	--	
	115	0.10	0.12	0.23	0.28	0.37	0.51	---------- 12.5 @ 0.64 ----------							
	125	0.07	--	--	--	0.32	0.40	---------- 12.5 at 0.52 ----------							
	150	0.1	--	--	0.19	0.28	0.32	0.42	------- 0.46 at 25 ma/cm^2 --------						
2918-33-1 HCHO, reduced in presence of $Al(OH)_3$	100	--	0.22	--	0.34	0.44	Dead	--	--	--	--	--	--	--	
	115	--	0.18	0.26	0.30	0.38	0.56	--	--	--	--	--	--	--	
	125	--	0.11	--	0.26	0.34	0.39	---------- 0.48 at 15 ma/cm^2 ----------							
	150	--	0.06	--	0.18	0.26	0.28	0.38	------- 0.42 at 25 ma/cm^2 --------						
Commercial Pt Black (1)	100	0.14	--	--	0.29	0.38	0.42	---------- 0.71 at 15 ma/cm^2 ----------							
	115	0.06	--	--	0.24	0.35	0.39	---------- 0.41 at 15 ma/cm^2 ----------							
	125	0.09	--	--	0.22	0.30	0.24	0.42	0.46	0.52	0.77	--	--	--	
	150	0.05	--	--	0.15	0.24	0.26	0.30	0.33	0.36	0.37	0.41	0.62	--	
2918-32-1 Prep 1 HCHO, reduced in presence of $NaAlO_2$.	100	0.12	--	--	--	--	0.41	0.52 @ 15 ----------							
	115	0.11	--	--	0.20	0.28	0.34	0.40	0.46	0.59	0.66	--	--	--	
	125	0.12	--	--	0.17	--	0.28	0.33	0.38	0.42	0.46	0.52	0.58 at 120		
	150	0.10	--	--	0.12	--	0.20	0.24	0.28	0.31	0.34	0.36	0.44	0.52	
	80	0.11	--	--	0.32	0.42	0.48	---------- 0.64 @ 15 ma/cm^2 ----------							
2918-32-1 Prep 2 HCHO, reduced in presence of $NaAlO_2$	150	0.10	--	--	0.14	--	0.22	0.27	0.30	0.33	0.38	0.38	0.42	0.64	
2918-32-1 Second electrode	150	0.08	0.11	0.11	0.20	--	0.33	0.40	0.42	0.50	--	--	--	--	
Commercial Pt Black	100	0.09	0.09	--	0.25	0.34	0.36	0.49	--	--	--	--	--	--	
	115	0.13	0.16	--	0.25	0.32	0.35	0.43	--	--	--	--	--	--	
	125	0.08	0.12	0.16	0.20	0.30	0.32	0.36	0.40	0.44	--	--	--	--	
	150	0.07	0.07	0.11	0.14	0.22	0.25	0.30	0.36	0.38	0.40	0.40	0.49	Dead	0.52 at 175.
Low Bulk Density Commercial Pt Black	100	0.17	0.35	0.50	--	--	--	--	--	--	--	--	--	--	
	115	0.09	0.24	0.35	0.47	--	--	--	--	--	--	--	--	--	
	125	0.06	0.07	0.28	0.32	0.60	--	--	--	--	--	--	--	--	
	150	0.12	0.16	--	0.30	0.42	0.62	--	--	--	--	--	--	--	

(1) Data not used in Tables A-2 and A-3 and Figure A-6 of text, due to contamination of catalysts during preparation with high surface area impurity.

(2) Higher density material.

APPENDIX A-12

CATALYST STRUCTURE STUDIES--SINTERED PLATINUM TEFLON ELECTRODES

3.7 M H_2SO_4, 100°C, Butane Fuel, 85% Platinum, 15% Teflon Electrodes

Catalyst Description	Polarization from Butane Theory at Indicated ma/cm^2, volts												
	0	0.1	0.5	1.0	5	7.5	10	12.0	15	20	25	30	40
2918-31-1	----------Too poor to deter ine----------												
2918-35	0.17	--	--	0.28	----------Dead at 5----------								
2918-39	0.12	0.12	0.21	0.24	0.35	--	0.43	Dead	--	--	--	--	--
2918-34-1	0.13	--	--	0.26	0.32	Dead	--	--	--	--	--	--	--
2918-38	0.14	0.20	--	--	--	--	0.54	--	--	--	--	--	--
2918-33-1	0.09	0.14	--	0.19	--	--	0.35	Dead	--	--	--	--	--
Commercial Pt(1)	0.14	0.19	0.21	0.25	0.35	0.42	0.51	--	0.59	0.67	--	--	--
2918-32-1	0.12	--	--	0.16	--	--	0.26	--	0.29	0.32	0.37	0.44	0.66
Low Density Pt Black	0.06	--	0.07	0.24	0.38	--	--	--	--	--	--	--	--

(1) See Appendix A-11 for details.

APPENDIX A-13

CATALYST STRUCTURE STUDIES--SINTERED PLATINUM TEFLON ELECTRODES

14.7 M H_3PO_4, 100°C, Hydrogen, 85% Pt/15% Teflon Electrodes

Catalyst Preparation[1]	Polarization from Theoretical Hydrogen at Indicated ma/cm^2, volts													
	0	1	10	20	40	60	80	100	150	200	400	600	800	1000
2918-31-1	0.03	0.04	0.04	0.05	0.07	0.09	0.12	0.29	Dead	--	--	--	--	--
2918-35	0.00	0.00	0.00	0.00	0.00	0.02	0.04	0.08	0.15	--	--	--	--	--
2918-39	0.03	0.03	0.04	0.08	0.12	0.16	0.23	0.27	0.44	0.59	--	--	--	--
2918-34-1	0.00	0.00	0.00	0.00	0.03	0.08	0.11	0.11	--	0.33	--	--	--	--
2918-38	0.03	0.03	0.03	--	--	0.05	--	0.07	--	0.10	---Did not complete---			
2918-33-1	0.03	----------Same----------					--	0.05	--	0.07	0.10 at 300 ma/cm^2			
Commercial Pt	0.00	0.00	0.00	0.00	0.02	0.04	0.06	0.00	0.13	0.18	0.44	--	--	--
2918-32-1	0.03	0.03	0.03	--	--	--	--	0.35	--	0.04	0.06	0.08	0.10	0.16

(1) See Appendix A-11 for details.

APPENDIX A-14

STATISTICAL EVALUATION OF PLATINUM ON CARBON PREPARATION VARIABLES

I. Estimate of Standard Deviation.

The data below represent the replications used to establish the repeatability of the screening runs on the platinum-on-carbon catalysts. The replicates are imperfect, actually including variations in the percent Teflon, the means of mixing the carbon and the Teflon, and the pH of the wash water, all of which had small effects relative to the improvements being sought. Therefore, the calculated variance is undoubtedly higher than the true variance. The logarithm of the current density is used in these analyses in accordance with electrochemical theory. The current densities have been corrected to a fixed catalyst loading and a fixed polarization.

Table A-3

Calculation of Independent Measure of Variance

Description		Log Activity @ η = 0.40 volts(4)	Sum of Squares	Degrees of Freedom
Catalyst	Reduction Method(1)			
Colloidal Pt/C	Citrate	0.477, 0.602	0.0078	1
"	" (3)	0.380, 0.505	0.0078	1
"	HCHO	1.000, 1.176	0.0155	1
"	Citrate (2)	0.270, 0.330	0.0018	1
"	CO (2)	0.301, 0.699	0.0792	1
Pt-Ir/C	$NaBH_4$ (3)	0.945, 1.265	0.0515	1
"	$NaBH_4$	1.000, 1.146, 1.301	0.0453	2
Adsorbed Pt on C-5SiO_2	High Temp. (3)	1.362, 1.398 1.447, 1.544 1.591, 1.602	0.0525	5
Total			0.2614	13

Variance = 0.0201 $\quad \phi = 13$

(1) Activation treatment except where noted.
(2) No activation.
(3) SCTE electrodes; all others are C-T II type.
(4) Activity measured in ma/cm^2 adjusted to 2 mg/cm^2 catalyst loading.

Conclusions

The standard deviation of the logarithm indicated a one sigma variation extending from 72% to 139% of a given value.

II. Effect of Electrode Type

Two different electrode structures were used in evaluating the catalysts prepared. Each of these was evaluated using three different catalysts. The numbers given are averages of the logarithims of the specific current densities. There were minor differences between the preparations averaged as discussed in I but all were activated (See III).

Table $\bar{A}$-4

Data Used in Electrode Evaluation

Electrode Type	Logarithm of Average Butane Performance, ma/mg, @ η = 0.40 volts, 14.7M H_3PO_4, 150°C.		
	CO Reduced Colloidal Pt/C	Citrate Reduced Colloidal Pt/C	Impregnated Pt-Ir/C
C-T II	0.699	0.239	0.848
SCTE	1.000	0.142	0.804

Table $\bar{A}$-5

Statistical Evaluation of Electrode Activity

Source	Sum of Squares	Degrees of Freedom	Variance	Variance Ratio (1)
Catalyst Preparation	0.5591	2	0.2796	13.9 (2)
Electrode Type	0.0042	1	0.0042	0.21 (3)
Interaction	0.0468	2	0.0234	1.2 (3)
Total	0.6101	5		
Independent Measure of Variance		13	0.0201	

(1) Based on Independent Measure of Variance
(2) Significant at 99+% confidence level
(3) Not statistically significant

Conclusions

While the effect of catalyst preparation is very large and statistically significant there is no effect of electrode type. It is recognized that since some of the points represent averages, a more exact but more complicated analysis could have been done. However, the effect of electrode structure was so small that it could not have been made statistically significant by the additional analysis. With this shown, data on both electrode types could be combined in the next analysis.

III. Benefit of Activation Technique

Experiments were carried out to determine whether the activation technique commonly used with platinum on carbon catalysts was still valuable for the new catalyst preparation techniques. Three different catalysts were tested with and without the activation technique (Tables A-6 and A-7).

Table A-6

Data Used in Evaluation of Activation Technique

Logarithm of Average Butane Performance, ma/mg, @ η = 0.40 volts, 14.7M H_3PO_4, 150°C.

	CO Reduced Colloidal Pt/C	Citrate Reduced Colloidal Pt/C	Adsorbed Pt/C-5SiO_2
Activation Treat	0.855	0.190	1.190
No Activation	0.097	-1.001	0.929

Table A-7

Statistical Evaluation of Activity

Source	Sum of Squares	Degrees of Freedom	Variance	Variance Ratio (1)
Catalyst Preparation	2.1757	2	1.0879	54.1 (2)
Activation Treat	0.8137	1	0.8137	40.5 (2)
Interaction	0.2165	2	0.1083	5.4 (3)
Total	3.2059	5		
Independent Measure of Variance		13	0.0201	

(1) Based on Independent Measure of Variance
(2) Significant at 99+% confidence level
(3) Significant at 95+% confidence level

Conclusions

The difference between the catalysts is highly significant. The activation technique also gives a significant benefit. The interaction is probably significant. One of the catalyst preparation techniques does not benefit as much from the activation as the other two. The chemistry of the situation verifies that this may be the case, since one of the steps in the catalyst preparation probably performs the same function as one of the activation steps.

APPENDIX A-15

PLATINUM ON CARBON CATALYSTS

Reference	Catalyst	Reduction Method	Catalyst Treatment	Electrode Type (6)	Pt Loading mg/cm²	Polarization from Butsoe Theory at Indicated ma/cm², volts													Polarization from Oxygeo Theory at Indicated ma/cm², volts				
						0	1	3	5	10	15	20	25	30	35	40	45	50	0	50	100	200	300
3371-5-1	Pt	L[illegible]	KOH, H_2O (4)	C-T II	50	0.13	0.16			0.35	0.40	0.44		0.50		0.58 (1)							
3371-18-2	6% Pt Black, C Mixture	Commercial	(4)	C-T II	2	0.48	Dead																
3371-18-1	4.2% Colloidal Pt on C	Sodium Citrate	KOH, H_2O (4)	C-T II	0.7	0.22	Dead												0.22	0.45	0.50		
3371-18-3	4.2% Colloidal Pt on C	Sodium Citrate	KOH, H_2O (4)	C-T II	1.4	0.25	Dead												0.25	0.48	0.52		
3371-22	4.2% Colloidal Pt on C	Sodium Citrate	KOH, H_2O (4)	C-T II	1.4	0.20	Dead												0.25	0.45	0.46		
3371-26-1	4.2% Colloidal Pt on C	Sodium Citrate	KOH, H_2O (3)	C-T II	1.4	0.22	0.36	0.46	Dead										0.25	0.41	0.45	0.49	
3371-26-2	4.5% Colloidal Pt on C	Sodium Citrate	KOH, H_2O (3)	C-T II	1.5	0.16	0.31	0.41	0.47	Dead									0.25	0.42	0.45	0.50	
3371-42-1	6% Colloidal Pt on C	Formaldehyde	KOH, H_2O (3)	C-T II	2	0.24	0.36	0.47	Dead										0.21	0.38	0.41	0.44	
3371-42-2	6% Colloidal Pt on C	Formaldehyde	KOH, H_2SO_4, H_2O (3)	C-T II	2	0.21	0.41	Dead											0.25		0.52	0.64	
3473-3-2	6% Colloidal Pt on C	Sodium Citrate	H_2SO_4, H_2O (3)	SCTE	2.5	0.17	0.28		0.42	Dead									0.24	0.43	0.49		
3473-3-2	6% Colloidal Pt on C	Sodium Citrate	H_2SO_4, H_2O (3)	RSCTE	2.5	0.22		0.41	0.44	Dead									0.22	0.34	0.38		
3473-3-1	6% Colloidal Pt on C	Carbon Monoxide	H_2SO_4, H_2O (3)	RSCTE	2.5	0.16	0.24		0.34	0.38	0.42	0.45	0.48 (5)	Dead					0.17	0.29	0.35		
3473-3-1	6% Colloidal Pt on C	Carbon Monoxide	H_2SO_4, H_2O (3)	SCTE	2.5	0.14	0.24		0.35	0.45	Dead								0.25	0.47	0.60		
3472-35-1	12% Colloidal Pt on C	Carbon Moooxide	H_2O (4)	C-T II	4	0.18	0.29	Dead											0.23		0.45	0.51	
3472-35-2	12% Colloidal Pt on C	Carbon Monoxide	H_2SO_4, H_2O (4)	C-T II	4	0.21	0.28		0.39	Dead									0.20		0.35	0.40	
3473-13-3	6% Pt-10 Ir on C	Li	H_2SO_4, H_2O (3)	C-T II	2	0.17	0.24		0.35	0.41	Dead								0.24		0.53	0.71	
3473-15-1	6% Colloidal Pt-5 Au on C	Carbon Monoxide	H_2SO_4, H_2O (3)	RSCTE	2.5	0.17	0.21		0.30	0.36	0.40	Dead							0.27	0.43	0.49		
3473-9	6% Colloidal Pt-5 Au on C	Carbon Monoxide	H_2SO_4, H_2O (3)	SCTE	2.5	0.21	0.31	Dead											0.28	0.49	0.55		
3473-36-1	6% Colloidal Pt-5 Au on C (2)	Carbon Monoxide	H_2SO_4, H_2O (3)	RSCTE	2.5	0.14	0.22		0.31	0.39	Dead								0.31	0.41	0.49	0.57	
3473-41-1	6% Colloidal Pt-10 Ir on C	Borohydride	H_2SO_4, H_2O (3)	RSCTE	2.5	0.24	0.33			0.48	Dead								0.28	0.42	0.53		
3473-13-2	6% Colloidal Pt on C	Carbon Monoxide	H_2SO_4, H_2O (3)	C-T II	2	0.17	0.23		0.33	0.41	Dead								0.25	0.41	0.48		
3371-31-2	6% Pt-10 Ir oo C	Borobydride	H_2SO_4, H_2O (3)	C-T II	2	0.14	0.24		0.36	0.40	0.47	Dead							0.20	0.36	0.42	0.47	
3371-31-1	6% Pt-10 Ir on C	Borohydride	H_2SO_4, H_2O (3)	C-T II	2	0.15	0.24		0.32	0.37	0.41	0.43	0.46	0.49	0.51	Dead			0.18		0.36		0.45
3472-10-1	6% Pt-10 Ir on C	Borohydride	H_2SO_4, H_2O (3)	SCTE	2.5	0.10				0.28	0.32	0.37	0.42	Dead					0.19	0.40	0.45		
3472-8-2	6% Pt-10 Ir on C	Borohydride	H_2SO_4, H_2O (3)	C-T II	2	0.16	0.20		0.29	0.33		0.40	0.44	Dead					0.20	0.31	0.36	0.40	0.43
3472-21-1	6% Pt-10 Ir on C	Borohydride	H_2SO_4, H_2O (3)	RSCTE	2.5	0.13	0.18		0.26	0.39	Dead								0.19	0.61			
3473-45-1	4-5% Pt on C-5 SiO_2Gel	High Temp	H_2O (3)	RSCTE		0.12	0.17		0.22	0.27	0.31	0.35	0.37	0.42	Dead				0.24	0.36	0.42	0.52	
3473-45-2	4-5% Pt on C-5 SiO_2Gel	High Temp	H_2O,CH_3OH (3)	RSCTE	2	0.14			0.23		0.30		0.37		0.40			0.45	0.22	0.32	0.37	0.43	
3473-9-1	4-5% Pt on C-5 SiO_2Gel	High Temp	H_2O,CH_3OH (3)	SCTE	2	0.14			0.25		0.35		0.40	Dead					0.23	0.42	0.56		
3933-17-1	4-5% Pt on C-5 SiO_2Gel	High Temp	H_2O,CH_3OH (3)	RSCTE	2	0.17			0.26		0.33	0.36	0.42	Dead					0.24	0.33	0.39	0.45	
3933-28-1	4-5% Pt on C-5 SiO_2Gel	High Temp	H_2O,CH_3OH (4)	RSCTE	2	0.15			0.24	0.30	0.37	Dead							0.27	0.43	0.54		
3933-37-2	4-5% Pt on C-5 SiO_2Gel	High Temp	H_2O,CH_3OH (3)	RSCTE	2	0.13	0.18		0.25		0.33	0.35	0.37		0.39		0.41	0.44	0.25	0.37	0.47		
3933-21-1	4-5% Pt on C-5 SiO_2 Colloid	High Temp	H_2O,CH_3OH (3)	RSCTE	2	0.13	0.18		0.25		0.35		0.43	Dead					0.25	0.39	0.48		
3934-3-3	4-5% Pt on C-5 SiO_2Gel	High Temp	H_2O,CH_3OH (3)	RSCTE	2	0.13	0.18		0.24	0.28	0.31	0.33	0.35	0.365	0.38	0.41		0.42 Dead	0.23	0.33	0.39		

(1) Unstable
(2) Different carbon used
(3) Activation step after drying.
(4) No activation after drying.
(5) Performance data after 3-1/2 hrs @ 25 ma/cm²; 0.40 volts for first hour.
(6) Abbreviations defined in Appendix A-16

APPENDIX A-16

PLATINIZED CARBON TEFLON ELECTRODES

	C-T I Carbon-Teflon 7 (absolute)	C-T II Carbon-Teflon 7	SCTE Carbon-Teflon 41 BX	Rapid Equilibration RSCTE
Compoaition				
% Teflon	33	33	5-30(15)[1]	10
% Artificial voida	25	25	--	--
Mixing Mode	Ball Mill	Ball Mill	Gelation	Gelation
Mixing time, mina	30	30	3-5 mina	3-5 mins
Fabrication				
Molding Preaaure, cold	10,000	10,000	500	500
Heat Treatment Temp. °C.	193	--	--	--
Heat Treatment	--	--	--	--
Time, mina	120	--	--	--
Sintering Preaaure	--	0	1100-10,000(2200)[1]	2200
Sintering Temperature °C.	--	383	349	349
Sintering Time, mins	--	120	2	1
Catalyst Loading, mg/cm^2	2.5[2]	2.0[2]	0.6→5	2.5 or 5.0
Electrode thickneas, em, less screen	0.060	0.048	0.007-0.059	0.028 or 0.059
Characteriatica				
Mechanical Integrity	Very poor	Poor	Satisfactory to excellent depends on thickness	Excellent at low thickness
Repeatability	Poor	Poor depend	Good	Good

(1) Preferred.
(2) Maximum effective in 14.7 M H_3PO_4.

APPENDIX A-17

GAS PHASE ELECTRODES--SINTERED CARBON-TEFLON STRUCTURES

Anode Performance

	Fabrication Conditions						Platinum on Carbon, wt %	Thickness, mils	Electrolyte Composition	Temp, °C	Z, mg Pt/cm²	Polarization from Butane — Theory at Indicated ma/cm², volts											
Reference	Temp, °C	Pressure, psi	Time, min	Mixing Mode	Cold Press, psi	Teflon, wt%						0	0.1	0.5	1.0	2.0	4.0	6.0	8.0	10.0	15	20	30	40
3444-5	193	0	120	Ball Mill	10,000	33	6	--	14.7 M H_3PO_4	150	2.1	0.16	--	--	0.25	--	--	0.35	0.44	Dead	--	--	--	--
3444-7	193	0	"	"	"	"	"	--	"	"	"	0.05	--	--	0.26	--	--	0.35	Dead	--	--	--	--	--
3444-9	382	0	"	"	"	"	"	--	"	"	"	0.14	0.15	--	0.26	0.31	--	0.40	Dead	--	--		--	--
3444-10	382	0	"	"	"	"	"	--	"	"	"	0.18	0.19	--	0.32	0.38	0.42	Dead	--	--	--	--	--	--
3444-11	382	0	"	"	"	"	"	--	"	"	"	0.15	0.18	--	0.27	0.30	0.38	0.39	Dead	--	--	--	--	--
3444-11A	382	0	"	"	"	"	"	--	"	125	"	0.16	0.22	--	0.35	0.42	Dead	--	--	--	--	--	--	--
3444-11B	382	0	"	"	"	"	"	--	"	100	"	0.17	0.28	--	0.38	Dead	--	--	--	--	--	--	--	--
Batch #2 Catalyst--Teflon Emulsion																								
3444-12-1	350	1100	1	Beaker	500	15	"	31.5	"	150	5.0	0.15	0.20	0.22	0.25	0.30	0.36	0.09	0.44	0.45	Dead	--	--	--
3444-12-2	350	2200	2	"	"	"	"	29.0	"	"	"	0.16	0.16	0.18	0.21	0.265	0.30	0.34	0.36	0.38	0.46	--	--	--
3444-12-3	350	2200	1	"	"	30	"	34	"	"	"	0.14	0.24	--	0.27	0.34	0.45	Dead	--	--	--	--	--	--
3444-12-4	350	1100	2	"	500	"	"	32	"	"	"	0.23	0.25	0.31	0.36	0.44	Dead	--	--	--	--	--	--	--
3444-12-2	350	2200	2	"	"	15	"	29	"	"	"	0.12	0.13	0.18	0.21	0.24	0.28	0.31	0.33	0.35	0.38	0.42	0.44@ 25 ma/cm²	
3444-12-2	350	2200	2	"	"	"	"	29	"	"	"	0.12	0.12	0.16	0.18	0.21	0.27	0.30	0.32	0.31	0.36	0.39	0.41	0.45
3444-12-2	350	2200	"	"	"	"	"	"	"	125	"	0.12	--	--	0.25	0.29	0.34	0.38	0.40	0.42	0.45	0.49	Dead	--
3444-12-2	350	2200	"	"	"	"	"	"	"	100	"	0.12	--	0.28	0.33	0.36	0.45	0.49	0.53	--	--	--	--	--
3444-16	350	2200	1	"	"	10	"	30	"	150	"	0.11	0.12	--	0.14	0.18	0.24	0.28	0.30	0.32	0.38	0.40 @ 17.5 ma/cm²		
3444-18	350	1100	"	"	"	"	"	27	"	"	"	0.12	0.12	0.18	0.22	0.26	0.32	0.36	0.39	0.43	Dead	--	--	--
3444-21	338	2200	2	Pallet	"	"	"	30	"	"	"	0.13	--	--	0.23	0.27	0.28	0.35	0.45	Dead	--	--	--	--
3444-21	338	2200	2	"	"	"	"	30	14.7 M H_3PO_4 0.05% FC 95	"	"	0.10	--	--	--	--	--	--	--	0.34	0.36	0.40	Dead	--
3444-24	350 After O_2 Treat	2200	2	"	"	15	"	31.5	14.7 M H_3PO_4	"	"	0.14	--	--	0.28	0.38	0.40	0.42	-----Oscillating at 8 ma/cm²-------					
												0.14	--	--	0.27	0.33	0.50	Dead	--	--	--	--	--	--
3444-25	338	2200	1	"	"	"	"	28	"	"	"	0.28	0.33	0.34	0.38	Dead	--	--	--	--	--	--	--	--
3444-25	338	2200	"	"	"	"	"	"	14.7 M H_3PO_4 0.05% FC 95	"	"	0.19	--	--	--	0.27	Dead	--	--	--	--	--	--	--
3444-26	338	1100	1	"	"	10	"	30	14.7 M H_3PO_4	----------2 ma/cm² @ 0.45 volts----------								--	--	--	--	--	--	--
3444-35	350	2200	2	Beaker	"	15	"	17.5	"	150	2.5	0.17	--	--	0.28	0.32	0.35	0.37	0.38	Dead	--	--	--	--
3444-36	350	2200	1	"	"	10	"	16	"	"	"	0.22	--	--	0.31	0.43	Dead	--	--	--	--	--	--	--
3444-37	350	2200	2	"	"	15	"	29	"	"	5.0	0.15	0.13	0.16	0.18	--	--	--	--	0.30	0.35	0.39	0.41	0.45
3444-28-1	350	2200	"	"	"	"	Diluted carbon	28	"	"	1.25	0.17	0.21	0.51	Dead	--	--	--	--	--	--	--	--	--
3444-28-2	350	2200	"	"	"	"	"	27	"	"	2.5	0.18	0.26	0.32	0.42	Dead	--	--	--	--	--	--	--	--
Loading Experiments																								
3444-30-1	350	2200	"	"	"	"	6	6.4	"	"	0.60	0.09	0.10	0.13	0.17	0.21	0.25	0.28	0.31	0.34	0.38 @ 12.5, 0.43 @ 13			
3444-30-2	350	2200	"	"	"	"	"	"	"	"	"	--	--	--	--	--	--	--	--	0.40	--	gave 7.5 ma/cm²		
3444-30-3	350	2200	"	"	"	"	"	8.7	"	"	1.25	0.12	0.14	--	0.25	0.31	0.36	0.46	Dead	--	--	--	--	--
3444-30-4	350	2200	"	"	"	"	"	11.0	"	"	"	0.15	--	--	--	--	0.35	0.45	0.50	0.40 @ 5.0 ma/cm²				
3444-30-5	350	2200	"	"	"	"	"	17.5	"	"	2.5	0.11	0.11	0.13	0.16	--	--	0.26	--	0.31	0.37	0.44	--	--
3444-30-6	350	5000	"	"	"	"	"	7.0	"	"	1.25	0.12	--	--	0.20	--	--	0.40	--	Dead	-------Poisoned------			
3444-32	350	2200	1	"	"	10	"	--	"	"	5.00	0.14	--	--	0.22	0.26	0.30	0.31	0.32	0.32	0.35	0.38	0.45 @ 25	
3444-33	350	10,000	2	"	"	15	"	7.5	"	"	1.25	0.13	0.13	0.18	0.18	0.19	0.29	0.28	0.38	0.37	0.42	--	--	--
3444-34	350	2200	"	"	"	"	"	6.5	"	"	0.63	0.13	0.14	--	0.24	0.27	0.33	0.44	--	--	--	--	--	--
3444-37	350	2200	"	"	"	"	3	6.8	"	"	0.4	0.15	--	0.19	0.26	0.30	0.37	0.42	Dead	--	--	--	--	--
3444-38	350	2200	"	"	"	"	"	9.8	"	"	0.6	0.19	--	0.24	0.27	0.30	0.36	0.41	Dead	Dead	--	--	--	--
3444-39	350	2200	"	"	"	"	"	17	"	"	1.25	0.13	--	0.21	0.24	0.31	0.36	0.41	0.49	--	7 at 0.45		Dead at 10	
3444-40	350	2200	"	"	"	"	"	30	"	"	2.5	0.19	--	--	0.26	0.30	0.34	0.40	0.44	0.47	Dead	--	--	--

APPENDIX A-18

HIGH SURFACE AREA ALLOYS

Alloy Composition	Notebook Reference	Reduction Temp, °C	Furnace	Observed Au Lattice Spacing	Calc % Non-Noble Metal in Gold	Other Results and Observations
Ni/50Au	3394-26	500	H_2 flow	4.05	10	Stable to pH 3 medium at room temperature. No stable potential with H_2 in 3 M KOH at 10 ma/cm^2.
Ni/20Au	3394-29	500	"	4.05	20	No stable potential with H_2 in 3 M KOH at 10 ma/cm^2.
Ni/50Au	3395-30	800	H_2 atm	--	--	Catalyst fused and not reduced.
Ni/50Ag	3395-46	700	H_2 flow	--	--	Catalyst reduced. No current with H_2 fuel in 3 M KOH at 100°C obtained.
Co/25Au	3394-22	500	"	4.08	0	No current from electrode. KOH electrolyte turned blue.
Co/50Au	3395-49	700	"	4.08	0	Some current obtained from electrode fabricated from catalyst. Runs not reproducible.
Fe/60Au	3394-34	700	"	4.01	20	No current from electrode.
Fe/40Au	3394-35	700	"	4.01	20	No current from electrode.
Fe/40Au	3394-47 3395-4	700	"	4.01	20	Catalyst pyrophoric. Electrode prepared from this sample, run in 3 M KOH at 98°C with H_2 fuel gave 100 ma/cm^2 at 0.08 volts polarization. With butane at 20 ma/cm^2 polarization was 0.18 volts. Neither run reproducible. Catalyst rusty looking at end of run.
Fe/40Au	3395-30	800	H_2 atm	--	--	Catalyst fused, not reduced.
Fe/40Ag	3395-34	700	H_2 flow	--	--	Metals not reduced.
Fe/60Ag	3395-34	700	"	--	--	Metals not reduced.
W/20Au	3394-41 3395-17	1000	H_2 atm	--	--	Fused catalyst, could not prepare electrode. No W-Au interaction.
Mo/20Au	3394-43 3395-17	1000	"	--	--	Metals not reduced. No Mo-Au interaction.

APPENDIX A-19

PREPARATION AND PROPERTIES OF PEROVSKITES

A. Nickel Compounds

Reference	Nominal Formula	Starting Materials	Firing Conditions: Atmosphere	Firing Conditions: Max Temp, °C	Product Formula[1]	Acid Resistance[2]: Percent Metal Retained	Acid Resistance[2]: Test Time (Hrs)	Conductance ($ohm^{-1}cm^{-1}$)
3440-36	$LaNi^{II}_{0.5}Ti_{0.5}O_3$	La_2O_3, NiO, TiO_2	N_2	1150	$LaNi^{II}_{0.5}Ti_{0.5}O_{2.5}$[10]	45	22[11]	2.6×10^{-6}
	Same Refired	--	Air	"	--[10]	--	--	--
3440-37	$LaNi^{II}_{0.5}Zr_{0.5}O_3$	" , " , ZrO_2	N_2	"	$LaNi^{II}_{0.5}Zr_{0.5}O_{2.57}$[10]	39	24[11]	2.2×10^{-3}
3440-45	$LaNi^{II}_{0.5}Sn_{0.5}O_3$	" , " , SnO_2	Air	"	$LaNi^{II}_{0.5}Sn_{0.5}O_{2.94}$	32	23[11]	6.7×10^{-6}
3440-48	$LaNi^{II}_{0.5}Hf_{0.5}O_3$	" , " , HfO_2	"	"	$LaNi^{II}_{0.5}Hf_{0.5}O_{2.94}$[10]	0	24	1.5×10^{-2}
3674-5	$LaNi^{II}_{0.5}V^{V}_{0.5}O_3$	" , Ni, NiO, V_2O_5	N_2	1200	$LaNi^{II}_{0.5}V_{0.5}O_{3.03}$	--	--	1.1×10^{-4}
3951-41	$SrNi^{II}_{0.33}V^{V}_{0.67}O_3$	$SrCO_3$, NiO, V_2O_5	"	1205	$SrNi^{II}_{0.33}V^{V}_{0.67}O_{3.15}$	--	--	1.7×10^{-11}
3951-45	$BaNi^{II}_{0.33}Ta_{0.67}O_3$	$BaCO_3$, NiO, Ta_2O_5	N_2	"	$BaNi^{II}_{0.33}Ta_{0.67}O_{2.88}$	92.2	101	1.8×10^{-9}
2814-38	$Sr(Ni^{II}_{0.3}Li_{0.033})Ta_{0.67}O_{2.98}$	$SrCO_3$, NiO, Li_2CO_3, Ta_2O_5	N_2	1260	$Sr(Ni^{II}_{0.3}Li_{0.033})Ta_{0.67}O_{2.86}$	--	--	1.1×10^{-9}
	Same Refired	--	Air	1205	--	--	--	4.7×10^{-9}
2814-39	$(Sr_{0.9}Li_{0.1})Ni^{II}_{0.33}Li_{0.67}O_{2.95}$	$SrCO_3$, NiO, Li_2CO_3, Ta_2O_5	N_2	"	$(Sr_{0.9}Li_{0.1})Ni^{II}_{0.33}Ta_{0.67}O_{2.90}$	--	--	1.8×10^{-9}
	Same Refired	--	Air	"	--	--	--	2.4×10^{-9}
3951-33	$Sr(Ni^{II}_{0.31}La_{0.031})Ta_{0.66}O_3$	$SrCO_3$, NiO, La_2CO_3, Ta_2O_5	N_2	"	$Sr(Ni^{II}_{0.31}La_{0.031})Ta_{0.66}O_{2.86}$	--	--	5.3×10^{-9}
	Same Refired	--	Air	"	--	--	--	8.8×10^{-9}
3951-35	$(Sr_{0.9}La_{0.1})Ni^{II}_{0.37}Ta_{0.63}O_3$	$SrCO_3$, NiO, La_2O_3, Ta_2O_5	N_2	"	$(Sr_{0.9}La_{0.1})Ni^{II}_{0.37}Ta_{0.63}O_{2.75}$	--	--	1.2×10^{-9}
	Same Refired	--	Air	"	--	89.3	101	1.4×10^{-9}
3951-32	$Sr_{0.97}Ni^{II}_{0.33}Ta_{0.60}W_{0.067}O_3$	$SrCO_3$, NiO, Ta_2O_5, WO_3	N_2	"	$Sr_{0.97}Ni^{II}_{0.33}Ta_{0.6}W_{0.067}O_{2.96}$	--	--	4.6×10^{-10}
	Same Refired	--	Air	"	--	--	--	1.1×10^{-9}
3951-23	$SrNi^{II}_{0.5}Mo_{0.5}O_3$	$SrCO_3$, NiO, MoO_3	N_2	"	--[6]	--	--	1.9×10^{-11}
3951-22	$SrNi^{II}_{0.5}W_{0.5}O_3$	$SrCO_3$, NiO, WO_3	"	"	--[6]	--	--	1.1×10^{-9}
3952-7	$Sr^{--}Ni^{II}_{0.675}V_{0.25}O_{2.30}$	$SrCO_3$, NiO, V_2O_5	"	"	$SrNi^{II}_{0.675}V_{0.25}O_{2.29}$	--	--	1.8×10^{-9}
3952-1	$SrNi^{II}_{0.675}Nb_{0.25}O_{2.30}$	$SrCO_3$, NiO, Nb_2O_5	"	1150	$SrNi^{II}_{0.675}Nb_{0.25}O_{2.28}$	--	--	3.6×10^{-7}
3951-48	$Sr_{0.8}Ni^{II}_{0.33}Ta_{0.67}O_{2.8}$	$SrCO_3$, NiO, Ta_2O_5	"	1205	$Sr_{0.8}Ni^{II}_{0.33}Ta_{0.67}O_{2.80}$	--	--	9.0×10^{-10}
3951-47	$SrNi^{III}_{0.5}Ta_{0.5}O_3$	$SrCO_3$, NiO, Ta_2O_5	Air	"	$SrNi^{II}_{0.5}Ta_{0.5}O_{2.78}$[9]	--	--	1.8×10^{-8}
3951-44	$SrNi^{II}_{0.5}Ta_{0.5}O_{2.75}$	$SrCO_3$, NiO, Ta_2O_5	N_2	"	$SrNi^{II}_{0.5}Ta_{0.5}O_{2.73}$	--	--	2.8×10^{-8}
3952-13	$SrNi^{II}_{0.75}Ta_{0.25}O_{2.38}$	$SrCO_3$, NiO, Ta_2O_5	"	"	$SrNi^{II}_{0.75}Ta_{0.25}O_{2.28}$	26[8]	8.3	2.7×10^{-7}
3951-29	$BaNi^{II}_{0.75}Ta_{0.25}O_{2.38}$	$BaCO_3$, NiO, Ta_2O_5	"	"	$BaNi^{II}_{0.75}Ta_{0.25}O_{2.29}$	48.7[8]	8.3	2.8×10^{-7}
3952-2	$CaNi^{II}_{0.675}Ta_{0.25}O_{2.30}$	$CaCO_3$, NiO, Ta_2O_5	"	1150	$CaNi^{II}_{0.675}Ta_{0.25}O_{2.30}$	--	--	1.1×10^{-9}
3952-17	$PbNi^{II}_{0.675}Ta_{0.25}O_{2.30}$	PbO, NiO, Ta_2O_5	"	1040	$Pb_{0.93}Ni^{II}_{0.675}Ta_{0.25}O_{2.30}$[4]	--	--	6.3×10^{-13}
2814-42	$SrNi^{II}_{0.6}Ta_{0.25}O_{2.23}$	$SrCO_3$, NiO, Ta_2O_5	"	1205	$SrNi^{II}_{0.6}Ta_{0.25}O_{2.20}$	--	--	2.2×10^{-7}
2814-36	$SrNi^{II}_{0.675}Ta_{0.25}O_{2.30}$	$SrCO_3$, NiO, Ta_2O_5	"	"	$SrNi_{0.675}Ta_{0.25}O_{2.32}$	66.5[3]	281	4.4×10^{-9}, 6×10^{-9}
	Same Refired	--	Air	"	--	--	--	4.1×10^{-6}
2814-40	$SrNi^{II}_{0.9}Ta_{0.1}O_{2.15}$	$SrCO_3$, NiO, Ta_2O_5	N_2	"	$SrNi^{II}_{0.9}Ta_{0.1}O_{2.12}$	--	--	3.2×10^{-8}, 5.9×10^{-8}
2814-47	$SrNi^{II}_{0.81}Ta_{0.1}O_{2.06}$	$SrCO_3$, NiO, Ta_2O_5	"	"	$SrNi^{II}_{0.81}Ta_{0.1}O_{2.02}$	--	--	2.8×10^{-8}
3951-30	$Sr(Ni^{II}_{0.61}Li_{0.068})Ta_{0.25}O_{2.27}$	$SrCO_3$, $LiCO_3$, NiO, Ta_2O_5	"	"	$Sr(Ni^{II}_{0.61}Li_{0.068})Ta_{0.25}O_{2.22}$	--	--	9.1×10^{-8}
	Same Refired	--	Air	"	--	--	--	9.3×10^{-7}

APPENDIX A-19 (CONT'D)

PREPARATION AND PROPERTIES OF PEROVSKITES

A. Nickel Compounds (Cont'd)

Reference	Nominal Formula	Starting Materials	Firing Conditions: Atmosphere	Firing Conditions: Max Temp, °C	Product Formula(1)	Acid Resistance(2): Percent Metal Retained	Acid Resistance(2): Test Time (Hrs)	Conductance ($ohm^{-1}cm^{-1}$)
3951-37	$(Sr_{0.9}Li_{0.1})Ni^{II}_{0.675}Ta_{0.25}O_{2.25}$	$SrCO_3$, Li_2CO_3, NiO, Ta_2O_5	N_2	1205	$(Sr_{0.9}Li_{0.1})Ni^{II}_{0.675}Ta_{0.25}$	2.20	--	4.8×10^{-8}
	Same Refired	--	Air	"	--	--	--	3.0×10^{-7}
3952-3	$Sr(Ni^{II}_{0.61}Ce_{0.068})Ta_{0.25}O_{2.26}$	$SrCO_3$, Ce_2CO_3, NiO, Ta_2O_5	N_2	1150	$Sr(Ni^{II}_{0.61}Ce_{0.068})Ta_{0.25}O_{2.14}$	--	--	2.1×10^{-7}
	Same Refired	--	Air	"	--	--	--	3.6×10^{-6}
3952-4	$(Sr_{0.9}Ce_{0.1})Ni_{0.675}Ta_{0.25}O_{2.25}$	$SrCO_3$, Ce_2CO_3 NiO, Ta_2O_5	N_2	"	$(Sr_{0.9}Ce_{0.1})Ni^{II}_{0.675}Ta_{0.25}O_{2.29}$	--	--	6.9×10^{-7}
	Same Refired	--	Air	"	--	--	--	4.0×10^{-6}
3951-31	$Sr(Ni^{II}_{0.61}La_{0.068})Ta_{0.25}O_{2.33}$	$SrCO_3$, La_2O_3, NiO, Ta_2O_5	N_2	1205	$Sr(Ni^{II}_{0.61}La_{0.063})Ta_{0.25}O_{2.22}$	--	--	4.6×10^{-7}
	Same Refired	--	Air	"	--	63.7(8)	8.3	3.6×10^{-5}
3951-34	$(Sr_{0.9}La_{0.1})Ni^{II}_{0.675}Ta_{0.25}O_{2.35}$	$SrCO_3$, NiO, La_2O_3, Ta_2O_5	N_2	"	$(Sr_{0.9}La_{0.1})Ni^{II}_{0.675}Ta_{0.25}O_{2.18}$	--	--	2.1×10^{-6}
	Same Refired	--	Air	"	--	--	--	3.4×10^{-5}
3952-10	$(Sr_{0.9}La_{0.9})Ni_{0.675}Ta_{0.25}O_{2.55}$	$SrCO_3$, La_2O_3, NiO, Ta_2O_5	N_2	"	--(7)	--	--	6.6×10^{-4}
	Same Refired	--	Air	"	--	--	--	6.2×10^{-3}
3952-23	$(Sr_{0.9}Tl^{III}_{0.1})Ni^{II}_{0.675}Ta_{0.25}O_{2.35}$	$SrCO_3$, Tl_2O_3, NiO. Ta_2O_5	N_2	1150	--(5)	--	--	1.8×10^{-7}
3952-22	$(Sr_{0.9}Bi^{III}_{0.1})Ni^{II}_{0.675}Ta_{0.25}O_{2.35}$	$SrCO_3$, Bi_2O_3, NiC. Ta_2O_5	"	"	$(Sr_{0.9}Bi^{III}_{0.1})Ni_{0.675}Ta_{0.25}O_{2.14}$	--	--	1.7×10^{-7}
3952-9	$SrNi^{II}_{0.675}(V_{0.125}Ta_{0.125})O_{2.30}$	$SrCO_3$, NiO, V_2O_5, Ta_2O_5	"	1205	$SrNi^{II}_{0.675}(V_{0.125}Ta_{0.125})O_{2.30}$	--	--	2.1×10^{-9}
3951-16	$SrNi^{II}_{0.67}Mo_{0.33}O_{2.66}$	$SrCO_3$, NiO, MoO_3	"	"	--(6)	--	--	6.6×10^{-11}
3951-17	$SrNi^{II}_{0.75}Mo_{0.25}O_{2.50}$	$SrCO_3$, NiO, MoO_3	"	"	--(6)	--	--	2.9×10^{-10}
3951-19	$SrNi^{II}_{0.67}W_{0.33}O_{2.66}$	$SrCO_3$, NiO, WO_3	"	"	--(6)	--	--	1.7×10^{-10}
3951-18	$SrNi^{II}_{0.75}W_{0.25}O_{2.50}$	$SrCO_3$, NiO, WO_3	"	"	--(6)	--	--	1.1×10^{-10}
3952-14	$SrNi^{II}_{0.675}W_{0.25}O_{2.43}$	$SrCO_3$, NiO, WO_3	"	"	--(7)	--	--	1.0×10^{-9}
3952-8	$SrNi^{II}_{0.675}(Mo_{0.125}V_{0.125})O_{2.36}$	$SrCO_3$, NiO, V_2O_5, MoO_3	"	"	$SrNi^{II}_{0.675}(Mo_{0.125}V_{0.125})O_{2.40}$	--	--	1.1×10^{-8}
	Same Refired	--	Air	"	--	--	--	5.0×10^{-8}

(1) Calculated from weight changes during firing.
(2) Percent of original metal, e.g. nickel, retained after heating with 3.7 M H_2SO_4 for specified number of hours.
(3) In the presence of 0.07 molar $NiSO_4$ in 3.7 M H_2SO_4.
(4) Product badly fused to boat.
(5) Fuming occurred during initial stages of firing; weights unreliable.
(6) Partial CO_2 loss occurred during drying of pilled firing mixtures; weight changes meaningless.
(7) Material spilled during firing; weights unreliable.
(8) With 0.08 M $NiSO_4$ in 3.62 M H_2SO_4 as corroding medium.
(9) Failure of nickel to oxidize probably due to stoppage of air stream to firing zone.
(10) X-ray pattern shows presence of more than one phase.
(11) At room temperature.
(12) X-ray pattern fits perovskite-type structure.

APPENDIX A-19 (CONT'D)

PREPARATION AND PROPERTIES OF PEROVSKITES

B. Cobalt Compounds

Refsrence	Nominal Formula	Starting Materials	Firing Conditions: Atmosphsre	Firing Conditions: Max Temp, °C	Product Formula	Acid Resistance: Percent Metal Retained	Acid Resistance: Test Time (Hrs)	Conductance ($ohm^{-1}cm^{-1}$)
3440-50	$LaCo^{II}_{0.5}Ti_{0.5}$	La_2O_3, $CoCO_3$, TiO_2	Air	1200	--(7),(12)	0	21	8.6×10^{-9}
3440-6	$SrCo^{IV}_{0.297}Ti_{0.67}O_{2.93}$	$BaCO_3$, $CoCO_3$, TiO_2	"	"	$SrCo^{IV}_{0.297}Ti_{0.67}O_{3.25}$(6),(12)	2	256(11)	3.0×10^{-3}
3440-34	$BaCo^{IV}_{0.33}Zr_{0.67}O_3$	La_2O_3, $CoCO_3$, ZrO_2	"	1150	$BaCo^{IV}_{0.33}Zr_{0.67}O_{2.90}$	0	21	4.6×10^{-5}
3261-40	$SrCo^{IV}_{0.1}Hf_{0.9}O_3$	$SrCO_3$, $CoCO_3$, HfO_2	"	1200	$SrCo^{IV}_{0.1}Hf_{0.9}O_{2.86}$	0	141(11)	2.1×10^{-8}
3440-33	$BaCo^{IV}_{0.33}Hf_{0.67}O_3$	$BaCO_3$, $CoCO_3$, HfO_2	"	1150	$BaCo^{IV}_{0.33}Hf_{0.67}O_{2.90}$(11)	15	21	7.6×10^{-5}
3261-41	$SrCo^{IV}_{0.45}Hf_{0.50}O_{2.90}$	$SrCO_3$, $CoCO_3$, HfO_2	"	1260	$SrCo^{IV}_{0.45}Hf_{0.50}O_{2.70}$(10)	0	170(11)	8.3×10^{-2}
3440-12	$SrCo^{IV}_{0.75}Hf_{0.25}O_3$	$SrCO_3$, $CoCO_3$, HfO_2	"	1200	$SrCo^{IV}_{0.75}Hf_{0.25}O_{3.81}$(6)	10	189(11)	4.3×10^{-2}
3674-4	$LaCo^{II}_{0.5}V^{IV}_{0.5}O_3$	$SrCO_3$, Co, CoO, V_2O_5	N_2	"	$LaCo^{II}_{0.5}V_{0.5}O_{3.02}$	--	--	7.3×10^{-6}
3951-4	$SrCo^{II}_{0.33}Ta_{0.67}O_3$	$SrCO_3$, $CoCO_3$, Ta_2O_5	"	1260	$SrCo^{II}_{0.33}Ta_{0.67}O_{2.88}$	81.8	321	2.6×10^{-10}
3951-2	$SrCo^{II}_{0.33}Ta_{0.67}O_3$	$SrCO_3$, CoO, Ta_2O_5	"	"	$SrCo^{II}_{0.33}Ta_{0.67}O_{2.91}$ --(6)	--	--	6.8×10^{-10}
3952-11	$SrCo^{II}_{0.5}Mo_{0.5}O_3$	$SrCO_3$, $CoCO_3$, MoO_3	"	"		48.4	101	7.5×10^{-8}
3952-12	$SrCo^{II}_{0.5}Mo_{0.5}O_3$	S[illegible], CoO, MoO_3	"	1205	$SrCo^{II}_{0.5}Mo_{0.5}O_{2.88}$	--	--	2.2×10^{-9}
	Same refired	SrO, CoO, MoO_3	"	1260	$SrCo^{II}_{0.5}Mo_{0.5}O_{2.86}$	--	--	5.3×10^{-9}
3952-15	$BaCo^{II}_{0.5}Mo_{0.5}O_3$	BaO, CoO, MoO_3	"	1205	$BaCo^{II}_{0.5}Mo_{0.5}O_{2.91}$	--	--	5.8×10^{-8}
	Same Refired	--	"	1260	$BaCo^{II}_{0.5}Mo_{0.5}O_{2.88}$	80.1	101	4.9×10^{-9}
3952-16	$CaCo^{II}_{0.5}Mo_{0.5}O_3$	CaO, CoO, MoO_3	"	1205	$CaCo^{II}_{0.5}Mo_{0.5}O_{2.94}$	--	--	7.3×10^{-12}
	Same Refired	--	"	1260	$CaCo^{II}_{0.5}Mo_{0.5}O_{2.93}$	--	--	1.2×10^{-10}
3951-40	$PbCo^{II}_{0.5}Mo_{0.5}O_3$	$PbCO_3$, $CoCO_3$, MoO_3	Air	1205	$Pb_{0.88}Co^{II}_{0.5}Mo_{0.5}O_{3.0}$ (14)	--	--	--
3952-18	$PbCo^{II}_{0.5}Mo_{0.5}O_3$	PbO, CoO, MoO_3	"	1040	$Pb_{0.98}Co^{II}_{0.5}Mo_{0.5}O_{3.0}$(14)	--	--	--
3951-28	$SrCo^{II}_{0.5}W_{0.5}O_3$	$SrCO_3$, $CoCO_3$, WO_3	N_2	1205	$SrCo^{II}_{0.5}W_{0.5}O_{3.29}$ --(6)	--	--	5.1 x 10^{-8}
2814-43	$SrCo^{II}_{0.75}Ta_{0.25}O_{2.9}$	$SrCO_3$, $CoCO_3$, Ta_2O_5	"	1260		0.0(15)	569	3.8×10^{-4}
3951-3	$SrCo^{II}_{0.75}Ta_{0.25}O_{2.38}$	$SrCO_3$, CoO, Ta_2O_5	"	"	$SrCo^{II}_{0.75}Ta_{0.25}O_{2.36}$ --(6)	11.1(15)	545	7.4×10^{-6}
2814-44	$SrCo^{II}_{0.675}Ta_{0.25}O_{2.30}$	$SrCO_3$, $CoCO_3$, Ta_2O_5	"	"		--	--	1.0×10^{-4}
3951-5	$SrCo^{II}_{0.675}Ta_{0.25}O_{2.30}$	$SrCO_3$, CrO, Ta_2O_5	"	1205	$SrCo^{II}_{0.675}Ta_{0.25}O_{2.31}$ --(6)	0.0(15)	265	2.7×10^{-5}
2814-45	$SrCo^{II}_{0.6}Ta_{0.25}O_{2.23}$	$SrCO_3$, $CoCO_3$, Ta_2O_5	"	1260		--	--	6.6×10^{-5}
2814-46	$SrCo^{II}_{0.5}Ta_{0.1}O_{2.15}$	$SrCO_3$, $CoCO_3$, Ta_2O_5	"	"	--(6)	3.9(15)	266	1.8×10^{-3}, 2.9×10^{-3}
2814-41	$SrCo^{II}_{0.81}Ta_{0.1}O_{2.06}$	$SrCO_3$, $CoCO_3$, Ta_2O_5	"	"	--(6)	--	--	(13)
3951-26	$SrCo^{II}_{0.67}Mo_{0.33}O_{2.66}$	$SrCO_3$, $CoCO_3$, MoO_3	"	1205	--(6)	21.7(15)	546	9.5×10^{-5}, 1.6×10^{-4}
3951-27	$SrCo^{II}_{0.75}W_{0.25}O_{2.50}$	$SrCO_3$, $CoCO_3$, WO_3	"	"	$SrCo^{II}_{0.75}W_{0.25}O_{2.69}$ --(6)	6.7(15)	545	2.0×10^{-3}, 3.8×10^{-3}
3951-21	$SrCo^{II}_{0.75}Mo_{0.25}O_{2.50}$	$SrCO_3$, $CoCO_3$, MoO_3	"	"	--(6)	0.0(15)	548	1.9×10^{-2}, 2.2×10^{-2}
3951-25	$SrCo^{II}_{0.67}Mo_{0.25}O_{2.43}$	$SrCO_3$, $CoCO_3$, MoO_3	"	"	--(6)	0.9(15)	401	3.3×10^{-2}, 4.5×10^{-2}
3951-24	$SrCo^{II}_{0.8}Mo_{0.25}O_{2.35}$	$SrCO_3$, $CoCO_3$, MoO_3	"	"	--(6)	0.0(15)	565	2.9×10^{-2}, 2.7×10^{-2}

(6) Partial CO_2 loss occurred during drying of pilled firing mixtures; weight changes meaningless.
(7) Material spilled during firing; weights unreliable.
(10) X-ray pattern shows presence of more than one phase.
(11) At room temperature.
(12) X-ray pattern fits perovskite-type structure.
(13) Samples ruined during attempt to refirs in silica boat at 1370°C.
(14) No product could be recovered; sample fused into boat.
(15) Corroding solution: 0.927 M cobalt sulfate in 2.8 M H_2SO_4.

APPENDIX A-19 (CONT'D)

PREPARATION AND PROPERTIES OF PEROVSKITES

C. Iron Compounds

Reference	Nominal Formula	Starting Materials	Firing Conditions: Atmosphere	Firing Conditions: Max Temp, °C	Product Formula(1)	Acid Resistance(2): Percent Metal Contained	Acid Resistance(2): Test Time (Hrs)	Conductance ($ohm^{-1}cm^{-1}$)
3440-38	$LaFe^{II}_{0.5}Ti_{0.5}O_3$	La_2O_3, Fe, Fe_2O_3, TiO_2	N_2	1205	$LaFe^{II}_{0.5}Ti_{0.5}O_{2.58}$	45	186(11)	1.2×10^{-9}
3440-14	$SrFe^{IV}_{0.5}Ti_{0.5}O_3$	$SrCO_3$, Fe_2O_3, TiO_2	Air	"	$SrFe^{IV}_{0.5}Ti_{0.5}O_{2.86}$(12)	2	64	3.8×10^{-4}
3440-13	$SrFe^{IV}_{0.5}Zr_{0.5}O_3$	$SrCO_3$, Fe_2O_3, ZrO_2	"	"	$SrFe^{IV}_{0.5}Zr_{0.5}O_{2.85}$	0	64	7.1×10^{-4}
3440-15	$SrFe^{IV}_{0.5}Hf_{0.5}O_3$	$SrCO_3$, Fe_2O_3, HfO_2	"	"	$SrFe^{IV}_{0.5}Hf_{0.5}O_{2.87}$	0	64	6.8×10^{-3}
3951-7	$SrFe^{III}_{0.5}Ta_{0.5}O_3$	$SrCO_3$, Fe_2O_3, Ta_2O_5	N_2	"	$SrFe^{III}_{0.5}Ta_{0.5}O_{2.92}$	57.1	381	1.4×10^{-9}
3951-6	$SrFe^{II}_{0.33}Ta_{0.67}O_3$	$SrCO_3$, Fe, Fe_2O_3, Ta_2O_5	"	"	$SrFe^{II}_{0.33}Ta_{0.67}O_{3.02}$	80.7	381	1.9×10^{-9}
2814-48	$SrFe^{II}_{0.6}Ta_{0.25}O_{2.23}$	$SrCO_3$, Fe, Fe_2O_3, Ta_2O_5	"	1260	$SrFe^{III}_{0.6}Ta_{0.25}O_{2.51}$(16)	9.2	64	1.5×10^{-3}
2814-50	$SrFe^{II}_{0.90}Ta_{0.1}O_{2.15}$	$SrCO_3$, Fe, Fe_2O_3, Ta_2O_5	"	"	$SrFe^{(II,III)}_{0.9}Ta_{0.1}O_{2.35}$(18)	6.4	64	3.9×10^{-5}
2814-49	$SrFe^{II}_{0.81}Ta_{0.1}O_{2.06}$	$SrCO_3$, Fe, Fe_2O_3, Ta_2O_5	"	"	$SrFe^{III}_{0.81}Ta_{0.25}O_{2.45}$(17)	1.5	64	4.1×10^{-3}
3952-5	$SrFe^{III}_{0.75}Mo_{0.25}O_{2.88}$	$SrCO_3$, Fe_2O_3, MoO_3	"	1205	--(6)	--	--	6.0×10^{-3}
3952-6	$SrFe^{III}_{0.75}W_{0.25}O_{2.88}$	$SrCO_3$, Fe_2O_3, WO_3	"	"	--(6)	--	--	2.4×10^{-3}

(1) Calculated from weight changes during firing.
(2) Percent of original metal, e.g. nickel, retained after heating with 3.7 M H_2SO_4 for specified number of hours.
(6) Partial CO_2 loss occurred during drying of pilled firing mixtures; weight changes meaningless.
(11) At room temperature.
(12) X-ray pattern fits perovskite-type structure.
(16) 95% Fe^{III}, sample badly fused to boat.
(17) 96% Fe^{III}, sample badly fused to boat.
(18) 54% Fe^{III}, sample badly fused to boat.

APPENDIX A-19 (CONT'D)

PREPARATION AND PROPERTIES OF PEROVSKITES

D. Manganese Compounds

Reference	Nominal Formula	Starting Materials	Firing Conditions: Atmosphere	Firing Conditions: Max Temp, °C	Product Formula[1]	Acid Resistance[2]: Percent Metal Retained	Acid Resistance[2]: Test Time (Hrs)	Conductance ($ohm^{-1}cm^{-1}$)
3440-7	$SrMn^{IV}_{0.297}Ti_{0.67}O_{2.93}$	$SrCO_3$, MnO_2, TiO_2	Air	1200	$SrMn^{IV}_{0.297}Ti_{0.67}O_{2.83}$	74.9	124	1.7×10^{-8}
3440-23	$LaMn^{II}_{0.5}Ti_{0.5}O_3$	La_2O_3, $MnCO_3$, TiO_2	N_2	1150	$LaMn^{II}_{0.5}Ti_{0.5}O_{2.5}$(10)	--	--	3.6×10^{-5}
3261-34	$SrMn^{IV}_{0.09}Zr_{0.9}O_{2.98}$	$SrCO_3$, MnO_2, ZrO_2	Air	1200	$SrMn_{0.09}Zr_{0.9}O_{2.94}$	--	--	5.6×10^{-11}
3261-33	$SrMn^{IV}_{0.1}Zr_{0.9}O_3$	$SrCO_3$, MnO_2, ZrO_2	"	"	$SrMn_{0.1}Zr_{0.9}O_{2.94}$(12)	--	--	4.8×10^{-11}
3261-35	$SrMn^{IV}_{0.675}Zr_{0.25}O_{2.85}$	$SrCO_3$, MnO_2, ZrO_2	"	"	$SrMn_{0.675}Zr_{0.25}O_{2.72}$	--	--	2.5×10^{-8}
3261-36	$SrMn^{IV}_{0.75}Zr_{0.25}O_3$	$SrCO_3$, MnO_2, ZrO_2	"	"	$SrMn_{0.75}Zr_{0.25}O_{2.80}$	90.7	104	1.9×10^{-8}
3261-46	$SrMn^{IV}_{0.45}Sn_{0.50}O_{2.90}$	$SrCO_3$, MnO_2, SnO_2	"	1260	$SrMn_{0.45}Sn_{0.50}O_{2.81}$(10)	--	--	1.8×10^{-9}
3261-44	$SrMn^{IV}_{0.1}Hf_{0.9}O_3$	$SrCO_3$, MnO_2, HfO_2	"	"	$SrMn_{0.1}Hf_{0.9}O_{2.87}$	--	--	1.2×10^{-10}
3261-45	$SrMn^{IV}_{0.45}Hf_{0.50}O_{2.90}$	$SrCO_3$, MnO_2, HfO_2	"	"	$SrMn_{0.45}Hf_{0.50}O_{2.80}$(10)	84.0	124	4.0×10^{-9}
3951-36	$SrMn^{II}_{0.33}Ta_{0.67}O_3$	$SrCO_3$, $MnCO_3$, Ta_2O_5	N_2	1205	$SrMn^{II}_{0.33}Ta_{0.67}O_{2.92}$	29.1	124	1.6×10^{-9}
3951-1	$SrMn^{II}_{0.75}Ta_{0.25}O_{2.38}$	$SrCO_3$, $MnCO_3$, Ta_2O_5	"	1260	--(19)	79.1	124	2.0×10^{-3}
3951-20	$SrMn^{II}_{0.675}Ta_{0.25}O_{2.30}$	$SrCO_3$, $MnCO_3$, Ta_2O_5	"	1205	--(19)	85.5	124	1.4×10^{-3}, 3.2×10^{-4}
3951-50	$SrMn^{II}_{0.75}W_{0.25}O_{2.50}$	$SrCO_3$, $MnCO_3$, WO_3	"	"	--(19)	66.1	124	1.0×10^{-3}, 2.0×10^{-3}

(1) Calculated from weight changes during firing.
(2) Percent of original metal, e.g. nickel, retained after heating with 3.7 M H_2SO_4 for specified number of hours.
(10) X-ray pattern shows presence of more than one phase.
(12) X-ray pattern fits perovskite-type structure.
(19) Probable loss of CO_2 during drying of pilled firing mixture precludes calculation of product formula. However, (a) low weight loss during firing, (b) dark colors, and (c) good acid resistance strongly suggest that manganese is in higher valence states (Mn^{III} and Mn^{IV}). CO_2 serves as oxidizing agent.

APPENDIX A-19 (CONT'D)

PREPARATION AND PROPERTIES OF PEROVSKITES

E. Copper Compounds

Reference	Nominal Formula	Starting Materials	Firing Conditions: Atmosphere	Firing Conditions: Max Temp, °C	Product Formula	Acid Resistance: Percent Metal Retained	Acid Resistance: Test Time (Hrs)	Conductance ($ohm^{-1}cm^{-1}$)
3951-10	$SrCu^{II}_{0.33}Ta_{0.67}O_3$	$SrCO_3$, CuO, Ta_2O_5	Air	1150	$SrCu_{0.33}Ta_{0.67}O_{2.91}$	79.9	148	8.2×10^{-10}
3951-11	$SrCu^{II}_{0.5}W_{0.5}O_3$	$SrCO_3$, CuO, WO_3	"	1205	$SrCu_{0.5}W_{0.5}O_{3.03}$	29.7	"	2.8×10^{-11}, 1.0×10^{-11}
3951-13	$SrCu^{II}_{0.75}Ta_{0.25}O_{2.38}$	$SrCO_3$, CuO, Ta_2O_5	"	"	$SrCu^{II}_{0.75}Ta_{0.25}O_{2.44}$	40.4	"	8.0×10^{-6}
3952-21	$SrCu^{II}_{0.675}Ta_{0.25}O_{2.30}$	$SrCO_3$, CuO, Ta_2O_5	"	1090	$SrCu^{(I,II)}_{0.675}Ta_{0.25}O_{2.10}$ (20)	4.3	"	1.6×10^{-5}
3951-39	$SrCu^{II}_{0.75}Mo_{0.25}O_{2.50}$	$SrCO_3$, CuO, MoO_3	"	1205	--(6)	21.7	"	5.9×10^{-6}
3951-38	$SrCu^{II}_{0.75}W_{0.25}O_{2.50}$	$SrCO_3$, CuO, WO_3	"	"	$SrCu^{(I,II)}_{0.75}W_{0.25}O_{2.24}$ (21)	25.2	"	3.3×10^{-5}
3440-44	$LaCu^{II}_{0.5}Ti_{0.5}O_3$	La_2O_3, CuO, TiO_2	"	"	$LaCu^{II}_{0.5}Ti_{0.5}O_{2.64}$ (12)	13.7	"	5.3×10^{-6}
		F. Chromium Compounds						
3951-14	$SrCr^{III}_{0.5}Ta_{0.5}O_3$	$SrCO_3$, Cr_2O_3, Ta_2O_5	N_2	1205	$SrCr^{III}_{0.5}Ta_{0.5}O_{2.92}$	--	--	1.3×10^{-9}
3951-15	$SrCr^{III}_{0.75}Ta_{0.25}O_{2.75}$	$SrCO_3$, Cr_2O_3, Ta_2O_5	"	1260	$SrCr^{(III,IV)}_{0.75}Ta_{0.25}O_{3.15}$ (22)	--	--	1.5×10^{-5}
3951-49	$SrCr^{III}_{0.75}W_{0.25}O_{2.88}$	$SrCO_3$, Cr_2O_3, WO_3	"	1205	$SrCr^{III}_{0.75}W_{0.25}O_{2.93}$	--	--	1.6×10^{-4}
3440-49	$BaCr^{III}_{0.33}Ti_{0.67}O_{2.84}$	$BaCO_3$, Cr_2O_3, TiO_2	"	"	$BaCr_{0.33}Ti_{0.67}O_{3.12}$ (10)	--	--	9.1×10^{-8}
		G. Noble Metal Compounds (Pt, Ru, Rh, Ir)						
2814-34	$BaRu^{IV}_{0.33}Ti_{0.67}O_3$	$BaCO_3$, Ru, TiO_2	Air	1260	$BaRu_{0.33}Ti_{0.67}O_{2.86}$	--	--	4.6×10^{-4}
2814-35	$BaRh^{IV}_{0.33}Ti_{0.67}O_3$	$BaCO_3$, Rh, TiO_2	"	"	$BaRh_{0.33}Ti_{0.67}O_{2.81}$	--	--	5.2×10^{-3}
3951-42	$BaPt^{IV}_{0.1}Ti_{0.9}O_3$	$BaCO_3$, PtO_2, TiO_2	"	1205	$BaPt_{0.1}Ti_{0.9}O_{2.76}$	--	--	1.1×10^{-8}
3951-43	$BaIr^{IV}_{0.33}Ti_{0.67}O_3$	$BaCO_3$, Ir, TiO_2	"	"	--(7)	--	--	2.6×10^{-4}
		H. Silver Compounds						
3951-12	$SrAg^{II}_{0.33}Ta_{0.67}O_3$	$SrCO_3$, Ag_2O, Ta_2O_5	Air	1205	$SrAg^{(?)}_{0.33}Ta_{0.67}O_{2.44}$ (23)	99.8	26.5	1.9×10^{-8}
3952-20	$SrAg^{II}_{0.75}Ta_{0.25}O_{2.38}$	$SrCO_3$, Ag_2O, Ta_2O_5	"	1150	$SrAg^{(?)}_{0.75}Ta_{0.25}O_{1.59}$ (23)	99.9	"	1.3×10^{-8}
3952-19	$SrAg^{II}_{0.675}Ta_{0.25}O_{2.30}$	$SrCO_3$, Ag_2O, Ta_2O_5	"	"	$SrAg^{(?)}_{0.675}Ta_{0.25}O_{1.604}$ (23)	99.4	"	6.3×10^{-9}

(7) Material spilled during firing; weights unreliable.
(10) X-ray pattern shows presence of more than one phase.
(12) X-ray pattern fits perovskite-type structure.
(20) Boat badly attacked, product formula corresponds to 59% Cu^I.
(21) Boat badly attacked, product formula corresponds to 69.5% Cu^I.
(22) Weight increasing at end of firing period, indicating pick-up of oxygen.
(23) Calculated assuming no silver loss during firing.

APPENDIX A-20

CORROSION TESTS ON PEROVSKITES

A. Nickel

Nominal Formula	Test Period	Accumulated Hrs at 86°C	Ni^{+2} Conc in Acid (M/L)(1) At Start of Period	Ni^{+2} Conc in Acid (M/L)(1) At End of Period	Ni in Solid (% of Original) At Start	Ni in Solid (% of Original) At End
$BaNi^{II}_{0.33}Ta_{0.67}O_3$	1	27.2	0.000	0.00798	100.0	83.9
(Reference 2815-13)(3)	2	40.8	0.00645	0.00664	83.9	82.9
	3	159.6	0.00558	0.0117	82.9	71.7
	4	199	0.00983	0.0145	71.7	60.5
	5	242	0.0122	0.00806	60.5	70.5
	6	265	0.00877	0.0119	70.5	60.2
	7	288	0.0260(2)	0.0237	60.2	64.8
	8	308	0.0481(2)	0.0415	64.8	78.3
	9	334	0.0428(2)	0.0446	78.3	74.8
	10	402	0.0534(2)	0.0456	74.8	92.7
	11	451	0.0630(2)	0.0659	92.7	84.7
$SrNi_{0.33}Ta_{0.67}O_3$	1	27	0.000	0.00021	100	99.6
(Reference 2815-15)(3)	2	40.8	0.00017	0.00019	99.6	99.5
	3	159.6	0.00015	0.00469	99.5	90.6
	4	199	0.00394	0.00652	90.6	84.4
	5	242	0.00548	0.00932	84.4	76.9
	6	265	0.0102(2)	0.00940	76.9	78.4
	7	288	0.0159(2)	0.0119	78.4	86.3
	8	308	0.0260(2)	0.0273	86.3	83.8
	9	354	0.0269(2)	0.0267	83.8	84.3
	10	402	0.0304(2)	0.0283	84.3	87.6
	11	451	0.0513(2)	0.0394	87.6	105.0
$SrNi^{II}_{0.33}Ta_{0.67}O_3$	1	27.2	0.000	0.00047	100.0	99.0
(Reference 2815-26)(3)	2	40.8	0.00039	0.00028	99.0	99.4
	3	159.6	0.00024	0.00657	99.4	87.3
	4	199	0.00552	0.00646	87.3	82.8
	5	242	0.00543	0.00705	82.8	80.2
	6	265	0.00833(2)	0.0105	80.2	74.8
	7	288	0.0168(2)	0.0148	74.8	78.9
	8	308	0.0284(2)	0.0239	78.9	88.0
	9	354	0.0241(2)	0.0236	88.0	89.1
	10	402	0.0278(2)	0.0249	89.1	95.0
	11	451	0.0489(2)	0.0461	95.0	100.6
$SrNi^{II}_{0.33}Ta_{0.67}O_3$	1	27.2	0.000	0.00098	100.0	98.0
(Reference 2815-25)	2	40.8	0.00082	0.00063	98.0	98.4
	3	159.6	0.00054	0.0111	98.4	76.5
	4	199	0.00933	0.00742	76.5	79.4
	5	242	0.00623	0.00343	79.4	87.5
	6	265	0.00528(2)	0.00914	87.5	79.5
	7	288	0.0157(2)	0.0139	79.5	83.3
	8	308	0.0276(2)	0.0243	83.3	90.3
	9	354	0.0244(2)	0.0243	90.3	90.6
	10	402	0.0284(2)	0.0265	90.6	94.4
	11	451	0.0500(2)	0.0333	94.4	129.2
$BaNi^{II}_{0.5}Mo_{0.5}O_3$	1	24.7	0.0000	0.00155	100.0	97.0
(Reference 2814-31)(3)	2	40.5	0.00130	0.00317	97.0	93.4
	3	83.8	0.00266	0.00778	93.4	83.5
	4	135	0.00654	0.0136	83.5	69.8
	5	156	0.0114	0.0115	69.8	69.7
	6	180	0.0257(2)	0.0174	69.7	85.7
	7	204	0.0306(2)	0.0282	85.7	90.3
$BaNi^{II}_{0.5}Mo_{0.5}O_3$	1	24.7	0.0000	0.0330	100	34.6
(Reference 2815-18)(3)	2	40.5	0.0277	0.0314	34.6	27.2
	3	83.8	0.0264	0.0299	27.2	12.2
	4	135	--	0.0281	12.2	14.4
	5	156	0.0316(2)	0.0303	14.4	17.0
	6	180	0.0414(2)	0.0447	17.0	10.6
	7	204	0.0855(2)	0.0569	10.6	32.6

(1) 3.7 M H_2SO_4 unless otherwise specified.
(2) Added sulfate of metal in aqueous H_2SO_4.
(3) See Reference (6).

APPENDIX A-20 (CONT'D)

CORROSION TESTS ON PEROVSKITES

Nominal Formula	Test Period	Accumulated Hrs at 86°C	Ni^{+2} Conc in Acid (M/L)(1) At Start of Period	At End of Period	Ni in Solid (% of Original) At Start	At End
$BaNi^{II}_{0.5}W_{0.5}O_3$	1	24.7	0.0000	0.0117	100	78.3
(Reference 2815-34)(3)	2	40.5	0.00983	0.0133	78.3	71.9
	3	83.8	0.0112	0.0176	71.9	59.9
	4	135	0.0148	0.0180	59.9	53.8
	5	156	0.0232(2)	0.0246	53.8	51.1
	6	180	0.0367(2)	0.0328	51.1	58.3
	7	204	0.0756(2)	0.0538	58.3	98.7
$BaNi^{II}_{0.33}Nb_{0.67}O_3$	1	27.2	0.0000	0.00932	100	81.9
(Reference 2815-12)(3)	2	41.4	0.00783	0.00760	81.9	82.4
	3	85	0.00638	0.01532	82.4	65.0
	4	163	0.0128	0.0120	65.0	66.7
	5	251	0.0260(2)	0.0341	66.7	51.1
	6	275	0.0447(2)	0.0327	51.1	74.3
	7	299	0.0506(2)	0.0574	74.3	69.1
$SrNi^{II}_{0.33}Nb_{0.67}O_3$	1	27.2	0.0000	0.00953	100	79.0
(Reference 2815-14)(3)	2	41.4	0.00800	0.0125	79.0	69.1
	3	85	0.00105	0.0256	69.1	35.8
	4	163	0.0215	0.0299	35.8	17.4
	5	251	0.0571(2)	0.0509	17.4	31.2
	6	275	0.0907(2)	0.0639	31.2	90.3
	7	299	0.140	0.142	90.3	86.4
$BaNi^{IV}_{0.33}Ti_{0.67}O_3$	1	19.8(4)	0.0000	0.0199	100	60.0
(Reference 2815-17)(3)	2	45.4(4)	0.0167	0.0299	60.0	33.6
	3	458(4)	0.0252	0.0273	33.6	28.4
	4	601(4)	0.0339(2)	0.0384	28.4	30.3
	5	813(4)	0.0483(2)	0.0483	30.3	30.2
	6	25.2(5)	0.0485(2)	0.0481	30.2	31.1
	7	50(5)	0.0647(2)	0.0618	31.1	37.0
	8	76(5)	0.119(2)	0.115	37.0	47.4
$BeNi^{IV}_{0.33}Ti_{0.67}O_3$	1	20.8(4)	0.0000	0.0175	100	65.2
(Reference 2815-46)(3)	2	45.3(4)	0.0147	0.0197	65.2	55.3
	3	459(4)	0.0166	0.0175	55.3	53.2
	4	814(4)	0.0307(2)	0.0309	53.2	52.9
	5	25.2(5)	0.0420(2)	0.0524	52.9	32.1
	6	50(5)	0.0676(2)	0.0680	32.1	31.5
	7	76(5)	0.1237(2)	0.1066	31.5	71.9
$BeNi^{IV}_{0.33}Zr_{0.67}O_3$	1	22(4)	0.0000	0.0144	100	71.9
(Reference 2815-29)(3)	2	46(4)	0.0121	0.0199	71.9	56.6
	3	168(4)	0.0167	0.0230	56.6	44.3
	4	457(4)	0.0194	0.0260	44.3	31.2
	5	601(4)	0.0379(2)	0.0353	31.2	36.2
	6	812(4)	0.0456(2)	0.0425	36.2	42.3
	7	25.2(5)	0.0437(2)	0.0429	42.3	41.9
	8	50(5)	0.0529(2)	0.0515	41.9	44.6
	9	76(5)	0.0913	0.0887	44.6	49.7
$Sr_{0.8}Ni^{II}_{0.33}Te_{0.67}O_{2.80}$	1	19.1	0.0000	0.0353	100	29.0
(Reference 2815-45)(3)	2	35.3	0.0297	0.0263	29.0	35.3
	3	78	0.0221	0.0212	35.3	37.5
	4	180	0.0178	0.0236	37.5	25.8
	5	221	0.0664(2)	0.0368	25.8	85.3
	6	257	0.0389(2)	0.0567	85.3	49.7
	7	281	0.0476	0.0448	49.7	55.2
	8	305	0.0215	0.0327	55.2	29.1
$SrNi^{III}_{0.5}Te_{0.5}O_3$	1	23.3(4)	0.0000	0.0178	100.0	65.0
(Reference 2815-25)(3)	2	46(4)	0.0150	0.0109	65.0	73.0
	3	169(4)	0.0091	0.0135	73.0	64.5
	4	457(4)	0.0113	0.0089	64.5	69.2
	5	812(4)	0.0235(2)	0.0229	69.2	70.3
	6	25.2(5)	0.0273(2)	0.0373	70.3	50.5
	7	50(5)	0.0474	0.0504	50.5	44.6
	8	76(5)	0.0903	0.0806	44.6	70.1

(1) 3.7 M H_2SO_4 unless otherwise specified.
(2) Added sulfate of metal in aqueous H_2SO_4.
(3) See Reference (6).
(4) Hours in contact with acid at room temperature.
(5) Hours at 86°C in addition to listed hours at room temperature.

CORROSION TESTS ON PEROVSKITES

Nominal Formula	Test Period	Accumulated Hrs at 86°C	Ni^{+2} Conc in Acid (M/L)(1) At Start of Period	Ni^{+2} Conc in Acid (M/L)(1) At End of Period	Ni in Solid (% of Original) At Start	Ni in Solid (% of Original) At End
$Pb_{0.9}Ni^{II}_{0.33}Ta_{0.67}O_?$	1	26.9	0.0000	0.00780	100	84.4
(Reference 3261-3)(3)	2	41	0.00655	0.00868	84.4	80.1
	3	85	0.00728	0.0192	80.1	56.4
	4	163	0.0161	0.0218	56.4	45.1
	5	251	0.0343(2)	0.0355	45.1	42.5
	6	275	0.0458(2)	0.0422	42.5	49.8
	7	299	0.0607(2)	0.0634	49.8	45.5
$Pb_{0.8}Ni^{II}_{0.33}Ta_{0.67}O_?$	1	26.9	0.0000	0.00754	100	84.9
(Reference 2815-16)(3)	2	41	0.00633	0.00881	84.9	79.9
	3	85	0.00740	0.0158	79.9	63.1
	4	163	0.0133	0.0181	63.1	53.4
	5	251	0.0312(2)	0.0356	53.4	45.5
	6	275	0.0460(2)	0.0326	45.5	71.3
	7	299	0.0542(2)	0.0636	71.3	52.6
$SrNi^{II}_{0.75}Ta_{0.25}O_{2.38}$	1	19.1	0.0000	0.0330	100	40.6
	2	35.1	0.0277	0.0404	40.6	17.7
(Reference 2815-40)(3)	3	78	0.0340	0.0340	17.7	17.6
	4	180	0.0284	0.0325	17.6	10.6
	5	209	0.0703(2)	0.0567	10.6	35.1
	6	257	0.0956(2)	0.0819	35.1	59.8
	7	281	0.0688	0.0757	59.8	47.3
	8	305	0.0394	0.0549	47.3	19.5
$SrNi^{II}_{0.75}Ta_{0.25}O_{2.38}$	1	18.9	0.0000	0.0402	100	26.9
	2	35.1	0.0338	0.0291	26.9	45.2
(Reference 2814-37)(3)	3	78	0.0245	0.0353	45.2	15.7
	4	180	0.0297	0.0264	15.7	21.6
	5	209	0.0676(2)	0.0574	21.6	40.1
	6	257	0.0962(2)	0.0865	40.1	57.8
	7	281	0.0796	0.0855	57.8	47.1
	8	305	0.0445	0.0567	47.1	24.9
$SrNi^{II}_{0.675}Ta_{0.25}O_{2.30}$	1	18.9	0.0000	0.0386	100	29.2
(Reference 2814-36)(3)	2	35.1	0.0324	0.0327	29.2	28.7
	3	78	0.0275	0.0288	28.7	26.1
	4	180	0.0242	0.0239	26.1	26.8
	5	209	0.0665(2)	0.0559	26.8	46.3
	6	257	0.0949(2)	0.0852	46.3	64.1
	7	281	0.0716	0.0703	64.1	66.5
	8	305	0.0366	0.0448	66.5	44.0
			B. Cobalt			
$SrCo^{II}_{0.33}Ta_{0.67}O_3$	1	53.8	0.0000	0.00597	100	88.0
(Reference 3951-4)	2	123	0.00501	0.00767	88.0	82.8
	3	194	0.00644	0.00827	82.8	79.1
	4	321	0.155(2)	0.154	79.1	81.8
	5	488	0.463(2)	0.374	81.8	100(?)
$BaCo^{II}_{0.5}Mo_{0.5}O_3$	1	28	0.0000	0.0246	100	50.8
(Referencc 2815-50)(3)	2	117	0.0207	0.0294	50.8	33.4
	3	139	0.0247	0.0265	33.4	29.7
	4	163	0.0303(2)	0.0323	29.7	25.6
	5	187	0.0432(2)	0.0393	25.6	34.2
	6	211	0.0810(2)	0.0784	34.2	38.8
" " (6)	1	24	0.927	1.004	100	76.5
	2	96.5	0.996	1.030	76.5	66.3
	3	265	1.019	1.014	66.3	66.8
	4	425	1.005	1.064	66.8	51.0
	5	569	1.050	1.062	51.0	47.4

(1) 3.7 M H_2SO_4 unless otherwise specified.
(2) Added sulfate of metal in aqueous H_2SO_4.
(3) See Reference (6).
(6) Corroding medium used in this test: 0.0793 M cobalt sulfate in 2.9 M H_2SO_4.

APPENDIX A-20 (CONT'D)

CORROSION TESTS ON PEROVSKITES

Nominal Formula	Test Period	Accumulated Hrs at 86°C	Co^{+2} Conc in acid (M/L)[1] At Start of Period	Co^{+2} Conc in acid (M/L)[1] At End of Period	Co in Solid (% of Original) At Start	Co in Solid (% of Original) At End
$SrCo^{II}_{0.5}Mo_{0.5}O_3$	1	28	0.000	0.0308	100	38.5
	2	117	0.0259	0.0380	38.5	14.2
(Reference 2815-49)[3]	3	139	0.0319	0.0318	14.2	14.4
	4	163	0.0347[2]	0.0381	14.4	7.6
	5	187	0.0480[2]	0.0425	7.6	10.6
	6	211	0.0837[2]	0.0881	10.6	9.9
" " [6]	1	24	0.927	1.088	100	51.4
	2	96.5	1.071	1.117	51.4	37.7
	3	265	1.097	1.049	37.7	54.3
	4	425	1.036	1.104	54.3	33.9
	5	569	1.086	1.060	33.9	42.4
$BaCo^{II}_{0.5}W_{0.5}O_3$	1	28	0.000	0.0163	100	67.5
(Reference 2815-35)[3]	2	117	0.0137	0.0281	67.5	38.6
	3	139	0.0236	0.0254	38.6	34.9
	4	163	0.0294[2]	0.0317	34.9	30.3
	5	187	0.0426[2]	0.0412	30.3	33.1
	6	211	0.0826[2]	0.0900	33.1	20.8
$BaCo^{II}_{0.33}Nb_{0.67}O_3$	1	28	0.0000	0.00997	100	80.1
(Reference 2815-39)[3]	2	117	0.00838	0.0213	80.1	54.2
	3	139	0.0178	0.0156	54.2	58.8
	4	163	0.0211[2]	0.0255	58.8	50.0
	5	187	0.0375[2]	0.0376	50.0	49.7
	6	211	0.0794[2]	0.0818	49.7	44.9
$BeCo^{IV}_{0.33}Ti_{C.67}O_3$	1	25.3[4]	0.0000	0.0182	100	63.6
(Reference 2815-37)[3]	2	100[4]	0.0152	0.0131	63.6	68.0
	3	151[4]	0.0110	0.0129	68.0	64.1
	4	268[4]	0.0108	0.0112	64.1	63.5
	5	28.3[5]	0.00908	0.0178	63.5	46.7
	6	52[5]	0.0310[2]	0.0410	46.7	26.7
	7	76[5]	0.0824[2]	0.0824	26.7	26.7
	8	100[5]	0.143[2]	0.142	26.7	26.9
$SrCo^{IV}_{0.297}Zr_{0.67}O_{2.93}$	1	27.6[4]	0.0000	0.0474	100	5.2
(Reference 3261-16)[3]	2	267[4]	0.0398	0.0399	5.2	5.0
	3	28.3[5]	0.0235	0.0317	5.0	8.6
$SrCo^{1V}_{0.45}Zr_{0.45}O_{2.90}$	1	28.9[4]	0.0000	0.0500	100	0.0
(Reference 3261-17)[3]	2	269[4]	0.0419	0.0260	0.0	32.0
	3	28.3[5]	0.218	0.0310	32.0	13.6
$SrCo^{IV}_{0.75}Zr_{0.25}O_3$	1	23.8[4]	0.0000	0.0501	100	0.0
(Reference 3261-19)[3]	2	269[4]	0.0426	0.0428	0.0	0.0
	3	28.3	0.0360	0.0361	0.0	0.0
$SrCo^{II}_{0.75}Te_{0.25}O_{2.38}$[3]	1	24	0.927	1.139	100	34.4
(Reference 2814-43)	2	96.5	1.118	1.142	34.4	26.7
	3	265	1.121	1.165	26.7	13.1
	4	425	1.141	1.161	13.1	6.8
	5	569	1.138	1.177	6.8	(-5.8)
$SrCo^{II}_{0.75}Te_{0.25}O_{2.38}$[6]	1	24	0.927	1.082	100	52
(Reference 3951-3)	2	96.5	1.066	1.151	52.0	25.5
	3	240	1.0862	1.078	25.5	28.2
	4	401	1.047	1.047	28.2	28.4
	5	545	1.035	1.090	28.4	11.1

(1) 3.7 M H_2SO_4 unless otherwise specified.
(2) Added sulfate of metal in aqueous H_2SO_4.
(3) See Reference (6).
(4) Hours in contact with acid at room temperature.
(5) Hours at 86°C in addition to listed hours at room temperature.
(6) Corroding medium used in this test: 0.0793 M cobalt sulfate in 2.9 M H_2SO_4.

APPENDIX A-20 (CONT'D)

CORROSION TESTS ON PEROVSKITES

Nominal Formula	Test Period	Accumulated Hrs at 86°C	Co^{+2} Conc in Acid (M/L)(1) At Start of Period	At End of Period	Co in Solid (% of Originel) At Start	At End
$SrCo_{0.675}Ta_{0.25}O_{2.30}$(6)	1	24	0.927	1.143	100.0	33.1
(Reference 3951-5)	2	96.5	1.121	1.175	33.1	16.5
	3	265	1.150	1.204	16.5	(-4.9)
	4	435	1.176	1.171	(-4.9)	1.3
$SrCo^{II}_{0.9}Ta_{0.1}O_{2.15}$(6)	1	24	0.927	1.185	100.0	26.0
(Reference 2814-45)	2	97.5	1.159	1.185	20.0	12.0
	3	266	1.159	1.185	12.0	3.9
$SrCo^{II}_{0.67}Mo_{0.33}O_{2.66}$(6)	1	24	0.927	--	100.0	--
(Reference 3951-26)	2	97.5	--	1.175	--	18.2(?)
	3	242	1.150	1.094	--	35.2
	4	402	1.080	1.116	35.2	23.5
	5	546	1.096	1.102	23.5	21.7
$SrCo^{II}_{0.75}Mo_{0.25}O_{2.50}$(6)	1	24	0.927	1.107	100	44.3
(Reference 3951-21)	2	97.5	1.089	1.146	44.3	26.9
	3	242	--	1.125	26.9	26.3
	4	402	1.105	1.131	26.3	18.3
	5	548	1.111	1.137	18.3	0.0
$SrCo^{II}_{0.675}Mo_{0.25}O_{2.43}$(6)	1	24	0.927	1.281	100	9.4
(Reference 3951-25)	2	97.5	1.245	1.175	9.4	12.4
	3	242	1.150	1.164	12.4	8.0
	4	401	1.140	1.153	8.0	0.9
$SrCo^{II}_{0.60}Mo_{0.25}O_{2.35}$(6)	1	24	0.927	1.217	100	10.6
(Reference 3951-24)	2	96	1.187	1.185	10.6	11.4
	3	260	1.165	1.131	11.4	19.9
	4	421	1.115	1.062(?)	19.9	35.1(?)
	5	565	1.048	1.200	--	0.0
$SrCo^{II}_{0.75}W_{0.25}O_{2.50}$(6)	1	24	0.927	1.082	100	52.3
(Reference 3951-28)	2	97.5	1.066	1.156	52.3	24.6
	3	242	--	1.060	24.6	47.1(?)
	4	401	1.046	1.105	--	29.0
	5	545	1.087	1.159	1.159	6.7
			C. Iron			
$SrFe^{II}_{0.33}Ta_{0.67}O_3$	1	45.2	0.0000	0.0354	100	64.6
(Reference 3951-6)	2	136	0.0326	0.0094	64.6	87.7
	3	253	0.0086	0.0269	87.7	69.5
	4	311	0.0247	0.0114	69.5	82.5
	5	381	0.00684	0.00899	82.5	80.7
$SrFe^{III}_{0.5}Ta_{0.5}O_3$	1	45.2	0.0000	0.0310	100	69.0
(Reference 3951-7)	2	136	0.0285	0.0504	69.0	46.9
	3	253	0.0464	0.0286	46.9	64.7
	4	311	0.0263	0.0315	64.7	59.5
	5	381	0.0189	0.0213	59.5	57.1
$BaFe^{IV}_{0.33}Ti_{0.67}O_3$	1	63.6	0.0000	0.0879	100	12.1
(Reference 2815-36)(3)	2	111	0.0809	0.0835	12.1	9.5
	3	141	0.341(2)	0.334	9.5	15.4
	4	162	0.726(2)	0.735	15.4	6.6

(1) 3.7 M H_2SO_4 unless otherwise specified.
(2) Added sulfate of metal in aqueous H_2SO_4.
(3) See Reference (6).
(6) Corroding medium used in this test: 0.0793 M cobalt sulfate in 1.9 M H_2SO_4.

APPENDIX A-20 (CONT'D)

CORROSION TESTS ON PEROVSKITES

Nominal Formula	Test Period	Accumulated Hrs at 86°C	Fe^{+3} Conc in Acid (M/L)(1) At Start of Period	Fe^{+3} Conc in Acid (M/L)(1) At End of Period	Fe in Solid (% of Original) At Start	Fe in Solid (% of Original) At End
$SrFe^{(II,III)}_{0.75}Ta_{0.25}O_{2.67}$ (7)	1	63.6	0.0000	0.0962	100.0	3.8
(Reference 2815-44)(3)	2	111	0.0885(2)	0.0868	3.8	5.4
	3	141	0.342(2)	0.346	5.4	1.7
	4	162	0.728(2)	0.728	1.7	1.4
$SrFe^{III}_{0.675}Ta_{0.25}O_{2.64}$ (8)	1	63.6	0.0000	0.0983	100	1.7
(Reference 2815-42)(3)	2	111	0.0904	0.0910	1.7	1.1
	3	135	0.344(2)	0.343	1.1	1.6
$SrFe^{III}_{0.675}Ta_{0.25}O_{2.64}$ (9)	1	63.6	0.0000	0.0983	100	1.7
(Reference 2815-43)(3)	2	111	0.0904	0.0910	1.7	1.1
	3	135	0.344(2)	0.343	1.1	1.6
$SrFe^{II}_{0.60}Ta_{0.25}O_{2.23}$ (10)	1	63.6	0.0000	0.0918	100	8.2
(Reference 2814-48)	2	90	0.0845	0.0863	8.2	6.3
	3	119	0.341(2)	0.342	6.3	6.2
	4	141	0.729(2)	0.747	6.2	0.0
$SrFe^{II}_{0.90}Ta_{0.10}O_{2.15}$ (11)	1	63.6	0.0000	0.0936	100	6.4
(Reference 2814-50)	2	90	0.0861	0.0884	6.4	4.1
	3	119	0.343(2)	0.341	4.1	6.2
	4	141	0.728(2)	0.744	6.2	0.0
$SrFe^{II}_{0.81}Ta_{0.10}O_{2.06}$ (12)	1	63.6	0.0000	0.0985	100	1.5
(Reference 2814-49)	2	90	0.0906	0.0889	1.5	4.2
	3	119	0.343(2)	0.348	4.2	0.0
	4	141	0.731(2)	0.731	0.0	0.0

(1) 3.7 M H_2SO_4 unless otherwise specified.
(2) Added sulfate of metal in aqueous H_2SO_4.
(3) See Reference (6).
(7) Product Formula. 80% Fe^{III}. Nominal Formula is $SrFe^{II}_{0.75}Ta_{0.25}O_{2.38}$.
(8) Product Formula. 100% Fe^{III}. Nominal Formula is $SrFe^{(II,III)}_{0.675}Ta_{0.25}O_{2.38}$.
(9) Product Formula. 100% Fe^{III}. Nominal Formula is $SrFe^{II}_{0.675}Ta_{0.25}O_{2.30}$.
(10) Product Formula is $SrFe^{III}_{0.60}Ta_{0.25}O_{2.51}$ (95% Fe^{III}).
(11) Product Formula is $SrFe^{(II,III)}_{0.90}Ta_{0.10}O_{2.39}$(54% Fe^{III}).
(12) Product Formula is $SrFe^{(II,III)}_{0.81}Ta_{0.10}O_{2.45}$ (96% Fe^{III}).

APPENDIX A-21

POLAROGRAPHIC METHODS FOR PEROVSKITE CORROSION TESTS

All analyses described below are for the metals in 3.7 M H_2SO_4, the acid employed in all corrosion testing

I. Manganese Analyses.

A 4.0 ml sample is neutralized with solid lithium carbonate to pH2.0 and stirred at room temperature until all carbonates are dissolved. Any discoloration of the solution due to formation of trivalent and tetravalent manganese compounds is discharged by heating at this point. The pH is then adjusted to 4.0 with saturated lithium carbonate. The neutralized solution is diluted to 100ml, and 3.0ml of gelatin solution (0.15g/100ml H_2O) added as maximum suppressor. The sample is de-aerated in the polarographic cell, and at least two polarograms giving the maximum wave height possible are recorded and measured.

Calibration data were obtained on solutions prepared by dissolving Fisher's Certified manganese in 3.7 M H_2SO_4. Calibration data are given below:

Concentration of Mn^{+2} in Polarograph Cell, moles/liter	Diffusion Current, microamps
3.88×10^{-3}	27.4
1.75×10^{-3}	11.5
5.83×10^{-4}	3.75
1.55×10^{-4}	0.993

II. Copper Analysis

Copper is determined polarographically using the ammonia complex. A 4.0ml sample is mixed with 15ml 6.0N NH_3. The ammoniacal complex is diluted to 100ml with deaerated water, and 3.0ml gelatin (0.15g/100ml H_2O) added as maximum suppressed. To avoid ammonia loss the polarograph cell is not deaerated with N_2

Fisher's certified copper oxide was used in preparing calibration solutions. The wave consists of two distinct portions, corresponding to $Cu^{II} \rightarrow Cu^{I}$ and $Cu^{I} \rightarrow Cu^{0}$ reactions. Calibration data for the overall wave are given below:

Concentration of Cu^{+2} in Polarograph Cell, moles/liter	Diffusion Current, microamps
3.88×10^{-3}	34.0
1.55×10^{-3}	15.7
6.22×10^{-4}	7.49
7.77×10^{-5}	0.778

III. Silver Analysis

Silver is also analyzed as the ammonia complex. An 8.0ml sample is mixed with 20ml 6 N NH_3, the complex diluted to 100ml with deaerated water, and 1.0ml of 0.2 wt% Triton X-100 added as maximum suppressor. The polarogram is run without N_2 in the cell to prevent ammonia loss.

Solutions for calibration were prepared by dissolving Fisher's certified silver oxide in 3.7 M H_2SO_4. Calibration data are given below:

Concentration of Ag^{+1} in Polarograph Cell, moles/liter	Diffusion Current, microamps
3.17×10^{-3}	21.5
1.58×10^{-3}	11.5
7.92×10^{-4}	7.35
3.96×10^{-4}	4.64
7.92×10^{-5}	3.06

APPENDIX A-22

CONDUCTIVITY TESTS ON CORRODED PEROVSKITES

Reference	Nominal Formula	Acid Treatment		% Metal Lost	Conductance ($ohm^{-1}cm^{-1}$)	
		Hours at 86°C	Corroding Solution		Before Acid Treatment	After Acid Treatment
3952-15	$BaCo^{II}_{0.5}Mo_{0.5}O_3$ (4)	101	0.834 M $CoSO_4$ in 2.9 M H_2SO_4	19.9	4.9×10^{-9}	7.0×10^{-10}(1) 3.8×10^{-11}(2)
3952-11	$SrCo^{II}_{0.5}Mo_{0.5}O_3$	"	"	51.6	7.5×10^{-8}	7.7×10^{-10}(1)
3951-26	$SrCo^{II}_{0.67}Mo_{0.33}O_{2.66}$	8.3	"	76.8	0.95×10^{-4}	4.5×10^{-11}(1)
3951-21	$SrCo^{II}_{0.75}Mo_{0.25}O_{2.50}$	"	"	69.7	3.8×10^{-3}	2.6×10^{-12}(2)
3951-24	$SrCo^{II}_{0.60}Mo_{0.25}O_{2.35}$	"	"	53.0(3)	2.9×10^{-2}	1.9×10^{-10}(1)
2815-25	$SrNi^{II}_{0.33}Ta_{0.67}O_3$	101	3.7 M H_2SO_4	14.3	7.1×10^{-9}	1.6×10^{-9}(1)
3951-45	$BaNi^{II}_{0.33}Ta_{0.67}O_3$	"	"	7.8	1.8×10^{-9}	5.0×10^{-9}(1)
3951-35	$(Sr_{0.9}La^{III}_{0.1})Ni^{II}_{0.37}Ta_{0.63}O_3$ (5)	"	"	10.7	1.4×10^{-9}	2.9×10^{-9}(2)
3951-23	$SrNi^{II}_{0.75}Ta_{0.25}O_{2.38}$	8.3	0.0832 M $NiSO_4$ in 3.62 M H_2SO_4	74.0	2.7×10^{-7}	3.1×10^{-8}(1) 2.5×10^{-8}(2)
3951-29	$BaNi^{II}_{0.75}Ta_{0.25}O_{2.38}$	"	"	51.3	2.8×10^{-7}	2.7×10^{-10}(1)
3951-31	$Sr(Ni^{II}_{0.61}La_{0.068})Ta_{0.25}O_{2.34}$ (5)	"	"	36.3	3.6×10^{-5}	4.4×10^{-9}(1)

(1) After drying in desiccator over P_2O_5.
(2) After drying in air oven at 110°C.
(3) Value probably too low.
(4) After refiring at 1260°C.
(5) After refiring under air.

APPENDIX A-23

PEROVSKITE X-RAY DATA

Notebook Reference	Perovskite	Firing Conditions: Atmosphere	Firing Conditions: Temperature, °C	Intensity of[1] Perovskite Peaks in Pattern	Presence of Extraneous Peaks
3440-49	$BaCr^{III}_{0.33}Ti_{0.67}O_{2.84}$	N_2	1150	Strong	Moderate
3261-41	$SrMn^{IV}_{0.1}Zr_{0.9}O_3$	Air	1200	Strong	Very Weak
3261-45	$SrMn^{IV}_{0.45}Hf_{0.50}O_{2.90}$	"	1260	Strong	Weak
3261-46	$SrMn^{IV}_{0.45}Sn_{0.50}O_{2.90}$	"	"	Moderate	"
3440-23	$LaMn^{II}_{0.5}Ti_{0.5}O_3$	N_2	1150	"	"
3440-14	$SrFe_{0.5}Ti_{0.5}O_3$	Air	1200	Strong	None
3440-6	$SrCo^{IV}_{0.30}Ti_{0.67}O_3$	"	"	"	"
3440-26	$LaCo^{II}_{0.5}Ti_{0.5}O_3$	N_2	1150[2]	Moderate	Moderate
3440-50	"	Air	1200[3]	Strong	None
3261-17	$SrCo^{IV}_{0.45}Zr_{0.50}O_{2.90}$	"	"	"	Moderate
3261-19	$SrCo^{IV}_{0.75}Zr_{0.25}O_3$	"	"	Moderate	Strong
3440-33	$BaCo^{IV}_{0.33}Hf_{0.67}O_3$	"	1150	Strong	None
3261-41	$SrCo^{IV}_{0.45}Hf_{0.50}O_{2.90}$	"	1260	"	Moderate
3440-36	$LaNi^{II}_{0.5}Ti_{0.5}O_3$	"	1150	"	"
3440-37	$LaNi^{II}_{0.5}Zr_{0.5}O_3$	N_2	"	Moderate	"
3440-48	$LaNi^{II}_{0.5}Hf_{0.50}O_3$	Air	"	"	"
3440-44	$LaCu^{II}_{0.5}Ti_{0.5}O_3$	"	"	Strong	Weak

(1) Typical perovskite d-spacings (Å) and relative intensities: 3.90 (W), 2.76 (VS), 2.26 (M), 1.95 (S), 1.60 (M), 1.38 (W), 1.24 (W), 1.18 (W).
(2) Fired 40 hours
(3) Fired 70 hours

APPENDIX A-24

EVALUATION OF CROUP IV PEROVSKITES FOR OXYGEN ACTIVITY

3 M KOH, 100°C

Notebook[1] Reference	Electrode[2]	Polarization From Oxygen Theory At Indicated ma/cm^2, Volts						
		0	1	10	50	100	300	400
	Blank 1[3]	0.295	0.395	0.445	0.490	0.520	0.580	0.605
	Blank 2[4]	0.350	0.400	0.455	--	--	--	--
3440-7	$SrMn^{IV}_{0.30}Ti_{0.67}O_{2.93}$	0.320	0.350	0.430	0.500	0.560	--	--
3621-45	$SrMn^{IV}_{0.45}Hf_{0.50}O_{2.90}$	0.330	0.380	0.430	0.515	0.555	--	--
3440-14	$SrFe^{IV}_{0.5}Ti_{0.5}O_3$	0.360	0.410	0.470	0.540	0.680	--	--
3440-15	$SrFe^{IV}_{0.5}Hf_{0.5}O_3$	0.335	0.410	0.465	0.515	0.550	0.640	0.730
3440-15	$SrFe^{IV}_{0.5}Hf_{0.5}O_3$[5]	0.280	0.570	--	--	--	--	--
3440-50	$LaCo^{II}_{0.5}Ti_{0.5}O_3$	0.250	0.275	0.390	0.460	0.550	--	--
3440-33	$BaCo^{IV}_{0.33}Hf_{0.67}O_3$	0.250	0.325	0.410	0.550	--	--	--
3440-44	$LaCu^{II}_{0.5}Ti_{0.5}O_3$	0.310	0.340	0.395	0.465	0.510	0.620	--
3440-49	$BaCr^{III}_{0.33}Ti_{0.67}O_{2.84}$	0.370	0.400	--	--	--	--	--

(1) Reference for perovskite preparation; electrochemical test data recorded in notebook 3371, pp. 17-35.
(2) Electrodes consisted of pressed porous mixtures of carbon, catalyst and Teflon.
(3) 50 Wt.% carbon
(4) 25 Wt.% $BaSO_4$, 25 Wt.% carbon
(5) No carbon support.

APPENDIX A-25

REDOX AND CYANO COMPLEXES

Reference	Catalyst (1)	Polarization From Methanol — Theory At Indicated ma/cm^2, Volts 0	1	2	5	10	20	50
3472-17-1	6% Pt Black + 25% Cupric Ferricyanide on C	0.56	Dead					
3472-17-2	6% Pt Black + 25% Cupric Ferricyanide on C	0.58	0.73 (2)	Dead				
3472-30	6% Pt on C	0.16	0.40	0.43	0.47	0.51	0.56	Dead
3472-28-1	10% Cupric Ferrocyanide on 6% Pt/C	0.45	0.62	0.66	0.69	0.72	0.86	
3472-28-2	10% Potassium Ferrocyanide on 6% Pt/C	.46	0.62	0.70	0.80	Dead		
3472-33-1	10% Cupric Ferrocyanide on C	0.58	Dead					
3472-33-2	10% Potassium Ferrocyanide on C	0.54	Dead					
3472-39-2	10% Ferric Ferrocyanide on 6% Pt/C	0.50	0.64	0.68	0.73	Dead		
3472-40-2	10% Ferric Ferrocyanide on C	0.69	Dead					
3472-43-3	10% Cupric Prusside on 6% Pt/C	0.61	0.75	0.78	0.81	0.85	Dead	
3472-43-4	10% Sodium Prusside on 6% Pt/C	0.54	0.79	0.85	Dead			
3371-48	6% Pt on C (3)	0.01	0.35	0.38	0.43	0.48	0.54	
3371-49	10% UO_2HPO_4 on C (3, 4)	0.27		0.66	0.78	Dead		

(1) Electrolyte 3.7 M H_2SO_4, 60°C, except where noted.

(2) Not stable.

(3) Electrolyte 50% Na_2HPO_4, 3% H_3PO_4; 80°C, -0.34 volts vs S.C.E. taken as theory.

(4) An estimated 90% of the catalyst flaked off the electrode leaving about half the area covered and about 0.5 mg UO_2HPO_4 per cm^2 (used in calculating the specific current density).

APPENDIX B-1

GASIFICATION WITHIN HYDROPHOBIC POROUS MATRICES

The passage of vapors through Teflon bonded electrodes is undoubtedly related to the hydrophobic nature of the pores within the structure. Pressure is required to force liquid into such pores as given by the equation used in porosimetry:

$$\Delta P = (\gamma_{gs} - \gamma_{sl})\sigma = (\gamma_{gl} \cos\theta)(\frac{2}{r})$$

where: ΔP = pressure difference between liquid and gas
γ_{gs} = gas-solid interfacial tension
γ_{sl} = liquid-solid interfacial tension
γ_{gl} = gas-liquid interfacial tension
σ = surface to volume ratio of matrix (=2/r for cylindrical pores)
r = average pore radius
θ = contact angle

The first expression for ΔP is general; the second applies to a cylindrical pore model of the structure. Since the external pressure is only one atmosphere there will be small highly wetproofed pores which will never fill with electrolyte, even if a perfect vacuum existed on the gas side. However, in a heterogeneous matrix there should be some pores which are filled with electrolyte at room temperature, but which fill with gas as the boiling point of the electrolyte is approached. In a sense, the boiling point of the liquid in such pores is lowered below its normal boiling temperature. This can be shown as follows:

Consider a porous hydrophobic matrix totally immersed in electrolyte. If equilibrium exists between a bubble of vapor and the liquid within such a matrix, the pressure within the bubble will be below atmospheric, as given by the porosimetry equation. The amount of boiling point lowering caused by this pressure drop can be estimated approximately using the Clausius-Clapeyron equation in the form:

$$\frac{dP}{dT} = \frac{\Delta H}{TV_v}$$

where T is the equilibrium temperature (boiling point)
ΔH is the heat of vaporization
V_v is the molar volume of the vapor

Combining the above with the differential form of the porosimetry equation, using the gas law for V_v, and integrating over σ, one obtains:

$$\frac{1}{T_B} - \frac{1}{T} = \frac{R}{\Delta H} \ln\left(\frac{Po + \sigma \gamma_{gl} \cos\theta}{Po}\right)$$

where T_B is the boiling point when σ is zero
Po is atmospheric pressure

Since $\cos\theta$ is negative for hydrophobic matrices, T is less than T_B. In heavily loaded platinum black electrodes, for example, σ can be $10^6 cm^2/cm^3$. A weighted average value of θ of only 90.4° will cause gasification to occur within the pores 20°C below the normal boiling point. It is observed that permeation begins about 20°C below the normal boiling point. (In the case of liquid fuels it begins

about 20°C below the fuel-electrolyte steam distillation temperature.) Apparently, the proper degree of wetproofing is provided by correct blending and sintering of the platinum and Teflon. Excessive wetproofing in a region of the electrode can give values of $\sigma \gamma_{gl} \cos \theta$ greater than one atmosphere. The pores in this region will remain free of liquid at all temperatures, as shown by the equation.

This phenomenon of internal gasification may explain the observation in Task A, Phase I that the platinum black in optimized Teflon bonded electrodes functions at near perfect efficiency. Simple calculations show that butane can diffuse only about 0.5 microns into the electrode from its surface at rates only about one fortieth the rates actually observed. However, the presence of open pores can provide the enlarged interface and the feed channels necessary to account for the high efficiencies observed. Furthermore, the opening and refilling of pores with changes in temperature may provide the "dynamic interface" considered necessary for efficient electrode operation.

APPENDIX C-1

HYDROCARBON PERFORMANCE ON SINTERED PLATINUM-TEFLON ELECTRODES IN PYROPHOSPHORIC ACID

Pt Content: 50 mg/cm^2

Fuel	Water Bath Temp, °C	Electrolyte Temp, °C	Polarization from Fuel Theory at Indicated ma/cm^2, volts									
			5	10	25	50	75	100	200	400	500	750
Ethane	25	200	0.37	0.43	0.48	0.56	--	--	--	--	--	--
Ethane	25	230	0.31	0.37	0.42	0.48	0.56	--	--	--	--	--
Ethane	--(1)	230	0.36	0.41	0.48	0.58	--	--	--	--	--	--
Ethane	25	250	0.23	0.31	0.38	0.45	0.54	--	--	--	--	--
Butane	--(1)	250	0.22	0.28	0.40	0.47	--	--	--	--	--	--
Butane	25	250	0.25	0.31	0.37	0.43	0.47	0.51	--	--	--	--
Butane	60	250	0.22	0.25	0.28	0.37	0.38	0.39	0.50	--	--	--
Butane	80	250	0.05	0.08	0.12	0.16	0.18	0.20	0.24	0.31	--	--
Butane	95	250	0.03	0.06	0.09	0.13	0.16	0.18	0.21	0.51	--	--
Butane	100	250	0.12	0.13	0.15	0.19	0.21	0.22	--	--	-	--
Butane	80	275	--	--	--	0.18	0.19	0.21	--	--	0.50	0.57-0.64
Decane	--(2)	250	0.08	0.17	0.23	0.24	0.28	0.39	--	--	--	--
Hexane	80	275	0.25	0.31	0.33	0.34	0.37	0.38	--	--	--	--
2-Methylpentane	80	275	0.29	0.31	0.34	0.36	0.38	0.42	0.45	--	--	--
Cyclohexane	80	275	0.37	0.41	0.45	0.50	0.51	0.52	--	--	--	--
1-Hexene	80	275	0.22	0.32	0.54	0.70	--	--	--	--	--	--
Benzene	80	275	0.52	0.56	0.63	--	--	--	--	--	--	--

(1) Fuel fed dry.
(2) Decane steam distilled.

APPENDIX C-2

BUTANE PERFORMANCE WITH CATALYZED CARBON ELECTRODES IN PYROPHOSPHORIC ACID

Catalyst Density: 5 mg/cm^2 Electrolyte Temperature: 275°C

Electrode Type	Relative Porosity	Carbon Catalyst Content, wt %	Water Bath Temp, °C	Polarization from Butane Theory at Indicated ma/cm^2, volts					
				5	10	25	50	75	100
CT-1a	Low	6	80	--	--	--	--	--	--
CT-1b	Low	6	80	0.28	0.37	0.41	--	--	--
CT-1b	Low	6	95	0.18	0.23	0.27	0.36	0.49-0.53	--
CT-1(1)	High	6	80	--	--	--	--	--	--
CT-1a	High	6	80	0.30	0.41	--	--	--	--
CT-1a	High	6	80	0.42	0.48	--	--	--	--
CT-1a	High	6	95	0.29	0.36	--	--	--	--
CT-1	High	6	80	0.31	0.39	--	--	--	--
CT-1	Low	6	80	0.32	0.34	--	--	--	--
CT-1a	High	6	80	0.47	--	--	--	--	--
CT-1a	High	6	95	0.28	--	--	--	--	--
CT-1	Low	6	80	0.30	0.34	--	--	--	--
CT-1a	Low	12	80	0.13	0.16	0.31	0.35	--	--
CT-1a	Low	12	80	0.13	0.16	0.32	0.48	--	--
CT-1	High	12	80	0.19	0.26	0.34	0.36-0.41	0.44-0.51	--
CT-1	High	12	80	0.37	0.31-0.56	--	--	--	--
CT-1a	Low	12	80	0.22	0.27	--	--	--	--
CT-1	High	12	80	0.20	0.24	0.39	--	--	--
CT-1	Low	12	80	0.33	0.33	0.43-0.69	--	--	--
CT-1	Low	18	80	0.26-0.31	0.35	0.40	--	--	--
CT-1	Low	18	95	--	0.24-0.28	0.36	0.38-0.43	0.44	--
CT-1	High	18	80	0.32-0.35	0.36	0.38-0.43	0.44	--	--
CT-1	Low	18	80	0.32	0.33	0.36	--	--	--
CT-1	Low	18	95	0.20	0.24	0.27	0.29	0.35	--
CT-1	High	18	80	0.37	0.42	0.46	--	--	--
CT-1(1)	High	18	95	0.26	0.30	0.37	--	--	--
CT-1	High	18	80	0.34	0.37	0.50	--	--	--
CT-2	High	6	80	0.57	--	--	--	--	--
--	--	6	80	0.26	--	--	--	--	--
Pt-Au-Teflon	--	--	80	--	--	--	--	--	--

(1) Leaked badly.

(2) 1.4 mg/cm^2 of catalyst.

APPENDIX C-3

OXYGEN PERFORMANCE IN PYROPHOSPHORIC ACID

Electrode Type	Electrolyte Temp , °C	Polarization from Oxygen Theory at Indicated ma/cm^2, volts					
		5	10	25	50	100	150
Pt-Teflon	200	0.12	0.16	0.20	0.25	0.30	0.33
Pt-Teflon	230	0.10	0.12	0.17	0.22	0.28	0.30
Pt-Teflon	250	0.08	0.09	0.13	0.18	0.24	0.28
Pt-Teflon	200	0.06	0.07	0.10	0.13	0.17	0.18
Pt-Teflon	230	0.08	0.09	0.10	0.12	0.15	0.16
Pt-Teflon	200	0.11	0.14	0.16	0.19	0.22	0.24
Pt-Teflon	230	0.10	0.11	0.12	0.14	0.18	0.20
Pt-Teflon	230	0.03	0.05	0.05	0.06	0.08	0.09
Pt-Teflon	250	0.03	0.05	0.05	0.07	0.08	0.09
Pt-Teflon	230(1)	0.06	0.10	0.14	0.18	0.25	0.30
Pt-Teflon	230(2)	0.11	0.12	0.14	0.16	0.19	0.21
Pt-Teflon	250(3)	--	--	--	0.06	0.07	0.09
Pt-Teflon	250	--	--	--	0.05	0.08	--
5 mg/cm^2 Catalyst on Carbon	275(4)	0.27	0.31	0.37	0.42	0.45	0.48
5 mg/cm^2 Catalyst on Carbon	275(5)	0.21	0.25	0.31	0.35	0.40	0.42
5 mg/cm^2 Catalyst on Carbon	275(6)	0.29	0.43	0.55	0.80	--	--
5 mg/cm^2 Catalyst on Carbon	275(7)	0.21	0.25	0.31	0.42	0.61	0.82

(1) Tested with air.

(2) Oxygen humidified with water bath at 25°C.

(3) Oxygen humidified with water bath at 80°C.

(4) Low porosity, 18 wt % catalyst on carbon.

(5) High porosity, 12 wt % catalyst on carbon.

(6) High porosity, 18 wt % catalyst on carbon.

(7) Low porosity, 12 wt % catalyst on carbon.

APPENDIX C-4

ELECTRODE PERFORMANCES IN EQUILIBRATED CONCENTRATED BUFFER
Pt Catalyst

Reactant	Initial Electrolyte Composition	Temp, °C	Polarization from Reactant Theory at Indicated ma/cm^2, volts						
			5	10	25	50	75	100	150
Methanol (vapor fed)	3 M Cs_2HPO_4 + 3 M Cs_3PO_4	130	0.17	0.24	0.34	0.43	0.51	0.54	--
" (syringe fed)	"	"	--	--	--	0.37	0.44	0.47	--
" (dead-ended anode chamber)	"	"	--	--	--	--	0.37	0.40	--
" (dissolved)	"	100	0.24	0.29	0.36	0.44	0.46	0.49	0.55 (1)
Oxygen	3.3 M Cs_2HPO_4 + 3.3 M Cs_3PO_4	130	0.29	0.37	0.39	0.75	0.90	--	--
Hydrogen	" "	"	--	0.02	0.05	0.14	0.27	--	--
Oxygen	1 M Cs_2HPO_4 + 1 M Cs_3PO +	80	--	0.26	0.29	0.34	0.37	0.42	0.46
Hydrogen	" "	"	0.00	0.00	0.03	0.06	0.09	0.12	0.17

(1) Polarization was 0.53 volts when electrolyte was stirred.

APPENDIX C-5

EFFECT OF DUAL ELECTRODE ARRANGEMENT ON PERFORMANCE

Temp: 60°C, Electrolyte: 1 M each K_2CO_3 - $KHCO_3$, pH: 10.6

Test Number	First Sheet(1)	Insulating Separator	Second Sheet(2)	Oxidant	Polarization from Oxygen Theory at Indicated ma/cm², volts 1	10	20	50	100	Remarks
2272-50a	Pt-Teflon, Electronically Connected	2 Teflon rings, 5 ml thick each	Pt-Teflon, Electronically Insulated	Air	0.25	0.35	0.41	0.62	0.95	
2272-50b	Pt-Teflon, Electronically Insulated	2 Teflon rings, 5 ml thick each	Pt-Teflon, Electronically Connected	Air	0.25	0.50	0.75	--	--	
2272-28	Pt-Teflon	None	Ni-Teflon	Air	0.31	0.40	0.55	0.70	0.81	Both sheets connected to external circuit.
2272-28	Pt-Teflon	None	Ni-Teflon	O_2	0.24	0.35	0.45	0.60	0.68	Both sheets connected to external circuit.
2272-42	Pt-Teflon	None	Teflon	Air	0.23	0.29	0.33	0.47	0.78	
2272-42	Pt-Teflon	None	Teflon	O_2	0.20	0.28	0.32	0.43	0.64	
2272-37	Ag-Teflon	None	2 Ag-Teflon	Air	0.54	0.68	0.72	0.82	0.92	Both sheets connected to external circuit.
2272-26	Ni-Teflon	None	Ni-Teflon	Air	0.81	--	--	--	--	Both sheets connected to external circuit.
2272-17	Ni-Teflon	None	Pt-Teflon	Air	0.37	0.77	--	--	--	Both sheets connected to external circuit.

(1) Facing air chamber.
(2) Facing electrolyte.

APPENDIX C-6

CATHODE PERFORMANCES IN CONCENTRATED BUFFER ELECTROLYTE

Test Number	Electrode	Electrolyte	Oxidant	Temp, °C	Polarization from Oxygen Theory at Indicated ma/cm^2, volts				
					1	10	20	50	100
3403-22a	Dual Ag-Teflon	3.3 M Cs_2HPO_4 + 3.3 M Cs_3PO_4	Air	130	0.61	0.69	0.73	0.79	0.89
3403-22b	Dual Ag-Teflon	3.3 M Cs_2HPO_4 + 3.3 M Cs_3PO_4	O_2	130	0.59	0.61	0.63	0.67	0.71
3403-23a	Single Ag-Teflon	3.3 M Cs_2HPO_4 + 3.3 M Cs_3PO_4	Air	130	0.63	0.70	0.71	0.77	0.91
3403-23b	Single Ag-Teflon	3.3 M Cs_2HPO_4 + 3.3 M Cs_3PO_4	O_2	130	--	0.63	0.64	0.68	0.72
3403-24c	Dual Pt-Teflon	3.3 M Cs_2HPO_4 + 3.3 M Cs_3PO_4	Air	133	0.43	0.99	--	--	--
3403-24d	Dual Pt-Teflon	3.3 M Cs_2HPO_4 + 3.3 M Cs_3PO_4	O_2	133	0.37	0.48	0.56	0.70	--
3403-24a	Single Pt-Teflon	3.3 M Cs_2HPO_4 + 3.3 M Cs_3PO_4	Air	130	0.47	--	--	--	--
3403-24b	Single Pt-Teflon	3.3 M Cs_2HPO_4 + 3.3 M Cs_3PO_4	O_2	130	--	0.51	--	0.87	--
3403-25a	Pt-Teflon (air side) + Ag-Teflon	2.8 M Cs_2HPO_4 + 2.8 M Cs_3PO_4	Air	80	0.62	0.70	0.72	0.77	0.85
3403-25b	Pt-Teflon (air side) + Ag-Teflon	0.7 M Cs_2HPO_4 + 0.7 M Cs_3PO_4	Air	80	0.50	0.58	0.60	0.64	0.69
3403-3a	Dual Ag-Teflon	2.8 M Cs_2HPO_4 + 2.8 M Cs_3PO_4	Air	125	0.59	0.67	0.68	0.74	0.78
3403-3b	Dual Ag-Teflon(1)	2.8 M Cs_2HPO_4 + 2.8 M Cs_3PO_4	Air	125	0.55	0.60	--	0.65	0.69
3403-40a	Dual Ag-Teflon	6 M Cs_2CO_3	Air	118	0.36	0.44	0.48	--	--
3403-40a	Dual Ag-Teflon	6 M Cs_2CO_3	O_2	118	--	0.37	--	0.42	0.46
3403-40b	Dual Ag-Teflon	4 M K_2CO_3 + 2 M Cs_2CO_3	Air	112	0.32	0.38	0.40	0.45	0.52
3403-40b	Dual Ag-Teflon	4 M K_2CO_3 + 2 M Cs_2CO_3	O_2	112	0.26	0.33	0.35	0.38	0.41
3403-40c	Dual Ag-Teflon	6 M K_2CO_3	Air	112	0.32	0.39	0.41	0.45	0.51
3403-40c	Dual Ag-Teflon	6 M K_2CO_3	O_2	112	0.27	0.33	0.35	0.38	0.42
3403-40d	Dual Ag-Teflon	6 M K_2CO_3	Air	100	--	--	--	--	0.52
3403-40d	Dual Ag-Teflon	6 M K_2CO_3	Air	80	--	--	--	--	0.54
3403-40d	Dual Ag-Teflon	6 M K_2CO_3	Air	60	0.33	0.43	0.46	0.51	0.57
3403-49	Dual Ag-Teflon	6 M K_2CO_3	Air	112	0.34	0.40	0.43	0.47	0.52

(1) High porosity sheets.

APPENDIX C-7

EFFECT OF METHANOL ON SILVER CATHODE

Cathode: 2Ag-Teflon + 1 Teflon, Electrolyte: 6 M K_2CO_3, Oxidant: Air, Temp: 105°C

Current Density, ma/cm^2	Polarization from Oxygen Theory, volts	Methanol Concentration, vol%	Air Flow Rate, cc/min	Ratio of Air Flow Rate to Stoichiometric Requirement	Carbon Dioxide Concentration, vol%	Change in Oxygen Content
0	0.18	0	81	----	0.0005	
"	"	1	"	----	"	none
"	"	2	"	----	"	"
"	"	3	"	----	"	"
100	0.61	3	"	2.2	0.0003	
"	"	4	"	2.2	"	none
0	0.3	0	59.5	----	0.0004	
"	"	1	"	----	"	none
"	"	2	"	----	"	"
0	0.18	0	128	----	0.0001	
1	0.36	"	"	348	"	
10	0.46	"	"	34.8	"	
20	0.49	"	"	17.5	"	
50	0.53	"	"	6.96	"	
100	0.61	"	"	3.48	"	
1	0.35	4	81	220	0.0003	
10	0.43	"	"	22.0	"	
20	0.46	"	"	11.0	"	
50	0.52	"	"	4.4	"	
100	0.62	0	128	3.48	<0.0001	
"	"	0.83	"	"	"	none
"	"	1.66	"	"	"	"
"	0.61	2.49	"	"	"	"
"	0.62	3.33	"	"	"	"
"	"	4.16	"	"	"	"
"	"	4.99	"	"	"	"
"	"	6.3	"	"	"	"

APPENDIX C-8

BUFFER TOTAL CELL PERFORMANCE

Anode: P-Type Catalyst + 2 AA-1, Cathode: 2 Ag-Teflon, Electrolyte: 6 M K_2CO_3

Cell Temp, °C			104	
Fuel Concentration, M			0.5	
Electrolyte Flow Rate, cc/min			14	
Oxidant	Air			O_2
Current Density, ma/cm^2	0	50	100	100
Cell Potential, volts	0.91	0.36	0.17	0.31
Anode Polarization, volts	0.10	0.21	--	--
Ohmic Loss, volts	--	0.10	0.20	0.20
Cathode Polarization (calculated), volts	0.14	0.48	--	--
Cell Potential EX IR, volts	0.91	0.46	0.37	0.51
Terminal Power Output, mwatts/cm^2	--	18	17	31
Power EX IR, mwatts/cm^2	--	23	37	51

APPENDIX C-9

CATALYST SCREENING STUDIES ON METHANOL

Electrode Number	Catalyst	Electrolyte	Catalyst Density, mg/cm^2	Temp °C	Polarization from Methanol Theory at Indicated ma/cm^2, volts 0	1	5	10	20	50	100
230B-1	NiWS	1 M K_2HPO_4 + 1 M K_3PO_4	21.3	80	0.57	0.82	--	--	--	--	--
				90	0.45	0.88	--	--	--	--	--
232A-1	WS_2 on C	"	2.5	80	0.67	--	--	--	--	--	--
				90	0.54	0.89	--	--	--	--	--
202B-1	42 Mo-Pd on C	"	1.4	80	0.45	0.64	--	--	--	--	--
				90	0.33	0.55	0.76	--	--	--	--
226A-1	30% $CoMoO_4$ on C	"	5.6	80	0.24	0.28	0.31	0.37	0.85	--	--
				90	0.28	0.79	--	--	--	--	--
226A-2	30% $CoMoO_4$ on C	"	5.7	80	0.27	0.30	0.32	0.38	--	--	--
235A-1	$NiMoO_4$	"	2.3	80	0.52	0.75	--	--	--	--	--
				90	0.48	0.79	--	--	--	--	--
227D-1	Pt on B_4C	"	0.5	80	0.27	0.40	0.60	0.75	--	--	--
				90	0.24	0.38	0.54	0.66	0.82	--	--
233A-1	Co	"	20	60	0.67	--	--	--	--	--	--
				80	0.56	--	--	--	--	--	--
234A-1	Co-5 Ru	"	--	60	0.59	--	--	--	--	--	--
				80	0.32	0.64	--	--	--	--	--
238A-1	Ti-33 Ni	"	30	60	0.57	0.95	--	--	--	--	--
				80	0.36	0.63	--	--	--	--	--
198B-1	Bi-Tl	"	1.8	80	0.61	0.80	--	--	--	--	--
				90	0.56	0.77	--	--	--	--	--
204B-1	Sb-48 Ni	"	1.8	80	0.44	0.48	--	--	--	--	--
				90	0.41	0.66	--	--	--	--	--
205B-1	15.5 Fe-44 Sb-40.5 Co	"	1.8	80	0.49	0.60	--	--	--	--	--
				90	0.47	0.87	--	--	--	--	--
206B-1	7.5 Fe-54 Sb-38.5 Ni	"	1.9	80	0.44	0.49	--	--	--	--	--
				90	0.46	0.89	--	--	--	--	--
207B-1	Co-43 Sb	"	1.9	80	0.48	0.62	--	--	--	--	--
				90	0.53	0.78	--	--	--	--	--
203B-1	38 Au-23 Ag-39 Cu	"	1.9	80	0.67	--	--	--	--	--	--
				90	0.60	0.85	--	--	--	--	--
238B-1	Ti-33 Ni	"	12.1	80	0.59	0.89	--	--	--	--	--
				90	0.43	0.79	--	--	--	--	--
243A-1	20% $MnNi_3$ on C	"	4.0	80	0.58	0.84	--	--	--	--	--
				90	0.46	0.81	--	--	--	--	--
200B-1	Au-35 Ni	"	1.7	80	0.58	0.90	--	--	--	--	--
				90	0.54	0.82	--	--	--	--	--

APPENDIX C-9 (CONT'D)

CATALYST SCREENING STUDIES ON METHANOL

Electrode Number	Catalyst	Electrolyte	Catalyst Density, mg/cm^2	Temp, °C	Polarization from Methanol Theory at Indicated ma/cm^2, volts						
					0	1	5	10	20	50	100
230C-1	NiWS	1 M K_2HPO_4 + 1 M K_3PO_4	15.3	80	0.59	0.68	0.87	--	--	--	--
				90	0.48	0.63	0.91	--	--	--	--
191B-1	$AuCu_3$	"	1.9	80	0.77	0.93	--	--	--	--	--
				90	0.66	0.86	--	--	--	--	--
234A-2	Co-5 Ru	"	12.3	80	0.46	0.77	--	--	--	--	--
				90	0.35	0.60	--	--	--	--	--
		6.9 M KOH		80	0.28	0.38	0.51	0.89	--	--	--
				90	0.23	0.32	0.44	0.46	0.92	--	--
		1 M K_2HPO_4 + 1 M K_3PO_4		80	0.48	0.86	--	--	--	--	--
				90	0.30	0.59	--	--	--	--	--
226A-3	30% $CoMoO_4$ on C	6.9 M KOH	5.8	80	0.50	0.54	0.81	1.03	--	--	--
				90	0.37	0.46	0.85	1.03	--	--	--
226A-4	"	1 M K_2HPO_4 + 1 M K_3PO_4	6.1	80	0.92	--	--	--	--	--	--
				90	0.59	--	--	--	--	--	--
226A-5	"	6.9 M KOH	7.6	80	0.52	0.56	0.80	1.0	--	--	--
				90	0.42	0.51	0.92	--	--	--	--
		1 M K_2HPO_4 + 1 M K_3PO_4		80	0.63	0.87	--	--	--	--	--
				90	0.51	0.76	--	--	--	--	--
238A-2	Ti-33 Ni	"	46.9	80	0.48	0.75	--	--	--	--	--
				90	0.32	0.63	--	--	--	--	--
238A-3	Ti-33 Ni	6.9 M KOH	52.9	80	0.26	0.36	0.47	0.55	0.77	--	--
				90	0.24	0.36	0.47	0.54	0.66	--	--
233A-3	Co	1 M K_2HPO_4 + 1 M K_3PO_4	11.2	80	0.53	--	--	--	--	--	--
				90	0.40	0.81	--	--	--	--	--
233A-2	Co	6.9 M KOH	4.4	80	0.29	0.40	0.60	--	--	--	--
				90	0.29	0.43	0.57	0.59	0.67	--	--
238C-1	Ti-33 Ni	"	18.8	80	0.29	0.38	0.51	0.60	--	--	--
				90	0.17	0.31	0.45	0.52	0.63	--	--
238D-1	Ti-33 Ni	"	31.7	80	0.24	0.32	0.42	0.47	0.54	0.75	--
				90	0.19	0.29	0.36	0.42	0.48	0.61	--
		1 M K_2HPO_4 + 1 M K_3PO_4		80	0.47	0.61	0.94	--	--	--	--
				90	0.33	0.55	0.81	--	--	--	--
238X-1	Ti-33 Ni	6.9 M KOH	38.9	80	0.15	0.31	0.43	0.49	0.81	--	--
				90	0.11	0.27	0.38	0.44	0.51	0.65	--
		1 M K_2HPO_4 + 1 M K_3PO_4		80	0.53	0.69	1.0	--	--	--	--
				90	0.43	0.63	0.87	--	--	--	--
244A-1	Ti-33 Ni	6.9 M KOH	25.1	80	0.15	0.30	0.43	0.49	0.56	--	--
				90	0.01	0.23	0.34	0.40	0.46	0.56	0.70
		1 M K_2HPO_4 + 1 M K_3PO_4		80	0.32	0.55	0.81	--	--	--	--
				90	0.22	0.50	0.72	0.91	--	--	--

APPENDIX C-9 (CONT'D)

CATALYST SCREENING STUDIES ON METHANOL

Electrode Number	Catalyst	Electrolyte	Catalyst Density, mg/cm^2	Temp, °C	Polarization from Methanol Theory at Indicated ma/cm^2, volts 0	1	5	10	20	50	100
244A-1	Ti-33 Ni	1 M $KHCO_3$ + 1 M K_2CO_3	25.1	80	0.37	0.57	--	--	--	--	--
				90	0.07	0.37	0.56	0.69	--	--	--
244B-1	Ti-33 Ni	6.9 M KOH	--	80	0.22	0.35	0.45	0.51	0.58	--	--
				90	0.14	0.30	0.43	0.50	0.59	--	--
--	Pt flag	6.9 M KOH	--	80	0.18	0.39	0.53	0.58	--	--	--
		After activation(1)	--	80	0.06	0.34	0.49	0.55	0.62	--	--
				90	0.10	0.33	0.52	0.58	0.63	--	--
		1 M $KHCO_3$ + 1 M K_2CO_3	--	80	0.46	0.68	--	--	--	--	--
		After activation	--	80	0.27	0.48	0.72	--	--	--	--
				90	0.14	0.46	0.68	--	--	--	--
		1 M K_2HPO_4 + 1 M K_3PO_4	--	80	0.29	0.49	--	--	--	--	--
		After activation	--	80	0.07	0.39	0.72	--	--	--	--
				90	0.10	0.46	0.75	--	--	--	--
	Au plated Pt flag	6.9 M KOH	--	80	0.37	0.59	0.85	0.92	--	--	--
		After activation	--	80	0.23	0.38	0.51	0.59	0.81	--	--
		1 M K_2HPO_4 + 1 M K_3PO_4	--	80	0.67	--	--	--	--	--	--
		After activation	--	80	0.50	0.72	--	--	--	--	--
		1 M $KHCO_3$ + 1 M K_2CO_3	--	90	0.53	--	--	--	--	--	--
187F	Pt button	1 M K_2HPO_4 + 1 M K_3PO_4	--	80	0.07	0.75	--	--	--	--	--
				90	0.20	--	--	--	--	--	--
187G	Au button	6.9 M KOH	--	80	0.11	0.50	0.68	--	--	--	--
				90	0.05	0.53	0.69	--	--	--	--
		1 M K_2HPO_4 + 1 M K_3PO_4	--	80	0.17	0.47	0.60	0.79	--	--	--
				90	0.15	0.45	0.65	0.80	0.94	--	--
		6.9 M KOH	--	80	0.07	0.24	0.35	0.41	0.49	0.65	--
				90	0.06	0.25	0.40	0.48	0.60	0.68	--
		3.7 M H_2SO_4	--	80	0.36	0.49	0.57	0.63	0.72	1.00	--
				90	0.38	0.52	0.63	0.72	0.87	--	--
187GA-1	Au powder	1 M K_2HPO_4 + 1 M K_3PO_4	--	80	0.31	0.70	--	--	--	--	--
		6.9 M KOH	--	80	0.27	0.43	0.55	0.60	0.68	--	--
				90	0.20	0.44	0.58	0.62	0.69	1.02	--

(1) Activation consisted of cathodizing at 400 ma for three minutes, anodizing at 400 ma for three minutes, cathodizing at 400 ma for three minutes.

APPENDIX C-9 (CONT'D)

CATALYST SCREENING STUDIES ON METHANOL

Electrode Number	Catalyst	Electrolyte	Catalyst Density, mg/cm^2	Temp, °C	Polarization from Methaool Theory at Indicated ma/cm^2, volts 0	1	5	10	20	50	100
245B	Au foil	6.9 M KOH	--	80	0.21	0.42	0.73	0.91	1.00	--	--
		1 M K_2HPO_4 + 1 M K_3PO_4	--	80	0.50	--	--	--	--	--	--
				90	0.48	--	--	--	--	--	--
245 A	Au button	1 M K_2HPO_4 + 1 M K_3PO_4	--	80	0.38	--	--	--	--	--	--
		After activation	--	80	0.08	0.93	--	--	--	--	--
		6.9 M KOH	--	80	0.44	1.01	--	--	--	--	--
		After activation	--	80	0.25	0.56	0.91	1.00	--	--	--
				90	0.24	0.62	0.93	--	--	--	--
187GB-1	Au powder <325 mesh	1 M K_2HPO_4 + 1 M K_3PO_4	20.5	80	0.47	0.69	--	--	--	--	--
				90	0.24	0.62	0.93	--	--	--	--
		6.9 M KOH	--	80	0.15	0.44	0.59	0.66	0.73	0.85	0.94
246A-1	Pt powder <325 mesh	1 M K_2HPO_4 + 1 M K_3PO_4	16.3	80	0.20	0.31	0.41	0.47	0.56	0.71	0.92
				90	0.08	0.27	0.39	0.46	0.55	0.71	0.92
		6.9 M KOH		80	0.07	0.18	0.26	0.30	0.34	0.42	0.50
				90	0.09	0.19	0.26	0.30	0.34	0.42	0.51
187GB-1	Au powder <325 mesh	1 M K_2CO_3 + 1 M $KHCO_3$	20.5	80	0.32	0.57	--	--	--	--	--
				90	0.25	0.61	--	--	--	--	--
		30% H_2SO_4	--	80	0.22	0.67	--	--	--	--	--
				90	0.42	0.68	--	--	--	--	--
	Au flag	1 M K_2HPO_4 + 1 M K_3PO_4	--	80	0.78	--	--	--	--	--	--
				90	0.58	--	--	--	--	--	--
		6.9 M KOH		80	0.67	0.91	--	--	--	--	--
				90	0.63	1.04	--	--	--	--	--
239A-1	Ti-33 Co	1 M K_2HPO_4 + 1 M K_3PO_4	25.7	80	0.45	--	--	--	--	--	--
				90	0.31	0.90	--	--	--	--	--
		6.9 M KOH	--	80	0.27	0.49	0.71	0.90	1.05	--	--
				90	0.28	0.45	0.60	0.74	0.88	--	--
240A-1	Ti-17.6 Mo	1 M K_2HPO_4 + 1 M K_3PO_4	--	80	0.29	0.51	--	--	--	--	--
				90	0.07	0.54	--	--	--	--	--
		6.9 M KOH	--	80	0.46	0.55	0.94	1.03	--	--	--
				90	0.38	0.55	0.78	0.86	--	--	--
236A-1	Ti-17.6 Mo	1 M K_2HPO_4 + 1 M K_3PO_4	3.2	80	0.43	--	--	--	--	--	--
				90	0.10	0.91	--	--	--	--	--
		6.9 M KOH	--	80	0.29	0.48	0.66	--	--	--	--
				90	0.01	0.33	0.56	0.67	--	--	--
237A-1	Cr-51 Fe	1 M K_2HPO_4 + 1 M K_3PO_4	17.1	80	0.48	0.83	--	--	--	--	--
				90	0.29	0.74	--	--	--	--	--
		6.9 M KOH	--	80	0.29	0.39	0.52	0.61	0.73	--	--
				90	0.27	0.35	0.48	0.57	0.65	--	--

APPENDIX C-9 (CONT'D)

CATALYST SCREENING STUDIES ON METHANOL

Electrode Number	Catalyst	Electrolyte	Catalyst Density, mg/cm^2	Temp, °C	Polarization from Methanol Theory at Indicated ma/cm^2, volts						
					0	1	5	10	20	50	100
244A-2	Ti-33 Ni	1 M K_2HPO_4 + 1 M K_3PO_4 6.9 M KOH	31.2	80	0.55	--	--	--	--	--	--
				90	0.25	0.85	--	--	--	--	--
			--	80	0.43	0.52	0.65	1.01	--	--	--
				90	0.28	0.45	0.57	0.73	0.99	--	--
238C-2	Ti-33 Ni	6.9 M KOH	3.2	80	0.25	0.38	0.50	0.58	0.85	--	--
				90	0.14	0.28	0.39	0.46	0.52	0.65	0.87
237A-2	Cr-51 Fe	6.9 M KOH	42.8	80	0.50	0.60	0.80	0.95	--	--	--
				90	0.32	0.46	0.76	0.91	--	--	--
241A-2	Ti-17.6 Mo-1.0 Pd	6.9 M KOH	19.5	80	0.43	0.71	--	--	--	--	--
				90	0.23	0.47	0.74	0.87	1.01	--	--
242A-1	Ni-29.4 Mn	1 M K_2HPO_4 + 1 M K_3PO_4 6.9 M KOH	7.7	80	0.45	--	--	--	--	--	--
				90	0.26	0.67	--	--	--	--	--
			--	90	0.23	0.49	0.76	0.90	0.94	1.0	--
248A-1	Ti-25 Au	1 M K_2HPO_4 + 1 M K_3PO_4 6.9 M KOH	27.8	80	0.39	--	--	--	--	--	--
				90	0.25	0.89	--	--	--	--	--
			--	90	0.29	0.48	0.62	0.72	0.83	1.02	--
247A-1	Ti-4.4 Au	1 M K_2HPO_4 + 1 M K_3PO_4 6.9 M KOH	32.1	80	0.56	0.94	--	--	--	--	--
			--	90	0.32	0.50	0.75	0.89	1.0	--	--
249A-1	Ti-13.9 Cr	1 M K_2HPO_4 + 1 M K_3PO_4 6.9 M KOH	27.7	80	0.61	0.93	--	--	--	--	--
				90	0.26	0.91	--	--	--	--	--
			1st run	80	0.39	0.54	0.71	0.79	0.84	0.91	0.99
			2nd run	80	0.51	0.66	0.88	0.98	--	--	--
				90	0.32	0.55	0.76	0.87	0.96	--	--
250A-1	Au-6.4 Ni	1 M K_2HPO_4 + 1 M K_3PO_4 6.9 M KOH	24.5	80	0.74	--	--	--	--	--	--
				80	0.53	0.79	0.89	0.95	--	--	--
			--	90	0.25	0.73	0.86	0.93	--	--	--
252A-1	Au-6.1 Cu	1 M K_2HPO_4 + 1 M K_3PO_4 6.9 M KOH	22.1	80	0.69	--	--	--	--	--	--
				90	0.31	--	--	--	--	--	--
			--	90	0.35	0.68	0.81	0.89	1.0	--	--
253A-1	Au-6.3 Zr	6.9 M KOH	22.5	80	0.52	0.71	0.83	0.91	0.99	--	--
				90	0.31	0.58	0.70	0.77	0.84	0.97	--
		1 M K_2HPO_4 + 1 M K_3PO_4	--	80	0.66	--	--	--	--	--	--
				90	0.39	--	--	--	--	--	--
255A-1	Au-0.1 Ir	1 M K_2HPO_4 + 1 M K_3PO_4 6.9 M KOH	31.2	80	0.69	--	--	--	--	--	--
				90	0.66	--	--	--	--	--	--
			--	80	0.61	0.90	0.99	--	--	--	--
				90	0.39	0.74	0.89	0.96	--	--	--
256A-1	Au-0.2 Ag	1 M K_3PO_4 + 1 M K_3PO_4 6.9 M KOH	24.1	80	0.72	--	--	--	--	--	--
				90	0.66	--	--	--	--	--	--
			--	80	0.62	0.89	1.0	--	--	--	--
				90	0.45	0.77	0.91	0.97	--	--	--

APPENDIX C-9 (CONT'D)

CATALYST SCREENING STUDIES ON METHANOL

Electrode Number	Catalyst	Electrolyte	Catalyst Density, mg/cm²	Temp, °C	Polarization from Methanol Theory at Indicated ma/cm², volts						
					0	1	5	10	20	50	100
187G8-2	Au	1 M K_3PO_4 + 1 M K_2HPO_4 6.9 M KOH	37.6	80	0.60	--	--	--	--	--	--
			--	90	0.50	--	--	--	--	--	--
254A-1	Au-46 Zr	1 M K_2HPO_4 + 1 M K_3PO_4 6.9 M KOH	35.8	80	0.41	0.60	0.75	0.81	0.89	0.98	--
			--	90	0.25	0.50	0.60	0.65	0.73	0.83	0.92
257A-1	Zr-32.9 Ni	1 M K_2HPO_4 + 1 M K_3PO_4 6.9 M KOH	20.2	80	0.20	0.48	0.65	--	--	--	--
			--	90	0.21	0.44	0.69	--	--	--	--
251A-1	Ti-33.5 Cu	1 M K_2HPO_4 + 1 M K_3PO_4 6.9 M KOH	23.0	80	0.34	0.50	0.84	1.02	--	--	--
			--	90	0.38	0.82	0.92	0.97	--	--	--
258A-1	Zr-33.5 Cu	1 M K_2HPO_4 + 1 M K_3PO_4 6.9 M KOH	12.9	80	0.69	--	--	--	--	--	--
			--	90	0.55	--	--	--	--	--	--
260A-1	Zr-7.2 Mo	1 M K_2HPO_4 + 1 M K_3PO_4 6.9 M KOH	19.4	80	0.54	0.82	0.99	--	--	--	--
			--	90	0.36	0.69	0.88	0.96	--	--	--
244A-3	Ti-33 Ni	1 M K_2HPO_4 + 1 M K_3PO_4 6.9 M KOH	33.1	80	0.56	--	--	--	--	--	--
			--	90	0.28	0.89	--	--	--	--	--
249A-2	Ti-13.9 Cr	6.9 M KOH	22.4	80	0.59	0.87	1.02	--	--	--	--
				90	0.16	0.78	0.93	1.0	--	--	--
245A-1	Au	1 M K_2HPO_4 + 1 M K_3PO_4 6.9 M KOH	26.2	80	0.78	--	--	--	--	--	--
			--	90	0.60	--	--	--	--	--	--
261A-1	Au-25 Zr	1 M K_2HPO_4 + 1 M K_3PO_4 6.9 M KOH	28.5	90	0.60	0.83	0.96	--	--	--	--
			--	80	0.57	--	--	--	--	--	--
				90	0.58	--	--	--	--	--	--
				80	0.61	0.94	--	--	--	--	--
				90	0.43	0.84	0.87	1.03	--	--	--
				80	0.59	--	--	--	--	--	--
				90	0.26	--	--	--	--	--	--
				80	0.33	0.64	0.87	--	--	--	--
				90	0.30	0.64	0.91	0.99	--	--	--
				80	0.41	0.87	--	--	--	--	--
				90	0.33	0.78	0.93	0.99	--	--	--
				80	0.71	--	--	--	--	--	--
				90	0.68	--	--	--	--	--	--
				80	0.57	0.83	0.99	--	--	--	--
				90	0.32	0.70	0.91	--	--	--	--
				80	0.72	--	--	--	--	--	--
				90	0.50	--	--	--	--	--	--
				80	0.46	0.64	0.76	0.84	0.93	--	--
				90	0.37	0.58	0.68	0.74	0.81	0.92	--
				2nd run 90	0.29	0.51	0.61	0.67	0.75	0.89	1.01

APPENDIX C-9 (CONT'D)

CATALYST SCREENING STUDIES ON METHANOL

Electrode Number	Catalyst	Electrolyte	Catalyst Density, mg/cm^2	Temp, °C	Polarization from Methanol Theory at Indicated ma/cm^2, volts 0	1	5	10	20	50	100
262A-1	Co-33.7 Zr	1 M K_2HPO_4 + 1 M K_3PO_4 6.9 M KOH	26.2	80	0.69	--	--	--	--	--	--
				90	0.56	--	--	--	--	--	--
			--	80	0.54	0.86	--	--	--	--	--
				90	0.42	0.74	0.98	--	--	--	--
264A-1	Co-21 W	1 M K_2HPO_4 + 1 M K_3PO_4 6.9 M KOH	14.2	80	0.71	--	--	--	--	--	--
				90	0.62	--	--	--	--	--	--
			--	80	0.17	0.84	--	--	--	--	--
				90	(0.05)	0.76	(- [illegible]ion)	--	--	--	--
265A-1	Co-33 Ta	1 M K_2HPO_4 + 1 M K_3PO_4 6.9 M KOH	21.9	80	0.19	--	--	--	--	--	--
				90	0.12	--	--	--	--	--	--
			--	80	0.59	0.87	0.98	--	--	--	--
				90	0.47	0.76	0.92	0.99	--	--	--
266A-1	Co-13.5 Ta	1 M K_2HPO_4 + 1 M K_3PO_4 6.9 M KOH	20.6	80	0.57	--	--	--	--	--	--
				90	0.45	--	--	--	--	--	--
			--	80	0.58	0.84	0.98	--	--	--	--
				90	0.34	0.71	0.90	--	--	--	--
263A-1	Zr-28 Cr	1 M K_2HPO_4 + 1 M K_3PO_4 6.9 M KOH	27.5	80	0.74	--	--	--	--	--	--
				90	0.63	--	--	--	--	--	--
			--	80	0.66	0.92	--	--	--	--	--
				90	0.50	0.80	0.97	--	--	--	--
267A-1	Au-25 Zr	1 M K_2HPO_4 + 1 M K_3PO_4 6.9 M KOH	24.2	80	0.63	--	--	--	--	--	--
				90	0.49	--	--	--	--	--	--
			--	80	0.50	0.66	0.77	0.84	0.91	--	--
				90	0.39	0.63	0.77	0.84	0.91	--	--
268A-1	Ti-13.9 Cr	1 M K_2HPO_4 + 1 M K_3PO_4 6.9 M KOH	22.2	80	0.61	--	--	--	--	--	--
				90	0.56	--	--	--	--	--	--
			--	80	0.56	0.94	--	--	--	--	--
				90	0.35	0.71	0.89	0.97	--	--	--

APPENDIX C-10

SLURRY CATALYST EXPERIMENTS

Carbon[1] Content, mg	Teflon Content, mg	FC-95, wt %	Electrolyte	Temp, °C	Polarization from Decane Theory at Indicated ma, volts				Remarks
					1	2	5	10	
100	--	--	3.7 M H_2SO_4	106	0.47	--	--	--	
100	--	0.02	3.7 M H_2SO_4	106	0.46	--	--	--	
100	--	0.04	3.7 M H_2SO_4	106	0.42	0.54	0.78	--	
100	--	0.06	3.7 M H_2SO_4	106	--	--	0.73	--	
200	--	0.06	3.7 M H_2SO_4	106	0.52	--	0.53-0.70	--	Oscillating at 5 ma.
100	50	--	3.7 M H_2SO_4	106	0.56	--	0.68	--	
100	50	0.02	3.7 M H_2SO_4	106	0.46	--	0.72	0.85	
100	50	0.02	3.7 M H_2SO_4	106	0.50	0.56	0.70	0.78	Increased particle density by factor of 2.
100	50	--	14.7 M H_3PO_4	150	0.49	--	0.60	0.74	
16.7	8.3	--	3.7 M H_2SO_4	106	--	--	--	--	Pressed onto gauze at 1000 psi. Could not maintain 0.5 ma.
16.7	8.3	--	3.7 M H_2SO_4	106	--	--	--	--	Pressed onto gauze by hand. Could not maintain 1 ma.
16.7	8.3	--	3.7 M H_2SO_4	106	--	--	--	--	Pressed onto gauze at 50 psi. Could not maintain 1 ma.

(1) 6 wt % catalyst.

APPENDIX C-11

ANALYSIS OF SLURRY ELECTRODES

A preliminary analysis of the operation of slurry type electrodes has been carried out to provide a possible means of treating the experimental data and optimizing the system. The results must be considered tentative due to the qualifications and assumptions given below. Nevertheless a number of interesting relationships emerge.

The analysis assumes that a catalyst particle leaves the electrode at the potential of the electrode, and floats about in solution reacting with the fuel, following the Tafel equation. However, the current serves only to charge the double layer capacitance of the particle, thereby changing its voltage. When the particle again collides with the electrode, it transfers its accumulated charge and returns to the potential of the electrode, ready to repeat the cycle. It is assumed that collisions between the particles are of negligible importance. This may not be far from the truth, since it is probable that only near the electrodes are the velocity gradients in the fluid sufficiently abrupt to cause the particles to move to the edge of their watery sheaths and make solid-solid contact. Experimental evidence for this is that the current removed from a slurry electrode at a given polarization is directly proportional to the solids concentration as predicted by the analysis, whereas particle-particle interaction might be expected to cause second order non-linear effects. The apparent electronic conductivity of stirred suspensions does not contradict this hypothesis, since particles leaving one electrode and striking another at a different potential can give rise to electronic conduction. In fact the observed conductivity can be shown to be related to some of the key parameters of electrode performance.

These key parameters are the number of particles, the capacity of each particle, the "exchange current" of each particle, the Tafel slope, and the average time a particle spends in suspension between electrode contacts. The average suspension time and the total capacitance of the slurry should be obtainable from analysis of potentiostatic charging curves. The exchange current and Tafel slope should be determinable from performance run on static or dynamic electrodes under certain limiting conditions.

The details of the analysis are given below. The results, in terms of dependencies on various parameters, can be summarized as follows:

- The current is directly proportional to the slurry concentration.
- For short suspension times the current is exponentially related to the potential but at long suspension times the current is linearly related to the potential.
- The current is relatively insensitive to the system volume at long suspension times.
- The catalyst utilization in terms of the ratio of the current to that of an ideal static electrode improves as the suspension time becomes shorter, approaching unity at zero suspension time (static electrode).

The reason for the less than ideal catalyst utilization is that the time the catalyst particle spends at or near its open circuit potential is essentially time wasted, since little or no anodic reaction of fuel is occurring. Of course, actual static electrodes may also be less efficient than the ideal static electrode envisioned here, especially in the case of immiscible fuels. The relative catalyst efficiency of the two systems will depend on how closely each one can be made to approach the ideal. Other debits of the slurry system such as the energy and space requirements have not been considered in this analysis.

Steady State Performance of Slurry Electrode

At the surface of a particle a reaction occurs, with the current related to the voltage according to the Tafel equation:

$$i = i_o e^{\eta/s} \qquad [1]$$

i = current per particle (amperes)

i_o = exchange current per particle (amperes)

η = polarization (volts)

s = Tafel slope on natural log scale (volts)

The current generated moves the potential toward open circuit:

$$\frac{d\eta}{dt} = -\frac{i}{c} \qquad [2]$$

t = time in seconds

c = capacity of particle

Combining [1] and [2] and integrating one obtains the potential of the particle as a function of time:

$$\eta = \eta_e - s \ln \left(1 + \frac{i_o t}{sc} e^{\eta_e/s}\right) \qquad [3]$$

η_e = polarization of the electrode

According to [3], the potential of the particle versus time is as shown in Figure C-1.

Figure C-1

Particle Potential Versus Time

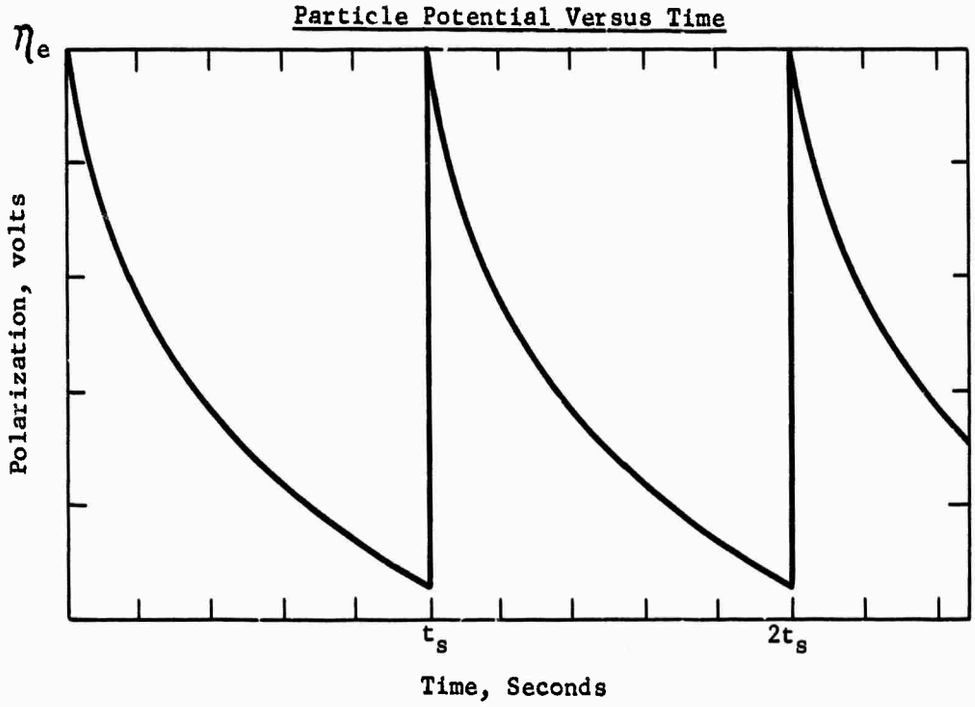

When the particle strikes the electrode it discharges enough coulombs to bring it to the potential of the electrode:

$$Q = (\eta - \eta_e)c \qquad [4]$$

Q = no. coulombs transferred per strike

The current depends on the number of particles striking the electrode per second, p:

$$I = (\eta - \eta_e)cp = (\eta - \eta_e)\frac{cN}{t_s} \qquad [5]$$

N = no. of particles in system

t_s = average time a particle stays in suspension between strikes

Inserting [3] in [5] gives

$$I = \frac{scN}{t_s} \ln \left(1 + \frac{i_o t_s}{sc} e^{\eta e/s}\right) \qquad [6]$$

This equation shows that the current density is directly proportional to the number of particles in the system. It also states that at small values of t_s the current follows the Tafel equation:

$$I_{(t_s \text{ small})} = Ni_o e^{\eta e/s} = I_e \qquad [7]$$

I_e is the current that would be obtained if the particles were always at η_e, the electrode potential. It can therefore be considered the current of an ideal static electrode, since approach of t_s to zero means the particle never leaves the electrode.

At large values of t_s the current is linearly related to the voltage

$$I_{(t_s \text{ large})} = \frac{scN}{t_s} \ln \frac{i_o t_s}{sc} + \eta_e \frac{cN}{t_s} \qquad [8]$$

At intermediate values of t_s behavior between linear and exponential should be obtained.

The catalyst efficiency can be obtained by taking the ratio of I/I_e using equations [7] and [6]

$$I/I_e = (1/K) \ln (1 + K) \qquad [9]$$

where $k = \frac{I_e t_s}{scN}$

A plot of catalyst efficiency versus K is drawn in Figure $\bar{C}$- 2.

Figure $\bar{C}$-2

Slurry Catalyst Efficiency

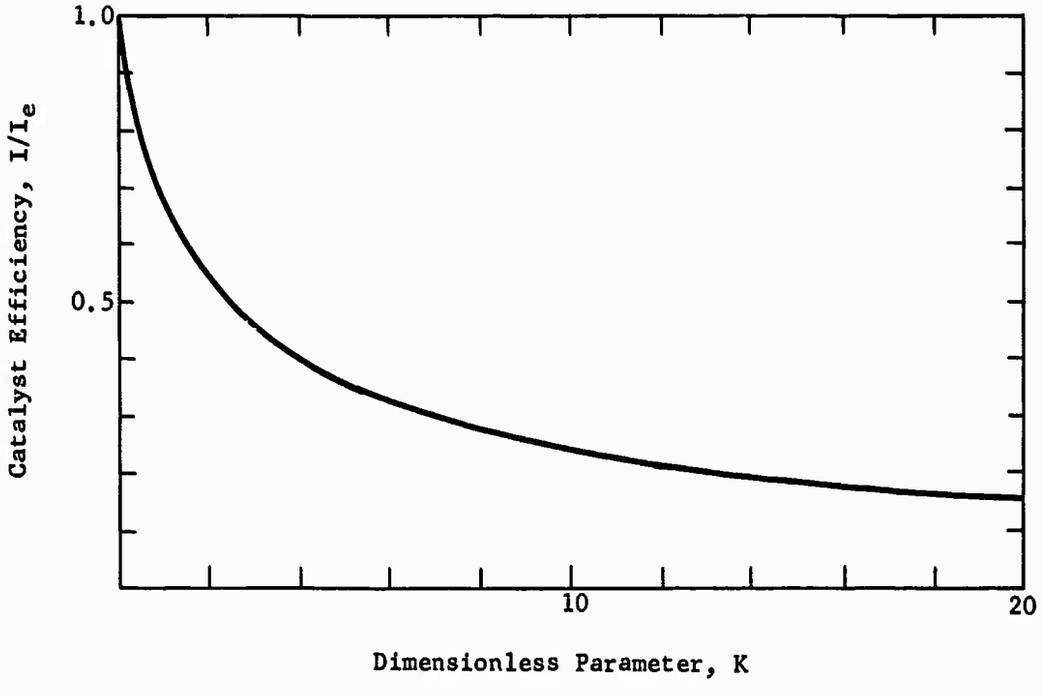

It will be noted from the above figure that I/I_e is never greater than one. It reaches one only when K = 0, which corresponds to a static electrode.

To find the effect of a volume change, v, at constant catalyst density, one notes that N is proportional to V and that t_s is also proportional to V in a well-stirred reactor. Thus equation [9] becomes

$$I = \frac{I^\circ_e}{K_o} \ln \left(1 + \frac{V}{V_o} K_o\right) \qquad [10]$$

I°_e is the ideal current of the standard volume system. Thus V is present only in the logarithmic term so that I is not very sensitive to it.

Determination of Parameters from
Potentiostatic Charging Curve

If the electrode is potentiostatted at a given voltage and then step changed by an amount ΔV, a charging current, I_p, will be observed:

$$I_p = \frac{N_u \, c \Delta V}{t_s} \qquad [11]$$

N_u is the number of particles whose voltage is unchanged at any time.

Initially all the particle voltages are unchanged and

$$I_{p(initial)} = \frac{N \, c \Delta V}{t_s} \qquad [12]$$

Since Nc, the total capacitance of the system, can be found by integrating the total charging curve, t_s can be determined.

As the charging process proceeds N_u will become appreciably less than N and the shape of the curve will depend on the mixing parameters. If one assumes perfect mixing then the number of unchanged particles striking the electrode is simply proportional to the number of such particles in suspension:

$$\frac{d N_u}{dt} = -\frac{N_u}{t_s} \qquad [13]$$

This expression integrates to

$$N_u = Ne^{-t/t_s} \qquad [14]$$

Substituting this into [11] gives the relation between charging current and time:

$$I_p = \frac{\Delta V \cdot Nc}{t_s} e^{-t/t_s} \qquad [15]$$

Thus a plot of ln I versus time should give a straight line of reciprocal slope t_s, which should verify the value of t_s from [12] or else give a measure of the mixing efficiency. (This type of system, incidentally should be well suited for an engineering study of mixing efficiency.)

Apparent Electronic Conductivity of the Suspension

If two wires at slightly different potentials are inserted into the slurry, current will be passed between them due to the bombardment of each electrode by particles which had previously collided with the other electrode. If neither electrode interferes with the flow pattern of the other the same t_s as before will apply. If the mixing is perfect then there is equal likelihood that the particles striking an electrode will have previously struck the same electrode or the other electrode. In this case the current will be

$$I = \frac{1}{2} \frac{Nc\Delta V}{t_s} \qquad [16]$$

Note how the apparent conductivity, $C = \frac{1}{2} \frac{Nc}{t_s}$ is related to the slope of the performance curve in the limiting case of equation [8]. The performance in that case appears to be "resistance limited".

In the absence of perfect mixing the factor of 1/2 in equation 16 would change. If the flow is laminar and the electrodes are in the same streamline, or if there is a pump-around system, the factor would approach one. If the electrodes are far apart or if there are eddy currents the factor could become lower than 1/2.

Qualifications of the Model

This model does not take into account the distribution of suspension times that must exist in a stirred reactor. However, in a slurry pump-around system the concept of a single suspension time may be more valid. The model also dodges the question of contact times. It can be calculated that the time constant for a one micron cube of Pt black discharging on one face is of the order of 10^{-11} seconds, which means that complete discharge will occur for any reasonable contact time. However, contact resistances could be large enough to prevent complete discharge during one strike. This would probably be accommodated by the model as a longer apparent suspension time.

Also neglected in the model are IR drops in the electrolyte, which are apparently large in these systems. These can probably be treated as a distributed current source obeying the relation:

$$\nabla^2 \eta_e^1 = \frac{R_e N i}{V}$$

R_e is the resistance of the electrolyte

V is the system volume

i is the current per particle, a function of η_e^1, the electrolyte potential.

The existence of these potential gradients in the solution causes the reaction at the surface of the particles to be faster in outlying regions of the electrolyte than near the electrode. The apparent i_o will probably be increased by this effect and the Tafel behavior may also be distorted. Taking into acoount the above complications, as well as the possibility of particle-particle collision in the suspension, would probably change the shape of all the relations without altering the basic variable dependencies.

APPENDIX D-1

DEPENDENCE OF ANODE POLARIZATION ON METHANOL CONCENTRATION

Stirred Half Cell Data
3.7 M H_2SO_4, 60°C, 6.4 cm^2 Electrodes
25 mg/cm^2 H_2 Reduced Ruthenium Modified P-type Catalyst

Methanol Molarity	Current, ma/cm^2	Anode Polarization from Methanol Theory, volts
.0312	2	.214
"	5	.244
"	10	.280
"	20	.335
"	50	>0.8
.0625	2	.210
"	5	.246
"	10	.275
"	20	.297
"	50	>0.8
.125	10	.270
"	20	.295
"	50	.336
"	100	.395
.25	10	.264
"	20	.285
"	50	.324
"	100	.351
.50	10	.262
"	20	.285
"	50	.315
"	100	.342
"	200	.365
1.0	10	.260
"	20	.280
"	50	.310
"	100	.335
"	200	.355
"	400	.380
"	5	.240
"	2	.210
"	1	.190

Methanol Molarity	Limiting Current, ma		
	No Stirring	Slow Stirring	Moderate Stirring
0	3	4	6
.0078	19	33	38
.0156	34	50	60
.0312	72	100	120
.0625	160	200	210
.125	610	610	650
.25	2250	2350	2400

APPENDIX D-2

EFFECT OF TEFLON SPRAY COAT ON METHANOL ELECTRODE PERFORMANCE

Electrode Identification(1)	Spray Coating(2)	Polarization from Methanol Theory at Indicated ma/cm^2, volts(3)						Ohmic Loss at 100 ma/cm^2, volts(4)
		0	1	5	10	50	100	
3372-40	Teflon 41-BX	0.04	0.09	0.21	0.24	0.28	0.32	0.020
3372-16	None	0.04	0.13	0.18	0.20	0.28	0.31	0.000 to 0.005

(1) Electrodes contain 25 mg/cm^2 of Ru-modified P-type catalyst pressed on 5.7 cm^2, 50 mesh Ta screen at 3000 psi.
(2) Teflon coating on driver-electrode side of anode.
(3) 60°C, 1 M CH_3OH in 3.7 M H_2SO_4 in anolyte chamber of glass half cell. 3.7 M H_2SO_4 in driver-electrode chamber.
(4) Measured with Kordesch-Marko bridge.

APPENDIX D-3

CATALYST ACTIVITY MAINTENANCE DURING STORAGE

1. Effect of Storage of Wet Catalyst Powder

Catalyst: Ru Modified P-type Catalyst, H_2 Reduced (Identification No. 2924-29P1)
Electrode Composition: 25 mg Catalyst/cm^2 on 50 Mesh Ta Screen, Pressed at 1000-2500 psi
Testing Conditions: 1 M CH_3OH in 3.7 M H_2SO_4 at 60°C.

Catalyst Stored in 1 M CH_3OH in H_2O								Catalyst Stored in 1 M CH_3OH in 3.7 M H_2SO_4[1]							
Electrode Identification	Cumulative Time Since Catalyst Preparation, Days	Polarization from Methanol Theory at Indicated ma/cm^2, volts						Electrode Identification	Cumulative Time Since Catalyst Preparation, Days	Polarization from Methanol Theory at Indicated ma/cm^2, volts					
		0	1	5	10	50	100			0	1	5	10	50	100
2924-34	0	0.03	0.14	0.21	0.23	0.30	0.31	2924-39	7	0.01	0.16	0.20	0.22	0.28	0.32
2924-36	1	0.04	0.18	0.24	0.26	0.32	0.35	2924-45	16	0.04	0.17	0.22	0.25	0.30	0.34
2924-39	7	0.01	0.16	0.20	0.22	0.28	0.31	3107-4	29	0.01	0.16	0.21	0.23	0.29	0.35
2924-45	16	0.06	0.17	0.22	0.25	0.32	0.36	3107-41	71	0.02	0.18	0.24	0.26	0.32	0.35
3107-4	30	0.01	0.16	0.21	0.24	0.30	0.34	3372-15	104	0.04	0.12	0.18	0.21	0.28	0.30
3107-41	70	0.40	0.17	0.23	0.26	0.32	0.37		160	0.11	0.20	0.24	0.26	0.32	0.34
3372-15	100	0.02	0.12	0.19	0.21	0.28	0.31								
	160	0.09	0.16	0.22	0.24	0.30	0.33								

(1) Catalyst placed in acid storage 4 days after preparation.

2. Effect of Storage of Methanol Anodes in 3.7 M Sulfuric Acid Containing Different Methanol Concentrations

Electrode Identification[1]	Methanol Concentration, M[2]	Storage Time, hours	Polarization from Methanol Theory at Indicated ma/cm^2, volts						Remarks
			0	1	5	10	50	100	
3372-30 (70)	0.00	1	0.01	0.15	0.19	0.22	0.28, 0.29	0.32	
		24	.05	.13	.19	.22	.28, .28	.32	
		72	.03	.13	.22	.24	.30, .30	.32	
		168	.03	.12	.22	.24	.30, .30	.33	
		336	.03	.12	.20	.22	.29, .30	.32	
		504	.02	.11	.19	.22	.29, .29	.32	
		744	.03	.13	.20	.23	.30, .30	.33	
3372-30 (71)	0.01	1	.05	.15	.21	.24	.30, .30	.33	
		24	.07	.15	.22	.24	.32, .33	.37	
		72	.06	.13	.22	.24	.32, .32	.35	About 20% catalyst lost off anode.
		168	.07	.15	.21	.24	.31, .32	.35	
		336	.10	.16	.23	.25	.34, .35	.40	
		504	.09	.17	.22	.26	.32, .32	.37	
		744	.05	.15	.21	.24	.30, .30	.34	
3372-30 (72)	0.10	1	.03	.13	.22	.24	.30, .31	.34	
		24	.08	.15	.22	.26	.32, .32	.36	
		72	.09	.17	.25	.28	.36, .36	.40	About 20% catalyst lost off anode.
		168	.09	.19	.26	.28	.36, .37	.41	
		336	.12	.17	[illegible]	.26	.33, .33	.38	
		384	.08	.17	.24	.26	.33, .33	.37	Test cell changed.
		552	.11	.17	.23	.26	.32, .32	.35	
		720	.11	.17	.24	.28	.35, .35	.40	
3372-30 (73)	1.0	1	.08	.13	.22	.25	.30, .32	.35	
		24	.08	.15	.21	.24	.32, .32	.36	
		72	.10	.17	.23	.26	.33, .33	.37	
		168	.11	.15	.23	.26	.33, .34	.37	
		336	.09	.13	.26	.29	.36, .36	.40	
		384	.08	.16	.26	.28	.36, .36	.40	Test cell changed.
		552	.10	.18	.25	.28	.35, .35	.40	
		720	.07	.18	.24	.28	.36, .36	.41	

(1) Ru-modified, P-type catalyst, 3372-16 H. Catalyst loading was 25 mg/cm^2 on 50 mesh Ta screen, pressed at 2500 psi on 5.7 cm^2 electrode area.
(2) Electrodes stored in indicated concentration solutions for specified time, removed and tested in glass half cell with 1 M CH_3OH in 3.7 M H_2SO_4 at 60°C. Electrodes were then removed, washed with 3.7 M H_2SO_4 and placed again in fresh storage solutions.

APPENDIX D-4

SUMMARY OF LIFE TESTING ON RUTHENIUM MODIFIED P-TYPE CATALYST

60°C
1 M Methanol
3.7 M Sulfuric Acid

Half Cell No.	Run No.	Current Density, ma/cm²	Starting Performance: Date	Starting Performance: Anode vs Theory, volts	Test Duration, hours	Life Performance: Before Activation, Anode vs Theory, volts	Life Performance: After Activation, Anode vs Theory, volts	Status 5/31/65	Comments
1	1*	44	7/2/64	0.35	6500	0.40	0.37	Terminated 4/1/65	
2	1*	48	7/2/64	0.35	8000	0.41	0.35	Running	
3	1*	48	7/2/64	0.35	8000	0.395	0.325	Running	
4	1*	46	7/2/64	0.35	5400	0.405	0.375	Terminated 4/23/65	
5	1*	46	7/1/64	0.35	6100	0.375	0.355	Terminated 3/16/65	
4	1a*	46	2/24/65	0.505	850	0.475	0.375	Terminated 4/1/65	Cell 4 Run 1 continued with acetone and propionaldehyde added.
5	1a*	46	3/17/65	0.375	1700	0.395	0.365	Running	Cell 5 Run 1 continued with distilled water instead of deionized.
1	2	44	4/14/65	0.26	1100	0.29	0.26	Running	
4	2	48	4/14/65	0.26	1100	0.30	0.25	Running	
III	1*	40	5/18/65	0.32	7500	0.33	--	Terminated 4/1/65	
IV	1*	40	5/15/64	0.35	7500	0.44	--	Terminated 4/1/65	Leaky calomel reference electrodes.
V	1*	40	6/26/64	0.36	6600	0.44	--	Terminated 4/1/65	Leaky calomel reference electrodes.

5 cm² electrodes on tantalum screens.

Total Cell No.	Run No.	Current Density, ma/cm²	Starting Performance: Date	Starting Performance: Cell Volts	Starting Performance: Anode Polarization, Volts vs Theory	Test Duration, Hours	Life Performance: Before Activation, Cell Volts	Life Performance: Before Activation, Anode vs Theory, volts	Life Performance: After Activation, Cell Volts	Life Performance: After Activation, Anode vs Theory, volts	Status 5/31/65	Comments
3	1	85	1/6/65	0.39	0.34	2300	0.29	0.45	--	--	Terminated	Cells accidentally driven during methanol starvation. (172 hours).
4	1	83	1/8/65	0.43	0.34	2800	0.25	0.45	--	--	Terminated	Cells accidentally driven during methanol starvation. (172 hours).
1	2	43	12/17/64	0.44	0.37	3800	0.33	0.42	0.39	0.34	Running	
2	2	46	12/17/64	0.43	0.29	3800	0.39	--	0.42	0.29	Running	
3	2	46	5/21/65	0.33	0.53	170	0.34	0.51	--	--	Running	New components. Storage test. Run 30 min. twice a week at room temp.
4	2	46	5/21/65	0.33	0.50	170	0.37	0.52	--	--	Running	New components. Storage test. Run 30 min. twice a week at room temp.

10 cm² anodes on platinum screens.
Permion 1010 Clad American Cyanamid AA-1 cathodes.
5 x Stoichiometric Air Rate.

* Reduced with potassium borohydride. All others reduced with hydrogen.

APPENDIX D-5

METHANOL CATALYST PERFORMANCE

H_2 Reduced Ru Modified P-type

Catalyst Identification	Electrode Identification[1]	Polarization from Methanol Theory at Indicated ma/cm^2, volts[2]						Remarks
		0	1	5	10	50	100	
3372-8A	3372-9	0.03	0.16	0.22	0.25	0.31	0.38	
3372-8B1	3372-9	.03	.16	.21	.24	.32	.35	
3372-8B2	3372-9	.04	.16	.21	.24	.30	.38	
3372-8C	3372-9	.04	.16	.21	.24	.30	.34	
3372-16A	3372-16	.01	.12	.19	.22	.29	.32	— Double KOH wash on remainder of samples
3372-16B1	"	.00	.12	.19	.22	.29	.34	
3372-16B2	"	.00	.14	.20	.23	.30	.34	
3372-16C	"	.04	.14	.20	.23	.30	.34	
3372-16D	"	.00	.15	.21	.24	.30	.34	
3372-16E	"	.03	.18	.24	.27	.32	.35	
3372-16F	"	.04	--	.18	.22	.28	.32	
3372-16G	"	.05	.15	.20	.23	.30	.34	
3372-16H	"	.05	.09	.18	.22	.29	.32	
3372-16I	"	--	.14	.18	.21	.27	.30	
3372-34 (A)	3372-34	.02	.11	.18	.20	.27	.30	
3372-34 (B)	"	.05	.12	.16	.19	.26	.29	
3372-34 (C)	"	.02	.10	.18	.20	.27	.30	
Composite V[3]	3372-16	.04	.13	.18	.20	.28	.31	
Composite VI[4]	3372-34	.04	.11	.17	.19	.26	.29	

(1) Electrodes contain about 25 mg/cm^2 catalyst on 5.7 cm^2 area, wet-pressed at 2500 psi on 50 mesh Ta screens.
(2) Testing conditions: 60°C, 1 M CH_3OH in 3.7 M H_2SO_4.
(3) Composite V: 3372-16A thru 3372-16G.
(4) Composite VI: 3372-16M, -16I, -34(1), -34(2), -34(3).

APPENDIX D-6

STATISTICAL EVALUATION OF METHANOL CATALYST ACTIVITY

A statistical evaluation was made of the activity differences between the potassium borohydride and recent samples of hydrogen reduced forms of ruthenium modified P-type methanol catalyst. Performance data were obtained from electrodes containing about 25 mg catalyst/cm^2, tested in 1 M methanol in 3.7 M sulfuric acid at 60°C. The data for each catalyst represent a sample from a population whose variance is caused by variations in catalyst preparation procedure per se and also variations in electrode fabrication and testing procedures. The individual data points are listed in Appendix D-5 of this report and in reference (6).

Table D-1

Data for Statistical Evaluation of Methanol Catalyst Activity

Catalyst Reduction Agent	Current Density, ma/cm^2	Number of Data Points	Mean Polarization from Methanol Theory, volts	Standard Error (± 1 sigma) volts(1)
KBH_4	50	19	0.346	0.011
	100	19	0.381	0.020
H_2	50	12(2)	0.288	0.014
	100	12	0.322	0.020

(1) Calculated from standard error = $\sqrt{\frac{\sum(x-\bar{x})^2}{N-1}}$, where x = polarization, N = number of data points.

(2) Data for double KOH-washed catalysts.

a. Significance of Differences between Variances (S^2)

Current Density ma/cm^2	KBH_4 Reduced Catalyst Variance(S^2)	$\emptyset$(1)	H_2 Reduced Catalyst Variance(S^2)	$\emptyset$	Variance Ratio, F
50	0.00013	18	0.00019	11	1.46(2)
100	0.00039	18	0.00040	11	1.03(2)

(1) Degrees of freedom, $\emptyset$ = N-1.

(2) Not significant at 90% confidence level.

b. Significance of Differences between Means

The above analysis shows that the variances for the two catalyst preparations are not significantly different. Therefore, one may use the conventional "t" test to compare the differences between means.

Current Density, ma/cm^2	Student's "t" Statistic
50	13.3(1)
100	8.0(1)

(1) Significantly different at greater than 99% confidence level.

c. Conclusions

The procedures used to prepare either form of the catalyst are under essentially the same degree of control, hence their variances are not significantly different. However, the mean performance of the H_2 reduced form of Ru modified P-type catalyst is clearly more active than the KBH_4 reduced form.

APPENDIX D-7

PERFORMANCE OF DILUTED CATALYST

Catalyst: Ruthenium-Modified P-Type Hydrogen Reduced
Test Conditions: 3-7 M Sulfuric Acid, 1 M Methanol, 60°C
Electrodes: 4 cm^2 Flag Type

Electrode Identification	Catalyst Mixture, wt %	Electrode Preparation	Catalyst Loading, mg/cm^2	Total Loading, mg/cm^2	Polarization from Methanol Theor. at Indicated ma/cm^2, Volts 0	1	10	50	100	Tafel Slope b	Current Density at 0.35 Volts Polarization, ma/cm^2	Catalyst Utilization at 0.35 Volts Polarization, mg/ma	Remarks
3378-5	33% catalyst + 67% Ta	Pressed at 3000 psi	,	27	0.18	0.23	0.32	0.40	0.46	0.10	20	2.2	
" -6	" " + " "	" " 6000 "	10	30	0.16	0.22	0.29	0.34	0.38	0.08	60	6.0	
" -11	" " + " "	" " 6000 "	10	30	0.16	0.23	0.32	0.38	0.42	0.09	20	2.0	100 mv IR at 100 ma/cm^2.
" -15	" " + " "	" " 6000 "	10	30	0.21	0.34	0.46	0.58	--	0.09	1	0.1	Screen exposed.
" -16	" " + " "	" " 6000 "	10	30	0.20	0.29	0.39	0.49	--	0.11	5	0.5	" "
" -22	20% " + 80% "	" " 4500 ", 0.5 wt % Teflon emulsion	10	50	0.10	0.19	0.27	0.36	0.42	0.09	45	4.5	
" -24	" " + " "	Pressed at 4500 psi	10	50	0.10	0.22	0.28	0.35	0.40	0.06	50	5.0	
" -20	100% Ta	" " 6000 "	50	50	0.40	0.44	0.60	--	--	--	--	--	
" -26	2 layers: bottom 10% cat + 90% Ta	" " 3000 "	2	20	0.12	0.20	0.28	0.36	0.40	0.08	45	3.6	Two layers, top layer
	Top: 50% cat + 50% Ta	" " 4500 "	10	20									50% catalyst.
" -13	33% catalyst + 67% Ta	" " 6000 ", 3% Kynar	10	30	0.20	0.25	0.33	0.45	0.51	0.10	12	1.2	
" -9	" " + " "	" " 4500 ", 5% "	10	30	0.10	0.24	0.32	0.42	0.52	0.08	18	1.8	
" -10	" " + " "	" " 4500 ", 5% Saran	10	30	0.17	0.21	0.29	0.40	0.48	0.10	28	2.8	
" -27	20% cat + 40% Ta + 40% Au	" " 4500 ", 0.5% Teflon	10	50	0.11	0.20	0.28	0.34	0.39	0.09	60	6.0	
" -12	33% catalyst + 67% Ta	" " 6000 ", 5% Teflon	10	30	0.23	0.36	0.53*	--	--	0.09	1	0.1	30% porous
" -14	" " + " "	" " 6000 ", 5% Kynar	10	30	0.16	0.26	0.43	0.56	0.63	0.17	4	0.4	30% "
" -25	20% " + 80% Ta	" " 4500 ", 0.5% Teflon	10	50	0.11	0.21	0.32	0.41	0.49	0.11	20	2.0	30% "
" -29	20% " + 80% Ta	" " 10000 ", 1% Teflon	10	50	0.18	0.23	0.31	0.39	0.45	0.09	24	2.4	40% "
" -30	20% " + 80% Ta	" " 10000 ", 1% Teflon	10	50	0.14	0.23	0.30	0.39	0.43	0.07	28	2.8	20% "
" -31	20% " + 80% Ta	" " 10000 ", 1% Teflon	10	50	0.14	0.22	0.30	0.37	0.41	0.08	35	3.5	20% "
" -32	20% " + 80% Ta	Pressed at 4500 psi, bottom 1% Teflon	10	50	0.13	0.21	0.28	0.35	0.38	0.06	50	5.0	Two layers, top layer pure catalyst.
" -33	20% " + 80% Au	Pressed at 4500 psi	10	50	0.11	0.20	0.27	0.33	0.36	0.07	78	7.8	
" -32	20% " + 80% Ta	" " 4500 "	10	50	0.12	--	0.26	0.31	0.35	0.06	100	--	Tested at 80° .
" -38	20% " + 80% Au	" " 3000 "	10	50	0.08	0.17	0.27	0.34	0.37	0.10	65	6.5	-140 mesh Au powder.
" -39	10% " + 90% Au	" " 4500 "	5	50	0.21	0.25	0.32	0.38	0.44	0.07	25	5.0	Two layers, top layer pure catalyst.
" -40	10% " + 90% Ta	" " 4500 "	5	50	0.20	0.29	0.40	0.58	--	0.11	5	0.6	Two layers, top layer pure catalyst.
" -45	10% " + 90% Ta C	" " 6000 " with 0.5% Teflon emulsion	10	100	0.23	0.29	0.42	--*	--	0.07	3	0.3	Run 1.
" -45	" " " " "	" " 6000 " " " "	10	100	0.36	0.42	0.54	--	--	0.06	0.1	0.01	Run 2.
" -46	10% " + 90% Ta	" " 6000 " " " "	10	100	0.19	0.26	0.36	0.48	0.56	0.07	8	0.8	Unstable above 100 ma/cm^2.
" -47	10% " + 90% WC	" " 6000 " " " "	10	100	0.20	0.24	0.32	0.44	0.90*	0.08	17	1.7	Unstable above 50 ma/cm^2.
" -48	10% " + 90% W	" " 6000 " " " "	10	100	0.18	0.23	0.30	0.38	0.44	0.07	27	2.7	
" -49	10% " + 90% ZrC	" " 4500 " " " "	7	70	0.22	0.45	--	--	--	--	1	0.1	Unstable above 1 ma/cm^2.
" -50	20% " + 80% Graphite	" " 6000 " 1% " "	5	25	0.24	0.26	0.32	0.40	0.46	0.07	16	3.2	Unstable above 100 ma/cm^2.
3468-5	20% " + 80% B_4C	" " 3000 " 2% " "	5	25	0.16	0.29	0.38	0.60*	--	0.09	4	0.9	
" -6	50% " + 50% Graphite	" " 3000 " 1% " "	5	10	0.18	0.22	0.29	0.39	0.46	0.07	27	5.4	
" -7	50% " + 50% Carbon	" " 3000 " 1% " "	5	10	0.22	0.25	0.33	0.43	0.49*	0.08	14	2.8	Unstable above 100 ma/cm^2.
" -28	25% " + 75% Ta	" " 4500 " " " "	12	50		0.22	0.31	0.38	0.45	0.10	25	2.1	
" -29	40% " + 60% Ta	" " 4500 " " " "	20	50		0.19	0.28	0.34	0.38	0.09	64	3.2	
" -30	80% " + 20% Ta	" " 4500 " " " "	40	50		0.18	0.26	0.33	0.37	0.09	74	1.9	

Unstable

APPENDIX D-8

PERFORMANCE OP RUTHENIUM MODIFIED P-TYPE CATALYST

Test Condition: 3.7 M Sulfuric Acid, 1 M Methanol, 60°C
Electrodes: 4 cm^2 Plag Type

Electrode Identification	Catalyst Preparation	Electroda Preparation	Catalyst Loadiog, mg/cm^2	Polsrizstion from Methanol Theory at Indicated ma/cm^2, volts					Tafel Slope	Curreot Density at 0.35 volts Polsrization, ma/cm^2	Catalyst Utilizstion at 0.35 volts Polarization, ma/mg	Remarks
				0	1	10	100	500				
3468-34	H_2 rad.	Pressad at 4000 psi	40	0.05	0.16	0.24	0.32	0.46	0.08	160	4.0	--
3378-18	H_2 red.	Pressed at 3000 psi	30	0.05	0.15	0.21	0.30	0.40	0.06	320	10.7	Hsodled wet.
3378-19	H_2 red.	Pressed at 3000 psi	30	0.07	0.16	0.22	0.29	0.40	0.06	330	11.0	--
3378-41	H_2 red.	Pressed at 4500 psi	13	0.10	0.19	0.26	0.36	0.42	0.08	80	6.2	--
3378-42	H_2 rad.	Pressed at 4500 psi	20	0.08	0.16	0.24	0.34	0.52	0.09	120	6.0	--
3378-43	H_2 red.	Pressed at 3000 psi	50	0.13	0.18	0.24	0.32	0.46	0.06	170	7.4	--
3378-3	H_2 red.	Pressed at 3000 psi	21	0.14	0.18	0.24	0.34	0.46	0.07	120	5.7	--
3378-30	H_2 red.	Pressed at 4000 psi	20	0.14	0.19	0.26	0.34	0.49	0.08	120	6.0	--
3378-35	H_2 red.	Prassed at 4000 psi	18	0.06	0.20	0.26	0.35	0.55	0.08	100	5.4	--
3378-36	H_2 red.	Pressed at 4000 psi	14	0.08	0.20	0.27	0.37	0.56	0.08	60	4.7	--
3378-36	H_2 red.	Pressed at 4000 psi	14	--	0.19	0.20	0.36	--	0.08	80	5.7	Rerun.
3378-37	H_2 red.	Pressed at 4000 psi	10	0.17	0.21	0.28	0.39	--	0.09	50	5.0	--
3378-37	H_2 red.	Pressed at 4000 psi	10	--	0.19	0.26	0.36	--	0.09	77	7.7	Rerun.
3378-38	H_2 red.	Pressed at 4000 psi	6	0.16	0.23	0.31	0.42	--	0.10	25	4.3	--
3378-40	H_2 red.	Pressed at 4000 psi	5	0.15	0.22	0.30	0.41	0.62	0.10	32	6.8	--
3378-40	H_2 red.	Pressed at 4000 psi	5	--	0.21	0.29	0.39	0.61	0.10	44	8.8	Rerun.
3378-10	H_2 red.	Pressed at 4000 psi	4	0.22	0.28	0.36	0.47	--	0.08	7	1.8	Cathodized.
3378-14	H_2 red.	Prassad at 4000 psi	4	0.21	0.26	0.33	0.46	--	0.08	13	3.2	--
3733-13	H_2 rad.	Pressed at 5000 psi	20	0.05	0.16	0.23	0.30	0.41	0.07	240	12.0	
3468-48	HCHO red. oo $NaAlO_2$	Pressad at 4000 psi	20	0.09	0.23	0.32	0.38	0.49	0.07	40	2.0	H_2SO_4 wash only.
3468-49	HCHO red. on $NaAlO_2$	Pressad at 4000 psi	20	0.09	0.20	0.26	0.33	0.48	0.06	170	8.5	--
3733-12	HCHO red. on $NaAlO_2$	Pressed at 5000 psi	20	0.04	0.20	0.26	0.32	0.41	0.06	210	10.5	--
3733-21	Radical anion red.	Pressad at 4000 psi	20	0.08	0.17	0.25	0.36	0.49	0.09	82	4.1	--
3733-23	CO reducad in sol.	Pressed at 4000 psi	20	0.20	0.27	0.35	0.45	0.57	0.08	10	0.5	--

APPENDIX D-9

PERFORMANCE OF PLATINUM-BLACK CATALYSTS

Test Conditions: 3.5 M Sulfuric Acid, 1 M Methanol, 60°C
Electrodes: 4 cm^2 Flag-Type

Electrode Identification	Catalyst Preparation	Electrode Preparation	Catalyst Loading, mg/cm^2	Polarization from Methanol Theory at Indicated ma/cm^2, volts					Tafel Slope, b	Current Density at 0.45 volts Polsrization, ma/cm^2	Catalyst Utilization at 0.45 volts Polarizstion, ma/mg
				0	1	10	50	100			
3397-3	Red. with Na-citrate, colloidal, 6% ads. on carbon.	10% Teflon 7, 8000 psi	10	0.38	0.40	0.45	0.53	0.57	0.08	9	0.9
3397-4	Reduced with $LiBH_4$.	Pressed at 2000 psi	30	0.22	0.33	0.39	0.44	0.46	0.06	80	2.7
3397-5	Reduced with HCHO.	Pressed at 2000 psi	23	0.19	0.39	0.44	0.48	0.50	0.06	13	0.6
3397-6	Reduced with Li/Biphenyl.	Pressed at 2000 psi	38	0.26	0.32	0.40	0.44	0.46	0.07	64	1.7
3397-7	Alloyed with Ag, Ag removed.	Pressed at 2000 psi	70	0.31	0.35	0.40	0.43	0.45	0.05	100	1.4
3397-8	Reduced with HCHO on Na aluminate.	Pressed at 3000 psi	34	0.10	0.23	0.39	0.44	0.46	0.07	70	2.0
3397-9	Alloyed with Ag, Ag removed.	Pressed at 4500 psi	100	0.28	0.35	0.41	0.44	0.46	0.05	62	0.6
3397-10	Commercial Pt-black.	Pressed at 3000 psi	23	0.24	0.34	0.43	0.50	0.55	0.08	15	0.7
3397-12	Reduced with HCHO on Na aluminate.	Pressed at 3000 psi	20	0.08	0.32	0.39	0.43	0.47	0.07	70	3.5
3397-13	Reduced with HCHO.	Pressed at 3000 psi	20	0.34	0.39	0.44	0.48	0.50	0.05	14	0.7
3397-14-1	Reduced with $LiBH_4$.	Pressed at 3000 psi	21	0.26	0.36	0.42	0.47	0.49	0.06	25	1.2
3468-12	Catalyzed carbon.	0.5% Teflon emulsion, 3000 psi	1.2	0.33	0.37	0.47	0.56	--	0.10	6.4	5.3
3468-13	Catalyzed carbon.	0.5% Teflon emulsion, 4000 psi	1.2	0.33	0.39	0.49	0.55	0.58	0.10	5.6	4.5
3733-30	" , colloidal, 6%	" " " , 4000 psi	0.6	0.25	0.38	0.48	0.56	0.60	0.11	5.5	9.0
3733-29	" , " " heat treated	" " " , " "	0.6	0.40	0.50	--	--	--	--	0.4	0.6

APPENDIX D-10

PERFORMANCE OF SUPPORTED CATALYSTS

Catelyst: Ruthenium Modified P-type
Test Conditions: 3.7 M Sulfuric Acid, 1 M Methanol, 60°C
Electrodes: 4 cm^2 Flag Type

Electrode Identificetioo	Catalyst Preparation	Cetalyst Content on Support, wt %	Electrode Preperetion	Catalyet Loeding on Electrode, mg/cm^2	Polerizetioo from Methanol Theory et Indicated ma/cm^2, volts 0	1	10	50	100	Tafel Slope b	Current Deoeity et 0.35 volts Polerization, ma/cm^2	Catalyst Utilization at 0.35 volts Polerizetion, ma/mg	Remarks
3468-24	Red. at high temp oo carbon	10	Pressed at 3000 psi with 2% Teflon emulsion	1	0.34	0.76	--	--	--	--	--	--	
3468-25	" " "	10	Pressed at 3000 psi with 2.5% Teflon emulsion	2	0.45	0.56	--	--	--	--	--	--	Steble to 30 ma/cm^2.
3468-32	Red with KBH_4 at room temp on cerbon	10	Prassed at 6600 psi with 0.5 Teflon emulsion	2	0.22	0.26	0.38	0.50	--	0.12	6	3	
3468-33	" " "	10	" "	2	0.22	0.27	0.41	--	--	0.14	4	2	5 wt % polyethylene binder edded.
3468-41	Red. with KBH_4 at room temp on carbon add. H_2 treat	10	" "	2	0.24	0.30	0.42	0.52	--	0.14	4.6	2.3	Physically steble to 50 ma/cm^2.
3468-31	Red. at high temp oo carboo	6	" "	1.2	0.32	0.39	0.52	0.60	0.64	0.13	0.4	0.3	52 at % Ru.
3468-45	Red. et 125°C with H_2 on cerbon	10	Pressed at 5000 psi with 0.5% Teflon emulsion	2	0.30	0.37	0.54	--	--	0.17	0.8	0.4	Steble to 20 ma/cm^2.
3468-46	" " "	20	" "	4	0.25	0.30	0.40	0.53	--	0.10	3.5	0.9	
3733-3	Red. et 125°C with H_2 on carbon, KOH weshed 0.01 N	10	" "	2	0.23	0.25	0.41	0.52	0.60	0.15	4.6	2.3	
3733-4	" " "	20	" "	2	0.21	0.27	0.35	0.42	0.46	0.08	10.0	5.0	Stable to 500 ma/cm^2.
3733-5	Red. at 125°C with H_2 on carbon, twice KOH washed	20	" "	1.5	0.23	0.27	0.37	0.45	0.49	0.10	6.6	4.4	Stable to 525 ma/cm^2.
3733-11	Red. at 225°C with H_2 oo pretreeted cerboo	20	Pressed at 6000 psi with 0.5% Teflon emulsion	2	0.26	0.31	0.42	0.56	0.64	0.11	2.5	1.2	Stable to 100 ma/cm^2, Pt-oucleii eeeded on cerbon.
3733-14	Red. at 225°C with H_2 on ballmilled coal	20	Preesed at 5000 psi with 1.0% Tefloo emulsioo	4	0.29	0.38	0.61	--	--	0.23	0.6	0.15	
3733-15-1	" " "	20	" "	4	--	0.37	0.52	0.72	--	0.14	0.8	0.2	Rerun.
3733-15-2	" " "	20	Pressed at 5000 psi with 0.5% Teflon emulsion	4	--	0.33	0.50	--	--	0.17	1.3	0.3	
3733-16-1	Red. et 225°C with H_2 on carboo, eeparate impregnation stepe	20	Preesed at 5000 psi with 0.5% Teflon emulsion	2	0.19	0.27	0.39	0.51	--	0.12	4.6	2.3	Componente impregnated aod reduced stepwise.
3733-16-2	" " "	20	Pressed at 5000 psi with 2.0% Teflon emulsioo	2	--	0.30	0.46	0.59	--	0.17	2.0	1.0	Rerun.
3733-17-1	Red. at 125°C with H_2 on carboo, dried.	20	Pressed et 5000 psi with 0.5% Teflon emulsion	2	0.17	0.27	0.35	0.44	--	0.08	10.0	5.0	Stable to 75 ma/cm^2.
3733-17-2	" " "	20	Pressed et 5000 psi with 2.0% Teflon emulsion	2	0.21	0.30	0.38	0.49	0.62	0.08	4.2	2.8	Steble to 100 ma/cm^2.
3733-18	Red. et 225°C with R_2 on cerboo, KOH weshed.	20	Pressed at 5000 psi with 0.5% Teflon emulsioo	2	0.22	0.27	0.36	0.46	0.55	0.09	8.2	4.1	Stable to 300 ma/cm^2.
3733-19-1	" " "	30	" "	3	0.26	0.32	0.42	0.53	0.60	0.10	2.0	0.7	Stable to 500 ma/cm^2.
3733-19-2	" " "	30	" "	3	0.16	0.22	0.30	0.40	0.49	0.08	24.0	8.0	Rerun.
3733-24-1	" " "	30	" "	2	0.22	0.27	0.36	0.44	0.49	0.09	8.0	4.0	
3733-24-2	" " "	30	" "	2	0.22	0.27	0.37	0.45	0.51	0.09	7.0	3.5	Rerun.
3733-20	Red. at 225°C with H_2 on B_4C, KOH weshed.	20	" "	2	0.03	0.25	0.35	0.47	--	0.10	10.0	5.0	Stable to 90 ma/cm^2.
3733-22-1	Red. with CO et room temp, edsorbed on carbon washed with H_2SO_4	16	" "	1.6	0.16	0.30	0.41	0.52	0.58	0.11	3.0	1.9	
3733-22-2	Red. with CO at room temp, adsorbed on carbon, washed with KOH	16	" "	1.6	0.32	0.36	0.44	0.52	0.56	0.08	0.7	0.4	
3733-25	Red. with H_2 at 225°C oo carboo, KOH washed.	20	" "	4	0.14	0.26	0.36	0.44	0.48	0.10	8.0	2.0	
3733-26-1	" " "	20	Pressed et 5000 psi with 1% latex	2	0.30	0.36	0.49	--	--	0.10	0.8	0.4	Stable to 30 ma/cm^2.
3733-26-2	" " "	20	Pressed at 5000 psi with 5% latex	2	0.26	0.32	0.43	0.58	0.68	0.10	2.0	1.0	

APPENDIX E-1

COATED ELECTRODE PERFORMANCE STUDIES

Tests Conducted in 1" Diameter Cell at 60°C
With Electrode Coating Facing Air Stream

Electrode Number	Description	Methanol Conc, M	Polarization From O_2 Theory at Indicated ma/cm^2, volts 0	1	5	10	50	100	Ohmic Losses at 100 ma/cm^2, volts[1]
M-3 }	Cyanamid AA-1 Coated with	0	0.23	0.27	0.32	0.35	0.47	0.60	0.015
M-4 }	Butyl Rubber Latex--Air Side	0	0.25	0.27	0.33	0.39	0.45	0.55	0
M-7	Cyanamid AA-1 Coated with Sulfur-free Butyl Rubber Latex	0	0.24	0.29	0.33	0.37	0.44	0.44	0.05
M-10	Cyanamid AA-1 Coated with Silastic Diluted with Decane	0	0.25	0.31	0.37	0.40	0.47	0.51	0.01
M-10		0.125	0.43	0.43	0.44	0.44	0.47	0.51	0
M-10		0.25	0.41	0.42	0.43	0.43	0.45	0.48	0
M-10		0.5	0.47	0.47	0.47	0.47	0.49	0.50	0
M-10		0.75	0.51	0.51	0.51	0.51	0.51	0.53	0
M-10		1	0.52	0.52	0.52	0.52	0.53	0.54	
83	Cyanamid AA-1 Spray Coated with Teflon 41 Bx	0	0.21	0.30	0.32	0.36	0.42	0.46	0.05
M-15	Cyanamid AA-1 Spray Coated with Fluoroglide Relative Thickness = 1	1	0.47	0.47	0.47	0.47	0.49	0.53	0
M-16	Cyanamid AA-1 Coated with Fluoroglide Relative Thickness = 10	1	0.45	0.45	0.45	0.45	0.47	0.49	0.005
M-22	Cyanamid AA-1 Coated with Fluoroglide Relative Thickness = 100	1	0.48	0.48	0.48	0.49	0.51	0.53	0.01

(1) Ohmic loss measured with Kordesch-Marko Bridge.

APPENDIX E-2

EFFECT OF SPRAY COATINGS ON CATHODE PERFORMANCE

Electrode Identification(1)	Run Identification(2)	Oxidant	Methanol Conc , M(3)	Polarization From O_2 Theory at Indicated ma/cm^2, volts(4)						Ohmic Losses at 100 ma/cm^2, volts(5)
				0	1	5	10	50	100	
A	3372-36A	Air	0	0.23	0.28	0.33	0.34	0.41	0.46	0.08
		Air	0.1	.37	.36	.37	.37	.43	.51	.08
		Air	0.5	.51	.50	.50	.50	.54	.58	.09
		Air	0	.23	.26	.32	.35	.58	.67	.06
		O_2	0	.19	.21	.28	.29	.37	.44	.08
		Air	0	--	--	--	--	--	.67	.06
B	3372-36B	Air	0	.23	.28	.32	.35	.40	.43	.04
		O_2	0	--	--	--	--	--	.32	.04
		Air	0.1	.34	.34	.34	.35	.40	.43	.04
		Air	0.5	.44	.44	.42	.42	.45	.47	.04
		Air	1.0	.47	.47	.47	.48	.49	.52	.04
		Air	2.0	.62	.62	.62	.62	.62	.64	.04
		O_2	2.0	--	--	--	--	--	.46	.06
		Air	2.0	.57	.56	.56	.56	.59	.62	.04
		Air	0	.24	.25	.30	.32	.40	.41	.04
		Air	0.1	.31	.31	.34	.36	.44	.46	.04
		Air	0.5	.40	.41	.42	--	--	--	--
		Air	0	.21	.26	.31	.33	.38	.43	--
		O_2	0	.21	.23	.25	.26	.31	--	--
		Air	0.1	.39	.37	.45	.44	.47	.48	.04
		O_2	0.1	.30	.31	.36	.37	.39	.39	.04
C	3372-37	O_2	0	.21	.28	--	--	--	.39	.03
		O_2	0.1	.28	.29	--	--	--	.39	.03
		Air	0.1	.31	.32	--	--	.45	.49	.02
D	3372-40	Air	0	.21	.30	.33	0.36	.42	.46	.07
		O_2	0	.18	.27	.27	.30	.34	.37	.07
		Air	0.1	.40	.39	.40	.40	.48	.49	.04
		O_2	0.1	.32	.32	.32	.32	--	--	--
		Air	0.5	.50	.50	.50	.50	.51	.54	.06
		Air	1.0	.52	.52	.55	.54	.58	.60	.04
		Air	1.0	.52	.52	.52	.52	.52	.54	.04
		Air	2.0	.57	.57	.57	.58	.58	.60	.02
E	3372-40	Air	0	.27	.32	.34	.37	.44	.48	.04
		Air	0.1	.43	.43	.43	.44	.48	.54	.03
		Air	0.5	.58	.57	.57	.57	.58	.61	.03
		Air	1.0	.60	.60	.60	.60	.62	.64	.04
		Air	1.0	.60	.60	.60	.60	.62	.64	.02
F	3372-40	Air	0	.25	.40	.49	.64	.80	--	--
		Air	0	.23	.35	.44	.47	.63	.93	.04
		O_2	0	.19	.26	.34	.36	.42	.42	.10
G	3372-40	Air	0	.33	.35	.46	.54	.81	--	--
		O_2	0	.27	.27	.32	.38	.56	.67	.025
		Air	0.1	.77	.77	.78	.79	--	--	--

(1) A: Permion 1010 membrane pressed onto electrolyte side of Cyanamid AA-1 cathode (5.7 cm^2 electrode area).
B: Same
C: Same, Teflon screen used as platen face during pressing.
D: Teflon 41 BX emulsion sprayed on oxidant side of Cyanamid AA-1 cathode. No membrane.
E: Same, but reversed so that Teflon-sprayed side faced electrolyte.
F: Permion 1010 membrane pressed onto electrolyte side of Cyanamid AA-1 cathode. Sprayed Teflon on oxidant side.
G: Ru-modified P-type catalyst (25 mg/cm^2) cathode with Teflon-sprayed oxidant side.

(2) 60°C, 3.7 M H_2SO_4, 50 cc/min oxidant rate. Note: Stoichiometric air rate = 0.095 I, cc air/min, where I = current density, ma/cm^2.

(3) Methanol concentration in electrolyte adjacent to cathode.

(4) Ex-IR values.

(5) Ohmic losses measured with Kordesch-Marko bridge.

APPENDIX E-3

EFFECT OF COATING THICKNESS ON POLARIZATION OF COATED CATHODES

Temperature : 60°C Oxidant: Air-5x Stoichiometric

Coating Type	Relative Coating Thickness	Cathode Polarization at Indicated ma/cm^2, volts 50	100
Electrolyte - 3.7 M H_2SO_4			
Fluoroglide Spray	1	0.49	0.53
" "	10	0.47	0.49
" "	100	0.51	0.53
Electrolyte - 1 M Methanol in 3.7 M H_2SO_4			
Silastic--Drip Coated	1	0.37	0.39
" " "	4	0.37	0.39

Figure E-1

Comparison of Teflon and Silastic Coated Cathodes

Silastic 60X

Teflon 60X

APPENDIX E-4

TESTING OF TEFLON SPRAY COATED CATHODE IN 9" x 5-3/4" TOTAL CELL

Oxidant(1)	Datum(2)	Performance at Indicated ma/cm^2, volts(3)						
		0	10	20	30	40	50	60
Air	Cell	0.47	0.33	0.32	0.12	0.04	--	--
	Anode	.12	.22	.29	.34	.36		
	Cathode	.61	.63	.55	.68	.72		
	IR	.00	.02	.04	.06	.08		
O_2	Cell	0.50	0.42	0.34	0.26	0.20	0.14	0.10
	Anode	.18	.23	.28	.32	.35	.38	.40
	Cathode	.52	.53	.54	.56	.57	.58	.58
	IR	.00	.02	.04	.06	.08	.10	.12

(1) Oxidant rates: Air = 8000 cc/min, O_2 = 1600 cc/min @ STP.

(2) Cell voltage, anode and cathode polarization, and ohmic losses. Latter measured by AC signal method.

(3) 62-66°C, 0.75 M methanol in 3.7 M sulfuric acid fed at 4000 cc/hr. Severe leakage of electrolyte from air exhaust was noted. Electrode data: Anode was 9" x 5-3/4" 50 mesh screen containing 25 mg/cm^2 of Ru-modified P-type catalyst. Cathode was Cyanamid AA-1 with Teflon 41 BX spray coat on oxidant side. Electrodes were mounted in bi-cell assembly. Run reference 3075-15, 16.

APPENDIX F-1

EFFECT OF GOLD ON METHANOL ELECTRODE PERFORMANCE

Electrode Identification[1]	Screen Composition[2]	Current Collector[3]	Gold Diluent Content mg/cm²[4]	Measurement	Polarizatioo from Methanol Theory or Ohmic Loss (IR) at Indicated ma/cm², volts[5] 0	1	5	10	50	100	200	500	1000	Remarks
3372-22(52)	Au-Ta	None	0	Polarization	0.06	0.14	0.24	0.27	0.33	0.37	0.40	0.45	0.50	
				IR	--	--	0.005	0.010	0.010	0.010	0.015	0.015	0.045	
				Polarization	0.05	0.18	0.25	0.28	0.34	0.38	0.42	0.46	0.50	Retested on same day.
				IR	--	--	--	0.005	0.010	0.015	0.020	0.025	0.045	
3372-22(53)	Au-Ta	PG	0	Polarization	0.10	0.17	0.23	0.26	0.32	0.34	0.38	0.42	0.46	
				IR	--	--	0.010	0.010	0.015	0.015	0.020	0.020	0.030	
3372-23(54)	Ta	None	25	Polarization	0.02	0.14	0.20	0.24	0.30	0.34	0.40	0.46	0.56	
				IR	--	--	0.005	0.010	0.010	0.015	0.030	0.055	0.100	
3372-23(55)	Ta	PG	25	Polarization	0.02	0.15	0.22	0.26	0.31	0.34	0.38	0.44	0.47	
				IR	--	--	0.005	0.005	0.010	0.005	0.010	0.015	0.030	
3372-23(58)	Au-Ta	PG	25	Polarization	0.04	0.14	0.22	0.26	0.30	0.34	0.38	0.42	0.46	
				IR	--	--	--	0.005	0.005	0.005	0.010	0.010	0.010	
3372-23(57)	Au-Ta	None	25	Polarization	0.02	0.16	0.20	0.22	0.30	0.34	0.39	0.46	0.54	
				IR	--	--	0.005	0.005	0.015	0.005	0.025	0.040	0.090	
				Polarizatioo	--	--	--	--	0.32	0.34	0.36	0.42	0.50	Retested oext day.
				IR	--	--	--	--	0.005	0.010	0.020	0.040	0.060	
3372-23(57)	Au-Ta	PG	25	Polarization	0.02	--	--	--	0.32	0.36	0.39	0.44	0.50	
				IR	--	--	--	--	0.005	0.010	0.010	0.015	0.025	
3372-6(31)	Au	None	0	Polarizatioo	0.04	0.14	0.22	0.26	0.34	0.38	0.42	0.46	0.50	6/0 Expanded metal screen. 40% cstalyst lost during run.
				IR	--	--	--	--	--	--	0.005	0.020	0.030	
3372-6(30)	Ta	PG	0	Polarization	0.02	0.18	0.24	0.26	0.32	0.36	0.38	0.44	0.50	
				IR	--	--	--	--	--	--	0.002	0.015	0.050	
3372-7(34)	Ta	None	0	Polarization	0.05	0.19	0.24	0.27	0.34	0.38	0.42	--	0.62	
				IR	--	--	--	--	--	--	0.015	--	0.055	
3372-7(35)	Ta	None	0	Polarization	0.04	0.17	0.25	0.28	0.36	0.40	0.45	0.53	0.62	0.02 wt % 3 M FC-95 surfactant added.
				IR	--	--	--	--	0.010	0.020	0.030	0.065	0.060	

(1) Electrodes contain 25 mg/cm² of H_2 reduced form of Ru modified P-type catalyst, pressed at 3000 psi to form 5.7 cm² area electrode. Data for last four electrodes reported previously (6).
(2) Ta: 50 mesh tantalum screen; Au-Ta: same gold-plated, contained about 0.2 mil gold coating; Au: all gold expanded metal screen.
(3) PG: peripheral gold ring used as curreot collecto:. Remaioing electrodes were connected to circuit by clipping leads directly to screen.
(4) Gold dilueot produced by reducing chloroplatinic acid with KBH_4. Reduced gold was ground and incorporated ioto catalyst powder prior to fabrication of electrode.
(5) Run conditions: 60°C, 1 M CH_3OH in 3.7 M H_2SO_4. Ohmic losses measured with Kordesch-Marko bridge.

APPENDIX F-2

EFFECT OF SCREEN COMPOSITION ON PERFORMANCE OF 9" x 5-3/4" METHANOL ELECTRODES

Electrode Identification[1]	Screen Composition[2]	Luggin Position Coordinates[3]	Measurement	Polarization from Methanol Theory or Ohmic Loss (IR) at Indicated ma/cm^2, volts[4] 0	5	10	20	30	40	50	60	70	80	90	Remarks
FC-87	Ta	(1, 1.5)	Polarization	0.06	0.24	0.28	0.32	0.36	0.40	0.42	0.46	0.50	0.54	0.56	
			IR	--	0.009	0.018	0.036	0.055	0.077	0.092	0.115	0.138	0.163	0.183	
		(9, 5.25)	Polarization	0.06	0.24	0.30	0.34	0.38	0.44	0.47	0.50	0.53	0.59	0.64	
			IR	--	0.012	0.026	0.051	0.081	0.116	0.138	0.158	0.185	0.220	0.248	
FC-88	Au-Ta	(1, 1.5)	Polarization	0.04	0.24	0.28	0.30	0.32	0.34	0.34	0.36	0.36	0.37	0.38	
			IR	--	0.002	0.003	0.007	0.010	0.013	0.017	0.021	0.023	0.028	0.031	
		(9, 5.25)	Polarization	0.01	0.26	0.28	0.32	0.34	0.34	0.36	0.38	0.38	0.40	0.40	
			IR	--	0.002	0.004	0.009	0.013	0.018	0.023	0.028	0.033	0.038	0.042	
FC-107	Pt	(1, 1.5)	Polarization	0.04	0.20	0.22	0.24	0.26	0.28	0.30	0.30	0.32	0.32	0.32	
			IR	--	0.01	0.002	0.004	0.006	0.008	0.011	0.013	0.016	0.018	0.020	
		(9, 5.25)	Polarization	0.04	0.20	0.22	0.25	0.27	0.30	0.30	0.32	0.32	0.32	0.33	
			IR	--	0.002	0.003	0.006	0.009	0.012	0.014	0.017	0.020	0.023	0.026	
		(1, 1.5)	Polarization	--	0.22	0.24	0.26	0.27	--	--	--	--	--	--	Loose contact between electrode and current collector.
			IR	--	0.001	0.003	0.005	0.008	--	--	--	--	--	--	
		(9, 5.25)	Polarization	--	0.24	0.27	0.30	0.32	--	--	--	--	--	--	
			IR	--	0.005	0.011	0.022	0.032	--	--	--	--	--	--	

(1) Electrodes contained 25 mg/cm^2 of H_2 reduced form of Ru modified P-type catalyst (composite V), pressed at 3000 psi.
(2) Screens were 9" x 5-3/4" Ta: 50 mesh tantalum; Au-Ta: same gold-plated, contained about 0.2 mil gold coating; Pt: 80 mesh platinum.
(3) Luggin positions on electrode surface. (1, 1.5) is close to current collector tab, (9, 5.25) is diagonally opposite. See reference (6) for additional details.
(4) Run conditions: 60°C, 1 M CH_3OH in 3.7 M H_2SO_4. Ohmic losses measured with AC method (6). Fan-shaped current collector used. Data obtained in 9" x 5-3/4" half cell (Reference 3372-29, 31) described previously (6).

APPENDIX F-3

EFFECT OF METHANOL CONCENTRATION ON PERFORMANCE OF 9" x 5-3/4" ELECTRODES

Methanol Concentration in 3.7 M H_2SO_4, M	Luggin Position Coordinates (1)	Measurement	Polarization from Methanol Theory or Ohmic Loss (IR) at Indicated ma/cm^2, volts (2) 0	10	20	30	40	50	60	70	80	90	Remarks
1.0	(1, 1.5)	Polarization	0.04	0.25	0.30	0.32	0.34	0.35	0.36	0.38	0.39	0.42	
		IR	--	0.004	0.008	0.012	0.016	0.020	0.023	0.028	0.032	0.036	
	(9, 5.25)	Polarization	0.04	0.27	0.31	0.34	0.36	0.38	0.40	0.41	0.42	0.44	
		IR	--	0.005	0.0108	0.015	0.021	0.026	0.031	0.036	0.041	0.046	
0.5	(1, 1.5)	Polarization	0.11	0.25	0.28	0.30	0.32	0.35	0.37	0.38	0.40	0.40	
		IR	--	0.003	0.008	0.012	0.015	0.017	0.022	0.027	0.030	0.033	
	(9, 5.25)	Polarization	0.11	0.26	0.30	0.32	0.34	0.37	0.40	0.41	0.44	0.46	
		IR	--	0.004	0.008	0.014	0.018	0.021	0.025	0.029	0.033	0.039	
0.1	(1, 1.5)	Polarization	0.06	0.32	0.38	0.40	0.44	0.48	0.50	0.52	0.55	0.59	
		IR	--	0.003	0.006	0.009	0.012	0.015	0.018	0.020	0.024	0.028	
	(9, 5.25)	Polarization	0.10	0.33	0.38	0.42	0.46	0.50	0.52	0.54	0.58	0.61	
		IR	--	0.004	0.007	0.011	0.014	0.018	0.022	0.025	0.030	0.032	
0.05	(1, 1.5)	Polarization	0.24	0.. (3)	--	--	--	--	--	--	--	--	Catalyst flaking
		IR	--	0.001 (3)	--	--	--	--	--	--	--	--	off electrode
	(9, 5.25)	Polarization	0.24	0.40 (3)	--	--	--	--	--	--	--	--	
		IR	--	0.001 (3)	--	--	--	--	--	--	--	--	

(1) Luggin Positions on electride surface. (1, 1.5) is close to current collector tab, (9, 5.25) is diagonally opposite. See reference (6).

(2) 9" x 5-3/4" electrode No. FC-88: 25 mg/cm^2 of H_2 reduced form of Ru modified P-type catalyst (composite V), pressed at 3000 psi on gold-plated 50 mesh Ta screen. Run conditions: 60°C with ohmic losses determined using AC method (6). Fan-shaped current collector employed.

(3) Data at 1 ma/cm^2; higher current densities ... not be maintained.

APPENDIX F-4

AIR HALF CELL STUDIES OF EFFECT OF METHANOL ON PERFORMANCE

Stirred Half Cell Data
3.7 M H_2SO_4 to 6.4 cm^2 Electrodes
Permion 1010 Membrane Clad Cyanamid AA1 Cathodes

Methanol Molarity	Current Density, ma/cm^2	Stoichiometric Air Rate	Cathode Polarization from O_2 Theory, volts	Percent CO_2 in Exhaust	Direct Oxidation, Equivalent ma/cm^2	Temp, °C	Identificat on
0	0	5	0.285	0	0	60	2292-50
0	40	"	0.380	0	0	"	"
0.125	0	"	0.37	--	--		"
"	40	5	0.39	--	--	"	"
.25	0	5 at 10 ma/cm^2	0.39	4.9	16.3	"	"
"	80	5	0.425	0.9	24.4	"	"
"	40	10	0.40	0.9	25.0	"	"
"	"	5	0.40	1.4	19.0	"	"
"	"	2.5	0.405	2.6	16.8	"	"
"	20	5	0.385	2.6	17.5	"	"
"	10	"	0.38	3.6	12.1	"	"
"	0	"	0.365	3.5	11.8	"	"
0.5	80	"	0.44	1.6	43.1	"	"
"	0	"	0.44	8.7	29.2	"	"
"	40	10	0.425	1.8	50.0	"	"
"	"	5	0.425	2.7	36.5	"	"
"	"	2.5	0.435	4.4	28.0	"	"
"	20	5	0.42	--	--	"	"
"	0	"	0.43	8.2	13.8	"	"
"	0	10	0.405	4.7	16.5	"	"
0	0	5	0.285	0	0	"	3629-3
"	80	5	0.395	"	"	"	"
"	40	10	0.36	"	"	"	"
"	"	5	0.36	"	"	"	"
"	"	2.5	0.36	"	"	"	"
"	20	5	0.34	"	"	"	"
"	10	"	0.32	"	"	"	"
"	0	"	0.255	"	"	"	"
0.0625	"	"	0.335	--	--	"	"
"	40	"	0.375	0.4	5.5	"	"
"	0	"	0.32	--	--	"	"
0.125	"	10	0.35	--	--	"	"

APPENDIX F-4 (Con't)

AIR HALF CELL STUDIES OF
EFFECT OF METHANOL ON PERFORMANCE

Methanol Molarity	Current Density, ma/cm^2	Stoichiometric Air Rate	Cathode Polarization from O_2 Theory, volts	Percent CO_2 in Exhaust	Direct Oxidation, Equivalent ma/cm^2	Temp, °C	Identification
0.125	80	1.25	0.415	1.3	8.0	60	3629-3
"	60	1.67	0.40	1.3	8.0	"	"
"	40	2.5	0.385	1.3	8.2	"	"
"	20	5	0.365	1.2	8.2	"	"
"	10	10	0.355	1.1	7.8	"	"
"	40	5	0.385	0.6	8.2	"	"
0.25	"	"	0.40	1.3	17.7	"	"
0.5	"	"	0.425	2.8	38.0	"	"
0.75	"	"	0.445	4.0	53.7	"	"
1.0	"	"	0.475	5.3	74.0	"	"
"	0	20	0.445	--	--	"	"
"	"	5	0.715	--	--	"	"
"	"	20	0.425	--	--	"	"
"	"	40	0.43	--	--	"	"
0	0	5	0.22	0	0	60	3629-4
"	80	"	0.385	"	"	"	"
"	0	"	0.235	"	"	"	"
"	"	"	0.225	"	"	80	"
"	80	"	0.37	"	"	"	"
"	40	10	0.34	"	"	"	"
"	"	5	0.34	"	"	"	"
"	"	2.5	0.34	"	"	"	"
"	20	5	0.32	"	"	"	"
"	10	"	0.305	"	"	"	"
"	0	"	0.235	"	"	"	"
0.125	"	"	0.35	--	--	"	"
"	80	"	0.395	0.6	16.4	"	"
"	40	10	0.37	0.6	16.8	"	"
"	"	5	0.37	0.8	11.8	"	"
"	"	2.5	0.38	2.0	13.0	"	"
"	20	5	0.36	1.8	12.2	"	"
"	10	"	0.345	3.3	11.1	"	"

APPENDIX F-4 (Con't)

AIR HALF CELL STUDIES OF
EFFECT OF METHANOL ON PERFORMANCE

Methanol Molarity	Current Density, ma/cm^2	Stoichiometric Air Rate	Cathode Polarization from O_2 Theory, volts	Percent CO_2 in Exhaust	Direct Oxidation, Equivalent ma/cm^2	Temp, °C	Identification
0.125	0	5	0.34	3.2	10.8	80	3629-4
0.25	"	"	0.385	--	--	"	"
"	40	"	0.395	2.1	28.4	"	"
"	0	"	0.38	--	--	"	"
"	"	10	0.365	--	--	"	"
0	0	5	0.345	0	0	45	3629-5
"	40	"	0.41	"	"	"	"
"	0	"	0.345	"	"	"	"

APPENDIX F-5

DETERMINATION OF RATE OF METHANOL OXIDATION AT THE CATHODE BY EXHAUST GAS ANALYSIS

The stoichiometric air rate and the extent of direct oxidation of methanol at the cathode are sufficient to fix the oxygen and carbon dioxide concentrations in the exhaust air from a cell. Thus the analysis of these components in the exhaust air is of great help in evaluating cell performance. A simple calculation is as follows:

Reaction	$CH_3OH + 3/2\ O_2 \longrightarrow CO_2 + 2\ H_2O$
Basis	1 mole CH_3OH consumed electrochemically
Inlet Air	79.021% N_2 + inerts
	20.946% O_2
	0.033% CO_2

The carbon dioxide produced by direct oxidation appears in exhaust air but the carbon dioxide from the electrochemical reaction is vented elsewhere. Exhaust gases are analyzed on a dry basis.

Picking three times stoichiometric air (based on electrochemical consumption) and a direct oxidation rate of 50% of the electrochemical oxidation:

Moles inlet gas:

$$O_2 = (3/2)\ (3) = 4.5$$

$$N_2 = \left(\frac{79.021}{20.946}\right)\ (4.5) = 17.0$$

$$CO_2 = \left(\frac{0.033}{20.946}\right)\ (4.5) = 0.0052$$

Moles O_2 Consumed:

$$\begin{array}{l} 3/2 \text{ electrochemically} \\ \underline{(.50)\ (3/2) = .75 \text{ by direct oxidation}} \\ 2.25 \text{ Total} \end{array}$$

Moles CO_2 produced in exhaust air stream = .5

Moles outlet gas:

$$O_2 \quad 4.5 - 2.25 = 2.25 = 11.40\%$$

$$N_2 \quad = 17.00 = 86.04\%$$

$$CO_2 \quad .005 + .5 = \frac{.505}{19.755} = \frac{2.56\%}{100.00\%}$$

For ease in actual application, since gas composition rather than direct oxidation rate is measured, a plot has been made of carbon dioxide vs oxygen concentrations, with percent direct oxidation as a parameter. Cross plotted on these lines are lines of constant stoichiometric air rate. Thus, measuring any two of the parameters of air rate (from a rotameter), percent oxygen or percent carbon dioxide, the third of these and also the per cent direct oxidation is found from the plot.

Gas compositions in present cell analyses are measured with a Beckmann F-3 oxygen analyzer and a Beckmann 1R-315 infrared analyzer referenced for CO_2.

Figure F-1

Analysis of Cell Operation from Exhaust Gas Composition

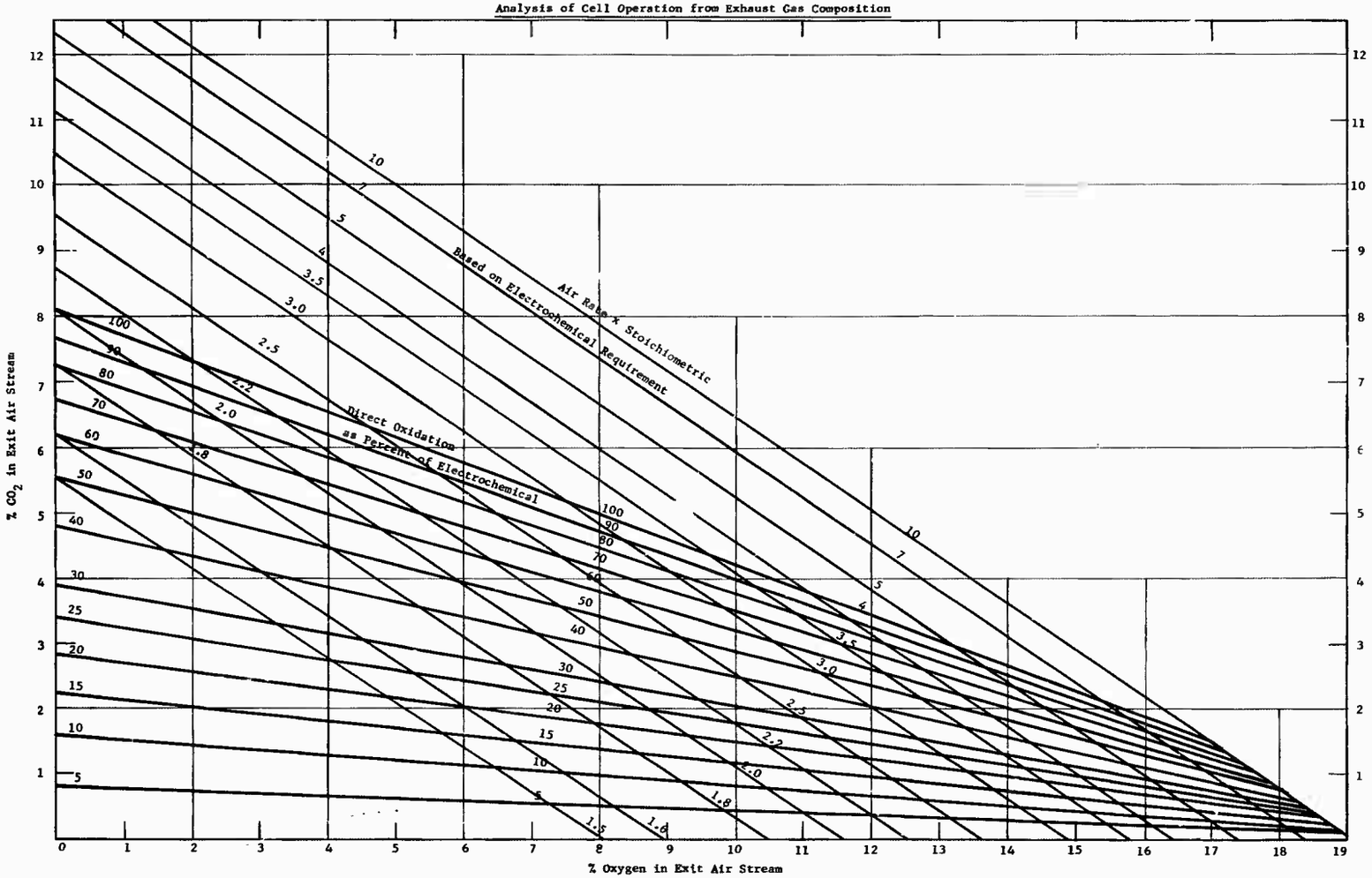

APPENDIX F-6

TOTAL CELL FACILITY USED TO EVALUATE EFFECT OF SURFACTANTS ON METHANOL BATTERY ELECTRODES

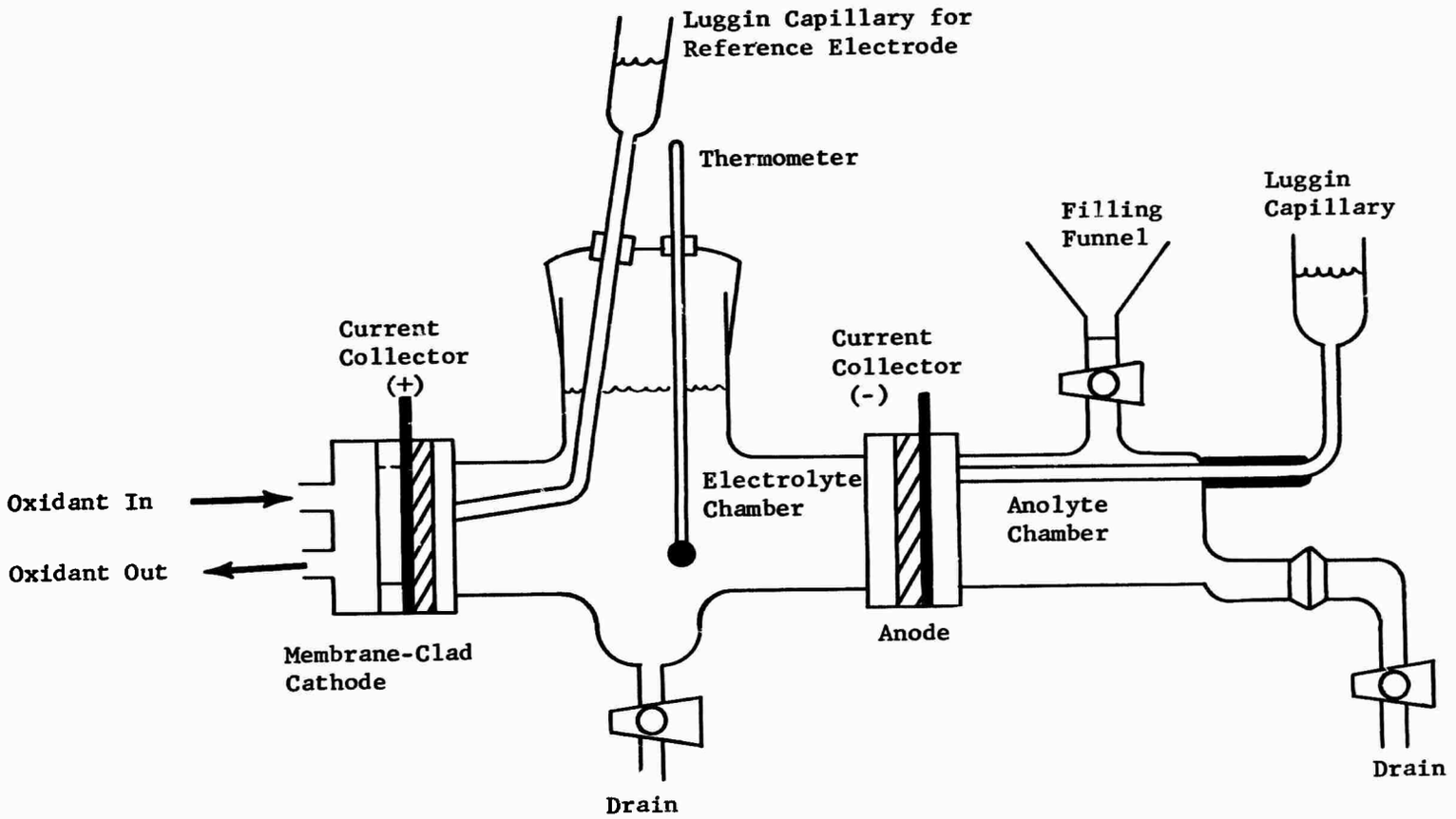

Note: Electrode area was 5.7 cm^2.

APPENDIX F-7

EFFECT OF SURFACTANT ON METHANOL BATTERY ELECTRODES

Oxidant	Surfactant Concentration, wt% (1)	CH_3OH Concentration In Electrolyte Chamber, M (2)	Datum (3)	Ohmic Loss-Free Performance at Indicated ma/cm^2, volts (4) 0	1	5	10	50	100
O_2	0	0	Cell	0.84	0.82	0.63	0.58	0.53	0.44
			Anode	0.03	0.17	0.22	0.25	0.32	0.37
			Cathode	0.33	0.33	0.35	0.36	0.33	0.37
O_2	0	0.5	Cell	0.82	0.73	0.63	0.60	0.50	0.44
			Anode	0.04	0.12	0.21	0.24	0.30	0.34
			Cathode	0.34	0.34	0.35	0.35	0.39	0.40
O_2	0.05	0	Cell	0.77	0.73	0.62	0.58	0.51	0.46
			Anode	--	0.10	0.20	0.23	0.29	0.32
			Cathode	0.34	0.35	0.35	0.35	0.38	0.40
Air	0	0	Cell	0.80	0.75	0.58	0.58	0.40	0.32
			Anode	0.05	0.06	0.22	0.22	0.30	0.33
			Cathode	0.35	0.37	0.39	0.39	0.47	0.53
Air	0	0.5	Cell	0.71	0.68	0.54	00	0.40	0.32
			Anode	0.06	0.10	0.21	--	0.34	0.33
			Cathode	0.43	0.43	0.44	--	0.49	0.54
Air	0.05	0	Cell	0.70	0.68	0.52	0.48	0.38	0.30
			Anode	0.04	0.07	0.20	0.25	0.30	0.32
			Cathode	0.43	0.44	0.45	0.45	0.50	0.55

(1) 3M FC-95 surfactant.

(2) See diagram of Test cell in Appendix F-6.

(3) Anode contained 25 mg/cm^2 H_2 reduced form of Ru modified p-type catalyst on 50 mesh Ta screen. Cathode was pressed Cyanamid AA1/Pernsion 1010 Membrane.

(4) Anolyte chamber contained 1 M CH_3OH in 3.7 M H_2SO_4. Cell temperature was 60°C. Ohmic-free performance measured with Kordesch-Marko bridge.

APPENDIX F-8

TOTAL CELL OPERATION STUDIES

3.7 M H_2SO_4
H_2 Reduced Ru Mod P-type Anode
Permion 1010 Membrane Clad, American Cyanamid AA1 Cathode

Ident.	Mode of Operation	Temp, °C	Feed Rate	Methanol Concentration in Feed, vol %	Cell Volts	Anode Polarization from Theoretical Methanol, volts	Current Density, ma/cm^2	IR, Volts	Air Times Stoichiometric	CO_2 % in Exhaust	Direct Oxidation, ma/cm^2	Comments
1216	Direct Feed	25	1.2 x Stoich.	50%	0.26	0.41	40	0.04	5	--	--	Leaky teed element.
"	"	"	"	"	0.28	0.41	"	0.04	10	--	--	
0105	"	62	1.4 x Stoich.	"	0.42	0.33	"	0.03	3.5	--	--	
0106	"	"	1.3 x Stoich.	"	0.36	0.39	"	0.03	3.0	--	--	
0107	"	"	1.4 x Stoich.	"	0.39	0.38	"	--	3.5	2.1	20	
"	Circulating	64	50 cc/hr	4%	0.41	0.34	"	--	3.5	5.1	46	
0122	Direct Feed	60	1.4 x Stoich.	50%	0.44	0.32	"	.035	3.5	--	--	Cell rebuilt-differences in end plate.
0225	"	"	1.4 x Stoich.	50%	0.44	0.27	"	0.032	3.0	2.1	17	
0226	"	"	1.21 "	"	0.365	0.435	"	0.035	3.5	--	--	
"	Circulating	"	50 cc/hr	4%	0.32	0.41	"	0.035	5.0	1.0	13	
0312	Circulating	"	42 cc/hr	4%	0.44	0.285	"	0.045	5.0	1.2	16	
"	Direct Feed	"	1.5 x Stoich.	50%	0.43	0.33	"	0.047	5.0	--	--	
"	Direct Feed	"	1.21 x Stoich.	"	0.36	0.44	"	0.05	5.0	0.45	6	
"	"	"	1.72 "	"	0.40	0.35	"	0.057	5.0	--	--	
0326	Circulating	"	90 cc/hr	2%	0.44	0.33	"	0.035	3.4	1.0	9	
0331	Direct Feed	"	1.3 x Stoich.	50%	0.50	0.27	"	0.032	2.7	2.1	15	
"	"	"	1.3 x Stoich.	"	0.32	0.32	80	0.07	2.5	1.6	10.5	
0401	Circulating	"	90 cc/hr	2%	0.43	0.34	40	--	3.5	0.7	6.5	New membrane installed.
0402	"	"	--	2%	0.45	0.325	"	--	3.5	0.85	8	
"	Direct Feed	"	1.21 x Stoich.	25%	0.465	0.305	"	--	3.5	1.3	10	

APPENDIX P-8 (Con't.)

TOTAL CELL OPERATION STUDIES

Ident.	Mode of Operetion	Temp, °C	Feed Rate	Methanol Concentretion in Feed, vol %	Cell Volts	Anode Polerizetion from Theoretical Methenol, volts	Current Density, ma/cm²	IR, Volts	Air Times Stoichiometric	CO_2 % in Exheust	Direct Oxidation ma/cm²	Comments
0421	"	"	1.21 x Stoich.	50%	0.425	0.26	"	0.06	3.5	1.05	10	Felt diffusion barrier.
"	"	"	1.10 x Stoich.	"	0.415	0.28	"	0.06	3.5	0.05	4.4	Felt diffusion barrier.
0430	Circuleting	"	117 cc/hr	2%	0.425	0.29	"	0.05	2.5	0.25	1.5	Polyox diffusion 1:20 p.m. barrier.
"	"	"	82 cc/hr	"	0.372	0.298	"	0.05	2.5	0.25	1.5	Polyox diffusion 2:00 p.m. barrier.
"	"	"	112 cc/hr	"	0.305	0.320	"	0.07	2.5	0.4	2.5	Polyox diffusion 4:30 p.m. barrier.
0506	"	"	117 cc/hr	"	0.425	0.29	"	0.05	2.5	0.25	1.5	Polyox diffusion 1:20 p.m. barrier.
		"	82 cc/hr	"	0.375	0.298	"	0.05	2.5	0.25	1.5	Polyox diffusion 2:00 p.m. barrier.
		"	112 cc/hr	"	0.305	0.320	"	0.07	2.5	0.4	2.5	Polyox diffusion 4:30 p.m. barrier.
0507		"	90 cc/hr	"	0.190	0.360	"	0.115	2.9	-	--	Polyox diffusion 4:30 p.m. barrier.
0527	Batch	25	--	"	0.57	--	1		--	--	--	Cell with cethode directly exposed to air.
	"	"	--	"	0.53	--	2	--	--	--	--	"
	"	"	--	"	0.46	--	5	--	--	--	--	"
	"	"	--	"	0.41	--	10	0.013	--	--	--	"
	"	"	--	"	0.36	--	20	0.023	--	--	--	"
	"	"	--	"	0.28	--	40	0.045	--	--	--	"
	"	"	--	"	0.20	--	70	0.075	--	--	--	"
	"	"	--	"	0.12	--	100	0.10	--	--	--	"
0528	"	"	--	"	0.66	0.105	1	--	--	--	--	"
	"	"	--	"	0.54	0.23	2	0.005	--	--	--	"
	"	"	--	"	0.46	0.27	5	0.008	--	--	--	"
	"	"	--	"	0.43	0.28	10	0.013	--	--	--	"
	"	"	--	"	0.30	0.33	40	0.045	--	--	--	"
	"	"	--	"	0.22	0.355	70	0.075	--	--	--	"
	"	"	--	"	0.14	0.37	100	0.09	--	--	--	"

APPENDIX G-1

METHANOL MULTICELL ASSEMBLY

The Methanol Multicell Assembly represented the center of the system. Enclosed in the metal case were the sixteen cell stack, the blower along with its controls, and meters for monitoring output current and voltage. The cells were connected in series to a receptacle located on the front panel. The blower operated directly from the stack. The electronic circuitry controlling the air flow produced by the blower was mounted inside the removable front panel.

Metal Case

The metal case was constructed of aluminum in two sections. The rear section housed the sixteen cells. These could be exposed to view by unlatching the metal catches at the base, then raising and unhooking the two panels. The stack could be detached from its base and the front section by removing all the screws except the bottom ones that were located along the seam between the front and rear sections. However, before sliding the stack out, the control knob had to be disengaged from its internal linkage by pulling it outward in its OFF position and rotating it counter-clockwise 180°. This knob controlled the butterfly valve located between the air blower and the stack. Its function was to prevent corrosive vapors from coming in contact with the blower during shutdown. The wires connecting the stack to the control panel in the front section were permanently attached.

Sixteen Cell Stack

The sixteen cell stack consisted of seventeen polypropylene frames, gasketed together with viton rubber to prevent leakage. With the exception of the two end frames, each frame supplied either electrolyte or air to two adjacent anodes or cathodes. The two end frames supplied air to only the end cathodes. Air entered from a common manifold through twenty holes along the top of each frame, flowed through the two separate cell compartments and exited through 14 holes along the bottom into a common exhaust manifold. Electrolyte containing methanol was fed to each frame from two inlet manifolds, flowed upwards and out two ports on the top sides of the frames. The carbon dioxide was carried out with this recycle stream and was exhausted outside the case. Figures G-1 and G-2 schematically illustrate the electrolyte and air flow patterns to the stack and within the frames.

Each individual cell contained an anode and cathode, two current collectors, two polypropylene support springs, an electrode separator also serving as the frame gasket, and a membrane. These components are shown in Figure G-3. The current collectors were connected to each other in series on top of the stack by means of two fixtures, which pressed the individual gold tabs together.

Figure G-1

Electrolyte and Air Flow Patterns to Sixteen Cell Stack

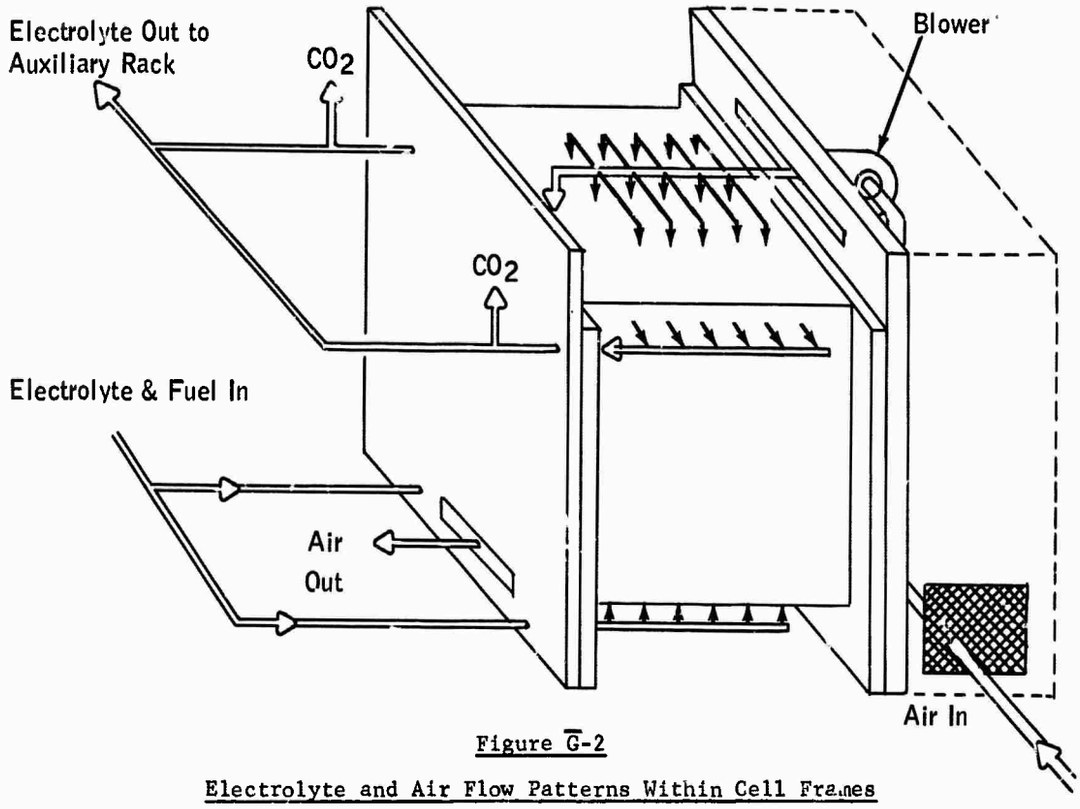

Figure G-2

Electrolyte and Air Flow Patterns Within Cell Frames

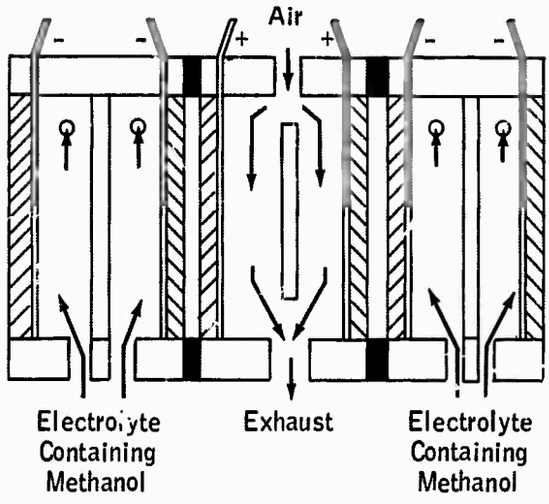

Figure G-3

Individual Cell Components

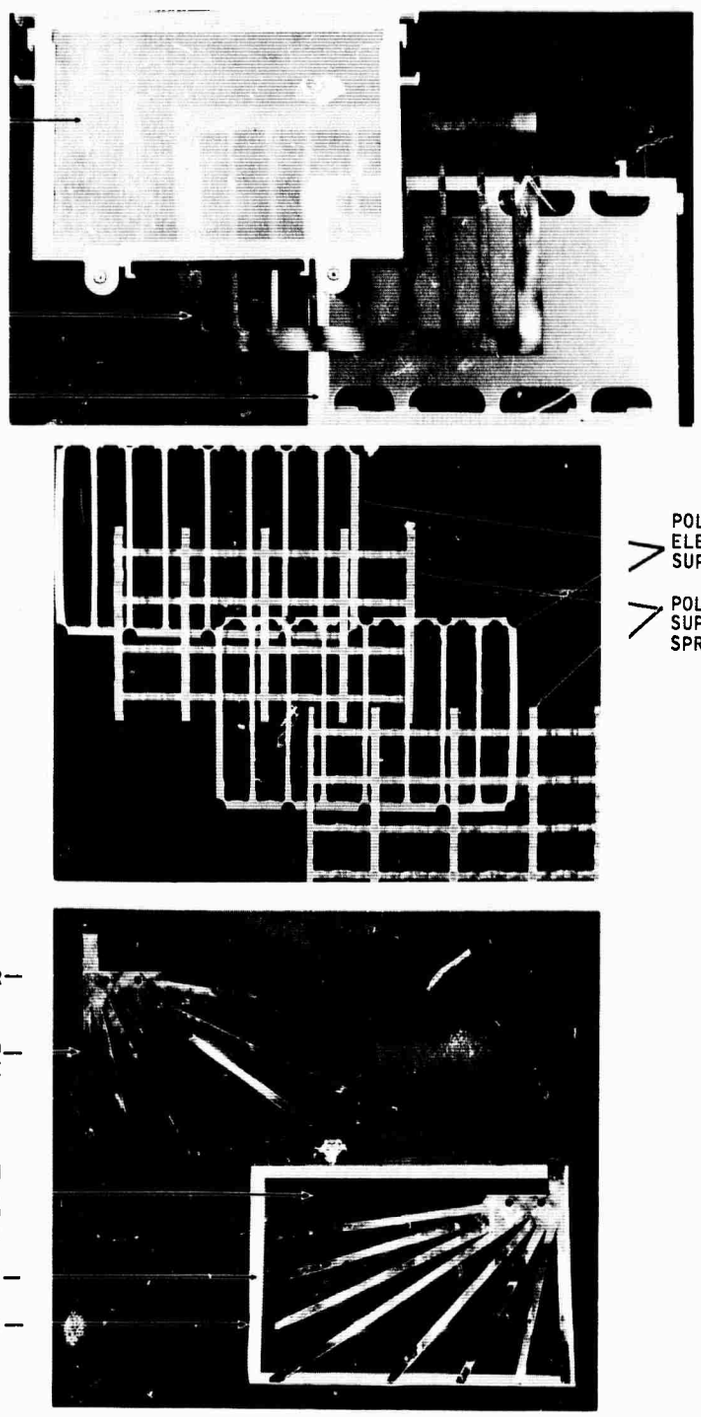

Electrical Circuitry

The electrical circuitry included in the Multicell Assembly was used to supply and monitor the power output from the unit and to control the air output of the blower. Figure G-4 illustrates the relationship between these components, most of which were mounted on the small removable front panel.

Figure G-4

Methanol Multicell Assembly
Electrical Circuit

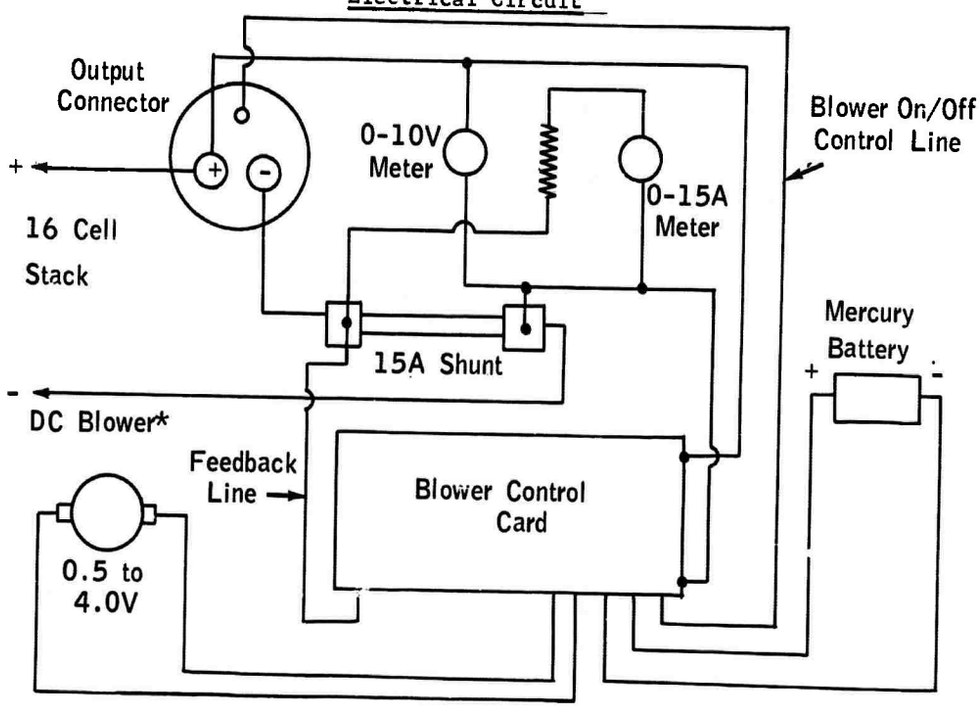

Two small meters on the front panel indicated output voltage and current The voltmeter was a 1000 ohm per volt instrument with a full scale range of 10 volts. Current, up to 15 amperes, was indicated on a 50 millivolt meter connected through a series resistor across a 15A-100 mv shunt. The shunt voltage drop was also used as feedback voltage to control the air supply blower speed.

A heavy duty output connector provided two large pins for connection to the load and a small pin which was used for blower circuit switching. Insertion of the load plug into the output connector socket actuated the blower circuit through a small wire jumper between the small connector pin at the negative side of the load. Removal of the load plug automatically stopped the blower.

Figure G-5

Blower Control Circuitry

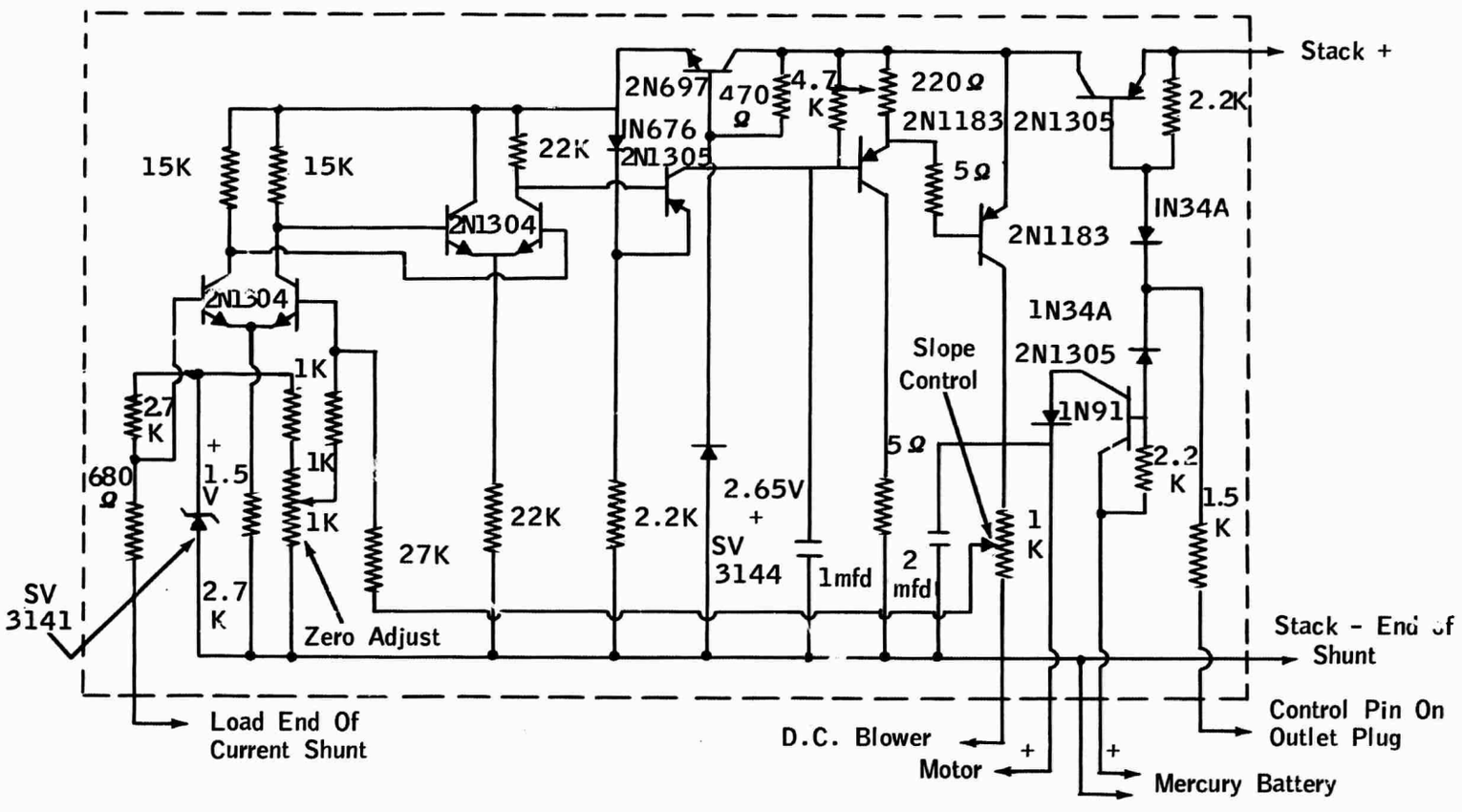

After extended periods of storage the stack voltage on start-up might have been below the blower starting level. Therefore, a 1.34 volt mercury battery was provided to start and operate the blower under this condition. Electronic circuitry in the blower control card automatically switched the blower to the battery when the load plug called for power and the stack voltage were below 1.3 volts. The battery was mounted on the back of a small removable plate on the right side of the assembly. Under typical operating conditions the battery might be replaced at six month intervals to ensure its operability.

The transistor circuitry used in the blower control system is shown in Figure G-5. This includes, a temperature stabilized DC amplifier, voltage reference diodes and switching circuits. Two switching transistors were actuated by the auxiliary contact in the output plug to connect the regulator circuit to the cell stack and the battery to the blower circuit. A small series diode prevented current flow in the dry cell loop when the stack voltage became the blower power source. The DC amplifier supplied voltage to the blower between a preset level at zero current through the reference shunt and an upper limit which was approached linearily as a function of increased current through the shunt. A typical performance curve is shown in Figure G-6.

Figure G-6

Blower Control Characteristics

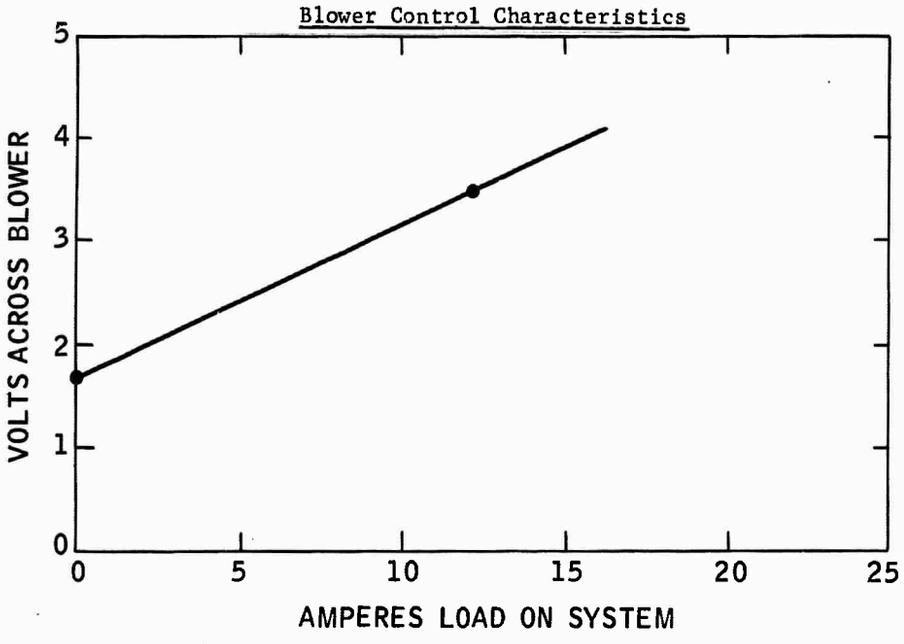

Increasing the voltage to the blower increased the air rate. Since blower voltage was controlled by the current, the air rate also responded to changes in current. Typical performance response to changes in blower voltage is shown in Figure G-7.

Figure G-7

Effect of Blower Voltage on Stack Performance

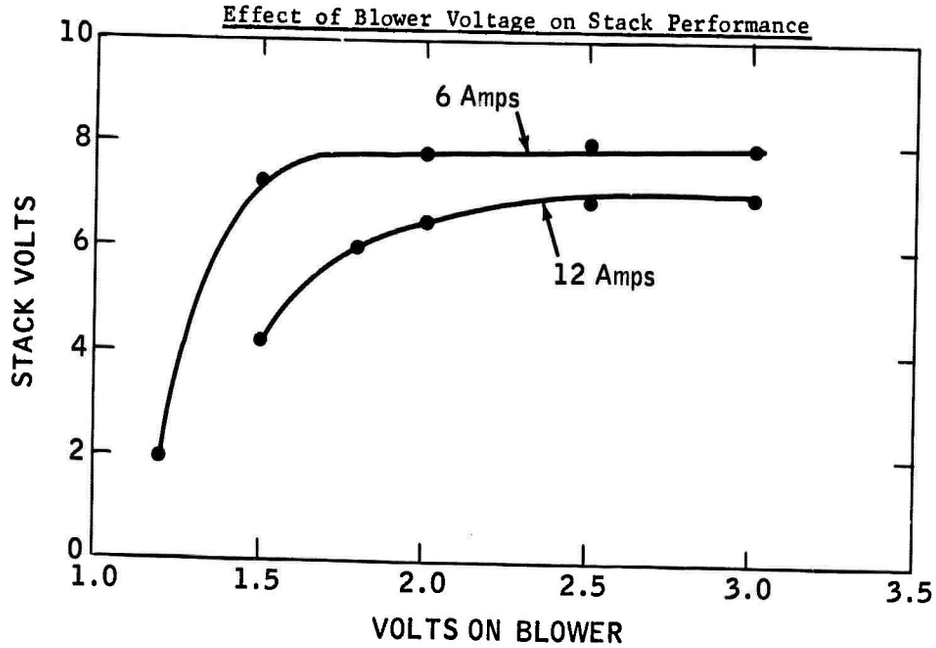

Two small holes in the front panel to the right of the ammeter provided means for adjusting the blower control with a 1/8" diameter screw driver. The lower adjustment hole lined up with the zero set control and was adjusted to about 1.7 volts at the blower. The upper adjustment controlled the control slope and was adjusted to provide about 3.5 volts at the blower with a 12 A load on the system. A small marked wire behind the dry cell plate was connected to the positive blower terminal. The negative side of the blower was common with the negative battery terminal. Regulation of the blower voltage was independent of stack voltage variations provided that the stack voltage exceeded the blower requirements by 0.5 volts.

APPENDIX G-2

AUXILIARY RACK

As previously indicated, the Auxiliary Rack contains the components essential to the operation of the individual cells, that had not yet been tailored for encorporation into the Multicell Assembly. These components were standard laboratory devices. Together, they controlled the methanol and sulfuric acid concentrations within the multicell stack. Functionally they controlled the methanol and water addition rates to the multicell assembly. Also, included on the rack was a load bank of resistors for conveniently dissipating the power produced by the Methanol Multicell Assembly.

The Auxiliary Rack

The Auxiliary Rack, itself, was a laboratory rod framework, 18" wide x 24" high x 15" wide. The major components mounted on it were the methanol, water, and electrolyte recycle tanks, their pumps, and controls. The overall assembly is shown in Figure G-8.

Figure G-8

Auxiliary Rack

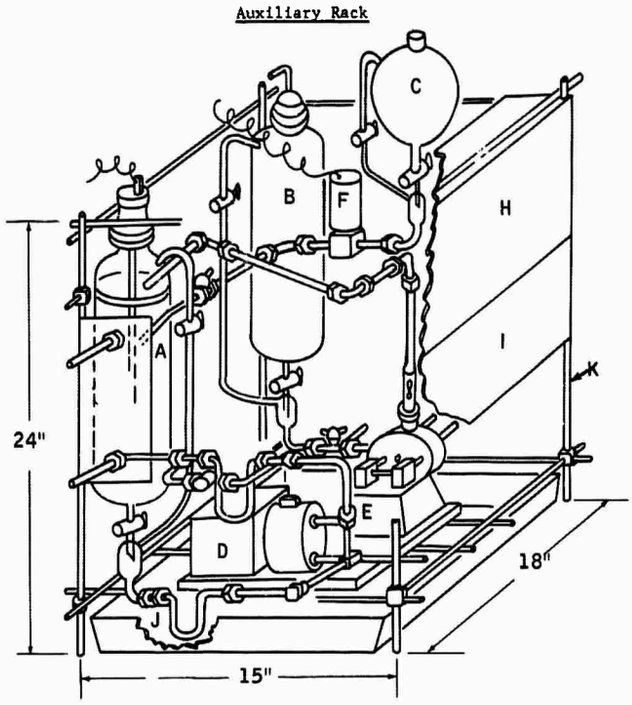

A = Electrolyte Recycle, Tank, 500 ml
B = Methanol Tank, 500 ml
C = Water Make-up Tank, 900 ml
D = Electrolyte Recycle Pump (Mace)
E = Methanol Pump (Buchler)
F = Water Level Control Solenoid (Mace N.C.)
G = Level Control Sensor
H = Electrical Load Panel
I = Rate and Level Controls
J = Auxiliary Electrolyte Pump Check Valves
K = Lab Rod (3/8")Frame: 15" x 18" x 24"

The functions of these components is best shown in the schematic drawing of the flow system represented in Figure G-9. Methanol was pumped to the electrolyte recycle tank at a rate dictated by the current flowing from the Multicell Assembly. Water loss from the system was reflected as a drop in the electrolyte recycle tank level. Water was gravity fed through a solenoid valve to this tank in response to a liquid level controller. The electrolyte with the added methanol was then circulated through the Multicell Assembly, its rate also being dictated by the current output from the Multicell Assembly.

Figure G-9

Schematic Flow Plan of Auxiliary Rack

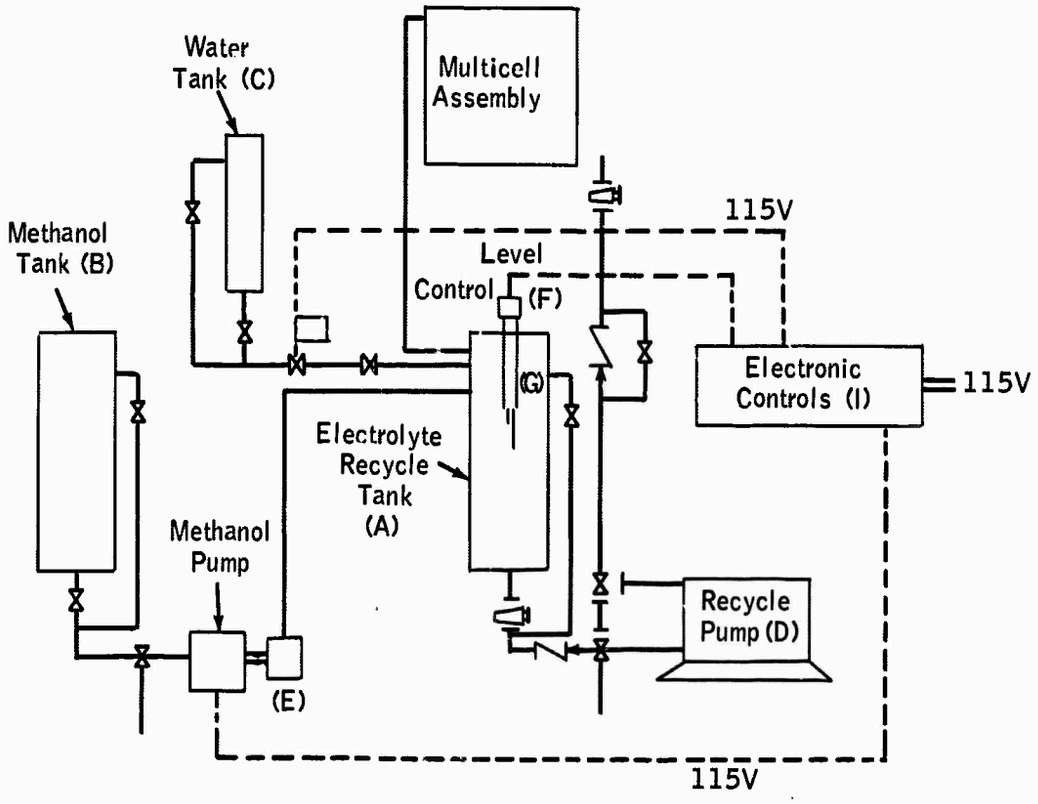

Methanol, Water and Electrolyte Feed Rate Controls

The lower chassis on the front of the Auxiliary Rack contained the electrical equipment for controlling the methanol feed rate, electrolyte recycle rate and the liquid level in the recycle tank. This equipment was powered by 115 v AC from the power line. The front panel of this chasis is shown in Figure G-10. Details of the AC power wiring are shown in Figure G-11.

Figure G-10

Front Panel of Feed Rate Controller

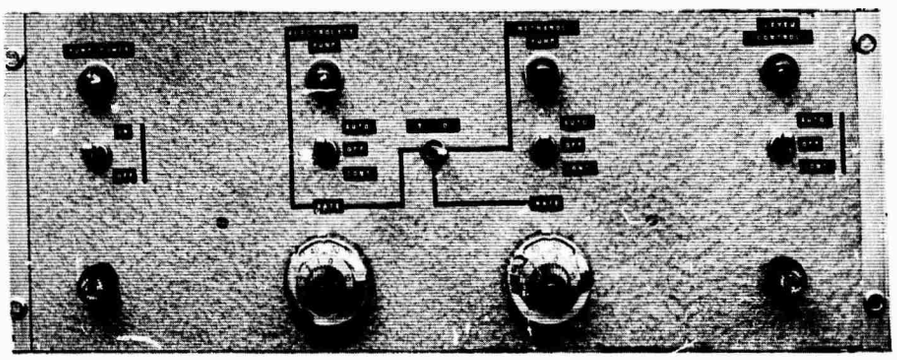

In addition to the main pump power switch, separate switches were provided for the electrolyte pump, methanol pump and liquid level controller. These switches had 3 positions: "OFF", "CONT." and "AUTO". The "CONT." position afforded a means for running the pumps at their maximum rate setting or for adding water at any time the operator desired. In the "AUTO" position the pumps and the water level controller were actuated by the electronic circuitry in the control chassis.

For water addition, the 115 v AC, solenoid was actuated by the lack of electrolyte at the proper level in the electrolyte recycle tank. If electrolyte was below the proper level, a very small DC current flowed through the circuit formed by the platinum wire level sensing probe. This current was amplified by a transistor amplifier and actuated a mercury relay which disconnected the AC power to the liquid level control solenoid.

Pumping rates in the "AUTO" position were varied by changing the percentage of time the pump operated. This was accomplished electronically by changing the time constant of an RC circuit in a hybrid timing circuit using a unijunction and two NPN transistors. The electrolyte pump control had a basic cycle of about 12 seconds. Percentage of time "ON" for this controller was adjusted from 5 to 95 percent depending on the setting of the electrolyte pump RATE dial. A complete rate calibration curve is shown in Figure G-12. The methanol pump rate controller had a basic cycle of about 120 seconds and was adjusted by the RATE dial under the methanol pump switch. The calibration for this rate controller is also shown in Figure G-12.

Figure G-11

AC Power Circuit for Auxiliary Rack

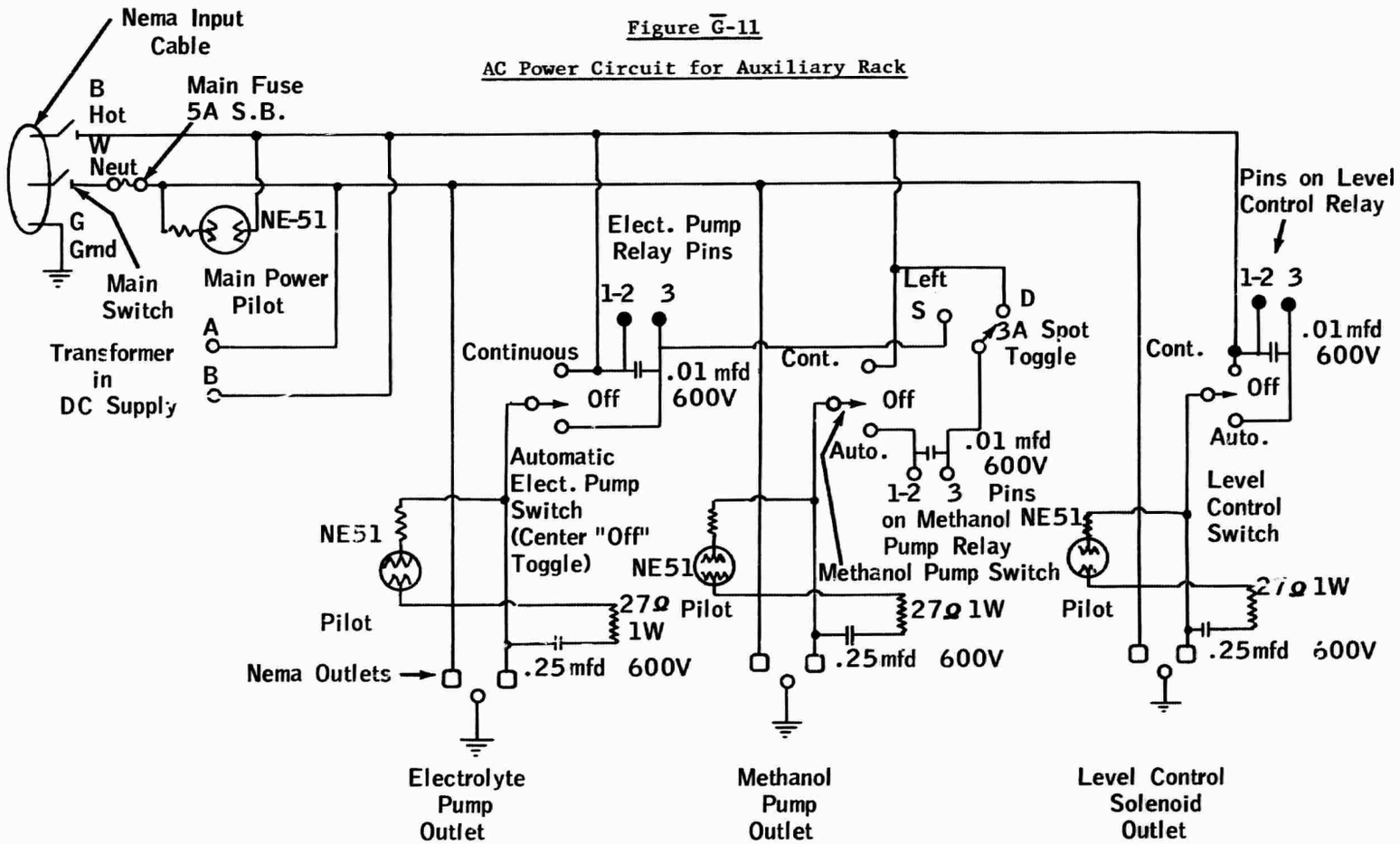

Figure G-12

Electrolyte and Methanol Pump Vernier Calibrations

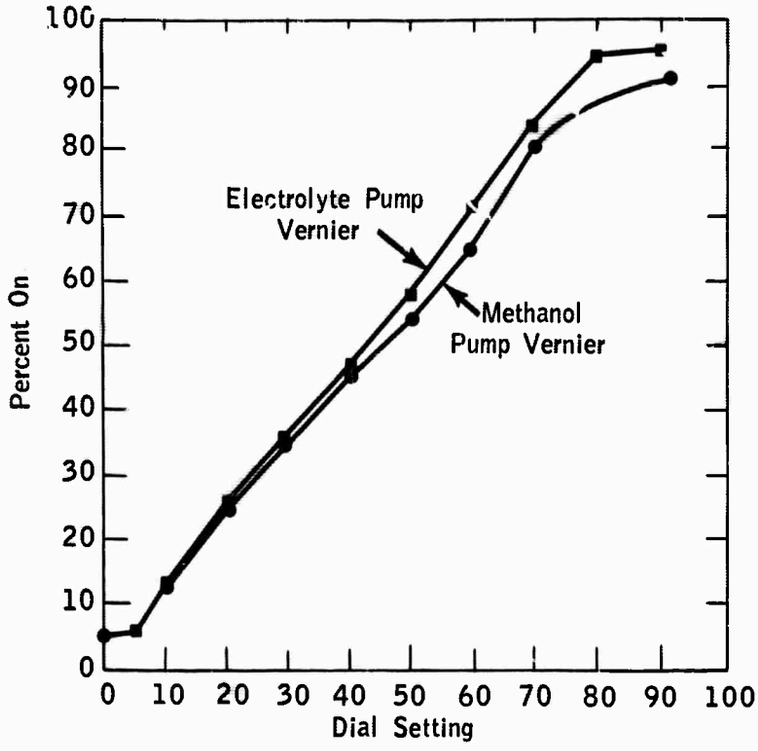

The complete circuit of the electronic controls and the DC power supply to operate the transistor and relay circuitry is shown in Figure G-13. It should be noted that the fuse below the liquid level control switch was connected to the DC power supply circuit.

The switch between the electrolyte pump switch and the methanol pump switch marked "S" and "D" provided a means for operating the methanol rate control directly (position "D") or as a percentage of the rate of the electrolyte pump controller (position "S"). However, this switch was generally position.

Electrical Load Panel

An electrical load panel was provided as a convenience for dissipating the output from the Methanol Multicell Assembly. The electrical load, designed to handle 15 amps, and 100 watts, was located at the top of the rack. The front panel is shown in Figure G-14.

Figure C-13

Pump Rate and Liquid Level Controls

For Methanol Multicell Assembly

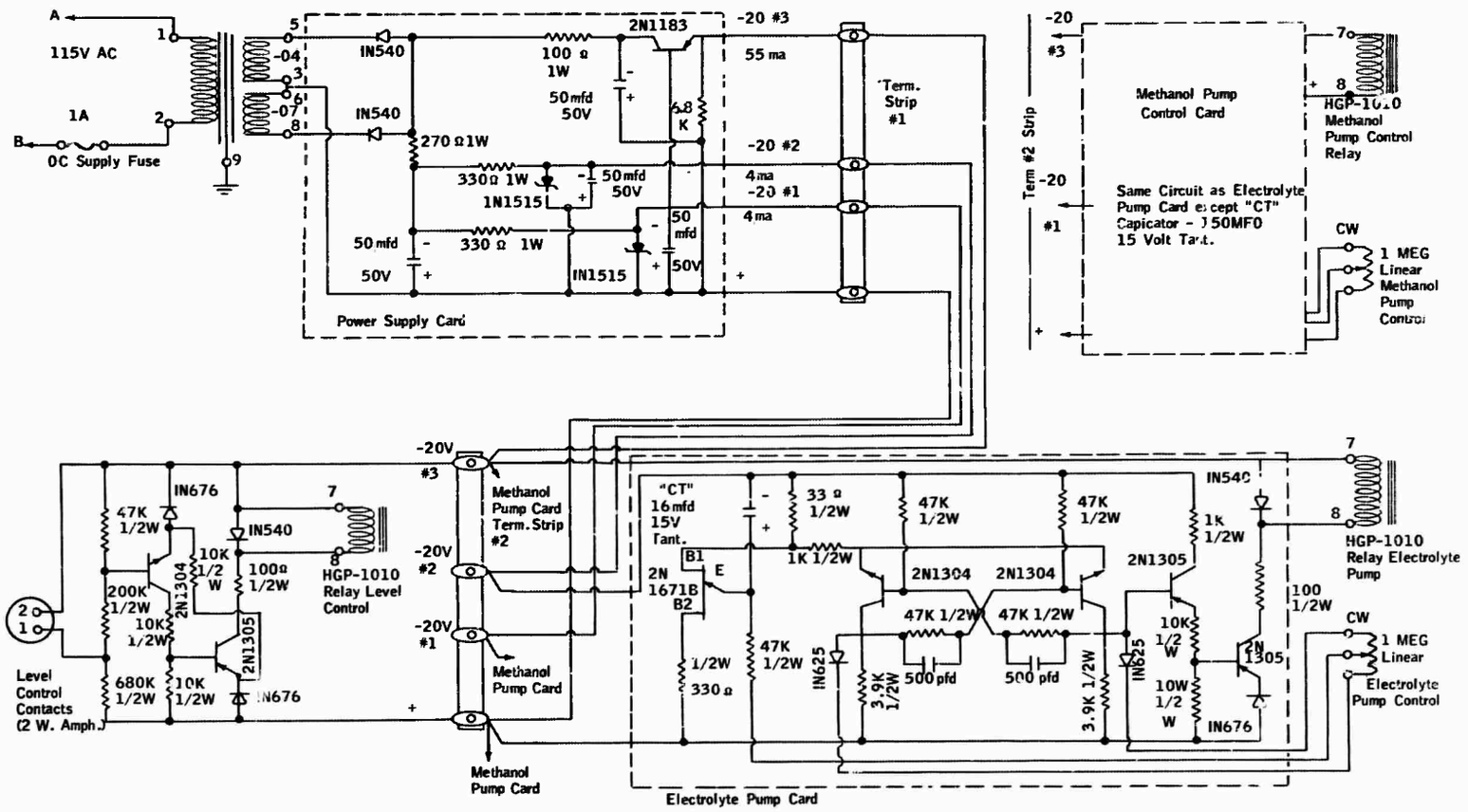

Figure G-14

Front Panel of Electrical Load

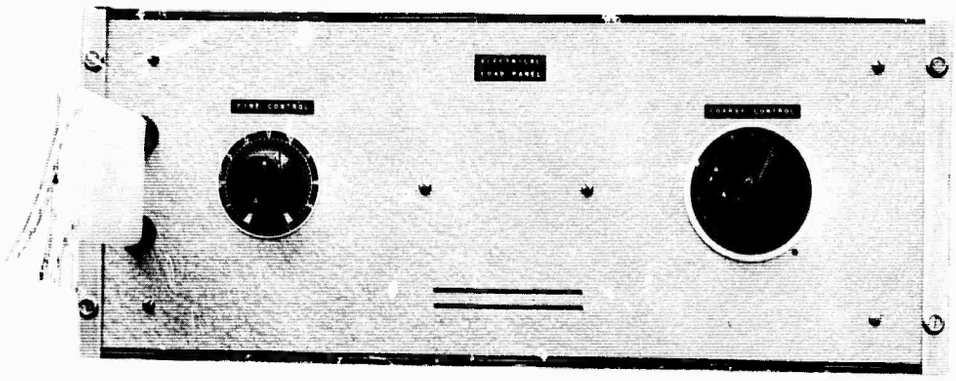

The left hand dial controlled a variable 0.5 ohm resistor. Additional series resistors were added by the switch on the right in 0.5 ohm steps up to 4 ohms on position 9. Position 10 added a 10 ohm series resistor to the load circuit. The circuit and resistor values are shown in Figure G-15.

Figure G-15

Electrical Load Panel

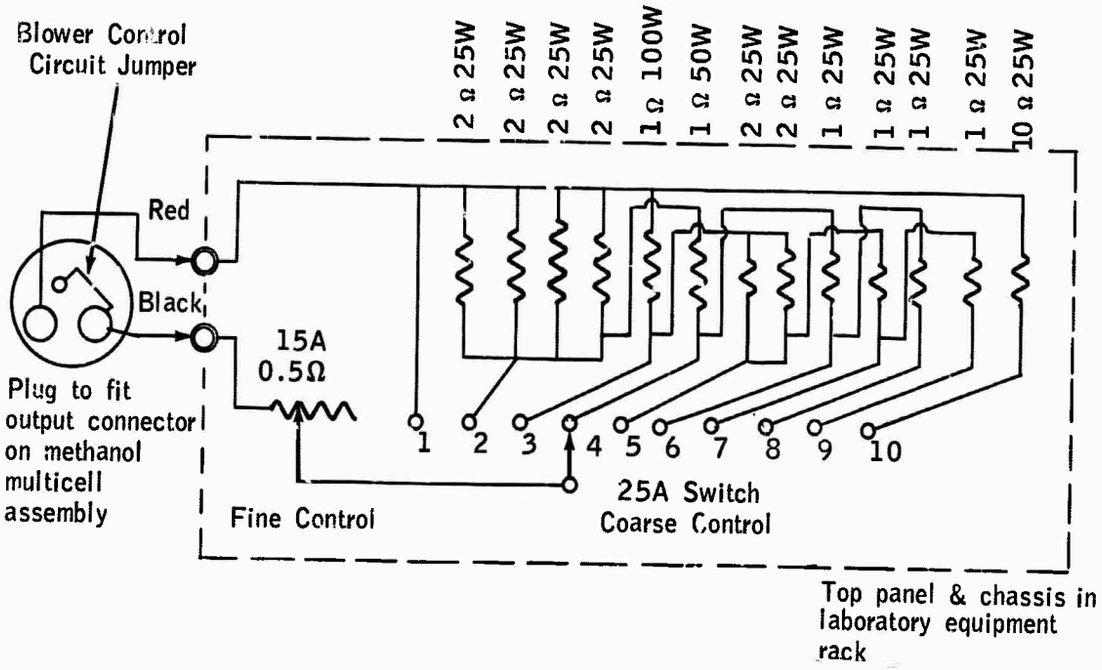

The lower panel and chassis contained the electrical equipment associated with the pumps and liquid level controller. This equipment was powered by 115 v AC from the power line. Details of the AC power wiring were also shown in Figure G-11.

Principles of Methanol Feed Control

The rate of methanol addition was programmed into the system rather than being independently controlled. The basis of this program is the fact that performance of the Methanol Multicell Assembly remained relatively constant over narrow, but reasonably controllable, ranges of methanol concentrations and electrolyte circulation rates.

The major factor dictating the size of this performance plateau was the methanol concentration in the cells. Too much methanol resulted in excessive methanol at the cathode, and too little starved the anode. However, other factors were also important. For example, a high electrolyte flow rate was undesirable, since it meant excessive pump sizes and high power demands. Figure G-16 shows a typical plateau pattern for this assembly. As can be seen in this figure, the methanol concentration and pump rate could each vary by about 25% without impairing performance.

Figure G-16

Typical Plateau for Maximum Performance

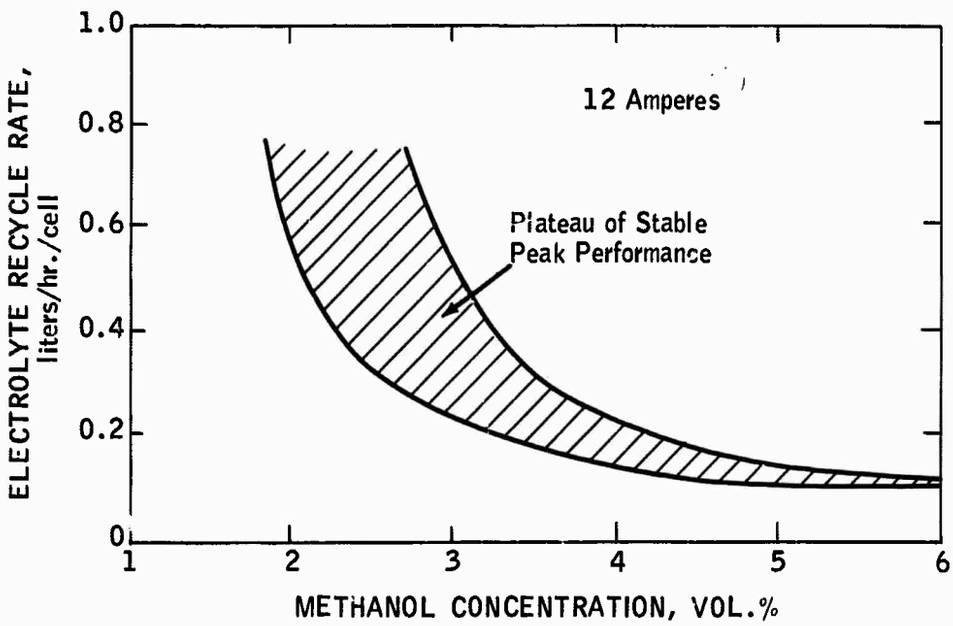

This latitude was needed to adjust for small errors in pump rates, and changes in the extent of chemical oxidation within the system. About 5 hours of unimpaired operation should have been obtained if the system was operating within the required limitations.

Various plateau profiles were obtained at currents up to 18 amperes. These were used to determine the recommended methanol feed rates and electrolyte, shown in Figures $\bar{G}$-17 and $\bar{G}$-18. The methanol feed rate took into account methanol consumed by chemical as well as by electrochemical oxidation. In addition, somewhat higher methanol feed rates were recommended during startup to ensure against the greater danger of methanol starvation.

Figure $\bar{G}$-17

Recommended Methanol Feed Rates

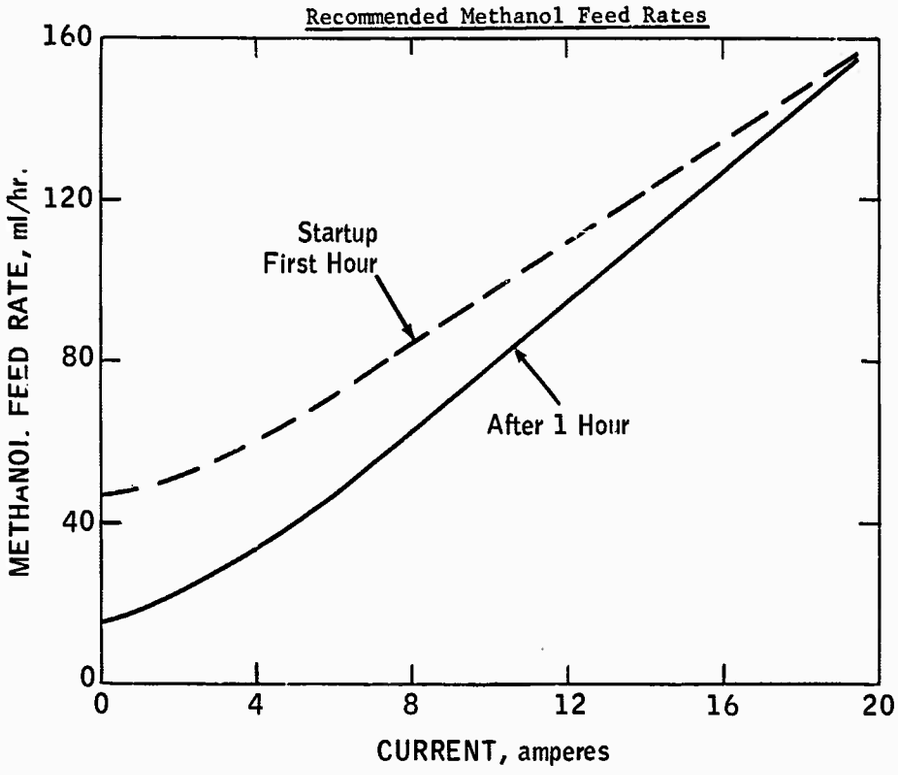

Figure G-18

Recommended Electrolyte Recycle Rates

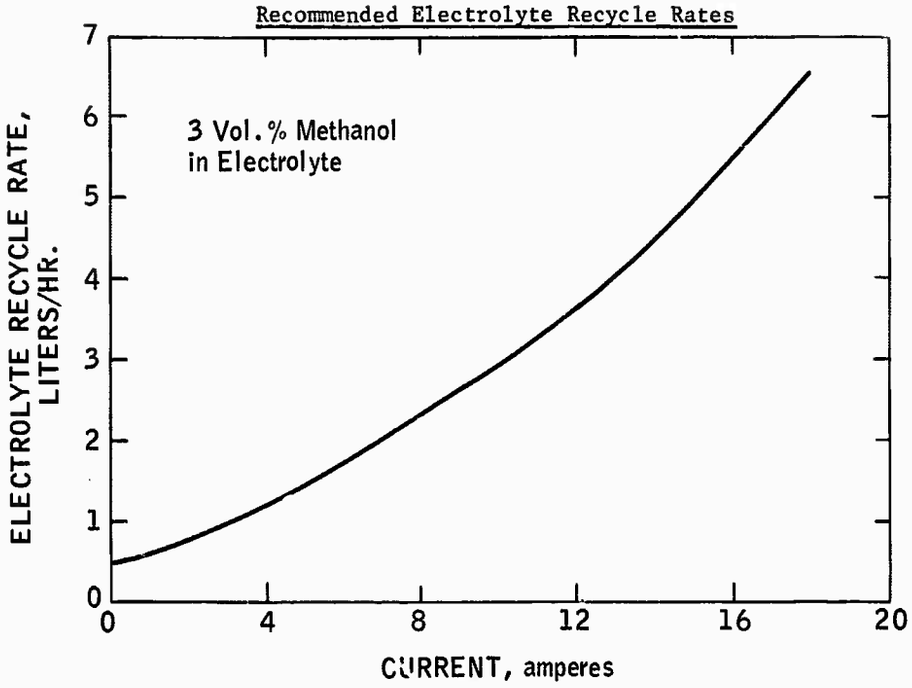

The methanol feed pump was set to feed fuel at a rate of 225 ml/hr. Its rate was changed by adjusting the back nuts, thus varying the pump stroke. The electrolyte rate was fixed at 8.2 liters/hr by setting the vernier on the pump to 8. The recommended flow rates, divided by the maximum rates, times 100, gives the required percentage of time the pumps were on. Figure G-12 gave the corresponding control panel vernier settings needed to accomplish this. Because of the importance of these pump rates, it was recommended that they be checked whenever the unit was not operating at the expected levels.

APPENDIX G-3

INITIAL PERFORMANCE OF METHANOL MULTICELL UNIT

Current Density, $ma./cm^2$	Battery Performance (1)	
	Voltage	Power, Watts
0	10.0+	0
3.3	10.0+	--
16.7	8.3	42
20	7.9	47
33.3	6.8	68
40	6.3	76
50	5.6	84

(1) Run 3330-8, 65-1-4.

APPENDIX G-4

METHANOL PERFORMANCE OF SIXTEEN CELL BATTERY WITH CONVENTIONAL TANTALUM SCREEN ANODES

Current Density ma/cm^2	Battery Performance (1)	
	Voltage	Power, Watts
0	11.5	0
10	7.8	23
20	6.0	36
40	4.2	50
50	3.0	45

(1) Run 3330-11, 65-1-29. 0.75 M CH_3OH in 3.7 M H_2SO_4, 50% nominal conversion per pass, 10 times stoichiometric air rate. Anode contained 25 mg/cm^2 of Ru modified P-type catalyst prepared by hydrogen reduction pressed at 3000 psi onto a 9" x 5 3/4" 50 mesh Ta screen. Cathodes were Cyanamid AA-1 with pressed Permion 1010 membrane.
Operating temperatures were:

Fuel in	38°C
Air in	27
Air out	62
Cell Range	60-71

Ohmic losses for battery were 4.26 volts at $100ma/cm^2$.

APPENDIX G-5

INITIAL PERFORMANCE OF SIXTEEN CELL METHANOL BATTERY WITH GOLD-PLATED TANTALUM SCREEN ANODES

Current Density, mA/cm^2	Battery Performance (1)	
	Voltage	Power, Watts
0	11.6	0
20	8.5	51
33.3	7.5	75
40	7.3	88
50	6.6	99
60	6.0	108
70	5.6	118

(1) Run 3330-14, 65-2-10. Run conditions same as those for Run 3330-11, 65-1-29 listed in Appendix G-4, except for use of gold-plated tantalum screens for anodes. Ohmic loss tor battery was 1.82 volts at 100ma/cm^2. Additional operating data for this run are given in Appendices G-9 and G-10.

APPENDIX G-6

VARIATION OF SIXTEEN CELL STACK PERFORMANCE WITH TIME

Time on Current, hrs	Current Density, ma/cm^2(1)	Stack Potential, Volts	Stack Power, watts	Average Cell Potential, volts
0	0	11.6	0	0.72
	20	8.5	51	.53
	33.3	7.75	78	.48
	40	7.3	88	.46
	50	6.6	99	.41
	60	6.0	108	.38
	70	5.6	118	.35
60	0	11.2	0	0.70
	10	8.8	26	.55
	40	6.9	83	.43
	50	6.0	90	.38
	80	4.6	110	.29
235	20	8.0	48	0.50
	40	6.6	79	.41
	80	4.4	106	.27
275	0	11.3	0	0.71
	3.3	9.7	10	.61
	10	9.0	27	.56
	20	8.05	48	.50
	40	6.8	82	.42
	60	5.85	105	.37
	80	4.95	119	.31

(1) 0.75 M CH_3OH in 3.7 M H_2SO_4, 50% conversion per pass, 8.4 times stoichiometric air rate.

APPENDIX G-7

VARIATION OF OHMIC LOSSES IN SIXTEEN CELL STACK WITH TIME

	Ohmic Losses at 100 ma/cm^2 at Indicated Hours on Current, mv:[1]					
Cell Number	1	20	45	94	163	213
1	108	-	121	158	165	123
2	113	-	113	117	125	117
3	108	-	119	133	125	125
4	107	-	113	117	117	123
5	109	-	125	135	127	133
6	113	-	113	109	113	113
7	125	-	137	145	141	141
8	117	-	125	125	137	145
9	117	-	113	158	153	141
10	113	-	121	121	133	133
11	125	-	133	141	137	137
12	113	-	121	113	113	113
13	107	-	129	133	111	113
14	113	-	133	141	119	125
15	108	-	111	117	129	117
16	119	-	137	158	141	137
Total	1818	1868	2016	2020	2020	2020
Average per Cell[2]	114	117	126	126	126	126

(1) Measured with AC technique (6).
(2) Calculated from measured value for total stack.

APPENDIX G-8

EXPLANATORY NOTES ON COMPUTED DATA

The data preaented in Appendices G-9 and G-10 were obtained from the sixteen cell stack during Run No. 3330-14. Explanatory notea on the atack components and computational procedurea are liated below.

A. Stack Detaila

The stack contained sixteen cella connected in series. The 9" x 5-3/4" anodea were numbered FC-108 through FC-123 and contained 25 mg/cm^2 of the hydrogen-reduced form of ruthenium modified P-type catalyat preaaed onto a gold-plated 50 mesh tantalum screen. The cathodea were numbered CYC-94 through CYC-109 and were American Cyanamid AA-1 electrodes to which waa pressed a Permion 1010 membrane.

B. Computational Procedurea

An electronic computer was used to facilitate the calculationa required for evaluating stack performance. The tabulated items liated in Appendices G-9 and G-10 are diacusaed below, as required for clarity.

1. Run Number and Condition Period: The atack was run intermittantly. Performance waa uaually noted during steady state at various operating conditiona. Exceptions were Runs 65-2-19 and 65-3-30, where tranaient data were obtained during atart-up:

Time After Start-Up, min

Condition Period	Run 65-2-19	Run 65-3-30
1	)	-
2	-	7
3	-	12
4	10	17
5	15	22
6	20	27
7	25	32
8	30	37
9	35	42
10	40	47
11	45	52
12	50	57
13	55	62
14	60	95
15	70	125
16	115	155
17	-	185
18	175	215
19	205	275
20	235	305
21	265	-
22	295	-

2. Time on Load: Cumulative time on current load.

3. Mode of Operation: R=recycle, S=single pass or once-through.

4. Nominal Conversion per Pass: Methanol consumption based on electrochemical conversion only.

5. Air Rate at STP: Standsrd conditions were 0°C and 1 atm.

6. Nominal Stoichiometric Excess Air: Multiples of air rate required for electrochemical oxidation of methanol.

7. Air Humidity: Dry air wss essentially bone-dry laboratory air that had been passed through a bed of Drierite. Wet air was passed counter current to a hot water stream in a packed column prior to entering the stack. This stream was presumed to be saturated at the indicated inlet air temperature.

8. Temperature: Reactant temperatures and temperatures within the stack were monitored with thermocouples mounted in polypropylene shields. The thermocouples were placed st various depths in several cells. Poth anolyte and air chamber measurements were made as follows:

Chamber	Cell No.	Thermocouple Location, Side of Stsck	Thermocouple Depth, inches
Anolyte	1	Back	1.5
	5	Front	1.0
	6	Bsck	1.5
	9	Front	1.5
	14	Back	1.5
	15	Front	1.5
Air	1	Front	1.0
	1	Back	4.1
	7	Front	2.8
	10	Bsck	2.8
	16	Front	4.1
	16	Bsck	0.8

It was noted that air chamber temperatures for cells 7, 10 and 16 formed smooth lines when superimposed on a plot of anolyte chamber temperature versus cell number. Temperatures for cells that did not contain a thermocouple were estimated by interpolation. Aversge cell temperature was the arithmetic average of the 16 individual cell values. The fuel outlet temperature was measured some distance from the stack and thus does not represent a true bulk mixing temperature for the anolyte chamber overflows.

9. Anode Polarization: Anode polarization was measured relative to a hydrogen reference electrode located in the anolyte chamber. Raw data were corrected to theoretical methanol potential st the observed cell temperature using the following equation derived from previous data (4):

$$\text{Anode Polarization at } T°C = \text{Measured Polarization} - 0.104 + 0.0013\ T_{cell}$$

where: T_{cell} = Cell tempersture, °C.

10. Anode Polarization at 60°C: In order to determine whether feed maldistribution existed, it was necessary to correct anode polarization data for the effects of cell temperature distribution within the stack. Anode polarization data were obtained at a variety of temperatures as indicated below:

Temperature, °C	Polarization from Methsnol Theory at 40 ma/cm^2, volts
55-57	0.28
58-59	.27
58-60	.26
60	.26
62-64	.26
65-66	.26
70	.24
75	.23
80	.22
95	.18

These values, together with data at lower temperature reported previously (6) were used to obtain the following correction factor, applicable in the range 38 to 95°C:

$$Z = 1.572 - 0.00952\ T_{cell}$$

where: T_{cell} = Cell temperature, °C

Z = Correction factor = $\frac{\text{Polarization at T°C}}{\text{Polarization at 60°C}}$

Thus anode polarization data were corrected to their equivalent values at 60°C.

11. Cathode Polarization: Cathode polarization data were calculated by subtracting the sum of (cell voltage + anode polarization at cell temperature + ohmic loss) from 1.20, the theoretical methanol-air cell voltage.

12. Ohmic Losses: Ohmic losses were measured at various times during Run No. 3330-14, and are listed in Appendix G-7.

13. Chemical Oxidation: The extent of chemical oxidation of methanol at the cathode was determined by measuring the CO_2 content of the exhaust gas. The equivalent current density corresponding to this level of methanol oxidation was calculated from:

$$\text{Chemical Oxidation, ma/cm}^2 = \frac{0.01\ Y\ (0.0899\ Q_A - 1.5\ I)}{1 + 0.025\ Y}$$

where: Y = CO_2 content of exhaust gas, mole %

Q_A = Inlet air rate, cc/min @ STP

I = Electrochemical current density, ma/cm^2

Values of carbon dioxide content were not obtained for all runs. The computer printout has assigned a value of "0" to these runs. Values of chemical oxidation as low as 0.0 were never observed experimentally.

14. Voltage Efficiency: Voltage efficiency for the sixteen cell stack was calculated from:

$$\text{Voltage Efficiency} = \frac{\text{Stack Voltage}}{(16)\ (1.20)} \times 100$$

15. Thermal Efficiency: Thermal efficiency was calculated from:

$$\text{Thermal Efficiency} = \frac{(\text{Stack Voltage})\ (I_{elec})}{(16)(1.23)(I_{elec} + I_{chem})} \times 100$$

where: I_{elec}, I_{chem} = Electrochemical and chemical oxidation current densities, respectively.

16. Water Balance Data: Water balance data were recorded for many runs by measuring the total condensate collected from the exhaust gas stream after it had been chilled to about 18°C in a series of condensers and knock-out traps. The final exhaust air was assumed to be saturated at this low temperature. The gross water loss rate was the sum of the condensate rate and the water lost in the final air exhaust. For runs made with dry inlet air, the gross and net water loss rates were identical, although the computer tables have listed the latter as 0.0. For runs made with wet inlet air, the net water loss represents the difference between the gross loss rate and the rate at which water is added to the stack via the saturated inlet air stream. This number is occassionally calculated to be negative, meaning that more water was added to the system than was recovered from the exhaust air stream. The rate of water production is calculated from the total rate of methanol consumption via electrochemical and chemical oxidation.

APPENDIX G-9

DETAILED PERFØRMANCE ØF METHANØL-AIR SIXTEEN CELL STACK(1)

RUN NØ. 65-	2-10
CØNDITIØN PERIØD	4
TIME ØN LØAD AT START ØF RUN, HRS.	0

RUN CØNDITIØNS

CURRENT DENSITY	40.0	CH3ØH IN FEED, M	0.75
FEED RATE, CC/HR.	3200	MØDE ØF ØPERATIØN	RECYCLE
NØM. CØNV. / PASS	50.2	TEMPERATURES, °C	
AIR RATE, CC/MIN. AT STP	30000	FUEL INLET	49
NØM. STØICH. EXCESS AIR	8.4	FUEL ØUTLET	61
AIR HUMIDITY	DRY	AIR INLET	28
		AIR ØUTLET	63

BATTERY PERFØRMANCE

STACK VØLTAGE	7.30
PØWER ØUTPUT, WATTS	87
PØWER DENSITY, MWATTS/SQ. CM.	18.2
VØLTAGE EFFICIENCY, PCT.	38.0
THERMAL EFFICIENCY, PCT.	37.1

CELL NØ.	CELL TEMP., °C	CELL VØLTS	PØLARIZATIØN, VØLTS ANØDE	CATHØDE	ØHMIC LØSS VØLTS	ANØDE PØL. @60 °C
1	58	0.38	0.36	0.42	0.043	0.36
2	62	0.40	0.33	0.42	0.045	0.34
3	65	0.46	0.31	0.39	0.043	0.33
4	68	0.42	0.32	0.41	0.043	0.35
5	72	0.43	0.23	0.49	0.052	0.26
6	73	0.50	0.35	0.31	0.045	0.40
7	73	0.47	0.31	0.37	0.050	0.36
8	70	0.43	0.21	0.52	0.047	0.23
9	67	0.46	0.26	0.43	0.047	0.28
10	72	0.44	0.27	0.45	0.045	0.30
11	66	0.48	0.30	0.37	0.050	0.32
12	61	0.48	0.17	0.50	0.045	0.17
13	55	0.39	0.29	0.48	0.043	0.27
14	50	0.46	0.26	0.44	0.045	0.24
15	57	0.42	0.31	0.43	0.043	0.30
16	49	0.44	0.30	0.41	0.048	0.27
AVERAGE	63	0.44	0.29	0.43	0.046	0.30
STD. DEV.	7.97	0.03	0.05	0.05	0.003	0.06

(1) See Appendix G-8 for additional details.

APPENDIX G-9 (Cont'd)

DETAILED PERFORMANCE OF METHANOL-AIR SIXTEEN CELL STACK[1]

RUN NO. 65-	4- 2
CONDITION PERIOD	2
TIME ON LOAD AT START OF RUN, HRS.	156

RUN CONDITIONS

CURRENT DENSITY	40.0	CH3OH IN FEED, M	0.25
FEED RATE, CC/HR.	9600	MODE OF OPERATION	ONCE-THRU
NOM. CONV. / PASS	50.2	TEMPERATURES, °C	
AIR RATE, CC/MIN. AT STP	30000	FUEL INLET	50
NOM. STOICH. EXCESS AIR	8.4	FUEL OUTLET	37
AIR HUMIDITY	DRY	AIR INLET	27
		AIR OUTLET	42

BATTERY PERFORMANCE

STACK VOLTAGE	4.80
POWER OUTPUT, WATTS	57
POWER DENSITY, MWATTS/SQ. CM.	12.0
VOLTAGE EFFICIENCY, PCT.	25.0
THERMAL EFFICIENCY, PCT.	20.4
CO2 IN AIR OUTLET, MOL PCT.	0.30
CHEM. OXID., MA/SQ. CM.	7.9

CELL NO.	CELL TEMP., °C	CELL VOLTS	POLARIZATION, VOLTS ANODE	CATHODE	OHMIC LOSS VOLTS	ANODE POL. @60 °C
1	55	0.31	0.42	0.41	0.066	0.40
2	56	0.35	0.41	0.39	0.050	0.40
3	58	0.25	0.40	0.50	0.050	0.39
4	59	0.34	0.40	0.41	0.047	0.40
5	61	0.22	0.40	0.47	0.051	0.47
6	60	0.36	0.46	0.33	0.045	0.46
7	60	0.37	0.45	0.32	0.056	0.45
8	59	0.29	0.43	0.42	0.055	0.43
9	57	0.36	0.51	0.27	0.061	0.50
10	55	0.29	0.44	0.42	0.053	0.42
11	54	0.25	0.53	0.37	0.055	0.50
12	54	0.30	0.49	0.36	0.045	0.47
13	53	0.30	0.45	0.40	0.044	0.43
14	52	0.27	0.45	0.43	0.048	0.42
15	51	0.27	0.48	0.40	0.052	0.44
16	46	0.27	0.48	0.40	0.056	0.42
AVERAGE	55	0.30	0.45	0.39	0.052	0.44
STD. DEV.	3.98	0.05	0.04	0.06	0.006	0.03

(1) See Appendix G-8 for additional details.

APPENDIX G-10

PERFØRMANCE ØF METHANØL-AIR SIXTEEN CELL STACK(1)

RUN NØ. 65-	2-10	2-10	2-10	2-11	2-11	2-11	2-11	2-11	2-17	2-17
CØNOITIØN PERIØO	1	3	5	9	10	11	12	14	3	4
TIME ØN LØAO AT START, HRS.	0	0	0	1	1	1	1	1	14	14
RUN CØNOITIØNS										
CH3ØH IN FEEO, M	0.75	0.75	0.75	0.75	0.75	0.75	0.75	0.75	0.75	0.75
MØOE ØF ØPERATIØN	R	R	R	R	R	R	R	R	S	S
CURRENT DENSITY, MA/SQ. CM.	0.	33.3	70.0	33.3	33.3	33.3	33.3	40.0	40.0	40.0
FEEO RATE, CC/HR.	0	2670	5600	2670	2670	2670	2670	3200	3200	3200
NØM. CØNV. / PASS	0.	50.2	50.2	50.2	50.2	50.2	50.2	50.2	50.2	50.2
AIR RATE, CC/MIN. AT STP	24780	24780	52100	24780	24780	24780	24780	30000	30000	30000
NØM. STØICH. EXCESS AIR	0.	8.3	8.3	8.3	8.3	8.3	8.3	8.4	8.4	8.4
AIR HUMIDITY	DRY	ORY	ORY	ORY	DRY	DRY	ORY	DRY	ORY	DRY
TEMPERATURES, °C										
AVG. CELL	45	59	63	74	72	71	68	71	60	67
FUEL INLET	37	46	53	52	51	50	50	55	26	48
FUEL ØUTLET	41	58	65	66	67	62	51	68	30	65
AIR INLET	27	27	28	27	28	28	29	29	27	27
AIR ØUTLET	26	58	65	78	76	74	72	73	40	45
8ATTERY PERFØRMANCE										
STACK VØLTAGE	11.60	7.50	5.60	7.70	7.65	7.75	7.70	7.15	6.90	6.60
CELL VØLTAGE, AVG.	0.71	0.47	0.35	0.47	0.48	0.48	0.48	0.44	0.43	0.40
STD. OEV.	0.03	0.02	0.05	0.06	0.04	0.03	0.02	0.05	0.03	0.07
PØLARIZATIØN, VØLTS										
ANØOE, AVG.	0.12	0.34	0.29	0.26	0.28	0.30	0.30	0.31	0.38	0.27
STO. OEV.	0.04	0.10	0.07	0.06	0.05	0.04	0.05	0.07	0.04	0.06
CATHØOE, AVG.	0.37	0.35	0.47	0.44	0.41	0.38	0.38	0.40	0.34	0.49
STO. DEV.	0.04	0.10	0.07	0.10	0.08	0.05	0.06	0.09	0.04	0.12
ØHMIC LØSSES, VØLTS	0.	0.04	0.08	0.04	0.04	0.04	0.04	0.05	0.05	0.05
;02 IN AIR ØUTLET, MØL. PCT.	0.	0.	0.	1.40	I.70	1.60	1.70	2.20	0.80	1.60
CHEM. ØXIO., MA/SQ. CM.	0.	0.	0.	29.5	35.5	33.5	35.5	55.0	20.7	40.6
PØWER ØUTPUT, WATTS	0.	75.	118.	77.	76.	77.	77.	86.	83.	79.
PØWER DENSITY, MWATTS/SQ. CM.	0.	15.6	24.5	16.0	15.9	I6.1	16.0	17.9	17.2	16.5
V.LTAGE EFFICIENCY, PCT.	60.4	39.1	29.2	40.I	39.8	40.4	40.1	37.2	35.9	34.4
THERMAL EFFICIENCY, PCT.	0.	38.I	28.5	20.8	18.8	19.6	18.9	I5.3	23.1	I6.6
WATER 8ALANCE OATA										
WATER LØSS, CC/MIN.										
GRØSS	0.	0.	0.	0.	0.	0.	0.	0.	2.63	2.62
NET	0.	0.	0.	0.	0.	0.	0.	0.	0.	0.
WATER PRØOUCEO, CC/MIN.	0.	0.	0.	0.	0.	0.	0.	0.	1.09	1.44

(I) See Appendix G-8 for additional details.

APPENDIX G-10 (Cont'd.)

PERFØRMANCE ØF METHANØL-AIR SIXTEEN CELL STACK[1]

RUN NØ. 65-	2-17	2-17	2-17	2-18	2-18	2-18	2-18	2-18	2-19	2-19
CØNOITIØN PERIØO	5	6	7	6	8	10	12	14	1	4
TIME ØN LØAO AT START, HRS.	14	14	14	19	19	19	19	19	26	26
RUN CØNOITIØNS										
CH3ØH IN FEED, M	0.75	0.75	0.75	0.75	0.75	0.75	0.75	0.75	0.75	0.75
MØDE ØF ØPERATIØN	S	S	S	S	S	S	S	S	S	S
CURRENT OENSITY, MA/SQ. CM.	40.0	40.0	40.0	40.0	40.0	40.0	40.0	40.0	0.	40.0
FEEO RATE, CC/HR.	3200	3200	3200	3200	3200	3200	3200	3200	3200	3200
NØM. CØNV. / PASS	50.2	50.2	50.2	50.2	50.2	50.2	50.2	50.2	0.	50.2
AIR RATE, CC/MIN. AT STP	30000	30000	30000	30000	30000	30000	30000	30000	30000	30000
NØM. STØICH. EXCESS AIR	8.4	8.4	8.4	8.4	8.4	8.4	8.4	8.4	0.	8.4
AIR HUMIOITY	ORY	ORY	ORY	ORY	ORY	ORY	ORY	ORY	ORY	ORY
TEMPERATURES, °C										
AVG. CELL	68	58	65	65	63	64	65	60	29	46
FUEL INLET	26	35	36	36	36	37	36	36	26	29
FUEL ØUTLET	53	52	55	58	57	58	57	51	26	36
AIR INLET	28	27	28	27	27	27	27	28	25	26
AIR ØUTLET	45	43	46	48	47	47	47	42	25	33
BATTERY PERFØRMANCE										
STACK VØLTAGE	7.05	6.60	6.90	7.00	6.95	6.85	6.90	6.85	10.00	6.30
CELL VØLTAGE, AVG.	0.44	0.41	0.43	0.44	0.43	0.42	0.43	0.42	0.64	0.40
STO. OEV.	0.03	0.05	0.02	0.02	0.02	0.03	0.03	0.02	0.03	0.02
PØLARIZATIØN, VØLTS										
ANØOE, AVG.	0.36	0.35	0.39	0.37	0.39	0.37	0.37	0.39	0.24	0.40
STO. OEV.	0.04	0.06	0.04	0.05	0.04	0.07	0.06	0.04	0.06	0.03
CATHØOE, AVG.	0.35	0.39	0.34	0.34	0.34	0.36	0.35	0.34	0.32	0.36
STD. DEV.	0.04	0.09	0.05	0.05	0.04	0.09	0.06	0.04	0.05	0.04
ØHMIC LØSSES, VØLTS	0.05	0.05	0.05	0.05	0.05	0.05	0.05	0.05	0.	0.05
C02 IN AIR ØUTLET, MØL. PCT.	1.00	0.80	1.00	1.00	1.00	0.90	1.00	0.80	0.75	1.30
CHEM. ØXIO., MA/SQ. CM.	25.7	20.7	25.7	25.7	25.7	23.2	25.7	20.7	19.9	33.2
PØWER ØUTPUT, WATTS	85.	79.	83.	84.	83.	82.	83.	82.	0.	76.
PØWER OENSITY, MWATTS/SQ. CM.	17.6	16.5	17.2	17.5	17.4	17.1	17.2	17.1	0.	15.7
VØLTAGE EFFICIENCY, PCT.	36.7	34.4	35.9	36.5	36.2	35.7	35.9	35.7	52.1	32.8
THERMAL EFFICIENCY, PCT.	21.8	22.1	21.3	21.6	21.5	22.0	21.3	22.9	0.	17.5
WATER 8ALANCE OATA										
WATER LØSS, CC/MIN.										
GRØSS	2.63	2.63	0.	3.04	2.62	2.62	2.60	2.60	0.	1.50
NET	0.	0.	0.	0.	0.	0.	0.	0.	0.	0.
WATER PRØOUCEO, CC/MIN.	1.18	1.09	0.	1.18	1.18	1.13	1.18	1.09	0.	1.31

(1) See Appendix G-8 for additional details.

APPENDIX G-10 (Cont'd.)

PERFØRMANCE ØF METHANØL-AIR SIXTEEN CELL STACK[1]

RUN NØ. 65-	2-19	2-19	2-19	2-19	2-19	2-19	2-19	2-19	2-19	2-19
CØNDITIØN PERIØD	5	6	7	8	9	10	11	12	13	14
TIME ØN LØAD AT START, HRS.	26	26	26	26	26	26	26	26	26	26
RUN CØNDITIØNS										
CH3ØH IN FEED, M	0.75	0.75	0.75	0.75	0.75	0.75	0.75	0.75	0.75	0.75
MØDE ØF ØPERATIØN	S	S	S	S	S	S	S	S	S	S
CURRENT DENSITY, MA/SQ. CM.	40.0	40.0	40.0	40.0	40.0	40.0	40.0	40.0	40.0	40.0
FEED RATE, CC/HR.	3200	3200	3200	3200	3200	3200	3200	3200	3200	3200
NØM. CØNV. / PASS	50.2	50.2	50.2	50.2	50.2	50.2	50.2	50.2	50.2	50.2
AIR RATE, CC/MIN. AT STP	30000	30000	30000	30000	30000	30000	30000	30000	30000	30000
NØM. STØICH. EXCESS AIR	8.4	8.4	8.4	8.4	8.4	8.4	8.4	8.4	8.4	8.4
AIR HUMIDITY	DRY	DRY	DRY	DRY	DRY	DRY	DRY	DRY	DRY	DRY
TEMPERATURES, °C										
AVG. CELL	52	56	58	60	62	62	63	64	64	64
FUEL INLET	35	35	33	28	30	28	29	30	28	33
FUEL ØUTLET	43	49	50	52	56	56	56	57	56	57
AIR INLET	26	25	25	25	26	26	27	26	26	26
AIR ØUTLET	38	41	43	43	43	46	43	46	46	46
BATTERY PERFØRMANCE										
STACK VØLTAGE	6.60	6.75	6.90	7.00	7.00	7.05	7.05	7.00	6.45	7.00
CELL VØLTAGE, AVG.	0.41	0.42	0.43	0.43	0.43	0.44	0.44	0.44	0.44	0.44
STD. DEV.	0.02	0.02	0.02	0.02	0.02	0.02	0.02	0.02	0.02	0.02
PØLARIZATIØN, VØLTS										
ANØDE, AVG.	0.39	0.39	0.38	0.38	0.38	0.38	0.38	0.38	0.39	0.38
STD. DEV.	0.04	0.04	0.04	0.04	0.04	0.04	0.04	0.04	0.04	0.04
CATHØDE, AVG.	0.35	0.34	0.34	0.34	0.34	0.34	0.34	0.34	0.33	0.34
STD. DEV.	0.04	0.03	0.05	0.04	0.04	0.04	0.04	0.04	0.04	0.04
ØHMIC LØSSES, VØLTS	0.05	0.05	0.05	0.05	0.05	0.05	0.05	0.05	0.05	0.05
C02 IN AIR ØUTLET, MØL. PCT.	1.20	1.15	1.15	1.10	1.10	1.10	1.20	1.10	1.10	1.00
CHEM. ØXID., MA/SQ. CM.	30.7	29.5	29.5	28.2	28.2	28.2	30.7	28.2	28.2	25.7
PØWER ØUTPUT, WATTS	7[illegible].	81.	83.	84.	84.	85.	85.	84.	77.	84.
PØWER DENSITY, MWATTS/SQ. CM.	16.5	16.9	17.2	17.5	17.5	17.6	17.6	17.5	16.1	17.5
VØLTAGE EFFICIENCY, PCT.	34.4	35.2	35.9	36.5	36.5	36.7	36.7	36.5	33.6	36.5
THERMAL EFFICIENCY, PCT.	19.0	19.7	20.2	20.9	20.9	21.0	20.3	20.9	19.2	21.6
WATER BALANCE DATA										
WATER LØSS, CC/MIN.										
GRØSS	1.70	1.50	2.30	2.50	2.70	2.70	2.90	2.30	2.50	1.90
NET	0.	0.	0.	0.	0.	0.	0.	0.	0.	0.
WATER PRØDUCED, CC/MIN.	1.27	1.24	1.24	1.22	1.22	1.22	1.27	1.22	1.22	1.18

(1) See Appendix G-8 for additional details.

APPENDIX G-10 (Cont'd.)

PERFØRMANCE ØF METHANØL-AIR SIXTEEN CELL STACK[1]

RUN NØ. 65-	2-19	2-19	2-19	2-19	2-19	2-19	2-24	2-24	2-24	2-24
CØNOITIØN PERIØO	15	16	18	19	21	22	3	5	7	8
TIME ØN LØAO AT START, HRS.	26	26	26	26	26	26	32	32	32	32
RUN CØNOITIØNS										
CH3ØH IN FEEO, M	0.75	0.75	0.75	0.75	0.75	0.75	0.75	0.75	0.75	0.75
MØOE ØF ØPERATIØN	S	S	S	S	S	S	S	S	S	S
CURRENT OENSITY, MA/SQ. CM.	40.0	40.0	40.0	40.0	40.0	40.0	40.0	40.0	10.0	10.0
FEEO RATE, CC/HR.	3200	3200	3200	3200	3200	3200	3200	3200	800	800
NØM. CØNV. / PASS	50.2	50.2	50.2	50.2	50.2	50.2	50.2	50.2	50.2	50.2
AIR RATE, CC/MIN. AT STP	30000	30000	30000	30000	30000	30000	30000	30000	9000	9000
NØM. STØICH. EXCESS AIR	8.4	8.4	8.4	8.4	8.4	8.4	8.4	8.4	10.0	10.0
AIR HUMIDITY	ORY	ORY	ORY	ORY	ORY	ORY	ORY	ORY	ORY	ORY
TEMPERATURES, °C										
AVG. CELL	64	65	66	65	66	65	69	65	62	65
FUEL INLET	33	37	38	38	38	38	37	37	37	39
FUEL ØUTLET	58	58	59	60	60	58	61	57	53	54
AIR INLET	27	27	27	27	27	27	27	27	28	28
AIR ØUTLET	46	47	47	47	47	48	48	47	47	45
BATTERY PERFØRMANCE										
STACK VØLTAGE	6.95	6.95	6.90	6.85	6.85	6.85	7.00	6.80	9.00	7.20
CELL VØLTAGE, AVG.	0.43	0.43	0.43	0.43	0.43	0.43	0.44	0.43	0.57	0.58
STO. OEV.	0.03	0.03	0.02	0.02	0.02	0.02	0.03	0.02	0.06	0.02
PØLARIZATIØN, VØLTS										
ANØOE, AVG.	0.37	0.37	0.39	0.37	0.38	0.39	0.38	0.39	0.28	0.33
STO. OEV.	0.05	0.06	0.05	0.06	0.05	0.05	0.07	0.05	0.11	0.05
CATHØOE, AVG.	0.35	0.35	0.34	0.36	0.35	0.34	0.33	0.33	0.35	0.28
STO. OEV.	0.05	0.06	0.05	0.06	0.05	0.05	0.08	0.04	0.16	0.04
ØHMIC LØSSES, VØLTS	0.05	0.05	0.05	0.05	0.05	0.05	0.05	0.05	0.01	0.01
C02 IN AIR ØUTLET, MØL. PCT.	1.05	1.10	1.00	1.00	1.00	1.00	1.00	0.80	1.80	1.50
CHEM. ØXIO., MA/SQ. CM.	27.0	28.2	25.7	25.7	25.7	25.7	25.7	20.7	13.7	11.5
PØWER ØUTPUT, WATTS	83.	83.	83.	82.	82.	82.	84.	82.	27.	26.
PØWER OENSITY, MWATTS/SQ. CM.	17.4	17.4	17.2	17.1	17.1	17.1	17.5	17.0	5.6	5.7
VØLTAGE EFFICIENCY, PCT.	36.2	36.2	35.9	35.7	35.7	35.7	36.5	35.4	46.9	47.9
THERMAL EFFICIENCY, PCT.	21.1	20.7	21.3	21.2	21.2	21.2	21.6	22.8	19.3	21.8
WATER 8ALANCE OATA										
WATER LØSS, CC/MIN.										
GRØSS	2.50	2.77	2.68	2.60	2.71	2.79	2.67	2.77	2.95	0.98
NET	0.	0.	0.	0.	0.	0.	0.	0.	0.	0.
WATER PRØOUCEO, CC/MIN.	1.20	1.22	1.18	1.18	1.18	1.18	1.18	1.09	0.42	0.38

(1) See Appendix G-8 for additional details.

APPENDIX G-10 (Cont'd.)

PERFØRMANCE ØF METHANØL-AIR SIXTEEN CELL STACK[1]

RUN NØ. 65-	2-24	2-24	2-26	2-26	2-26	2-26	2-26	2-26	2-26	2-26
CØNDITIØN PERIØD	13	14	3	4	5	6	7	8	9	10
TIME ØN LØAD AT START, HRS.	32	32	39	39	39	39	39	39	39	39
RUN CØNDITIØNS										
CH3ØH IN FEED, M	0.75	0.75	0.75	0.75	0.75	0.75	0.75	0.75	0.75	0.75
MØDE ØF ØPERATIØN	S	S	S	S	S	S	S	S	S	S
CURRENT DENSITY, MA/SQ. CM.	80.0	80.0	40.0	10.0	10.0	10.0	10.0	10.0	10.0	10.0
FEED RATE, CC/HR.	6400	6400	3200	800	800	800	1600	1600	1600	533
NØM. CØNV. / PASS	50.2	50.2	50.2	50.2	50.2	50.2	25.1	25.1	25.1	75.4
AIR RATE, CC/MIN. AT STP	58000	58000	30000	4500	7200	4500	9000	9000	4500	4500
NØM. STØICH. EXCESS AIR	8.1	8.1	8.4	5.0	8.0	5.0	10.0	10.0	5.0	5.0
AIR HUMIDITY	DRY	DRY	DRY	DRY	DRY	DRY	DRY	DRY	DRY	DRY
TEMPERATURES, °C										
AVG. CELL	57	62	66	65	66	67	65	64	69	70
FUEL INLET	38	33	38	35	37	40	45	43	43	36
FUEL ØUTLET	57	62	61	57	55	53	54	54	55	51
AIR INLET	27	27	27	28	28	29	28	28	29	29
AIR ØUTLET	46	47	48	47	42	41	45	45	41	42
BATTERY PERFØRMANCE										
STACK VØLTAGE	4.60	4.60	7.00	6.80	7.90	7.90	9.20	9.15	9.00	7.50
CELL VØLTAGE, AVG.	0.30	0.30	0.43	0.42	0.53	0.50	0.57	0.56	0.48	0.49
STD. DEV.	0.02	0.03	0.03	0.15	0.07	0.08	0.02	0.03	0.08	0.09
PØLARIZATIØN, VØLTS										
ANØDE, AVG.	0.43	0.43	0.37	0.24	0.28	0.25	0.32	0.30	0.20	0.22
STD. DEV.	0.05	0.06	0.06	0.10	0.10	0.12	0.06	0.07	0.10	0.13
CATHØDE, AVG.	0.38	0.37	0.35	0.52	0.38	0.43	0.30	0.32	0.51	0.48
STD. DEV.	0.04	0.06	0.07	0.25	0.17	0.20	0.06	0.08	0.17	0.22
ØHMIC LØSSES, VØLTS	0.10	0.10	0.05	0.01	0.01	0.01	0.01	0.01	0.01	0.01
C02 IN AIR ØUTLET, MØL. PCT.	0.40	0.40	1.00	3.30	2.70	3.00	2.50	2.80	4.70	4.00
CHEM. ØXID., MA/SQ. CM.	20.2	20.2	25.7	11.9	16.0	10.9	18.7	20.8	16.4	14.2
PØWER ØUTPUT, WATTS	110.	110.	84.	20.	24.	24.	28.	27.	27.	22.
PØWER DENSITY, MWATTS/SQ. CM.	23.0	23.0	17.5	4.2	4.9	4.9	5.7	5.7	5.6	4.7
VØLTAGE EFFICIENCY, PCT.	24.0	24.0	36.5	35.4	41.1	41.1	47.9	47.7	46.9	39.1
THERMAL EFFICIENCY, PCT.	18.7	18.7	21.6	15.8	15.4	19.2	16.3	15.1	17.3	15.8
WATER BALANCE DATA										
WATER LØSS, CC/MIN.										
GRØSS	3.31	5.21	2.70	1.45	0.62	0.45	0.92	1.21	0.65	0.54
NET	0.	0.	0.	0.	0.	0.	0.	0.	0.	0.
WATER PRØDUCED, CC/MIN.	1.79	1.79	1.18	0.39	0.47	0.37	0.51	0.55	0.47	0.43

(1) See Appendix G-8 for additional details.

APPENDIX G-10 (Cont'd.)

PERFØRMANCE ØF METHANØL-AIR SIXTEEN CELL STACK[1]

RUN NØ. 65-	2-26	2-26	3- 1	3- 1	3- 1	3- 1	3- 1	3- 1	3- 1	3- 1
CØNOITIØN PERIØO	11	12	2	3	4	5	6	7	8	9
TIME ØN LØAO AT START, HRS.	39	39	45	45	45	45	45	45	45	45
RUN CØNOITIØNS										
CH3ØH IN FEED, M	0.75	0.75	0.75	0.75	0.75	0.75	0.75	0.75	0.75	0.75
MØOE ØF JPERATIØN	S	S	S	S	S	S	S	S	S	S
CURRENT OENSITY, MA/SQ. CM.	10.0	10.0	40.0	40.0	40.0	40.0	40.0	40.0	40.0	40.0
FEEO RATE, CC/HR.	533	533	3200	3200	3200	3200	6400	6400	2264	2264
NØM. CØNV. / PASS	75.4	75.4	50.2	50.2	50.2	50.2	25.1	25.1	71.0	71.0
AIR RATE, CC/MIN. AT STP	4500	4500	30000	12200	10800	7200	30000	30000	30000	12200
NØM. STØICH. EXCESS AIR	5.0	5.0	8.4	3.4	3.0	2.0	8.4	8.4	8.4	3.4
AIR HUMIOITY	ORY	ORY	ORY	ORY	ORY	ORY	DRY	ORY	ORY	ORY
TEMPERATURES, °C										
AVG. CELL	70	69	65	76	80	79	76	70	68	72
FUEL INLET	37	37	38	36	35	30	32	32	38	39
FUEL ØUTLET	53	54	60	71	70	67	63	55	41	42
AIR INLET	29	30	29	29	29	29	29	29	29	29
AIR ØUTLET	44	43	47	47	47	44	48	43	47	47
BATTERY PERFØRMANCE										
STACK VØLTAGE	8.00	8.20	7.20	5.90	5.70	1.90	6.87	6.85	6.40	5.20
CELL VØLTAGE, AVG.	0.51	0.49	0.45	0.38	0.36	0.18	0.43	0.42	0.40	0.33
STO. OEV.	0.09	0.07	0.03	0.09	0.09	0.16	0.03	0.02	0.05	0.12
PØLARIZATIØN, VØLTS										
ANØOE, AVG.	0.25	0.29	0.36	0.31	0.31	0.31	0.32	0.36	0.38	0.35
STD. OEV.	0.12	0.12	0.05	0.08	0.08	0.07	0.06	0.05	0.05	0.08
CATHØOE, AVG.	0.43	0.41	0.35	0.46	0.49	0.67	0.40	0.37	0.37	0.52
STO. OEV.	0.21	0.18	0.06	0.16	0.16	0.19	0.07	0.05	0.09	0.18
OHMIC LØSSES, VØLTS	0.01	0.01	0.05	0.05	0.05	0.05	0.05	0.05	0.05	0.
IN AIR ØUTLET, MØL. PCT.	2.60	2.00	1.40	2.80	3.20	1.70	2.20	1.70	0.60	1.40
ØXIO., MA/SQ. CM.	9.5	7.4	35.7	27.1	27.0	9.6	55.0	43.0	15.6	14.0
POWER ØUTPUT, WATTS	24.	25.	86.	71.	68.	23.	82.	82.	77.	62.
POWER OENSITY, MWATTS/SQ. CM.	5.0	5.1	18.0	14.7	14.2	4.7	17.2	17.1	16.0	13.0
VØLTAGE EFFICIENCY, PCT.	41.7	42.7	37.5	30.7	29.7	9.9	35.8	35.7	33.3	27.1
THERMAL EFFICIENCY, PCT.	20.8	23.9	19.3	17.9	17.3	7.8	14.7	16.8	23.4	19.6
WATER BALANCE DATA										
WATER LØSS, CC/MIN.										
GRØSS	0.59	0.53	1.31	1.51	1.11	0.95	2.09	2.59	2.52	1.57
NET	0.	0.	0.	0.	0.	0.	0.	0.	0.	0.
WATER PRØOUCEO, CC/MIN.	0.35	0.31	1.35	1.20	1.20	0.89	1.70	1.49	1.00	0.97

(1) See Appendix G-8 for additional details.

APPENDIX G-10 (Cont'd.)

PERFORMANCE OF METHANOL-AIR SIXTEEN CELL STACK[1]

RUN NO. 65-	3- 2	3- 2	3- 2	3- 2	3- 2	3- 2	3- 2	3- 2	3- 2	3- 4
CONDITION PERIOD	2	3	4	5	6	7	8	9	10	1
TIME ON LOAD AT START, HRS.	51	51	51	51	51	51	51	51	51	56
RUN CONDITIONS										
CH3OH IN FEED, M	0.75	0.75	0.75	0.75	0.75	0.75	0.75	0.75	0.75	0.75
MODE OF OPERATION	S	S	S	S	S	S	S	S	S	S
CURRENT DENSITY, MA/SQ. CM.	40.0	40.0	40.0	40.0	40.0	10.0	10.0	80.0	80.0	40.0
FEED RATE, CC/HR.	3200	3200	3200	6400	6400	533	533	6400	6400	3200
NOM. CONV. / PASS	50.2	50.2	50.2	25.1	25.1	75.4	75.4	50.2	50.2	50.2
AIR RATE, CC/MIN. AT STP	30000	30000	12200	12200	12200	9000	9000	58000	30000	30000
NOM. STOICH. EXCESS AIR	8.4	8.4	3.4	3.4	3.4	10.0	10.0	8.1	4.2	8.4
AIR HUMIDITY	DRY	DRY	DRY	DRY	DRY	DRY	DRY	DRY	DRY	DRY
TEMPERATURES, °C										
AVG. CELL	61	66	78	71	70	72	68	63	71	51
FUEL INLET	37	37	33	33	34	37	40	35	32	30
FUEL OUTLET	33	36	40	37	37	38	37	36	38	47
AIR INLET	25	26	26	27	27	27	27	26	27	40
AIR OUTLET	47	47	47	37	36	50	47	46	47	53
BATTERY PERFORMANCE										
STACK VOLTAGE	7.10	7.10	6.05	5.65	5.65	9.00	9.10	4.60	4.05	6.65
CELL VOLTAGE, AVG.	0.44	0.44	0.38	0.36	0.35	0.56	0.56	0.29	0.25	0.42
STD. DEV.	0.02	0.02	0.09	0.06	0.06	0.09	0.04	0.02	0.07	0.02
POLARIZATION, VOLTS										
ANODE, AVG.	0.36	0.37	0.33	0.33	0.32	0.28	0.35	0.40	0.38	0.35
STD. DEV.	0.05	0.05	0.07	0.04	0.05	0.11	0.07	0.05	0.05	0.04
CATHODE, AVG.	0.35	0.35	0.45	0.46	0.48	0.35	0.28	0.41	0.47	0.39
STD. DEV.	0.05	0.06	0.15	0.09	0.09	0.19	0.09	0.05	0.10	0.04
OHMIC LOSSES, VOLTS	0.05	0.05	0.05	0.05	0.05	0.01	0.01	0.10	0.10	0.05
CO2 IN AIR OUTLET, MOL. PCT.	1.20	1.00	2.40	3.70	3.90	1.60	1.10	0.50	1.50	1.50
CHEM. OXIO., MA/SQ. CM.	30.7	25.7	23.5	35.1	36.8	12.2	8.5	25.2	37.3	38.1
POWER OUTPUT, WATTS	85.	85.	73.	68.	68.	27.	27.	110.	97.	80.
POWER DENSITY, MWATTS/SQ. CM.	17.7	17.7	15.1	14.1	14.1	5.6	5.7	23.0	20.2	16.6
VOLTAGE EFFICIENCY, PCT.	37.0	37.0	31.5	29.4	29.4	46.9	47.4	24.0	21.1	34.6
THERMAL EFFICIENCY, PCT.	20.4	22.0	19.4	15.3	14.9	20.6	25.0	17.8	14.0	17.3
WATER BALANCE DATA										
WATER LOSS, CC/MIN.										
GROSS	2.11	2.29	1.19	0.98	0.62	0.99	1.24	4.06	2.84	0.
NET	0.	0.	0.	0.	0.	0.	0.	0.	0.	0.
WATER PRODUCED, CC/MIN.	1.27	1.18	1.14	1.34	1.38	0.40	0.33	1.88	2.10	0.

(1) See Appendix G-8 for additional details.

APPENDIX G-10 (Cont'd.)

PERFØRMANCE ØF METHANØL-AIR SIXTEEN CELL STACK[1]

RUN NØ. 65-	3- 4	3- 4	3- 4	3- 4	3- 4	3- 4	3- 4	3- 4	3- 5	3- 5
CØNDITIØN PERIØD	2	3	4	5	6	7	8	9	1	5
TIME ØN LØAD AT START, HRS.	56	56	56	56	56	56	56	56	63	63
RUN CØNDITIØNS										
CH3ØH IN FEED, M	0.75	0.75	0.75	0.75	0.75	0.75	0.75	0.75	0.75	0.75
MØDE ØF ØPERATIØN	S	S	S	S	S	S	S	S	S	S
CURRENT DENSITY, MA/SQ. CM.	40.0	80.0	80.0	80.0	80.0	80.0	0.	0.	40.0	10.0
FEED RATE, CC/HR.	3200	8800	8800	4832	4832	4832	3200	3200	3200	4000
NØM. CØNV. / PASS	50.2	36.5	36.5	66.6	66.6	66.6	0.	0.	50.2	10.0
AIR RATE, CC/MIN. AT STP	30000	58000	30000	58000	46200	58000	12200	30000	30000	9000
NØM. STØICH. EXCESS AIR	8.4	8.1	4.2	8.1	6.4	8.1	0.	0.	8.4	10.0
AIR HUMIDITY	DRY	DRY	DRY	DRY	DRY	DRY	DRY	DRY	DRY	DRY
TEMPERATURES, °C										
AVG. CELL	64	61	74	67	68	68	55	54	62	68
FUEL INLET	28	32	35	32	36	37	42	40	40	41
FUEL ØUTLET	56	59	72	63	65	68	48	48	55	57
AIR INLET	27	26	27	27	27	27	28	27	37	27
AIR ØUTLET	45	42	48	44	48	47	42	42	46	42
BATTERY PERFØRMANCE										
STACK VØLTAGE	6.90	4.55	3.90	3.65	3.95	3.75	11.20	11.10	6.90	8.50
CELL VØLTAGE, AVG.	0.43	0.29	0.25	0.23	0.25	0.24	0.69	0.68	0.42	0.53
STD. DEV.	0.03	0.03	0.07	0.08	0.05	0.04	0.09	0.04	0.03	0.05
PØLARIZATIØN, VØLTS										
ANØDE, AVG.	0.36	0.40	0.35	0.41	0.39	0.40	0.14	0.18	0.36	0.23
STD. DEV.	0.05	0.05	0.05	0.05	0.05	0.05	0.06	0.06	0.04	0.07
CATHØDE, AVG.	0.36	0.41	0.51	0.46	0.46	0.46	0.37	0.34	0.37	0.42
STD. DEV.	0.05	0.05	0.10	0.11	0.07	0.07	0.10	0.05	0.05	0.10
ØHMIC LØSSES, VØLTS	0.05	0.10	0.10	0.10	0.10	0.10	0.	0.	0.05	0.01
C02 IN AIR ØUTLET, MØL. PCT.	1.10	1.00	1.60	0.30	0.50	0.30	2.00	1.40	1.00	4.90
CHEM. ØXID., MA/SQ. CM.	28.2	49.7	39.6	15.2	19.9	15.2	20.9	36.5	25.7	34.7
PØWER ØUTPUT, WATTS	83.	109.	94.	88.	95.	90.	0.	0.	83.	25.
PØWER DENSITY, MWATTS/SQ. CM.	17.2	22.7	19.5	18.2	19.7	18.7	0.	0.	17.2	5.3
VØLTAGE EFFICIENCY, PCT.	35.9	23.7	20.3	19.0	20.6	19.5	58.3	57.8	35.9	44.3
THERMAL EFFICIENCY, PCT.	20.6	14.3	13.2	15.6	16.1	16.0	0.	0.	21.3	9.7
WATER BALANCE DATA										
WATER LØSS, CC/MIN.										
GRØSS	2.50	3.01	2.25	3.46	2.11	4.15	1.40	1.35	0.	0.62
NET	0.	0.	0.	0.	0.	0.	0.	0.	0.	0.
WATER PRØDUCED, CC/MIN.	1.22	2.32	2.14	1.70	1.79	1.70	0.37	0.65	0.	0.80

(1) See Appendix G-8 for additional details.

APPENDIX G-10 (Cont'd.)

PERFØRMANCE ØF METHANØL-AIR SIXTEEN CELL STACK[1]

RUN NØ. 65-	3- 5	3- 5	3- 8	3- 8	3- 8	3- 9	3- 9	3- 9	3- 9	3-11
CØNDITIØN PERIØD	6	7	5	7	9	1	2	4	6	1
TIME ØN LØAD AT START, HRS.	63	63	69	69	69	75	75	75	75	82
RUN CØNDITIØNS										
CH3ØH IN FEED, M	0.75	0.75	0.75	0.75	0.75	0.75	0.75	0.75	0.75	0.75
MØDE ØF ØPERATIØN	S	S	S	S	S	S	S	S	S	S
CURRENT DENSITY, MA/SQ. CM.	10.0	20.0	20.0	20.0	20.0	40.0	50.0	10.0	10.0	40.0
FEED RATE, CC/HR.	4000	3200	3200	1600	1213	3200	4000	4000	4000	3200
NØM. CØNV. / PASS	10.0	25.1	25.1	50.2	66.3	50.2	50.2	10.0	10.0	50.2
AIR RATE, CC/MIN. AT STP	4500	9000	9000	9000	9000	30000	38100	9000	9000	30000
NØM. STØICH. EXCESS AIR	5.0	5.0	5.0	5.0	5.0	8.4	8.5	10.0	10.0	8.4
AIR HUMIDITY	DRY	DRY	DRY	DRY	DRY	DRY	DRY	DRY	DRY	DRY
TEMPERATURES, °C										
AVG. CELL	64	79	75	70	67	62	65	70	72	66
FUEL INLET	41	43	34	45	46	40	40	46	47	40
FUEL ØUTLET	55	67	51	57	52	57	56	54	57	57
AIR INLET	28	28	27	28	28	26	27	28	28	27
AIR ØUTLET	35	47	45	48	46	47	47	46	51	47
BATTERY PERFØRMANCE										
STACK VØLTAGE	7.20	7.25	7.55	7.60	7.85	6.90	6.00	8.40	8.00	6.75
CELL VØLTAGE, AVG.	0.45	0.45	0.48	0.48	0.48	0.42	0.37	0.51	0.49	0.42
STD. DEV.	0.06	0.06	0.05	0.05	0.04	0.02	0.03	0.06	0.06	0.03
PØLARIZATIØN, VØLTS										
ANØDE, AVG.	0.18	0.20	0.24	0.23	0.35	0.35	0.38	0.19	0.16	0.37
STD. DEV.	0.06	0.08	0.09	0.07	0.04	0.04	0.03	0.08	0.09	0.04
CATHØDE, AVG.	0.56	0.52	0.46	0.41	0.34	0.37	0.39	0.49	0.53	0.36
STD. DEV.	0.10	0.13	0.14	0.10	0.05	0.04	0.04	0.13	0.15	0.06
ØHMIC LØSSES, VØLTS	0.01	0.02	0.02	0.02	0.02	0.05	0.06	0.01	0.01	0.05
C02 IN AIR ØUTLET, MØL. PCT.	6.70	4.20	4.40	2.50	1.90	1.10	0.65	4.35	4.70	0.70
CHEM. ØXID., MA/SQ. CM.	22.4	29.6	30.9	18.3	14.1	28.2	21.4	31.2	33.4	18.1
PØWER ØUTPUT, WATTS	22.	43.	45.	47.	47.	83.	90.	25.	24.	81.
PØWER DENSITY, MWATTS/SQ. CM.	4.5	9.1	9.4	9.7	9.8	17.2	18.7	5.2	5.0	16.9
VØLTAGE EFFICIENCY, PCT.	37.5	37.8	39.3	40.6	40.9	35.9	31.2	43.7	41.7	35.2
THERMAL EFFICIENCY, PCT.	11.3	14.8	15.1	20.7	23.4	20.6	21.3	10.4	9.4	23.6
WATER BALANCE DATA										
WATER LØSS, CC/MIN.										
GRØSS	0.43	0.77	0.57	1.15	0.93	1.80	2.91	0.81	1.04	0.
NET	0.	0.	0.	0.	0.	0.	0.	0.	0.	0.
WATER PRØDUCED, CC/MIN.	0.58	0.89	0.91	0.69	0.61	1.22	1.28	0.74	0.78	0.

(1) See Appendix G-8 for additional details.

APPENDIX G-10 (Cont'd.)

PERFORMANCE OF METHANOL-AIR SIXTEEN CELL STACK[1]

RUN NO. 65-	3-11	3-11	3-11	3-11	3-11	3-11	3-11	3-11	3-12	3-12
CONDITION PERIOD	2	3	4	5	6	7	8	9	1	2
TIME ON LOAD AT START, HRS.	82	82	82	82	82	82	82	82	88	88
RUN CONDITIONS										
CH3OH IN FEED, M	0.75	0.75	0.75	0.75	0.75	0.75	0.75	0.75	0.75	0.50
MODE OF OPERATION	S	S	S	S	S	S	S	S	S	S
CURRENT DENSITY, MA/SQ. CM.	40.0	60.0	60.0	80.0	80.0	100.0	100.0	20.0	40.0	20.0
FEED RATE, CC/HR.	2440	4800	4000	6400	4880	8000	6130	1600	3200	2400
NOM. CONV. / PASS	65.9	50.2	60.3	50.2	65.9	50.2	65.6	50.2	50.2	50.2
AIR RATE, CC/MIN. AT STP	30000	46200	46200	58000	58000	70200	70200	12200	30000	12200
NOM. STOICH. EXCESS AIR	8.4	8.6	8.6	8.1	8.1	7.8	7.8	6.8	8.4	6.8
AIR HUMIDITY	DRY	DRY	DRY	DRY	DRY	DRY	DRY	DRY	DRY	DRY
TEMPERATURES, °C										
AVG. CELL	63	63	63	67	63	60	62	58	64	64
FUEL INLET	37	36	36	32	29	27	27	52	39	40
FUEL OUTLET	52	55	55	66	65	62	64	27	57	55
AIR INLET	27	27	27	26	26	26	26	41	26	27
AIR OUTLET	47	47	47	47	45	43	45	60	46	43
BATTERY PERFORMANCE										
STACK VOLTAGE	6.55	5.45	5.45	4.60	4.20	2.75	2.80	7.85	6.75	7.90
CELL VOLTAGE, AVG.	0.40	0.33	0.33	0.28	0.25	0.17	0.17	0.48	0.41	0.49
STD. DEV.	0.02	0.03	0.03	0.03	0.03	0.05	0.04	0.03	0.04	0.04
POLARIZATION, VOLTS										
ANODE, AVG.	0.38	0.39	0.38	0.40	0.42	0.44	0.44	0.33	0.36	0.34
STD. DEV.	0.03	0.05	0.04	0.03	0.03	0.05	0.05	0.05	0.03	0.04
CATHODE, AVG.	0.36	0.40	0.41	0.41	0.42	0.46	0.46	0.36	0.38	0.34
STD. DEV.	0.04	0.05	0.05	0.04	0.04	0.07	0.04	0.06	0.05	0.06
OHMIC LOSSES, VOLTS	0.05	0.08	0.08	0.11	0.11	0.13	0.13	0.03	0.05	0.03
CO2 IN AIR OUTLET, MOL. PCT.	0.45	0.50	0.40	0.35	0.20	0.30	0.25	1.40	1.10	1.55
CHEM. OXID., MA/SQ. CM.	11.7	20.1	16.1	17.7	10.1	18.3	15.3	14.4	28.2	15.9
POWER OUTPUT, WATTS	79.	98.	98.	110.	101.	82.	84.	47.	81.	47.
POWER DENSITY, MWATTS/SQ. CM.	16.4	20.4	20.4	23.0	21.0	17.2	17.5	9.8	16.9	9.9
VOLTAGE EFFICIENCY, PCT.	34.1	28.4	28.4	24.0	21.9	14.3	14.6	40.9	35.2	41.1
THERMAL EFFICIENCY, PCT.	25.7	20.8	21.8	19.1	18.9	11.8	12.3	23.2	20.1	22.4
WATER BALANCE DATA										
WATER LOSS, CC/MIN.										
GROSS	0.	0.	0.	0.	0.	0.	0.	0.	0.	0.76
NET	0.	0.	0.	0.	0.	0.	0.	0.	0.	0.
WATER PRODUCED, CC/MIN.	0.	0.	0.	0.	0.	0.	0.	0.	0.	0.64

(1) See Appendix G-8 for additional details.

APPENDIX G-10 (Cont'd.)

PERFØRMANCE ØF METHANØL-AIR SIXTEEN CELL STACK[1]

RUN NØ. 65-	3-12	3-12	3-12	3-12	3-16	3-16	3-16	3-16	3-19	3-19
CØNOITIØN PERIØO	3	4	5	6	1	3	4	5	1	2
TIME ØN LØAO AT START, HRS.	88	88	88	88	94	94	94	94	102	102
RUN CØNOITIØNS										
CH30H IN FEED, M	0.50	0.50	0.50	0.50	0.75	0.75	0.75	0.75	0.75	0.75
MØOE ØF ØPERATIØN	S	S	S	S	S	S	S	S	S	S
CURRENT OENSITY, MA/SQ. CM.	20.0	40.0	40.0	60.0	20.0	10.0	10.0	40.0	40.0	40.0
FEEO RATE, CC/HR.	1830	4800	3660	7200	1600	800	610	3200	3200	3200
NØM. CØNV. / PASS	65.9	50.2	65.9	50.2	50.2	50.2	65.9	50.2	50.2	50.2
AIR RATE, CC/MIN. AT STP	12200	30000	30000	46200	12200	9000	9000	12200	30000	12200
NØM. STØICH. EXCESS AIR	6.8	8.4	8.4	8.6	6.8	10.0	10.0	3.4	8.4	3.4
AIR HUMIOITY	ORY	ORY	ORY	ORY	ORY	ORY	ORY	ORY	ORY	ORY
TEMPERATURES, °C										
AVG. CELL	64	60	61	63	66	58	56	73	60	75
FUEL INLET	40	38	37	33	29	42	42	46	40	39
FUEL ØUTLET	55	52	40	60	51	45	43	62	37	43
AIR INLET	27	27	27	26	27	26	27	82	26	27
AIR ØUTLET	43	43	44	45	44	40	40	50	48	51
BATTERY PERFØRMANCE										
STACK VØLTAGE	7.00	6.30	5.40	5.00	8.00	8.70	8.50	5.75	6.60	6.00
CELL VØLTAGE, AVG.	0.45	0.39	0.37	0.32	0.49	0.54	0.52	0.36	0.41	0.37
STO. OEV.	0.12	0.04	0.10	0.07	0.02	0.02	0.02	0.09	0.02	0.11
PØLARIZATIØN, VØLTS										
ANØOE, AVG.	0.40	0.38	0.42	0.40	0.35	0.34	0.36	0.31	0.36	0.32
STO. OEV.	0.11	0.03	0.11	0.05	0.03	0.02	0.02	0.06	0.02	0.10
CATHØOE, AVG.	0.32	0.37	0.36	0.40	0.33	0.30	0.30	0.47	0.38	0.46
STO. OEV.	0.03	0.04	0.03	0.06	0.04	0.03	0.03	0.14	0.03	0.11
ØHMIC LØSSES, VØLTS	0.03	0.05	0.05	0.08	0.03	0.01	0.01	0.05	0.05	0.05
C02 IN AIR ØUTLET, MØL. PCT.	1.00	0.75	0.55	0.25	1.10	0.90	0.60	1.50	0.85	2.80
CHEM. ØXIO., MA/SQ. CM.	10.4	19.4	14.3	10.1	11.4	7.0	4.7	15.0	21.9	27.1
PØWER ØUTPUT, WATTS	42.	76.	65.	90.	48.	26.	25.	69.	79.	72.
PØWER OENSITY, MWATTS/SQ. CM.	8.7	15.7	13.5	18.7	10.0	5.4	5.3	14.4	16.5	15.0
VØLTAGE EFFICIENCY, PCT.	36.5	32.8	28.1	26.0	41.7	[illegible].3	44.3	29.9	34.4	31.2
THERMAL EFFICIENCY, PCT.	23.4	21.6	20.2	21.7	25.9	[illegible].0	29.4	21.3	21.7	18.2
WATER 8ALANCE OATA										
WATER LØSS, CC/MIN.										
GRØSS	0.71	1.55	2.04	2.21	0.	0.66	0.70	0.	0.	1.30
NET	0.	0.	0.	0.	0.	0.	0.	0.	0.	0.
WATER PRØOUCEO, CC/MIN.	0.54	1.06	0.97	1.25	0.	0.30	0.26	0.	0.	1.20

(1) See Appendix G-8 for additional details.

APPENDIX G-10 (Cont'd.)

PERFØRMANCE ØF METHANØL-AIR SIXTEEN CELL STACK(1)

RUN NØ. 65-	3-19	3-19	3-19	3-19	3-22	3-22	3-22	3-22	3-22	3-22
CØNDITIØN PERIØD	3	4	5	6	1	2	3	4	5	6
TIME ØN LØAD AT START, HRS.	102	102	102	102	109	109	109	109	109	109
RUN CØNDITIØNS										
CH3ØH IN FEED, M	0.75	0.75	0.75	0.75	0.75	0.75	0.75	0.75	0.75	0.75
MØDE ØF ØPERATIØN	S	S	S	S	S	S	S	S	S	S
CURRENT DENSITY, MA/SQ. CM.	40.0	20.0	20.0	10.0	40.0	10.0	60.0	60.0	80.0	80.0
FEED RATE, CC/HR.	2440	1600	1220	800	3200	610	4800	3660	6400	4880
NØM. CØNV. / PASS	65.9	50.2	65.9	50.2	50.2	65.9	50.2	65.9	50.2	65.9
AIR RATE, CC/MIN. AT STP	12200	9000	9000	4500	30000	9000	21300	21300	30000	30000
NØM. STØICH. EXCESS AIR	3.4	5.0	5.0	5.0	8.4	10.0	4.0	4.0	4.2	4.2
AIR HUMIDITY	ORY	ORY	ORY	ORY	DRY	ORY	ORY	DRY	ORY	DRY
TEMPERATURES, °C										
AVG. CELL	77	70	65	63	64	65	73	73	73	73
FUEL INLET	33	28	39	40	34	37	31	26	26	26
FUEL ØUTLET	46	38	37	36	37	36	42	39	43	43
AIR INLET	27	27	27	27	26	27	26	26	26	26
AIR ØUTLET	51	46	46	40	42	38	49	50	45	45
BATTERY PERFØRMANCE										
STACK VØLTAGE	5.60	8.20	7.60	8.60	6.80	7.60	5.80	4.20	3.90	2.40
CELL VØLTAGE, AVG.	0.36	0.51	0.47	0.53	0.42	0.48	0.35	0.26	0.24	0.19
STD. DEV.	0.13	0.03	0.04	0.03	0.03	0.10	0.04	0.12	0.07	0.12
PØLARIZATIØN, VØLTS										
ANØDE, AVG.	0.34	0.30	0.36	0.32	0.34	0.25	0.33	0.38	0.39	0.41
STD. DEV.	0.14	0.06	0.03	0.04	0.07	0.11	0.07	0.05	0.04	0.07
CATHØDE, AVG.	0.45	0.36	0.35	0.34	0.39	0.45	0.44	0.48	0.46	0.50
STD. DEV.	0.10	0.07	0.04	0.07	0.07	0.19	0.08	0.11	0.09	0.11
ØHMIC LØSSES, VØLTS	0.05	0.03	0.03	0.01	0.05	0.01	0.08	0.08	0.11	0.11
C02 IN AIR ØUTLET, MØL. PCT.	2.80	2.40	1.30	2.10	1.00	2.10	1.60	1.00	1.10	0.80
CHEM. ØXID., MA/SQ. CM.	27.1	17.6	9.8	7.8	25.7	15.8	28.1	17.8	27.6	20.2
PØWER ØUTPUT, WATTS	67.	49.	46.	26.	82.	23.	101.	76.	94.	58.
PØWER DENSITY, MWATTS/SQ. CM.	14.0	10.2	9.5	5.4	17.0	4.7	21.0	15.7	19.5	12.0
VØLTAGE EFFICIENCY, PCT.	29.2	42.7	39.6	44.8	35.4	39.6	29.2	21.9	20.3	12.5
THERMAL EFFICIENCY, PCT.	17.0	22.1	25.9	24.6	21.0	14.9	19.4	16.5	14.7	9.7
WATER BALANCE DATA										
WATER LØSS, CC/MIN.										
GRØSS	1.41	1.01	0.84	0.	0.	0.46	2.53	2.60	2.57	3.16
NET	0.	0.	0.	0.	0.	0.	0.	0.	0.	0.
WATER PRØDUCED, CC/MIN.	1.20	0.67	0.53	0.	0.	0.46	1.58	1.39	1.93	1.79

(1) See Appendix G-8 for additional details.

APPENDIX G-10 (Cont'd.)

PERFORMANCE OF METHANOL-AIR SIXTEEN CELL STACK[1]

RUN NO. 65-	3-23	3-23	3-23	3-23	3-23	3-24	3-24	3-24	3-24	3-24
CONDITION PERIOD	1	2	3	4	5	1	2	3	4	5
TIME ON LOAD AT START, HRS.	116	116	116	116	116	122	122	122	122	122
RUN CONDITIONS										
CH3OH IN FEED, M	0.75	0.50	0.50	0.50	0.50	0.50	0.50	0.50	0.50	0.50
MODE OF OPERATION	S	S	S	S	S	S	S	S	S	S
CURRENT DENSITY, MA/SQ. CM.	40.0	10.0	10.0	10.0	10.0	40.0	40.0	40.0	40.0	40.0
FEED RATE, CC/HR.	3200	2400	1200	800	915	4800	8150	3660	4800	4000
NOM. CONV. / PASS	50.2	25.1	50.2	75.4	65.9	50.2	29.6	65.9	50.2	60.3
AIR RATE, CC/MIN. AT STP	30000	4500	4500	4500	4500	12200	12200	12200	30000	30000
NOM. STOICH. EXCESS AIR	8.4	5.0	5.0	5.0	5.0	3.4	3.4	3.4	8.4	8.4
AIR HUMIDITY	DRY	DRY	DRY	DRY	DRY	DRY	DRY	DRY	DRY	DRY
TEMPERATURES, °C										
AVG. CELL	60	63	62	59	59	69	68	68	56	56
FUEL INLET	32	41	43	43	44	39	36	36	42	43
FUEL OUTLET	34	36	35	33	42	34	39	34	35	35
AIR INLET	25	27	27	27	32	27	27	27	26	28
AIR OUTLET	42	35	40	38	27	42	37	37	44	45
BATTERY PERFORMANCE										
STACK VOLTAGE	6.65	8.30	8.65	7.10	8.55	6.20	6.40	5.50	6.00	5.60
CELL VOLTAGE, AVG.	0.41	0.51	0.53	0.44	0.52	0.39	0.38	0.34	0.37	0.34
STD. DEV.	0.02	0.05	0.03	0.10	0.04	0.04	0.04	0.15	0.04	0.10
POLARIZATION, VOLTS										
ANODE, AVG.	0.38	0.25	0.33	0.42	0.35	0.36	0.35	0.39	0.41	0.43
STD. DEV.	0.03	0.09	0.03	0.07	0.03	0.05	0.05	0.08	0.03	0.05
CATHODE, AVG.	0.35	0.43	0.32	0.33	0.32	0.39	0.41	0.41	0.37	0.38
STD. DEV.	0.04	0.13	0.05	0.08	0.05	0.07	0.08	0.10	0.04	0.06
OHMIC LOSSES, VOLTS	0.05	0.01	0.01	0.01	0.01	0.05	0.05	0.05	0.05	0.05
CO2 IN AIR OUTLET, MOL. PCT.	1.00	4.20	2.40	1.10	1.90	2.10	2.70	2.10	0.50	0.40
CHEM. OXID., MA/SQ. CM.	25.7	14.8	8.8	4.2	7.1	20.7	26.2	20.7	13.0	10.4
POWER OUTPUT, WATTS	80.	25.	26.	21.	26.	74.	77.	66.	72.	67.
POWER DENSITY, MWATTS/SQ. CM.	16.6	5.2	5.4	4.4	5.3	15.5	16.0	13.7	15.0	14.0
VOLTAGE EFFICIENCY, PCT.	34.6	43.2	45.0	37.0	44.5	32.3	33.3	28.6	31.2	29.2
THERMAL EFFICIENCY, PCT.	20.6	17.0	23.4	25.5	25.5	20.8	19.6	18.4	23.0	22.6
WATER BALANCE DATA										
WATER LOSS, CC/MIN.										
GROSS	0.	1.09	0.37	0.43	0.45	0.	0.88	1.11	2.08	2.23
NET	0.	0.	0.	0.	0.	0.	0.	0.	0.	0.
WATER PRODUCED, CC/MIN.	0.	0.44	0.34	0.25	0.31	0.	1.19	1.09	0.95	0.90

(1) See Appendix G-8 for additional details.

APPENDIX G-10 (Cont'd.)

PERFØRMANCE ØF METHANØL-AIR SIXTEEN CELL STACK[1]

RUN NØ. 65-	3-26	3-26	3-26	3-26	3-26	3-29	3-29	3-29	3-30	3-30
CØNOITIØN PERIØO	1	2	3	4	5	1	2	3	2	3
TIME ØN LØAO AT START, HRS.	129	129	129	129	129	136	136	136	142	142
RUN CØNOITIØNS										
CH3ØH IN FEED, M	0.50	0.50	0.50	1.00	1.00	1.00	1.00	1.00	0.50	0.50
MØOE ØF ØPERATIØN	S	S	S	S	S	S	S	S	S	S
CURRENT OENSITY, MA/SQ. CM.	40.0	40.0	40.0	40.0	40.0	40.0	10.0	10.0	40.0	40.0
FEEO RATE, CC/HR.	4800	8150	4000	2400	1846	4800	1200	600	4800	4800
NØM. CØNV. / PASS	50.2	29.6	60.3	50.2	65.3	25.1	25.1	50.2	50.2	50.2
AIR RATE, CC/MIN. AT STP	30000	30000	30000	12200	12200	12200	4500	4500	30000	30000
NØM. STØICH. EXCESS AIR	8.4	8.4	8.4	3.4	3.4	3.4	5.0	5.0	8.4	8.4
AIR HUMIOITY	DRY	ORY	ORY	ORY	DRY	ORY	DRY	DRY	DRY	DRY
TEMPERATURES, °C										
AVG. CELL	56	57	58	74	74	83	82	62	43	49
FUEL INLET	37	36	40	45	45	22	21	23	43	42
FUEL ØUTLET	35	35	34	40	40	38	39	22	32	36
AIR INLET	26	26	26	27	27	27	28	28	25	25
AIR ØUTLET	42	41	45	57	57	3i	32	42	26	30
BATTERY PERFØRMANCE										
STACK VØLTAGE	6.20	6.20	5.15	5.25	5.25	4.60	6.35	8.10	5.45	5.80
CELL VØLTAGE, AVG.	0.38	0.39	0.31	0.33	0.33	0.30	0.39	0.50	0.34	0.37
STO. OEV.	0.02	0.02	0.11	0.15	0.15	0.10	0.12	0.08	0.02	0.02
PØLARIZATIØN, VØLTS										
ANØOE, AVG.	0.40	0.40	0.45	0.27	0.27	0.27	0.16	0.24	0.40	0.39
STO. OEV.	0.03	0.04	0.07	0.07	0.07	0.05	0.08	0.12	0.02	0.02
CATHØOE, AVG.	0.36	0.36	0.38	0.54	0.55	0.58	0.63	0.44	0.40	0.39
STO. OEV.	0.03	0.03	0.08	0.19	0.21	0.12	0.17	0.18	0.03	0.03
ØHMIC LØSSES, VØLTS	0.05	0.05	0.05	0.05	0.05	0.05	0.01	0.01	0.05	0.05
C02 IN AIR ØUTLET, MØL. PCT.	0.60	0.80	0.50	2.55	2.30	5.40	4.90	2.70	0.90	1.00
CHEM. ØXIO., MA/SQ. CM.	15.6	20.7	13.0	24.9	22.5	49.3	17.0	9.9	23.2	25.7
PØWER ØUTPUT, WATTS	74.	74.	62.	63.	63.	55.	19.	24.	65.	70.
PØWER OENSITY, MWATTS/SQ. CM.	15.5	15.5	12.9	13.1	13.1	11.5	4.0	5.1	13.6	14.5
VØLTAGE EFFICIENCY, PCT.	32.3	32.3	26.8	27.3	27.3	24.0	33.1	42.2	28.4	30.2
THERMAL EFFICIENCY, PCT.	22.7	20.8	19.7	16.5	17.1	10.5	11.9	20.7	17.5	17.9
WATER BALANCE OATA										
WATER LØSS, CC/MIN.										
GRØSS	0.	1.89	2.14	1.55	2.19	0.	0.50	0.74	0.65	0.95
NET	0.	0.	0.	0.	0.	0.	0.	0.	0.	0.
WATER PRØOUCEO, CC/MIN.	0.	1.09	0.95	1.16	1.12	0.	0.48	0.36	1.13	1.18

(1) See Appendix G-8 for additional details.

APPENDIX G-10 (Cont'd.)

PERFØRMANCE ØF METHANØL-AIR SIXTEEN CELL STACK[1]

RUN NØ. 65-	3-30	3-30	3-30	3-30	3-30	3-30	3-30	3-30	3-30	3-30
CØNDITIØN PERIØD	4	5	6	7	8	9	10	11	12	13
TIME ØN LØAD AT START, HRS.	142	142	142	142	142	142	142	142	142	142
RUN CØNDITIØNS										
CH3ØH IN FEED, M	0.50	0.50	0.50	0.50	0.50	0.50	0.50	0.50	0.50	0.50
MØDE ØF ØPERATIØN	S	S	S	S	S	S	S	S	S	S
CURRENT DENSITY, MA/SQ. CM.	40.0	40.0	40.0	40.0	40.0	40.0	40.0	40.0	40.0	40.0
FEED RATE, CC/HR.	4800	4800	4800	4800	4800	4800	4800	4800	4800	4800
NØM. CØNV. / PASS	50.2	50.2	50.2	50.2	50.2	50.2	50.2	50.2	50.2	50.2
AIR RATE, CC/MIN. AT STP	30000	30000	30000	30000	30000	30000	30000	30000	30000	30000
NØM. STØICH. EXCESS AIR	8.4	8.4	8.4	8.4	8.4	8.4	8.4	8.4	8.4	8.4
AIR HUMIDITY	DRY	DRY	DRY	DRY	DRY	DRY	DRY	DRY	DRY	DRY
TEMPERATURES, °C										
AVG. CELL	53	55	56	58	59	60	60	60	60	60
FUEL INLET	41	41	40	40	39	39	39	39	40	40
FUEL ØUTLET	40	40	44	44	45	46	44	46	41	45
AIR INLET	25	25	26	26	26	25	26	26	26	26
AIR ØUTLET	34	36	37	38	38	38	38	38	38	38
BATTERY PERFØRMANCE										
STACK VØLTAGE	6.15	6.30	6.35	6.50	6.40	6.40	6.35	6.40	6.30	6.35
CELL VØLTAGE, AVG.	0.39	0.39	0.40	0.40	0.40	0.40	0.39	0.39	0.39	0.40
STD. DEV.	0.02	0.03	0.03	0.03	0.04	0.04	0.04	0.04	0.04	0.03
PØLARIZATIØN, VØLTS										
ANØDE, AVG.	0.38	0.38	0.38	0.37	0.37	0.37	0.38	0.37	0.37	0.37
STD. DEV.	0.02	0.02	0.03	0.03	0.03	0.03	0.03	0.04	0.04	0.03
CATHØDE, AVG.	0.38	0.37	0.37	0.38	0.38	0.38	0.38	0.38	0.38	0.38
STD. DEV.	0.03	0.04	0.04	0.05	0.06	0.06	0.05	0.05	0.06	0.05
ØHMIC LØSSES, VØLTS	0.05	0.05	0.05	0.05	0.05	0.05	0.05	0.05	0.05	0.05
C02 IN AIR ØUTLET, MØL. PCT.	0.90	0.85	0.80	0.80	0.80	0.80	0.75	0.75	0.70	0.70
CHEM. ØXID., MA/SQ. CM.	23.2	21.9	20.7	20.7	20.7	20.7	19.4	19.4	18.1	18.1
PØWER ØUTPUT, WATTS	74.	76.	76.	78.	77.	77.	76.	77.	76.	76.
PØWER DENSITY, MWATTS/SQ. CM.	15.4	15.7	15.9	16.2	16.0	16.0	15.9	16.0	15.7	15.9
VØLTAGE EFFICIENCY, PCT.	32.0	32.8	33.1	33.9	33.3	33.3	33.1	33.3	32.8	33.1
THERMAL EFFICIENCY, PCT.	19.8	20.7	21.3	21.8	21.4	21.4	21.7	21.9	22.0	22.2
WATER BALANCE DATA										
WATER LØSS, CC/MIN.										
GRØSS	1.67	1.28	1.30	1.44	1.65	1.62	1.35	1.62	1.38	1.50
NET	0.	0.	0.	0.	0.	0.	0.	0.	0.	0.
WATER PRØDUCED, CC/MIN.	1.13	1.11	1.09	1.09	1.09	1.09	1.06	1.06	1.04	1.04

(1) See Appendix G-8 for additional details.

APPENDIX G-10 (Cont'd.)

PERFØRMANCE ØF METHANØL-AIR SIXTEEN CELL STACK[1]

RUN NØ. 65-	3-30	3-30	3-30	3-30	3-30	3-30	3-30	3-31	3-31	3-31
CØNDITIØN PERIØD	14	15	16	17	18	19	20	1	3	4
TIME ØN LØAD AT START, HRS.	142	142	142	142	142	142	142	149	149	149
RUN CØNDITIØNS										
CH3ØH IN FEED, M	0.50	0.50	0.50	0.50	0.50	0.50	0.50	0.50	1.25	1.25
MØDE ØF ØPERATIØN	S	S	S	S	S	S	S	S	S	S
CURRENT DENSITY, MA/SQ. CM.	40.0	40.0	40.0	40.0	40.0	40.0	40.0	40.0	40.0	40.0
FEED RATE, CC/HR.	4800	4800	4800	4800	4800	4800	4800	4800	1920	1600
NØM. CØNV. / PASS	50.2	50.2	50.2	50.2	50.2	50.2	50.2	50.2	50.2	60.3
AIR RATE, CC/MIN. AT STP	30000	30000	30000	30000	30000	30000	30000	30000	30000	30000
NØM. STØICH. EXCESS AIR	8.4	8.4	8.4	8.4	8.4	8.4	8.4	8.4	8.4	8.4
AIR HUMIDITY	DRY	DRY	DRY	DRY	DRY	DRY	DRY	DRY	DRY	DRY
TEMPERATURES, °C										
AVG. CELL	63	62	61	62	63	64	64	58	71	68
FUEL INLET	40	41	46	51	47	50	50	37	16	15
FUEL ØUTLET	44	43	38	42	40	47	47	28	26	25
AIR INLET	26	26	26	26	26	26	26	25	26	26
AIR ØUTLET	38	45	46	47	47	47	47	41	46	46
BATTERY PERFØRMANCE										
STACK VØLTAGE	6.25	6.35	6.30	6.35	5.75	6.25	5.80	6.20	6.35	6.20
CELL VØLTAGE, AVG.	0.38	0.39	0.39	0.39	0.36	0.39	0.36	0.38	0.40	0.39
STD. DEV.	0.04	0.03	0.03	0.04	0.10	0.03	0.09	0.03	0.06	0.04
PØLARIZATIØN, VØLTS										
ANØDE, AVG.	0.37	0.38	0.37	0.38	0.40	0.37	0.41	0.39	0.31	0.34
STD. DEV.	0.04	0.03	0.02	0.03	0.08	0.04	0.09	0.03	0.08	0.09
CATHØDE, AVG.	0.39	0.38	0.38	0.38	0.39	0.39	0.38	0.38	0.44	0.42
STD. DEV.	0.07	0.04	0.04	0.04	0.07	0.06	0.04	0.04	0.13	0.12
ØHMIC LØSSES, VØLTS	0.05	0.05	0.05	0.05	0.05	0.05	0.05	0.05	0.05	0.05
CO2 IN AIR ØUTLET, MØL. PCT.	0.65	0.60	0.70	0.60	0.60	0.60	0.55	0.60	1.20	0.70
CHEM. ØXID., MA/SQ. CM.	16.9	15.6	18.1	15.6	15.6	15.6	14.3	15.6	30.7	18.1
PØWER ØUTPUT, WATTS	75.	76.	76.	76.	69.	75.	70.	74.	76.	74.
PØWER DENSITY, MWATTS/SQ. CM.	15.6	15.9	15.7	15.9	14.4	15.6	14.5	15.5	15.9	15.5
VØLTAGE EFFICIENCY, PCT.	32.5	33.1	32.8	33.1	29.9	32.5	30.2	32.3	33.1	32.3
THERMAL EFFICIENCY, PCT.	22.3	23.2	22.0	23.2	21.0	22.9	21.7	22.7	18.2	21.7
WATER BALANCE DATA										
WATER LØSS, CC/MIN.										
GRØSS	1.66	4.13	2.17	2.40	2.76	2.61	2.58	0.	2.18	2.79
NET	0.	0.	0.	0.	0.	0.	0.	0.	0.	0.
WATER PRØDUCED, CC/MIN.	1.02	1.00	1.04	1.00	1.00	1.00	0.97	0.	1.27	1.04

(1) See Appendix G-8 for additional details.

APPENDIX G-10(Cont'd.)

PERFØRMANCE ØF METHANØL-AIR SIXTEEN CELL STACK[1]

RUN NØ. 65-	3-31	4- 2	4- 5	4- 5	4- 5	4- 6	4- 6	4- 6	4- 6	4- 8
CØNDITIØN PERIØD	5	3	2	3	4	1	2	3	4	1
TIME ØN LØAD AT START, HRS.	149	156	159	159	159	163	163	163	163	170
RUN CØNDITIØNS										
CH3ØH IN FEED, M	1.25	0.25	0.50	0.50	0.50	0.75	0.75	0.75	0.75	0.75
MØOE ØF ØPERATIØN	S	S	S	S	S	S	S	S	S	S
CURRENT OENSITY, MA/SQ. CM.	40.0	40.0	80.0	80.0	80.0	40.0	40.0	40.0	40.0	40.0
FEEO RATE, CC/HR.	3840	16670	9600	7320	16670	3200	3200	3200	3200	3200
NØM. CØNV. / PASS	25.1	28.9	50.2	65.9	28.9	50.2	50.2	50.2	50.2	50.2
AIR RATE, CC/MIN. AT STP	30000	30000	30000	30000	30000	30000	30000	30000	30000	30000
NØM. STØICH. EXCESS AIR	8.4	8.4	4.2	4.2	4.2	8.4	8.4	8.4	8.4	8.4
AIR HUMIOITY	ORY	ORY	ORY	ORY	ORY	WET	WET	WET	WET	WET
TEMPERATURES, °C										
AVG. CELL	75	55	65	68	60	66	68	68	68	71
FUEL INLET	21	47	27	55	31	40	28	27	26	37
FUEL ØUTLET	27	33	27	26	30	28	27	27	27	26
AIR INLET	26	29	27	28	27	26	47	47	48	55
AIR ØUTLET	47	41	47	27	33	48	53	54	53	56
8ATTERY PERFØRMANCE										
STACK VØLTAGE	6.00	5.65	3.80	3.25	3.50	6.60	6.90	6.90	6.85	6.90
CELL VØLTAGE, AVG.	0.37	0.35	0.24	0.19	0.22	0.41	0.43	0.43	0.42	0.43
STO. OEV.	0.08	0.03	0.05	0.08	0.05	0.04	0.02	0.03	0.02	0.03
PØLARIZATIØN, VØLTS										
ANØDE, AVG.	0.28	0.41	0.41	0.44	0.39	0.33	0.34	0.32	0.33	0.32
STO. OEV.	0.07	0.04	0.04	0.06	0.03	0.05	0.03	0.05	0.05	0.06
CATHØOE, AVG.	0.50	0.39	0.44	0.46	0.48	0.41	0.38	0.39	0.39	0.40
STO. OEV.	0.12	0.02	0.06	0.08	0.07	0.08	0.04	0.07	0.07	0.08
ØHMIC LØSSES, VØLTS	0.05	0.05	0.10	0.10	0.10	0.05	0.05	0.05	0.05	0.05
C02 IN AIR ØUTLET, MØL. PCT.	2.30	0.45	0.80	0.60	1.10	0.80	0.80	0.80	0.85	1.10
CHEM. ØXIO., MA/SQ. CM.	57.4	11.7	20.2	15.2	27.6	20.7	20.7	20.7	21.9	28.2
PØWER ØUTPUT, WATTS	72.	68.	91.	78.	84.	79.	83.	83.	82.	83.
PØWER OENSITY, MWATTS/SQ. CM.	15.0	14.1	19.0	16.2	17.5	16.5	17.2	17.2	17.1	17.2
VØLTAGE EFFICIENCY, PCT.	31.2	29.4	19.8	16.9	18.2	34.4	35.9	35.9	35.7	35.9
THERMAL EFFICIENCY, PCT.	12.5	22.2	15.4	13.9	13.2	22.1	23.1	23.1	22.5	20.6
WATER BALANCE DATA										
HATER LØSS, CC/MIN.										
GRØSS	2.48	0.	0.	1.91	1.28	0.	0.	3.66	3.41	3.77
NET	0.	0.	0.	0.	0.	0.	0.	0.77	0.42	-0.76
WATER PRØOUCEO, CC/MIN.	1.74	0.	0.	1.[illegible]	1.93	0.	0.	1.09	1.11	1.22

(1) See Appendix G-8 for additional details.

APPENDIX G-10 (Cont'd.)

PERFØRMANCE ØF METHANØL-AIR SIXTEEN CELL STACK[1]

RUN NØ. 65-	4- 7	4- 8	4- 8	4- 8	4- 8	4- 9	4- 9	4- 9	4- 9	4-12
CØNDITIØN PERIØD	2	3	4	5	6	1	2	3	4	I
TIME ØN LØAD AT START, HRS.	170	170	170	170	170	176	176	176	176	183
RUN CØNDITIØNS										
CH3ØH IN FEED, M	0.75	0.75	0.75	0.75	0.75	0.75	0.75	0.75	0.75	0.75
MØDE ØF ØPERATIØN	S	S	S	S	S	S	S	S	S	S
CURRENT DENSITY, MA/SQ. CM.	40.0	40.0	40.0	40.0	40.0	40.0	40.0	40.0	40.0	40.0
FEED RATE, CC/HR.	3200	3200	3200	3200	3200	3200	3200	3200	3200	3200
NØM. CØNV. / PASS	50.2	50.2	50.2	50.2	50.2	50.2	50.2	50.2	50.2	50.2
AIR RATE, CC/MIN. AT STP	30000	30000	30000	30000	30000	30000	30000	30000	30000	30000
NØM. STØICH. EXCESS AIR	8.4	8.4	8.4	8.4	8.4	8.4	8.4	8.4	8.4	8.4
AIR HUMIDITY	WET	WET	WET	WET	WET	WET	WET	WET	WET	DRY
TEMPERATURES, °C										
AVG. CELL	70	70	70	71	72	71	71	70	64	67
FUEL INLET	38	38	38	49	49	48	48	50	48	41
FUEL ØUTLET	27	27	28	31	30	28	29	27	31	28
AIR INLET	48	51	51	51	51	51	50	48	50	53
AIR ØUTLET	53	54	54	56	56	57	57	57	55	50
BATTERY PERFØRMANCE										
STACK VØLTAGE	6.65	6.75	6.70	6.60	6.80	6.75	7.00	6.85	6.50	6.40
CELL VØLTAGE, AVG.	0.42	0.42	0.42	0.41	0.43	0.43	0.44	0.43	0.41	0.40
STD. DEV.	0.04	0.03	0.03	0.05	0.02	0.03	0.02	0.02	0.05	0.04
PØLARIZATIØN, VØLTS										
ANØDE, AVG.	0.31	0.33	0.33	0.31	0.32	0.36	0.34	0.34	0.35	0.35
STD. DEV.	0.06	0.05	0.06	0.06	0.05	0.04	0.04	0.04	0.07	0.07
CATHØDE, AVG.	0.41	0.39	0.40	0.43	0.40	0.36	0.37	0.38	0.39	0.40
STD. DEV.	0.08	0.07	0.08	0.11	0.06	0.04	0.05	0.05	0.06	0.10
ØHMIC LØSSES, VØLTS	0.05	0.05	0.05	0.05	0.05	0.05	0.05	0.05	0.05	0.05
C02 IN AIR ØUTLET, MØL. PCT.	1.10	1.00	1.00	0.90	0.90	0.70	0.75	0.75	0.70	0.80
CHEM. ØXID., MA/SQ. CM.	28.2	25.7	25.7	23.2	23.2	18.1	19.4	19.4	18.1	20.7
PØWER ØUTPUT, WATTS	80.	81.	80.	79.	82.	81.	84.	82.	78.	77.
PØWER DENSITY, MWATTS/SQ. CM.	16.6	16.9	16.7	16.5	17.0	16.9	17.5	17.1	16.2	16.0
VØLTAGE EFFICIENCY, PCT.	34.6	35.2	34.9	34.4	35.4	35.2	36.5	35.7	33.9	33.3
THERMAL EFFICIENCY, PCT.	19.8	20.9	20.7	21.2	21.9	23.6	23.9	23.4	22.7	21.4
WATER BALANCE DATA										
WATER LØSS, CC/MIN.										
GRØSS	3.81	4.28	5.89	4.25	4.53	0.	5.08	5.15	4.43	3.27
NET	0.73	0.77	2.27	0.63	0.91	0.	1.69	2.17	1.04	0.
WATER PRØDUCED, CC/MIN.	1.22	1.18	1.18	1.13	1.13	0.	1.06	1.06	1.04	1.09

(1) See Appendix G-8 for additional details.

APPENDIX G-10 (Cont'd.)

PERFØRMANCE ØF METHANØL-AIR SIXTEEN CELL STACK[1]

RUN NØ. 65-	4-12	4-12	4-12	4-13	4-13	4-13	4-13	4-13	4-15	4-15
CØNDITIØN PERIØD	2	3	4	1	2	3	4	5	1	2
TIME ØN LØAD AT START, HRS.	183	183	183	188	188	188	188	188	195	195
RUN CØNDITIØNS										
CH₃ØH IN FEED, M	0.75	0.75	0.75	0.75	0.50	0.50	0.50	0.50	0.75	0.75
MØDE ØF ØPERATIØN	S	S	S	S	S	S	S	S	R	R
CURRENT DENSITY, MA/SQ. CM.	40.0	40.0	40.0	40.0	40.0	40.0	40.0	40.0	40.0	40.0
FEED RATE, CC/HR.	3200	3200	3200	3200	4800	4800	4800	4800	3200	3200
NØM. CØNV. / PASS	50.2	50.2	50.2	50.2	50.2	50.2	50.2	50.2	50.2	50.2
AIR RATE, CC/MIN. AT STP	30000	30000	30000	30000	30000	30000	30000	30000	30000	30000
NØM. STØICH. EXCESS AIR	8.4	8.4	8.4	8.4	8.4	8.4	8.4	8.4	8.4	8.4
AIR HUMIDITY	DRY	DRY	DRY	DRY	DRY	DRY	DRY	DRY	DRY	DRY
TEMPERATURES, °C										
AVG. CELL	73	67	65	67	65	66	66	66	67	67
FUEL INLET	55	36	33	41	47	50	50	50	39	38
FUEL ØUTLET	30	27	28	27	35	36	37	37	26	28
AIR INLET	50	52	55	47	51	51	51	51	26	26
AIR ØUTLET	54	50	47	47	47	48	48	49	48	47
BATTERY PERFØRMANCE										
STACK VØLTAGE	6.35	6.65	6.40	6.40	6.20	6.25	6.25	6.25	6.30	6.25
CELL VØLTAGE, AVG.	0.37	0.41	0.40	0.40	0.39	0.39	0.39	0.39	0.39	0.38
STD. DEV.	0.11	0.03	0.02	0.03	0.04	0.04	0.04	0.04	0.05	0.07
PØLARIZATIØN, VØLTS										
ANØDE, AVG.	0.33	0.37	0.38	0.35	0.38	0.37	0.36	0.37	0.35	0.36
STD. DEV.	0.05	0.04	0.05	0.07	0.07	0.06	0.07	0.05	0.07	0.07
CATHØDE, AVG.	0.45	0.37	0.37	0.39	0.38	0.39	0.39	0.38	0.41	0.41
STD. DEV.	0.14	0.06	0.06	0.10	0.10	0.10	0.11	0.09	0.11	0.12
ØHMIC LØSSES, VØLTS	0.05	0.05	0.05	0.05	0.05	0.05	0.05	0.05	0.05	0.05
C02 IN AIR ØUTLET, MØL. PCT.	0.90	0.85	0.80	1.00	0.80	0.75	0.75	0.75	0.80	0.90
CHEM. ØXID., MA/SQ. CM.	23.2	21.9	20.7	25.7	20.7	19.4	19.4	19.4	20.7	23.2
PØWER ØUTPUT, WATTS	76.	80.	77.	77.	74.	75.	75.	75.	76.	75.
PØWER DENSITY, MWATTS/SQ. CM.	15.9	16.6	16.0	16.0	15.5	15.6	15.6	15.6	15.7	15.6
VØLTAGE EFFICIENCY, PCT.	33.1	34.6	33.3	33.3	32.3	32.5	32.5	32.5	32.8	32.5
THERMAL EFFICIENCY, PCT.	20.4	21.8	21.4	19.8	20.8	21.4	21.4	21.4	21.1	20.1
WATER BALANCE DATA										
WATER LØSS, CC/MIN.										
GRØSS	3.97	3.56	2.94	0.	2.55	2.74	2.90	2.79	0.	2.83
NET	0.	0.	0.	0.	0.	0.	0.	0.	0.	0.
WATER PRØDUCED, CC/MIN.	1.13	1.11	1.09	0.	1.09	1.06	1.06	1.06	0.	1.13

(1) See Appendix G-8 for additional details.

APPENDIX G-10 (Cont'd.)

PERFØRMANCE ØF METHANØL-AIR SIXTEEN CELL STACK[1]

RUN NØ. 65-	4-19	4-19	4-19	4-19	4-19	4-21	4-21	4-21	4-21	4-22
CØNDITIØN PERIØD	1	2	3	4	5	1	2	3	4	1
TIME ØN LØAD AT START, HRS.	200	200	200	200	200	207	207	207	207	212
RUN CØNDITIØNS										
CH3ØH IN FEED, M	0.75	0.75	0.75	0.75	0.75	0.75	0.75	0.75	0.75	0.75
MØDE ØF ØPERATIØN	S	S	S	S	S	S	S	S	S	S
CURRENT DENSITY, MA/SQ. CM.	40.0	40.0	40.0	40.0	40.0	40.0	40.0	40.0	40.0	40.0
FEED RATE, CC/HR.	3200	3200	3200	3200	4620	4620	4620	3200	3200	3200
NØM. CØNV. / PASS	50.2	50.2	50.2	50.2	34.8	34.8	34.8	50.2	50.2	50.2
AIR RATE, CC/MIN. AT STP	30000	30000	30000	46200	46200	30000	30000	30000	30000	30000
NØM. STØICH. EXCESS AIR	8.4	8.4	8.4	12.9	12.9	8.4	8.4	8.4	8.4	8.4
AIR HUMIDITY	WET	WET	WET	WET	WET	DRY	DRY	DRY	DRY	DRY
TEMPERATURES, °C										
AVG. CELL	70	73	72	69	63	64	66	70	71	69
FUEL INLET	48	53	50	52	49	26	26	27	27	47
FUEL ØUTLET	53	48	52	51	48	56	58	60	58	60
AIR INLET	59	58	61	57	56	18	25	27	27	47
AIR ØUTLET	55	57	56	53	51	42	40	42	42	55
BATTERY PERFØRMANCE										
STACK VØLTAGE	6.40	6.60	6.40	6.60	6.50	6.30	6.35	6.35	5.30	6.45
CELL VØLTAGE, AVG.	0.41	0.41	0.39	0.41	0.41	0.39	0.40	0.39	0.34	0.41
STD. DEV.	0.07	0.07	0.09	0.04	0.02	0.04	0.03	0.04	0.14	0.05
PØLARIZATIØN, VØLTS										
ANØDE, AVG.	0.34	0.34	0.34	0.38	0.37	0.36	0.36	0.36	0.37	0.34
STD. DEV.	0.06	0.05	0.06	0.04	0.04	0.06	0.05	0.06	0.06	0.06
CATHØDE, AVG.	0.40	0.40	0.42	0.35	0.37	0.39	0.39	0.40	0.44	0.40
STD. DEV.	0.12	0.12	0.14	0.06	0.05	0.09	0.07	0.09	0.18	0.10
ØHMIC LØSSES, VØLTS	0.05	0.05	0.05	0.05	0.05	0.05	0.05	0.05	0.05	0.05
C02 IN AIR ØUTLET, MØL. PCT.	1.00	1.00	0.75	0.40	0.55	1.20	1.25	1.40	1.00	0.85
CHEM. ØXID., MA/SQ. CM.	25.7	25.7	19.4	16.2	22.2	30.7	32.0	35.7	25.7	21.9
PØWER ØUTPUT, WATTS	77.	79.	77.	79.	78.	76.	76.	76.	64.	77.
PØWER DENSITY, MWATTS/SQ. CM.	16.0	16.5	16.0	16.5	16.2	15.7	15.9	15.8	13.2	16.1
VØLTAGE EFFICIENCY, PCT.	33.3	34.4	33.3	34.4	33.9	32.8	33.1	33.1	27.6	33.6
THERMAL EFFICIENCY, PCT.	19.8	20.4	21.9	23.9	21.2	18.1	17.9	17.2	16.4	21.2
WATER BALANCE DATA										
WATER LØSS, CC/MIN.										
GRØSS	0.	3.71	4.81	6.09	5.27	0.	2.09	1.88	1.98	3.91
NET	0.	-1.79	-1.66	-1.60	-2.18	0.	0.	0.	0.	0.
WATER PRØDUCED, CC/MIN.	0.	1.18	1.06	1.01	1.11	0.	1.29	1.35	1.18	1.11

(1) See Appendix G-8 for additional details.

APPENDIX G-10 (Cont'd.)

PERFORMANCE OF METHANOL-AIR SIXTEEN CELL STACK[1]

RUN NØ. 65-	4-22	4-26	4-26	4-26	4-26	4-26
CØNDITIØN PERIØD	2	1	2	3	4	5
TIME ØN LØAD AT START, HRS.	212	224	224	224	224	224
RUN CØNDITIØNS						
CH3ØH IN FEED, M	0.75	0.75	0.75	0.75	0.75	0.75
MØDE ØF ØPERATIØN	S	S	S	S	S	S
CURRENT DENSITY, MA/SQ. CM.	40.0	40.0	40.0	40.0	40.0	40.0
FEED RATE, CC/HR.	3200	3200	3200	3200	3200	3200
NØM. CØNV. / PASS	50.2	50.2	50.2	50.2	50.2	50.2
AIR RATE. CC/MIN. AT STP	30000	30000	30000	30000	30000	30000
NØM. STØICH. EXCESS AIR	8.4	8.4	8.4	8.4	8.4	8.4
AIR HUMIDITY	DRY	WET	WET	WET	DRY	DRY
TEMPERATURES, °C						
AVG. CELL	74	71	70	68	69	71
FUEL INLET	51	51	51	51	51	51
FUEL ØUTLET	62	57	56	57	53	53
AIR INLET	52	27	27	27	51	51
AIR ØUTLET	60	54	53	52	53	53
BATTERY PERFØRMANCE						
STACK VØLTAGE	6.55	5.90	5.50	5.80	6.00	6.10
CELL VØLTAGE, AVG.	0.41	0.37	0.36	0.37	0.37	0.38
STD. DEV.	0.06	0.11	0.13	0.11	0.11	0.08
PØLARIZATIØN, VØLTS						
ANØDE, AVG.	0.34	0.36	0.38	0.39	0.38	0.39
STD. DEV.	0.06	0.07	0.05	0.05	0.07	0.05
CATHØDE, AVG.	0.40	0.41	0.41	0.39	0.40	0.39
STD. DEV.	0.12	0.16	0.16	0.15	0.16	0.12
ØHMIC LØSSES, VØLTS	0.05	0.05	0.05	0.05	0.05	0.05
CØ2 IN AIR ØUTLET, MØL. PCT.	0.85	0.90	0.80	0.75	0.80	0.75
CHEM. ØXID., MA/SQ. CM.	21.9	23.2	20.7	19.4	20.7	19.4
PØWER ØUTPUT, WATTS	79.	71.	66.	70.	72.	73.
PØWER DENSITY, MWATTS/SQ. CM.	16.4	14.7	13.7	14.5	15.0	15.2
VØLTAGE EFFICIENCY, PCT.	34.1	30.7	28.6	30.2	31.2	31.8
THERMAL EFFICIENCY, PCT.	21.5	19.0	18.4	19.8	20.1	20.9
WATER BALANCE DATA						
WATER LØSS, CC/MIN.						
GRØSS	4.23	3.46	3.32	3.38	3.16	3.11
NET	0.	2.58	2.41	2.50	0.	0.
WATER PRØDUCED, CC/MIN.	1.11	1.13	1.09	1.06	1.09	1.06

(1) See Appendix G-8 for additional details.

APPENDIX G-11

OPERATION WITH FORMALDEHYDE AS FUEL

A. Operation of Sixteen Cell Battery

Current Density, ma/cm^2	Battery Performance[1]	
	Voltage	Power, Watts
16.6	10.2	51
40	8.8	106
50	8.0	120
56.7	7.5	128
70	7.0	147
90	6.2	167

(1) Run 3330-14 65-2-16 made in 16 cell battery after 9 hours prior operation with methanol feed. Feed for this run was 1 M HCHO in 3.7 M H_2SO_4, once-thru at 50% nominal conversion per pass with 15 times stoichiometric air rate. Peak battery temperatures maintained at 80°C by prechilling feed to about 16°C.

B. Anode Performance

Current Density, ma/cm^2	Polarization from Formaldehyde Theory, volts[1]
0	0.16
1	0.19
5	0.27
10	0.27
50	0.33
100	0.36
400	0.44

(1) 1 M HCHO in 3.7 M H_2SO_4 @ 60°C. Anode was 25 mg/cm^2 Ru modified P-type catalyst prepared with H_2 reducing agent on 5.7 cm^2 50 mesh Ta screen. Following are estimated relative potentials @ 60°C:

Formaldehyde	+ 0.135 volts
Hydrogen	0.000
Methanol	- 0.007
Oxygen	- 1.204

APPENDIX G-12

METHANOL ANALYZER TEST CELL

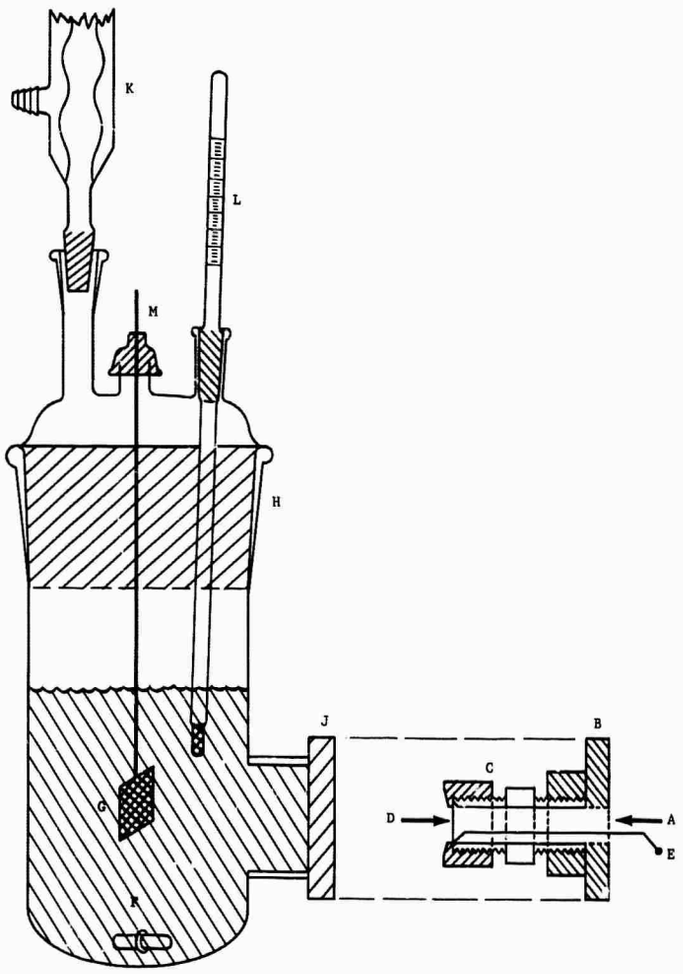

A. Aperture for CO_2 exit (N_2 sparged)
B. Teflon flange
C. Modified polypropylene tubing fitting
D. Membrane-electrode analyzer element
E. Current collector tab
F. Magnetic stirrer
G. Counter electrode
H. Standard taper joint
J. Glass flange
K. Condenser
L. Thermometer
M. Serum stopper

APPENDIX G-13

SUMMARY OF METHANOL ANALYZER DATA
CYANAMID AA-1-PERMION 1010 ELEMENT; 3.7 M H_2SO_4

Unit Identification	Temperature, °C.	Output Current, ma., @ Indicated Vol. % CH_3OH				Activation Energy(1), Kcal/Mole	Output Slope, ma./vol. %, @ Indicated Hours Running Time(4)					Remarks
		1	1.5	2	3		0	10	50	100	200	
0-41	26	10.5	15.8	--	--	--	10.5	--	--	--	--	--
0-42	26	10.0	15.5	20.5	28.5	--	10.2	--	--	--	--	35 ma. @ 4%
0-45	26	12.0	17.5	23.0	33.0	--	11.5	--	--	--	--	42.5 ma. @ 4%
1-46	29	--	--	42	--	--	21	18.2	--	--	--	Discontinued - Leaking
1-47	28	15.0	22.0	28.0	41.5	--	14.5	14.5	13.3	9	--	Fresh electrolyte at 100 hours (con't. 1-47A)
1-47A	31	--	--	--	42	--	14	14	14	--	--	Open circuit @ 25 hr.
1-414	30	--	--	--	41.5	--	13.5	13	9	13.5(2)	--	40 ppm Re in electrolyte(6)
1-420	60	21.5	32	42	--	--	21	21.5	20.7(40)	20	20	Added 28 ppm Ru @ ~40 hrs.
1-430	60	--	--	--	43	--	21.5	--	--	17	16.5(150)	Discontinued 150 hrs.
2-48	60	--	--	60	--	6.1	30	--	26.7(24)	19		
2-412	60	--	--	68	--	4.8	34	16	--	--	--	Discontinued
2-415	60	--	--	60	--	4.8	30	--	--	29	27	Pt black pressed on Nalfilm
3-519	60	18	--	35.5	53	5.5 (@ 4%)	18	--	--			69.5 ma. @ 4%
3-413	60	18.5	27.5	37	--	4.8	18.5	--	18.5	20	--	Discontinued
3-420	60	12.5	17.5	22	--	5.1	12	--	~8	--	8	Discontinued
4-414	60	17.5	26	34.5	--	4.8	17.5		17 (25)	20(3)		Continued as 4-419 with 40 ppm Re added(6)
4-419	60	--	--	40	--	4.8	20	20	19.5	--		Continued as 4-421 with 440 ppm Re_2O_7 added(6)
4-421	60	--	--	40	--	4.8	20	~20	20	--		Continued as 4-423 with temperature compensator
4-423	60	--	--	--	60(5)	--	20	--	--	20		Increased to 3 vol. % CH_3OH. Continued as 4-427 with 0.4% Re_2O_7(6)
4-427	60	--	--	--	60(5)	--	20	--	18.4(25)	17.1(75)		Replaced with fresh 3% CH_3OH soln., continued as 4-430
4-430	60	--	--	--	59		20	--	--	20(2)	20(600)	Total of 1030 hours running time

(1) In the range 30-60°C.
(2) Recover to this value upon change to fresh electrolyte (No Re).
(3) Abrupt change in response following temperature study after 25 hours - continued on new basis.
(4) Numbers in parentheses below indicate times other than those listed.
(5) Calculated from Temperature Compensator output and known conversion factor.
(6) Re and Re_2O_7 are know soluble redox reagents (3).

APPENDIX G-14

FIFTY AMPERE CONSTANT CURRENT LOAD AND DRIVER

A heavy duty, wide range electrical loading and measuring unit was designed and built for cell stack testing. Constant current loading, regulated to ± 1%, was provided from 200 ma to 50 amp. Voltage measurement ranges extended from 0.5 volts to 150 volts. All equipment was assembled in a single package except for the high current DC supplies. Solid state devices were used for rectification, amplification and regulation. A block diagram of the regulation system is shown in Figure G-20.

The main regulator consisted of 12 parallel connected 2N174 transistors mounted in a commercial stacking device provided with forced air cooling. Regulation was accomplished using negative feedback through a high gain voltage amplifier and a regulator driver. The regulated current level was established by adjusting the reference voltage level which was compared to the voltage drop across the regulator shunt by a differential error amplifier. A surge control circuit prevented the development of large current peaks during startup and shutdown periods.

The 50 amp regulated current span was covered in three ranges; 0.2 to 5.0 amp, 0.2 to 15 amp, and 0.2 to 50 amp. Range change was accomplished by shunt switching. Mechanical coupling in the current range switch provided automatic switching of the recorder circuit shunts as the current range was changed.

The voltage measuring circuit provided readout up to 150 volts full scale. Ranges of 0 to 0.5, 0 to 1.5, 0 to 5.0, 0 to 15, 0 to 50, and 0 to 150 volts were available. Mechanical coupling in the voltage range control switch provided automatic activation of the external DC power supplies needed to maintain good regulation below the 5 volt operating level.

Figure G-19

Constant Current Load And Driver
for 50 Amperes, 800 Watts Operation

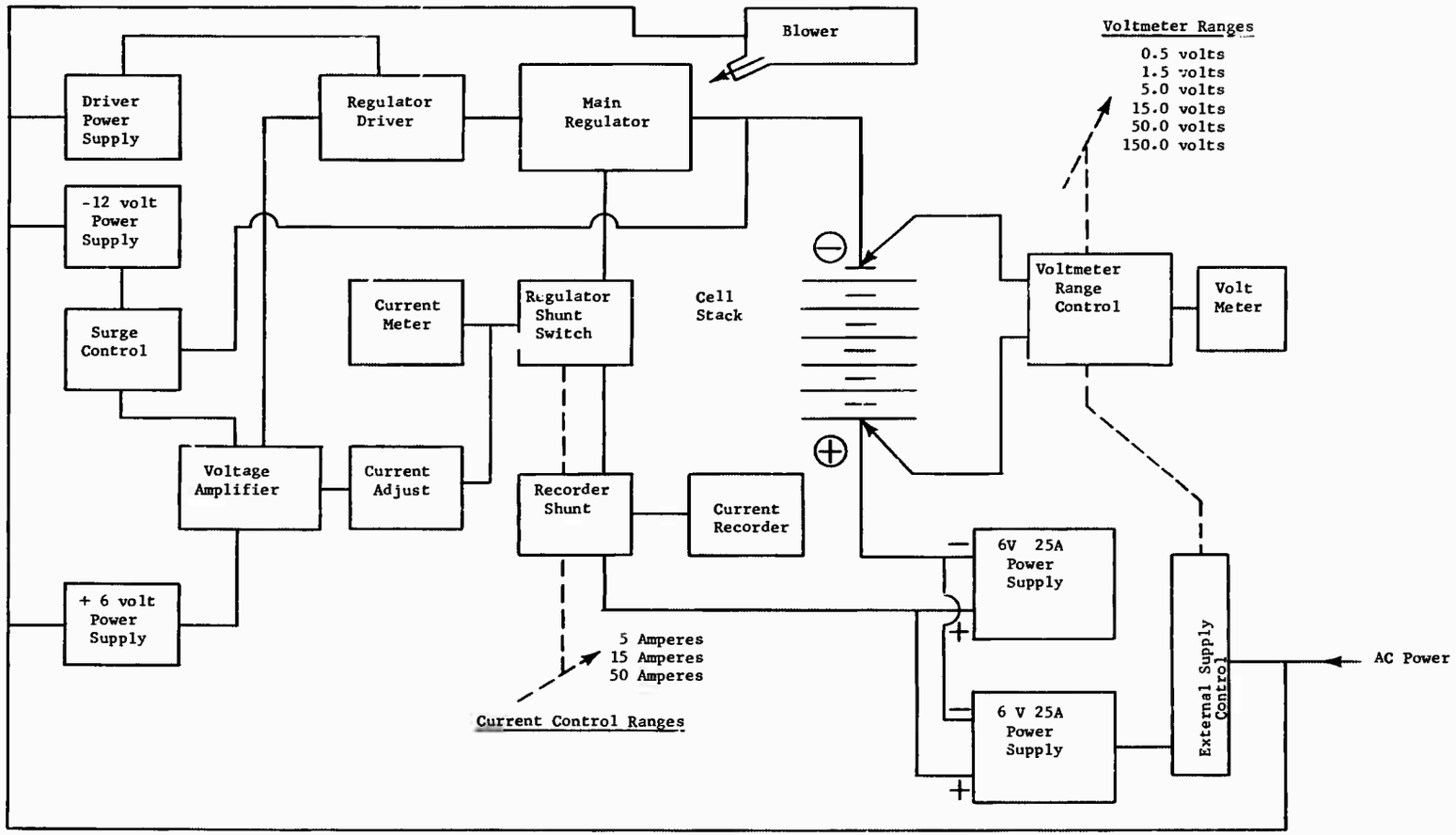

DOCUMENT CONTROL DATA - R&D

(Security classification of title, body of abstract and indexing annotation must be entered when the overall report is classified)

1. ORIGINATING ACTIVITY *(Corporate author)*
Esso Research and Engineering Company
Process Research Division
Linden, New Jersey

2a. REPORT SECURITY CLASSIFICATION
UNCLASSIFIED

2b. GROUP

3. REPORT TITLE

HYDROCARBON-AIR FUEL CELL

4. DESCRIPTIVE NOTES *(Type of report and inclusive dates)*
3rd Semi Annual - 1 Jan 1965 - 30 June 1965

5. AUTHOR(S) *(Last name, first name, initial)* William R. Epperly, Eugene L. Holt, Hugh H. Horowitz, Duane G. Levine, Charles E. Morrell, Barry L. Tarmy, James A. Wilson, Morton Beltzer, George Ciprios, I-Ming Feng, Donald E. LeClair, Martin Lieberman, John M. Matsen, Andreas W. Moerikofer, Eugene H. Okrent, Robert K. Resnik, (Contd in 11)

6. REPORT DATE	7a. TOTAL NO. OF PAGES	7b. NO. OF REFS
	288	24

8a. CONTRACT OR GRANT NO.	9a. ORIGINATOR'S REPORT NUMBER(S)
DA-36-039-AMC-03743(E)	
b. PROJECT NO. 7900.21.903.01.00	Report No. 7
c.	9b. OTHER REPORT NO(S) *(Any other numbers that may be assigned this report)*
d.	

10. AVAILABILITY/LIMITATION NOTICES

QUALIFIED REQUESTORS MAY OBTAIN COPIES OF THIS REPORT FROM DDC. DDC RELEASE TO CFSTI NOT AUTHORIZED.

11. SUPPLEMENTARY NOTES	12. SPONSORING MILITARY ACTIVITY
Joseph A. Shropshire, Charles E. Thompson, Herbert H. Vickers, Elliot A. Vogelfanger, Abraham A. Zimmerman	Command General U. S. Army Electronics Command Fort Monmouth, N.J. ATTN: AMSEL-KL-PB

13. ABSTRACT

Studies were continued aimed toward the ultimate development of fuel cells using either hydrocarbons or methanol as fuels and air as the oxidant at moderate temperatures and pressures. Included are work carried out on the effects of the fuel, catalyst composition, and other major operating variables on the design and operation of the fuel electrodes, experiments performed to improve the overall efficiency of the air electrodes, and tests designed to evaluate the operability of the fuel cell components in complete cells. These tests demonstrated the importance of various structural and catalytic parameters in hydrocarbon electrodes. They also demonstrated operability of liquid hydrocarbon electrodes in engineered cells. Finally, they demonstrated the practicality of sustained performance in a self-contained methanol-air multi-cell unit. (Author)

DD FORM 1 JAN 64 1473

14. KEY WORDS	LINK A		LINK B		LINK C	
	ROLE	WT	ROLE	WT	ROLE	WT
Power Supplies-Fuel Cells Hydrocarbons and Methanol CO_2 Rejecting Electrolyte Electrodes						

INSTRUCTIONS

1. ORIGINATING ACTIVITY: Enter the name and address of the contractor, subcontractor, grantee, Department of Defense activity or other organization *(corporate author)* issuing the report.

2*a*. REPORT SECURITY CLASSIFICATION: Enter the overall security classification of the report. Indicate whether "Restricted Data" is included. Marking is to be in accordance with appropriate security regulations.

2*b*. GROUP: Automatic downgrading is specified in DoD Directive 5200.10 and Armed Forces Industrial Manual. Enter the group number. Also, when applicable, show that optional markings have been used for Group 3 and Group 4 as authorized.

3. REPORT TITLE: Enter the complete report title in all capital letters. Titles in all cases should be unclassified. If a meaningful title cannot be selected without classification, show title classification in all capitals in parenthesis immediately following the title.

4. DESCRIPTIVE NOTES: If appropriate, enter the type of report, e.g., interim, progress, summary, annual, or final. Give the inclusive dates when a specific reporting period is covered.

5. AUTHOR(S): Enter the name(s) of author(s) as shown on or in the report. Enter last name, first name, middle initial. If military, show rank and branch of service. The name of the principal author is an absolute minimum requirement.

6. REPORT DATE: Enter the date of the report as day, month, year; or month, year. If more than one date appears on the report, use date of publication.

7*a*. TOTAL NUMBER OF PAGES: The total page count should follow normal pagination procedures, i.e., enter the number of pages containing information.

7*b*. NUMBER OF REFERENCES: Enter the total number of references cited in the report.

8*a*. CONTRACT OR GRANT NUMBER: If appropriate, enter the applicable number of the contract or grant under which the report was written.

8*b*, 8*c*, & 8*d*. PROJECT NUMBER: Enter the appropriate military department identification, such as project number, subproject number, system numbers, task number, etc.

9*a*. ORIGINATOR'S REPORT NUMBER(S): Enter the official report number by which the document will be identified and controlled by the originating activity. This number must be unique to this report.

9*b*. OTHER REPORT NUMBER(S): If the report has been assigned any other report numbers *(either by the originator or by the sponsor)*, also enter this number(s).

10. AVAILABILITY/LIMITATION NOTICES: Enter any limitations on further dissemination of the report, other than those imposed by security classification, using standard statements such as:

(1) "Qualified requesters may obtain copies of this report from DDC."

(2) "Foreign announcement and dissemination of this report by DDC is not authorized."

(3) "U. S. Government agencies may obtain copies of this report directly from DDC. Other qualified DDC users shall request through _____."

(4) "U. S. military agencies may obtain copies of this report directly from DDC. Other qualified users shall request through _____."

(5) "All distribution of this report is controlled. Qualified DDC users shall request through _____."

If the report has been furnished to the Office of Technical Services, Department of Commerce, for sale to the public, indicate this fact and enter the price, if known.

11. SUPPLEMENTARY NOTES: Use for additional explanatory notes.

12. SPONSORING MILITARY ACTIVITY: Enter the name of the departmental project office or laboratory sponsoring *(paying* for) the research and development. Include address.

13. ABSTRACT: Enter an abstract giving a brief and factual summary of the document indicative of the report, even though it may also appear elsewhere in the body of the technical report. If additional space is required, a continuation sheet shall be attached.

It is highly desirable that the abstract of classified reports be unclassified. Each paragraph of the abstract shall end with an indication of the military security classification of the information in the paragraph, represented as *(TS)*, *(S)*, *(C)*, or *(U)*.

There is no limitation on the length of the abstract. However, the suggested length is from 150 to 225 words.

14. KEY WORDS: Key words are technically meaningful terms or short phrases that characterize a report and may be used as index entries for cataloging the report. Key words must be selected so that no security classification is required. Idenfiers, such as equipment model designation, trade name, military project code name, geographic location, may be used as key words but will be followed by an indication of technical context. The assignment of links, rules, and weights is optional.